UNIVERSIDADE DE LISBOA
FACULDADE DE CIÊNCIAS

Sphingolipid domains in the plasma membrane of fungal cells
Interplay with membrane proteins and antifungal resistance

"Documento Definitivo"

Doutoramento em Bioquímica
Especialidade: Biofísica Molecular

Filipa Pedro Costa Santos

Tese orientada por:
Doutor Rodrigo F. M. de Almeida

Documento especialmente elaborado para a obtenção do grau de doutor

2022

UNIVERSIDADE DE LISBOA
FACULDADE DE CIÊNCIAS

Sphingolipid domains in the plasma membrane of fungal cells
Interplay with membrane proteins and antifungal resistance

Doutoramento em Bioquímica
Especialidade: Biofísica Molecular

Filipa Pedro Costa Santos

Tese orientada por:
Doutor Rodrigo F. M. de Almeida

Júri:
Presidente: Doutor Manuel Eduardo Ribeiro Minas da Piedade, Professor Catedrático e Presidente do Departamento de Química e Bioquímica da Faculdade de Ciências da Universidade de Lisboa
Vogais:

- Doutora Maria do Rosário Gonçalves dos Reis Marques Domingues, Professora Associada com Agregação do Departamento de Química da Universidade de Aveiro
- Doutor Jorge Manuel Martins, Professor Auxiliar da Faculdade de Ciências e Tecnologia da Universidade do Algarve
- Doutora Liana Casquinha da Silva, Professora Auxiliar com Agregação da Faculdade de Farmácia da Universidade de Lisboa
- Doutora Maria Luísa Mourato Oliveira Marques Serralheiro, Professora Associada com Agregação da Faculdade de Ciências da Universidade de Lisboa
- Doutora Ana Isabel Abrantes Coutinho, Professora Auxiliar da Faculdade de Ciências da Universidade de Lisboa
- Doutor Rodrigo Freire Martins de Almeida, Professor Auxiliar da Faculdade de Ciências da Universidade de Lisboa (orientador)

Documento especialmente elaborado para a obtenção do grau de doutor

Trabalho financiado pela Fundação para a Ciência e a Tecnologia através da bolsa de doutoramento SFRH/BD/108031/2015

2022

This thesis is in memory of

My beloved father

My beloved grandfather Vasco Grazina

My dear friend Gerson Lobo

My dear friend Professor Jorge Gaspar

My dear friend Fermelinda Vitorino

My dear friend Mário Póvoa

“Nothing in life is to be feared, it is only to be understood.
Now is the time to understand more, so that we may fear less”.
Marie Curie

List of Publications

My contribution to the articles and chapters included in this thesis:

(1) **Santos, F. C.**, Fernandes, A. S., Antunes, C. A. C., Moreira, F. P., Videira, A., Marinho, H. S., de Almeida, R. F. M. (2017) Reorganization of plasma membrane lipid domains during conidial germination, *Biochimica et Biophysica Acta (BBA) – Molecular and Cell Biology of Lipids*, 1862, 156 – 166, doi: 10.1016/j.bbalip.2016.10.011, IF: 5.547.

Took an active part in the planning of the work and performed all the experiments related with *Neurospora crassa*. C.A.C.A. and F.P.M. performed all the experiments related with *Saccharomyces cerevisiae*. Took an active part in the writing of the manuscript.

(2) **Santos, F. C.**, *Lobo, G. M.*, Fernandes, A. S., Videira, A., de Almeida, R. F. M. (2018) Changes in the biophysical properties of the cell membrane are involved in the response of Neurospora crassa to staurosporine, *Frontiers in Physiology – Membrane Physiology and Membrane Biophysics*, 9, 1375 – 1387, doi: 10.3389/fphys.2018.01375; IF: 3.394.

Took an active part in the planning of the work and performed all the experiments related with *Neurospora crassa*, except ABC-3 expression that was performed by A.S.F. G.M.L. performed the experiments with liposomes. Took an active part in the writing of the manuscript.

(3) de Almeida, R. F. M., **Santos, F. C.**, Marycz, K., Alicka, M., Krasowska, A., Suchodolski, J., Panek, J., Jezierska, A., Starosta, R. (2019) New diphenylphosphane derivatives of ketoconazole are promising antifungal agents, *Scientific Reports*, 9, 16214, doi: 10.1038/s41598-019-52525-7, IF 4.525.

Developed and performed the minimal inhibitory concentration (MIC) assays with the *Saccharomyces cerevisiae* BY4741 strains, *wt* and *erg6*Δ. The other MIC assays with *Saccharomyces cerevisiae* W303 and ADI-8 were developed and performed in A.K. laboratory, Faculty of Biotechnology, University of Wroclaw, Poland.

(4) Bento-Oliveira, A.[§], **Santos, F. C.[§]**, Marquês, J. T.[§], Paulo, P. M. R., Korte, T., Herrmann, A., Marinho, H. S., de Almeida, R. F. M. (2020) Yeast sphingolipid-enriched domains and membrane compartments in the absence of mannosyldiinositolphosphorylceramide. *Biomolecules*, 10, 871, doi:10.3390/biom10060871, IF 4.879. [§]Equally contributing authors.

Took an active part in the formal analysis, investigation, writing-original draft preparation, writing-review and editing and visualization. I performed the confocal FLIM experiments with *S. cerevisiae* living cells and data analysis. The analysis of the distribution heterogeneity was performed by A.B.O.

(5) **Santos, F. C.**, Marquês, J. T., Bento-Oliveira, A., de Almeida, R. F. M. (2020) Sphingolipid-enriched domains in fungi, *FEBS Letters*, 594, 3698-3718, doi: 10.1002/1873-3468.13986, IF 4.124.

Took an active part in the writing-original draft preparation, figure and table design.

(6) Sousa, C., **Santos, F. C.**, Bento-Oliveira, A., Mestre, B., Silva, L. C., de Almeida, R. F. M. (2021) Biophysical Analysis of Lipid Domains in Mammalian and Yeast Membranes by Fluorescence Spectroscopy. In *Lipid Rafts: Methods and Protocols*, Bieberich, E., Ed. Springer US: New York, NY, Chapter 14, 247-269, doi: 10.1007/978-1-0716-0814-2_14.

Took an active part in the writing of the manuscript, figure and table design.

(7) **Santos, F. C.**, Fernandes, A. S., Videira, A., de Almeida, R. F. M., Biophysical impact of a staurosporine challenge in the plasma membrane of high drug-sensitivity *Neurospora crassa* strains, **in preparation**.

Took an active part in the planning of the work and performed all the experiments. Took an active part in the writing of the manuscript.

Acknowledgments

First of all, I would like to express my most sincere and deepest thanks to Doctor Rodrigo de Almeida, for allowing me to perform this project in the Molecular Biophysics group (CQB/CQE, FCUL), specially for being my supervisor/ mentor, for providing all necessary conditions for the development of this work, for sharing his knowledge with me, for believing in my capacities and giving me incentive and opinions crucial for the development of this scientific project. Last but certainly not the least I want to thank his friendship, patience, and availability along my personal and scientific development journey.

I would like to direct my deepest gratitude to the institutions that supported the execution of this project: to Fundação para a Ciência e a Tecnologia (**FCT**) for giving financial support to its progress (PhD Scholarship – SFRH/BD/108031/2015), research grants PTDC/BBB-BQB/6071/2014 and EXPL/BIA-BFS/1034/2021, and research units UID/Multi/00612/2013-2019 and UIDB/00100/2020, to Faculdade de Ciências da Universidade de Lisboa (FCUL), for accepting me as a 3rd cycle student and Centro de Química e Bioquímica/ Centro de Química Estrutural facilities and equipment provided.

I also want to acknowledge the scholarships and travel funding from **EBSA** (European Biophysical Societies' Association) and **FEBS** (The Federation of European Biochemical Societies), that allowed me to attend the 59th International Conference on Bioscience of Lipids (ICBL), held in Helsinki, Finland, on September 4 – 7th 2018 and the FEBS Advanced Practical Course, held in Nijmegen/ Wageningen, The Netherlands, on September 11 – 20th 2018.

I would like to thank all Academic scientists, either Professors or not who have contributed directly or indirectly to this work and from whom I had the pleasure to learn immensely, namely Fernando Santos, Ana Viana, Jorge Correia, Andreia Fernandes, Arnaldo Videira, Luísa Serralheiro, Ana Isabel Tomaz, Helena Garcia Carla Real and Ana Tenreiro and Filipa.

A very special thanks to Professor Doctor Jorge Francisco Gaspar for teaching me that dreams can and will come true if you keep on fighting and off course for his friendship that will be forever in my memory.

A very special thanks to Professor Luísa Cyrne for her kindness and all the help during my first steps with *Saccharomyces cerevisiae* and whenever I had a doubt or just wanted to talk a little.

To Professor Susana Marinho, I want to thank for making the Redox Biology lab available and for all the scientific input to the project.

I also want to thank Professor Radoslaw Starosta aka Radek for the possibility to study the antifungal activity of new ketoconazole derivatives, which work was published in *Scientific Reports* 2019, entitled, "New diphenylphosphane derivatives of ketoconazole are promising antifungal agents", and for the possibility to study HSA and BSA, unravelling the rotational diffusion differences between them, which work was published in *Journal of Molecular Structure* 2020, entitled, "Human and bovine serum albumin time-resolved fluorescence: Tryptophan and tyrosine contributions, effect of DMSO and rotational diffusion".

I also want to thank Doctor Pedro Paulo for the help with FLIM, the access to the facilities and providing the necessary conditions to develop my experiments and sharing his knowledge and for giving advice on sample and microscope handling and data analysis.

To Professor Luísa Corvo, Catarina Faria-Silva and Francesca Fedeli, I want to thank for the Nys formulations, that allowed the start of the study of antifungal activity with liposomes as drug delivery systems.

In this part of the acknowledgments, I want to highlight the importance of all the colleagues and friendships along my scientific journey, and to thank all of them.

I want to firstly give a special and huge thanks to the amazing people/ friends I have met in Molecular Biophysics laboratory and that in some way or another became to be a second family to me, Ana Carreira, André Bastos, Andreia Giro, Andreia Oliveira, Andreia Sousa, António Flor, Beatriz Mestre, Catarina Antunes, Carla Sousa, Filipe Moreira, Gerson Lobo, Hugo Filipe, Inês Almeida, Joaquim Marquês, Telma Santos and Telmo Paiva. Well, Inês you were not really from the Molecular Biophysics lab, you were from the Interfacial Electrochemistry group, but you are included in this group of people that became to be like a second family. Thinking about that, well, both Ana and Beatriz were from FFUL, but I

completely forgot about that, sorry, from FFUL also Tânia Santos, thanks for the cloth tennis (actually I should be thanking to Tânia's mother 😊) and for the book it helped me a lot.

A very special thanks to my former colleague and especially good friend, Gerson Lobo, for helping me with the interaction of staurosporine with lipid model systems assays. And for helping me to see things differently and for the many laughs.

From the Organometallics group, I want to give a special thanks to Tânia Morais and Leonor Côrte-Real for their precious advice and help when I needed the most, but most of all for their friendship. To Bruno Demoro that I met when working with both Molecular Biophysics and Organometallics groups I want to give a special thanks for the friendship, the long talks and for letting me try the Yerba Mate Tea.

Many thanks to all the brilliant scientists who I gladly and proudly worked with during the FEBS Advanced Practical Course, held in Nijmegen/ Wageningen, The Netherlands, in special my roomie Emilia Holm. To Miguel Angel Casado a special thanks for creating a relaxed work environment, many laughs, talks and especially for his friendship.

To Fermelinda Vitorino a very special friend that will stay in my memory, a special thanks for staying with me many afternoons when I was younger and did not want to stay at home alone waiting my parents to arrive from work, and also for all the scholar material she gave to me, love those and work even more to give them a very good use.

To Mário Póvoa who had a grocery shop below my parents' home, and who saw me grow, I want to thank also for all the things he taught me and for his friendship that will remain always in my memory.

Liliana Carvalho, yes you are the last, but I ensure you, you are definitely not the least, you are the sister I never had. Thanks for the many talks until late hours, for the surprise visits when I needed them the most. Sincerely there are not enough words. Love you sis.

I want to give a special and huge thanks to my family. To my parents, to my father who always gave me strength to carry on, even when we did not agree about something or after a big fight, *miss those a lot, wish you were here with me*. To my mom I want to thank for the unconditional love, support, and patience during the worse time of our lives.

To Mimi, Luís and Vó to whom I am deeply grateful for the unconditional love, support, encouragement, and patience. To Ivo, besides, we have distanced from each other a little I want to thank the friendship, it means a lot to me.

To Zé, Jaime, Carlos and Eduardo, I want to give a special thanks for their support, during the worse time of my life.

To Vô Vasco, who I loss very young but with whom I learn so much about life and the love for books (the knowledge and the smell of a book, only book lovers will understand this one) reason way he loved to work surrounded by books in the old faculty library 😊 where I was so happy readding under the tables, while he was working, animals and nature (the botanical garden where I used to walk and run with him and his dog, Dic, the little fox, so beautiful.

Last but not least, I would like to remark the happiness and joyful moments that companion animals brought into my life. Mila who arrived when I have already told myself I did not want another pet, because it was too painful to overcome the loss of my previous cat, Mareka. However, nowadays I do not imagine my life without her, and for that reason and many more I want to give a special thanks to Catarina Antunes. Rebeco, my crazy and loving dog, that I have adopted in 2019 to help me and my mom during the worst time of our lives.

This thesis is dedicated to my family and friends.

This work was developed under the supervision of:

- Doctor Rodrigo Freire Martins de Almeida, Principal Investigator, Centro de Química e Bioquímica e Centro de Química Estrutural, and Assistant Professor, Departamento de Química e Bioquímica, Faculdade de Ciências, Universidade de Lisboa, Portugal

This work was developed at:

- Centro de Química e Bioquímica (grupo de Biofísica Molecular) e Centro de Química Estrutural (laboratório de Biofísica Molecular – Grupo 8), Institute of Molecular Sciences, Departamento de Química e Bioquímica, Faculdade de Ciências, Universidade de Lisboa, Campo Grande, 1749-016 Lisboa, Portugal

Filipa Pedro Costa Santos was financially supported by Fundação para a Ciência e a Tecnologia (FCT) with a PhD fellowship SFRH/BD/108031/2015 and 100AC9108-CC327-1A BI. The work developed during the PhD project was supported by FCT research grants PTDC/BBB-BQB/6071/2014 (RESYEAST) and EXPL/BIA-BFS/1034/2021 (SphingOHmyces), UID/Multi/00612/2013-2019 (Centro de Química e Bioquímica) and since January 1st, 2020, Centro de Química Estrutural (UIDB/00100/2020).

Aims and Outline

The work presented along this dissertation is focused on the relevance of sphingolipids and sphingolipid-enriched domains (SLEDs) for the biophysical properties of the fungal plasma membrane, namely of *Neurospora crassa* and *Saccharomyces cerevisiae*, in order to better understand their relationship with yeast functional membrane compartments and their interplay with antifungal resistance.

This was achieved recurring mainly to the combination of fluorescence-based techniques, steady-state and time-resolved fluorescence spectroscopy and fluorescence microscopy, Fluorescence Lifetime Imaging Microscopy (FLIM).

This work aimed at answering pressing questions concerning *Neurospora crassa* plasma membrane behaviour.

- Are there SLEDs in the membrane of *Neurospora crassa*?
- How does the absence of sterols impact its biophysical properties?
- Is the conidial growth from a dormancy state to the exponential phase (mycelial stage) accompanied by membrane reorganization?
- Is this dependent on growth conditions?
- How different are the membrane biophysical properties in a cell wall-less strain?
- Is there a biophysical response at the plasma membrane to a staurosporine challenge?
- In such a case, should membrane lipid composition and biophysical properties be considered to understand the physiological response of filamentous fungi to the drug?

While for *Saccharomyces cerevisiae* plasma membrane this work aimed at:

- Determining the major sphingolipid component(s) of gel and liquid ordered domains in the plasma membrane
- Evaluating the influence of the 2-hydroxylation of very-long-chain fatty acid and sphingolipid headgroup on plasma membrane organization and biophysical properties
- Disclosing the relations between sphingolipid (and ergosterol)-enriched domains and membrane compartments MCC and MCP

- Assessing the degree of resistance of sphingolipid biosynthetic mutants (versus *wt*) used in this project to antifungal agents of the azole and polyene families
- Understanding the role of sphingolipid domains and plasma membrane biophysical properties in fungal resistance

Most of the data obtained during the execution of this work has already been published in international peer-review scientific journals, hence a great part of this thesis corresponds to a compilation of the published work.

The dissertation is divided into 10 chapters. **Chapter I** comprises an overview of the thematic that contextualize the present thesis. In a first approach a brief introduction is given to fungal organisms and fungal infections, the fungal plasma membrane and the differences between the lifecycle of unicellular budding yeast *S. cerevisiae* and multicellular *N. crassa*, the notion of compartmentalization of fungal plasma membrane, and the different complex sphingolipids and membrane sterols found in fungi and mammals. Then an introduction to the biophysical characteristics of sphingolipid-enriched domains (SLEDs), allowing to distinguish between gel and liquid ordered phases, is made. A brief overview of membrane model systems, specially liposomes (multilamellar vesicles and unilamellar vesicles), a very brief notion of lipid phase diagrams to help interpret the observations made when working with a mixture of lipids, to realize that the higher the number of lipids included in the mixture, the more complex is the phase behaviour, and usually that there is a broad range of temperatures where two or more phases can coexist. Finally, liposomes as drug delivery systems and an introduction to the antifungal drugs used throughout this thesis is also made.

Chapter II comprises briefly the basic principles of the biophysical characterization techniques used during this thesis, mainly, fluorescence spectroscopy and microscopy.

Chapter III is the description of the material, techniques and experimental procedures carried out through this Ph.D. thesis.

Chapter IV concerns the results, discussion and conclusion of the work already published in **Santos, F. C.**, Fernandes, A. S., Antunes, C. A. C., Moreira, F. P., Videira, A., Marinho, H. S., de Almeida, R. F. M. (2017) Reorganization of plasma membrane lipid domains during conidial germination, *Biochimica et Biophysica Acta (BBA) – Molecular and Cell Biology of Lipids*, 1862, 156 – 166.

Chapter V covers the results, discussion and conclusion of the work already published in **Santos, F. C.**, *Lobo, G. M.*, Fernandes, A. S., Videira, A., de Almeida, R. F. M. (2018)

Changes in the biophysical properties of the cell membrane are involved in the response of Neurospora crassa to staurosporine, *Frontiers in Physiology – Membrane Physiology and Membrane Biophysics*, 9, 1375 – 1387.

Chapter VI deals with the results, discussion and conclusion of a work which publication is *in preparation*, and only one result, the steady-state fluorescence anisotropy of DPH in the plasma membrane of *N. crassa* conidia (Figure 42) is already published in the publication mentioned in the previous chapter.

In **Chapter VII**, the results, discussion and conclusions concerning the experiments I performed with *S. cerevisiae*, which have already been partially published in two different articles, de Almeida, R. F. M., **Santos, F. C.**, Marycz, K., Alicka, M., Krasowska, A., Suchodolski, J., Panek, J., Jezierska, A., Starosta, R. (2019) New diphenylphosphane derivatives of ketoconazole are promising antifungal agents, *Scientific Reports*, 9, 16214; and Bento-Oliveira, A., **Santos, F. C.**, Marquês, J. T., Paulo, P. M. R., Korte, T., Herrmann, A., Marinho, H. S., de Almeida, R. F. M. (2020) Yeast sphingolipid-enriched domains and membrane compartments in the absence of mannosyldiinositolphosphorylceramide. *Biomolecules*, 10, 871.

Chapters I and **VIII**, "INTRODUCTION" and "CONCLUDING REMARKS AND FUTURE PERSPECTIVES", respectively, in their majority were published in the following review, **Santos, F. C.**, Marquês, J. T., Bento-Oliveira, A., de Almeida, R. F. M. (2020) Sphingolipid-enriched domains in fungi, *FEBS Letters*, 594, 3698-3718.

Chapters IX and **X** contain the "REFERENCES" and "ANNEXES".

Abstract

Plasma membrane (PM) carries out multiple functions a tightly regulated dynamic organization into specialized domains of different size, stability, and composition. Sphingolipids are a major class of lipids of PM being crucial for its structure and function. A specific type of ergosterol-depleted PM domains in fungi, where lipids are tightly packed in a very rigid gel phase, comprises the sphingolipid-enriched domains (SLEDs). In this work, the presence of SLEDs in a mold, *Neurospora crassa*, was disclosed, as well as their involvement in the response to the antifungal staurosporine. A comparison with the budding yeast *Saccharomyces cerevisiae* was performed, taking into consideration the known differences between their PM sphingolipidomes. The studies with *N. crassa* were performed in conidial suspensions along different time points of conidial germination, using several fluorescence spectroscopy techniques and a multiprobe approach.

S. cerevisiae living cells were studied in mi-exponential phase. To evaluate the impact of changing sphingolipid composition in the organization of the two main yeast PM compartments, MCC (arginine/ H^+ symporter Can1p) and MCP (H^+ ATPase Pma1p), the time-resolved fluorescence properties of Can1p tagged with GFP and Pma1p tagged with mRFP, respectively, were studied by FLIM in *wt* and a mutant strain with a different sphingolipid profile, *ipt1*Δ.

IPT1 deletion strongly affects the rigidity of gel domains and Pma1p PM distribution, whereas no significant alterations could be perceived neither in ergosterol-enriched domains nor Can1p distribution.

Thus, this work strongly suggests that proper SLEDs hydrophobic chain packing is required for an adequate organization of the MCP, but not MCC.

Finally, considering that the PM is crucial for antifungal action, a biophysical connection between SLEDs and antifungal activity was explored in *S. cerevisiae*.

Keywords: Fungal plasma membrane, antifungal agents, Fluorescence, sphingolipid-enriched domains (SLEDs), membrane compartments (MCC and MCP).

Resumo

O principal objetivo deste projeto de doutoramento foi desvendar as propriedades estruturais e biofísicas dos esfingolípidos que determinam a organização dos microdomínios na membrana plasmática de fungos, nomeadamente, o *Neurospora crassa* e a *Saccharomyces cerevisiae*, esclarecendo a sua relação com os compartimentos funcionais da membrana de levedura e o seu papel na resistência a agentes antifúngicos.

A membrana plasmática desempenha diversas funções fisiológicas que requerem a sua organização dinâmica e fortemente regulada em domínios especializados de diferentes tamanhos, estabilidade e composição lipídica/ proteica. Os esfingolípidos são uma classe de lípidos, nos quais a membrana plasmática se encontra particularmente enriquecida, sendo por esse motivo cruciais para a sua estrutura e função. Um tipo específico de domínios de membrana plasmática onde os lípidos são compactados numa fase gel muito rígida, que é ainda mais enriquecida em esfingolípidos e pobre em ergosterol, é agora conhecido em várias espécies de fungos. Antes deste trabalho era conhecido em leveduras e com este trabalho foram também detetados em bolores/ fungos filamentosos. A importância desses domínios ricos em esfingolípidos (SLEDs) para a membrana plasmática fúngica foi estudada recorrendo tanto a fungos unicelulares como multicelulares.

O *Neurospora crassa* é um fungo filamentoso não patogénico, utilizado em larga escala como modelo eucariota multicelular, que na sua fase conidial unicelular possui as características ideais para estudar domínios enriquecidos em esfingolípidos, que de acordo com os resultados apresentados nesta tese, estão envolvidos em processos celulares fundamentais que poderão ir desde a resistência a antifúngicos à apoptose celular. Várias alterações no metabolismo lipídico e na composição da membrana do *N. crassa* ocorrem durante a germinação dos esporos. No entanto, o impacto biofísico dessas alterações era praticamente desconhecido. Por esse motivo tornou-se de extrema importância realizar-se um estudo biofísico da membrana plasmática do *N. crassa*, particularmente dos domínios enriquecidos em esfingolípidos, e da sua dinâmica durante o processo de germinação conidial. Foram estudadas inicialmente duas estirpes de *N. crassa*, a estirpe selvagem (*wt*) e uma estirpe mutada, o *slime* que não possui parede celular. O crescimento conidial da *wt* desde a fase de dormência até à fase de crescimento exponencial foi acompanhada por reorganização membranar, nomeadamente o aumento da fluidez de membrana, que se verificou ocorrer mais rapidamente

num meio de crescimento suplementado do que no meio de mínimo de Vogel's. Os domínios tipo gel, que se vieram a comprovar enriquecidos em esfingolípidos foram encontrados em ambas as estirpes de *N. crassa*, mas estes eram particularmente compactos, rígidos e abundantes no caso das células de *slime*, ainda mais do que na levedura *Saccharomyces cerevisiae*. Em *N. crassa*, os nossos resultados sugerem que a fusão dos domínios enriquecidos em esfingolípidos ocorre próximo da temperatura de crescimento (30 ºC) para a *wt*, mas a temperaturas superiores no caso do *slime*. Em relação às propriedades biofísicas fortemente afetadas pelo ergosterol, a membrana plasmática das conidias do *slime* situa-se entre as das células de *N. crassa wt* e as de *S. cerevisiae wt*. As diferenças nas propriedades biofísicas encontradas neste trabalho e as relações estabelecidas entre a composição lipídica da membrana e a dinâmica forneceram novas perspetivas/ informações sobre a organização e estrutura da membrana plasmática das estirpes de *N. crassa* ao longo do desenvolvimento conidial. Resumindo, as propriedades biofísicas da membrana plasmática conidial de *N. crassa* foram extensamente caracterizadas. Estas evoluem durante a germinação conidial numa velocidade que depende das condições de cultura/ crescimento, sugerindo uma importante associação entre a remodelação da membrana e a intensa biogénese da membrana que ocorre durante o processo germinativo.

A estaurosporina (STS) é um fármaco utilizado para induzir a morte celular programada em vários organismos. Em *N. crassa*, a STS induz a sobre expressão regulada do transportador ABC (ABC-3), que se localiza na membrana plasmática e bombeia STS para fora da célula. Para entender o papel das propriedades biofísicas da membrana plasmática na resposta fúngica a fármacos, *N. crassa wt* e o mutante sem o transportador ABC (*abc3*) foram submetidos ao tratamento com STS durante os estágios inicial e tardio do desenvolvimento conidial. Após 1 h de tratamento com STS, há um aumento na abundância dos domínios mais ordenados, enriquecidos em esfingolípidos, na membrana plasmática conidial, o que leva a uma maior fluidez em outras regiões da membrana. A ordem global da membrana permanece assim praticamente inalterada. Mudanças significativas nos domínios enriquecidos em esfingolípidos também foram observadas após 15 min de incubação com STS, mas foram essencialmente opostas às verificadas para o tratamento de 1 h, sugerindo diferentes tipos de respostas consoante o tempo de exposição ao fármaco. Os efeitos da STS nas propriedades da membrana que são mais dependentes dos níveis de ergosterol também dependem do estágio de desenvolvimento. Não houve alterações nas células crescidas durante 2 h, contrastando claramente com o que acontece em tempos de crescimento mais longos. Neste caso, as diferenças foram mais acentuadas para o tratamento mais prolongado com STS, e

racionalizadas considerando que o fármaco previne o aumento da relação ergosterol/glicerofosfolípido que normalmente ocorre no estágio conidial tardio/ transição para o estágio micelial. Isto pode ser percebido como uma paragem de desenvolvimento induzida pelo tratamento com STS após 5 h de crescimento, envolvendo ergosterol, e apontando para um papel das jangadas lipídicas possivelmente relacionadas com sobre expressão regulada do transportador ABC-3. Em suma, os nossos resultados sugerem o envolvimento de domínios ordenados de membrana nos mecanismos de resposta à STS em *N. crassa*.

As propriedades biofísicas dos domínios ricos em esfingolípidos foram analisadas em diferentes situações, tendo em consideração as principais diferenças no esfingolipidoma da membrana plasmática. Além disso, os seus possíveis papéis biológicos foram criticamente revistos, incluindo as suas relações com os compartimentos da membrana plasmática e o seu envolvimento na resposta a stress. Para avaliar o impacto da alteração da composição de esfingolípidos da membrana plasmática da levedura *S. cerevisiae* na organização dos compartimentos de membrana do transportador de simporte arginina/ H^+ Can1p (MCC) e (H^+ ATPase Pma1p) MCP, os dois principais compartimentos da membrana plasmática da levedura, as propriedades de fluorescência resolvidas no tempo das proteínas Can1p marcada com GFP (Can1p-GFP) e Pma1p marcada com mRFP (Pma1p-mRFP) foram estudadas por imagiologia de tempos de vida de fluorescência (*fluorescence lifetime imaging microscopy*, FLIM), tanto em células vivas de *S. cerevisiae wt* como em células mutantes, *ipt1*Δ, sem o principal esfingolípido da membrana plasmática de *wt*, manosil di-inositol fosforilceramida ($M(IP)_2C$), e que ao invés acumula manosil inositol fosforilceramida (MIPC). A proteína Can1p pode encontrar-se em domínios MCC que co-localizam com a coloração de ergosterol pela filipina, enquanto a proteína Pma1p se encontra no compartimento MCP que parece estar intimamente relacionada com os esfingolípidos, no entanto sem evidência direta de enriquecimento em esfingolípidos à data de realização destas experiências.

Os resultados mostraram que a deleção do gene *IPT1* afeta fortemente a rigidez dos domínios gel, mas não a sua abundância relativa, no entanto não se observou nenhuma alteração significativa nos domínios ricos em ergosterol. Além disso nas células *ipt1*Δ foram observadas alterações claras na distribuição da proteína Pma1p na membrana plasmática, mas o mesmo não se observou para a proteína Can1p. Assim, este trabalho reforça a noção de que os domínios enriquecidos em esfingolípidos são distintos das regiões ricas em ergosterol e estão presentes na membrana plasmática da levedura *S. cerevisiae* e sugere que $M(IP)_2C$ é importante para o empacotamento adequado das cadeias hidrofóbicas dos esfingolípidos presentes nos

domínios gel das células *wt*, que por sua vez é necessário para uma organização adequada do compartimento MCP. A Pma1p é a H^+-ATPase mais abundante encontrada na membrana plasmática fúngica, tendo importantes funções como criar e manter o potencial transmembranar, bem como regular o pH intracelular.

Finalmente, uma vez que a membrana plasmática é um excelente alvo terapêutico para vários compostos antifúngicos, foi explorada uma conexão biofísica entre os domínios enriquecidos em esfingolípidos de diversas estirpes da levedura *S. cerevisiae* e a atividade antifúngica de dois antifúngicos distintos, um pertencente aos azois, Cetoconazol, sendo que deste foram também estudados os seus derivados difenilfosfano e respetivos calcogenoides e outro da família dos polienos, a Nistatina.

A atividade antifúngica dos novos derivados do cetoconazol foi estudada em diferentes estirpes de *S. cerevisiae wt*, *erg6*Δ, *W303* e *AD1-8*, que apresentaram diferentes níveis de resistência comparativamente ao fármaco base, o Cetoconazol. Os novos derivados mostraram ser antifúngicos promissores, especialmente o derivado difenilfosfano e o respetivo óxido, que apresentaram para a generalidade das estirpes estudadas uma atividade antifúngica mais elevada.

Finalmente, resultados interessantes foram também obtidos para a atividade antifúngica da Nistatina e do Cetoconazol, contra diferentes estirpes com deleções em genes codificantes para enzimas envolvidas na via biossintética dos esfingolípidos da levedura às 24 e 48 horas. Enquanto as diferenças encontradas podem ser devido a vários fatores, de forma geral os resultados observados sugerem que a estrutura dos esfingolípidos e os domínios ricos em esfingolípidos, e a sua influência na compartimentação da membrana são aspetos essenciais a ter em atenção, quando o objetivo é compreender e melhorar o nosso conhecimento sobre o modo de ação de antifúngicos e a resistência ao tratamento com esses mesmos fármacos, que tem vindo a aumentar nomeadamente a nível hospitalar.

Palavras-chave: membrana plasmática de fungos, agentes antifúngicos, fluorescência, domínios ricos em esfingolípidos (SLEDs), compartimentos de membrana (MCC e MCP).

List of abbreviations and symbols

Abbreviations

(IP)$_2$C – diinositolphosphorylceramide

ABC – ATP-Binding Cassette

AmB – Amphotericin B

ANEP - aminonaphthylehenylpyridinium

ATP – Adenosine Triphosphate

ATPase – Adenosine Triphosphatase

CTRL – control

DHS – dihydrosphingosine

di-4-ANEPPS – 4-(2-(6-(dibutylamino)-2-naphthalenyl)ethenyl)-1-(3-sulfopropyl)-pyridinium

DM-11 - lysosomotropic aminoester *N*-*N*-dimethylaminoethyl dodecanoate hydrochloride

DmAMP1 – *Dahlia merckii* antimicrobial peptide 1

DMEM – Dulbecco's modified Eagle medium

DMSO – dimethylsulfoxide

DNA - Deoxyribonucleic acid

DPH – 1,6-diphenyl-1,3,5-hexatriene

DPPC - 1,2-dipalmitoyl-*sn*-glycero-3-phosphocholine

EDTA – 2,2',2",2"'-(Ethane-1,2-diyldinitrilo)tetraacetic acid

FCCP – p-trifluoromethoxycarbonylcyanide phenylhydrazone

FGSC – Fungal Genetics Stock Centre

FLIM – Fluorescence Lifetime Imaging Microscopy

FRET – Förster Resonance Energy Transfer

GalCer – galactosylceramide

GFP – green fluorescent protein

GlcCer – glucosylceramide

GM1 – ganglioside GM1

GPI - Glycosylphosphatidylinositol

GUV - giant unilamellar vesicle

HEPES – 4-(2-hydroxyethyl)-1-piperazineethanesulfonic acid

IC – internal conversion

IPC – inositolphosphorylceramide

IRF – instrument response function

ISC – intersystem crossing

Ke – Ketoconazole

LCB – long chain base

LUV - large unilamellar vesicle

M(IP)$_2$C – mannosyldiinositolphosphorylceramide

MCC – membrane compartment containing protein Can1

MCP – membrane compartment containing protein Pma1

MCT – membrane compartment containing the kinase complex TORC2

MCW – membrane compartment containing Wsc1

MIC – minimal inhibitory concentration

MIC$_{50}$ – half maximal inhibitory concentration

MIPC – mannosylinositolphosphorylceramide

MLVs – multilamellar vesicles

MMV – Vogel's Minimal Medium

mRNA – messenger RNA

Na$_2$ATP – Adenosine 5'-triphosphate disodium salt

Na$_2$EDTA – Disodium ethylenediaminetetraacetate

Na$_2$HPO$_4$ - disodium hydrogenphosphate

NaCl - sodium chloride

NaH$_2$PO$_4$ - sodium dihydrogenphosphate

Nys – Nystatin

ODDC – octenidine dihydrochloride

PBS – Phosphate Buffered Saline

PC – Phosphatidylcholine

PE – Phosphatidylethanolamine

PhyCer – Phytoceramide

PM – plasma membrane

PMSF – phenylmethylsulfonyl fluoride

POPC – 1-palmitoyl-2-oleoyl-*sn*-glycero-3-phosphocholine

RFP – red fluorescent protein

ROI – region of interest

S.D. – Standard Deviation

SC – Synthetic Complete Medium

SDS-PAGE – Sodium Dodecyl Sulfate Polyacrylamide Gel Electrophoresis

SeM – Supplemented Vogel's Medium

SL(s) – sphingolipid(s)

SLEDs – SL-enriched domains

SM – sphingomyelin

SPT – serine palmitoyltransferase

STS – Staurosporine

SUV - small unilamellar vesicle

TCSPC – Time-Correlated Single Photon Counting

T_m – main-phase transition temperature

***t*-PnA** – *trans*-parinaric acid

wt – wild-type

YPD – Yeast Extract – Peptone – Dextrose Medium

Symbols

ε - molar absorption coefficient

φ – rotation correlation time

⟨r⟩ – steady-state fluorescence anisotropy

⟨τ⟩ – intensity-weighted mean fluorescence lifetime

τ_{av} – amplitude-weighted mean fluorescence lifetime

I_{VH} – perpendicular component of fluorescence intensity

I_{VV} – parallel component of fluorescence intensity

k_{nr} **-** rate constant for non-radiative processes

lag – latency phase

l_d – liquid disordered

l_o – liquid ordered

log – exponential phase

r_∞ – limiting anisotropy

r_0 – fluorescence anisotropy in the absence of rotation

R^2 – squared linear correlation coefficient

rpm – rotation per minute

S_0 – fundamental electronic state

S_1 – lowest excited state energy level

s_o – solid ordered

t – time, s

α_i – normalized pre-exponential factor or amplitude

α_{long} – normalized amplitude of long component lifetime

τ_i – lifetime of decay component *i*

τ_{long} – long component lifetime

Contents

List of figures

List of tables

CHAPTER I - INTRODUCTION

1.1. Fungal organisms and fungal infections

Fungi are a unique group of organisms, different from all others in their behaviour and cellular organization. Fungi also have an enormous range of activities – as pathogens of crop plants or humans, as decomposer organisms, as experimental "model organisms" for investigating genetics and cell biology, and as producers of many important metabolites. The uniqueness of fungi is reflected in the fact that they have the status of a kingdom, equivalent to the plant and animal kingdoms (Deacon 2005).

The model organisms used in this Ph.D. research work were *Saccharomyces cerevisiae* (*S. cerevisiae*) and *Neurospora crassa* (*N. crassa*) wild-type (*wt*) and mutant strains. The importance of including *N. crassa* in the project, goes beyond extended the study from yeast to filamentous fungi. In fact, ergosterol levels are very low during conidial stage in *N. crassa*, therefore allowing to attribute the presence of ordered domains unequivocally to sphingolipids (SLs), as will become evident along this work.

N. crassa, a haploid ascomycete, has been extensively used as a biological model for multicellular eukaryotes, namely in the study of developmental processes, apoptosis (Fernandes et al. 2013), aging (Case et al. 2014), and in the molecular basis of the circadian rhythm observed in asexual spore formation, also known as conidiation (Nakashima and Onai 1996). *Neurospora* colonies are very perceptible due to the orange carotenoid neurosporaxanthin which accumulates in conidia and vegetative mycelia (Zalokar 1955). The biosynthesis of neurosporaxanthin in vegetative mycelia is induced by light, which serves as an environmental activator allowing *Neurospora* to adjust the circadian clock and anticipate possible changes occurring in the environmental surroundings (Luque et al. 2012).

N. crassa have also been used in studies of resistance to antifungal drugs (Castro et al. 2010, Fernandes et al. 2011), and others where we hypothesize that plasma membrane reorganization in the presence of an antifungal drug may have an important role (Bolard 1986, W.K.Ng and M.Wasan 2003, Maschmeyer et al. 2007, Francois et al. 2009, Chakrabarti 2011).

Detailed information concerning the plasma membrane (PM) organization during the germination and redifferentiation process as a *Neurospora* cell progresses from dormant conidia to a vegetative mycelium will be addressed in more detail in Chapter IV. Different reports present large variations in either the total lipid content per dry weight or in the content of major lipid classes, namely a reduction in the amount of triacylglycerols, and a net increase of membrane phospholipids found in conidia and mycelia. Also, small variations in

phospholipid subclasses and/or unsaturation have been reported (Bianchi and Turian 1967, Schmit and Brody 1976, Beck and Greenawalt 1977).

S. cerevisiae, a unicellular fungus, also from the Ascomycota division, is one of the most widely studied eukaryotes, which has a plasma membrane (PM) with high levels of ergosterol (van Meer et al. 2008). Yeast has several industrial applications, ranging from bakeries and breweries to the production of bioethanol. For example, Takagi *et al.* (Takagi et al. 2015) isolated the yeast mutant that overproduces isoamyl alcohol and its acetate, which gives sake its characteristic flavour (Takagi 2019). The budding yeast *S. cerevisiae* is possibly the eukaryotic organism most extensively used in fundamental research. A substantial part of our knowledge about cellular metabolism, cell cycle regulation, deoxyribonucleic acid (DNA) recombination, replication and repair, cell death, protein folding and biogenesis of organelles has been obtained in experimental work with this fungus (Khurana and Lindquist 2010).

The genome of the yeast *S. cerevisiae* has been completely sequenced through a worldwide collaboration. The sequence of 12,068 kilobases defines 5885 potential protein-coding genes, approximately 140 genes specifying ribosomal RNA, 40 genes for small nuclear RNA molecules, and 275 transfer RNA genes (Goffeau et al. 1996). In sharp contrast, *N. crassa* contains about 10,000 protein-coding genes, approximately twice as many genes as the yeasts and only slightly fewer than the invertebrate animals (Braun 2004).

Currently, there are a growing number of fungi causing diseases worldwide. These infections can be grouped into four types, which are superficial mycosis, cutaneous mycosis, subcutaneous mycosis and systemic mycosis (Chinnappan et al. 2020). Therefore, antifungal drug resistance is a major society concern, since the mortality rate associated with resistant fungal infections, especially infections caused by *Aspergillus spp.*, where the mortality rate crosses 50 %, has increased dramatically, particularly in hospital environment and in patients with decreased immunological response, HIV and cancer patients receiving immunosuppressive chemotherapy (Maschmeyer et al. 2007, Regional Committee for the Western 2019). Candidemia is the fourth leading cause of blood-stream infections in hospitals by antibiotic-resistant organisms and carries 35-55 % mortality (Wisplinghoff et al. 2004). Fungal infections also occur in plants, food stocks and cattle with negative consequences for health and economy.

1.2. Fungal plasma membrane

SLs comprise one of the major group of lipids in the PM of eukaryotes and their spatial arrangement in the PM is essential for several cellular vital functions, such as growth, survival, differentiation, cell senescence, inflammation, and immune and stress responses (Dickson and Lester 2002, Dickson 2008, Breslow and Weissman 2010, Singh and Del Poeta 2016, Hannun and Obeid 2018). SLs present large structural diversity, and any alterations of SL composition can potentially exert a strong impact on several biophysical properties of membranes such as fluidity, hydration, passive permeability, lateral diffusion of components, membrane curvature and thickness (Breslow and Weissman 2010, Del Poeta et al. 2014, Goñi et al. 2014, Carreira et al. 2015). These effects are considered an integral part of the mechanisms by which SLs fulfil their different biological functions. SLs play an important role in the lateral segregation of membrane components and in the formation of membrane ordered domains, contributing to both the stability and dynamics of membrane compartmentalization (Schuberth and Wedlich-Söldner 2015, Gournas et al. 2018, Marques et al. 2018).

SL-enriched domains (SLEDs) have been most comprehensively studied in the unicellular fungus *S. cerevisiae* (Figure 1A), a well-known model organism, the genome (Botstein and Fink 2011, Ralser et al. 2012, Dujon 2015) and lipidome of which have been thoroughly analysed (Gaspar et al. 2007, Ejsing et al. 2009, Klose et al. 2012) and used to study diverse PM features (Folmer et al. 2008, Guan et al. 2009, Aresta-Branco et al. 2011, Malinsky and Opekarova 2016, Marques et al. 2018). Conversely, the multicellular filamentous fungus *N. crassa* remains comparatively understudied (Figure 1B), even though its genome and genomic analysis have been reported (Galagan 2003, Mannhaupt et al. 2003, Borkovich et al. 2004). Together, these fungal species afforded important insights into the biophysical properties of biological membranes *in vivo*, especially those involving the SLEDs, as will be detailed. Due to their different degree of complexity and distinct lipidomes, *S. cerevisiae* and *N. crassa* provide complementary information on SLEDs. Of note, there is evidence for the presence of SLEDs in *Cryptococcus neoformans (Singh et al. 2012)*.

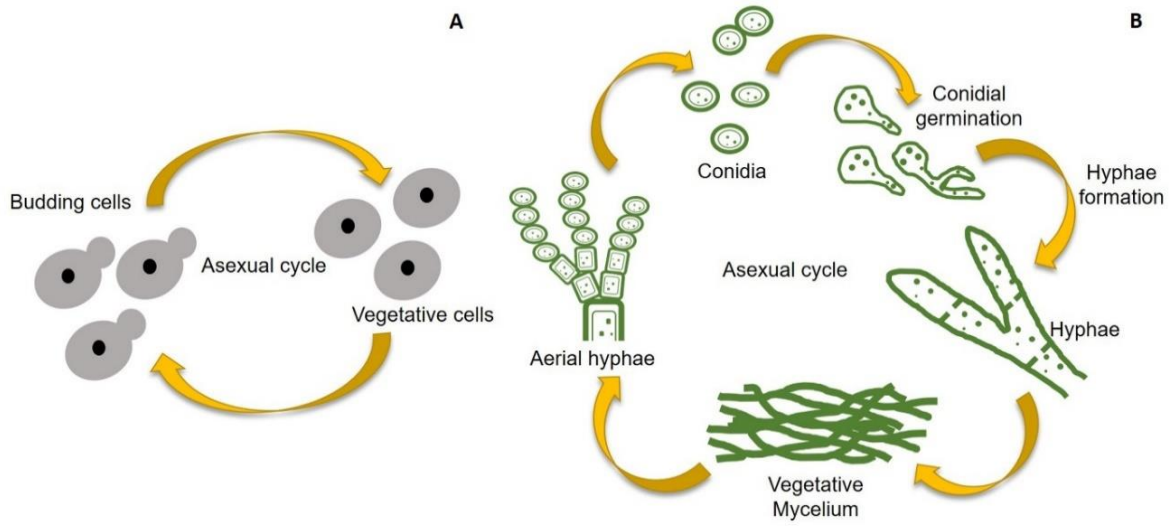

Figure 1 - Asexual cycle and morphological comparison between S. cerevisiae and N. crassa. A) S. cerevisiae and B) N. crassa. Further details on the life cycle of these organisms can be found, for example, in (Davis 2000, Carlile et al. 2001).

Restricting to the asexual reproduction cycle, *N. crassa* presents conidial germination during which the biophysical properties of the PM can be studied in conidial suspensions with approaches similar to those used for *S. cerevisiae* cells in suspension (Sousa et al. 2021). Additionally, in the conidial stage, the latency (*lag*) growth stage of *N. crassa*, is characterized by very low sterol levels, including ergosterol, the major sterol in *N. crassa* mycelium and in the PM of *S. cerevisiae* (Bianchi and Turian 1967, Zinser et al. 1993, Heese-Peck et al. 2002, Guan et al. 2009). While *S. cerevisiae* contains only inositolphosphorylceramide-based complex SLs, *N. crassa* contains also hexosylceramides (cerebrosides) (Lester et al. 1974, Costantino et al. 2011), which are also found in pathogenic fungi, such as *C. neoformans* (Singh et al. 2012, Munshi et al. 2018) and *Candida albicans* (Del Poeta et al. 2014, Singh and Del Poeta 2016), and in higher eukaryotes (Breslow and Weissman 2010, Marques et al. 2018).

Thus, we will focus our attention on highly ordered PM domains specifically found in fungi, which are rich in SLs but ergosterol-depleted. After summarising the current view of fungal PM organization, the main features that distinguish SLEDs from typical lipid rafts as well as the method that allows detecting SL-enriched gel domains in fungi will be presented. Furthermore, we will discuss the major biophysical properties of SLEDs in fungi, illustrating with key examples their relationship with the lipid composition of the PM and their possible interplay with other membrane domains/ compartments, biological functions, and potential impact on the activity of antifungal agents.

1.2.1. The fungal plasma membrane is highly compartmentalized

SLEDs coexist with a large variety of membrane compartments in the PM of fungi. In this section, we will briefly describe those compartments for which more evidence indicates that they are functionally related with SLs. Membrane compartments in the PM of fungi differ markedly from the mammalian lipid rafts since they are larger, more temporally stable microdomains with a better-defined localization, and therefore, they can be observed by conventional optical microscopy (Malinsky et al. 2013, Athanasopoulos et al. 2019, Bento-Oliveira et al. 2020). Of these distinct membrane compartments, the two major ones are the membrane compartment containing Pma1p (MCP), and the one containing Can1p (MCC) (Figure 2). Pma1p is the PM H^+-ATPase, the protein responsible for the creation and maintenance of fungal PM transmembrane potential and for regulating pH and intracellular ion concentration, with homologues found in all fungi (Kane 2016). While in *S. cerevisiae* Pma1p can constitute up to 50 % of the total protein in the PM, in *N. crassa* it comprises roughly 5 to 10 % (Fajardo-Somera et al. 2013). MCP is a large and very stable membrane compartment. Under a confocal microscope, it has a network appearance, however, super-resolution microscopy revealed that this network is not continuous, but rather made of isolated foci (Malinsky and Opekarova 2016, Gournas et al. 2018).

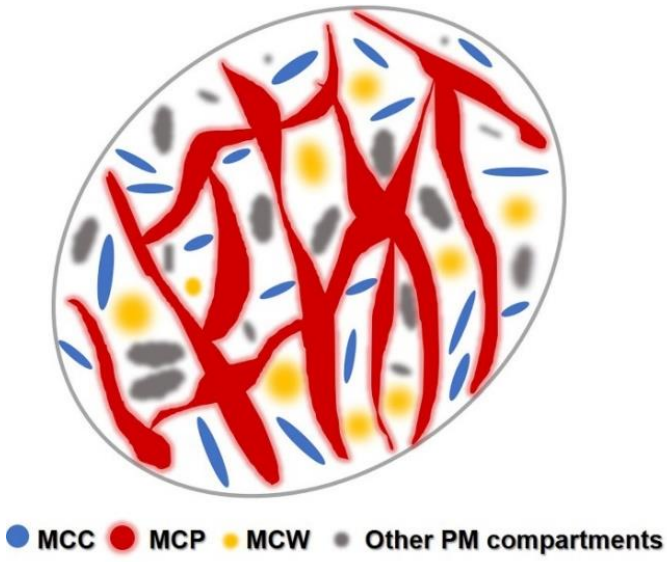

Figure 2 – The fungal PM is highly compartmentalized. Pictorial representation of the top view of an area of the fungal PM. See text and references therein for further information on the different membrane compartments.

The MCC is associated with furrow-like invaginations, which are maintained by a large cytosolic protein complex, the eisosome (Walther et al. 2006, Stradalova et al. 2009, Zahumensky and Malinsky 2019). It has been suggested that the MCC/eisosome is ergosterol-enriched (Grossmann et al. 2007). Distinct ergosterol-dependent nutrient transporters, such as Can1p (an arginine permease), Fur4p (an uracil permease) and Tat2p (high-affinity tryptophan permease) are found in this compartment and its integrity is compromised in mutants with deletions in some steps of the ergosterol biosynthesis (Spira et al. 2012, Zahumensky and Malinsky 2019). The nutrient uptake by MCC/eisosome H^+-symporters is dependent on the transmembrane potential created and sustained by the MCP protein Pma1p (Athanasopoulos et al. 2019).

The membrane compartment containing Wsc1 (MCW) in the PM of fungi is a domain associated with the maintenance of cell wall integrity (Figure 2). In addition to Wsc1, a cell wall mechanosensor, MCW contains four other known sensors involved in cell wall stress response and remodelling. Complex SLs, in particular mannosylinositolphosphorylceramide (MIPC), play a role in the maintenance of cell wall integrity. SL biosynthetic mutants exhibiting cell wall defects display more severe phenotypes when ergosterol synthesis is decreased or impaired and an hyperactivation of the cell wall integrity pathway (Tanaka and Tani 2018). There are several other membrane compartments in the fungal PM, for example, the one containing the kinase complex TORC2 (target of rapamycin complex 2) (MCT), a protein involved in the regulation of SL biosynthesis through mechanisms that also involve the MCC, amongst other important functions related to PM homeostasis (Busto et al. 2018, Athanasopoulos et al. 2019, Zahumensky and Malinsky 2019).

The development that took place over the last 2 decades regarding the study and characterization of the fungal PM, especially of the budding yeast, have enabled to build a more complete picture of its patchwork organization (Grossmann et al. 2007, Stradalova et al. 2009, Malinsky et al. 2013, Athanasopoulos et al. 2019, Zahumensky and Malinsky 2019). How its multiple membrane compartments interplay with each other and their functional dynamics are, however, far from fully unravelled. Still, the first steps for the understanding of the mechanisms behind the formation and stabilization of these compartments, and the relevance of lipid-lipid and lipid-protein interactions, are now taking place (Grossmann et al. 2007, Aresta-Branco et al. 2011, Spira et al. 2012, Vecer et al. 2014, Schuberth and Wedlich-Söldner 2015, Malinsky and Opekarova 2016, Busto et al. 2018, Gournas et al. 2018, Athanasopoulos et al. 2019, Zahumensky and Malinsky 2019, Bento-Oliveira et al. 2020, Khmelinskaia et al. 2020, van 't Klooster et al. 2020, van 't Klooster et al. 2020). Indeed, they are thought to be intimately

related with lipid lateral organization, and certainly a deeper knowledge of SLEDs will be crucial to clarify the mutual roles of lipids and proteins in PM compartmentalization.

1.2.2. Complex sphingolipids and membrane sterols

Lipid domains are currently acknowledged as essential in many cellular processes, but their study in eukaryotic living cells still raises many challenges (Sezgin et al. 2017). The presence of proteins which are also major components of biological membranes and can change the membrane lateral organization renders difficult to assert that the lipid-lipid interactions are indeed responsible for a given type of heterogeneity. Moreover, membrane dynamics and composition fluctuations must also be considered. The large diversity of lipids adds further complexity, and theoretically, there can be an almost equally large variety of different lipid domains, forming an almost continuum of biophysical properties, instead of abrupt changes that would be more easily detected. In this respect, studying lipid domains in yeast cells can be highly advantageous, as will become evident below. The biophysical properties of lipid domains are strongly dependent on the structure of the lipids that comprise them. In the case of SLEDs, it is thus crucial to know the structure of, at least, the main complex SLs. The structural differences between fungal and mammalian SLs may, in addition, help to understand the origin of the SLEDs specific of fungi.

In mammals, complex SLs are grouped in two types, sphingomyelins (SMs) and glycosphingolipids. There is a huge variety of sugar chain structures forming the headgroups of glycosphingolipids. In addition, the structural diversity of complex SLs is further augmented by structural variations in the fatty acyl chain and long chain (or sphingoid) base (LCB) in the ceramide backbone (Tani 2016, Carreira et al. 2019).

Fungi, especially the budding yeast *S. cerevisiae*, present a simpler sphingolipidome than mammalian cells, and a noticeably reduced number of genes involved in lipid metabolism (Ejsing et al. 2009, Dujon 2015, Singh and Del Poeta 2016). Inositolphosphorylceramides are an important group of complex SLs in fungi, which are absent in mammals. In *S. cerevisiae* and *N. crassa*, it is possible to find inositolphosphorylceramide (IPC), mannosylinositolphosphorylceramide (MIPC) and mannosyldiinositolphosphorylceramide ($M(IP)_2C$) (Figure 3), which differ not only in the size of their polar headgroup but also in the global net charge, which is -1 in IPC and MIPC, and -2 in $M(IP)_2C$ (Figure 3).

Diinositolphosphorylceramide ($(IP)_2C$) has also been found in *N. crassa* (Lester et al. 1974, Hanson and Brody 1979, Hanson and Lester 1980, Singh and Del Poeta 2016). The most common acyl chains in the inositol-based SLs of *N. crassa* are usually 2-OH-24:0 (shown in Figure 3) followed by 2-OH-22:0, which are shorter than the most abundant one in *S. cerevisiae wt* cells (2-OH-26:0) (Lester et al. 1974). The most abundant LCB in fungi is phytosphingosine, while in mammals is sphingosine. However, it is possible to find dihydrosphingosine, in both mammals and yeast (Dickson 2008, Sarmento et al. 2020). In yeast, phytosphingosine is 18 or 20 carbon long (Lester and Dickson 2001), though C18 phytosphingosine is more abundant (Dickson 2008). Although the most common acyl chain is 2-OH-26:0 (represented in Figure 3), species with lower or higher degree of hydroxylation are also present (Dickson and Lester 2002).

In *N.* crassa the glucosylceramide (GlcCer) backbone is usually composed by a 18 carbon length LCB, methylated at position C-9 and diunsaturated at positions C-4 and C-8, acylated with a 16 or 18 carbon chain fatty acid hydroxylated at C-2, the latter represented in Figure 3 (Lester et al. 1974, Huber et al. 2019). *N. crassa* GlcCer is very similar to the one found in *C. neoformans* (Singh et al. 2012), whereas in mammals the acyl chain length can vary from C14 to C26 and hydroxylation can also be present at position C-2, though at lower levels than those found in fungi (Hama 2010). In addition to the saturated acyl chain species, it is common to find a *trans* unsaturation at position C-3 of the acyl chain in *N. crassa* GlcCer (*E*-Δ(3)) which in some *wt* strains is in fact the major GlcCer acyl chain (Ferket et al. 2003, Huber et al. 2019).

A more complex glycosphingolipid (Neurosporaside, Figure 3) with four sugar residues forming a chain of 3 β-galactopyranoside residues and a glucopyranoside α-linked to the other galactopyranoside (Costantino et al. 2011) was also found in *N. crassa* (Lester et al. 1974, Costantino et al. 2011).

SLs and sterols (Figure 3) are major components of the PM in eukaryotic cells and their metabolism and distribution are inter-regulated (Guan et al. 2009, Tanaka and Tani 2018). Ergosterol is the main sterol found in the fungal PM, whereas it is cholesterol in the mammalian PM. The structural differences include one additional double bond in the B ring and in the aliphatic side chain of ergosterol as well as an additional methyl group in its side chain, as can be seen in Figure 3.

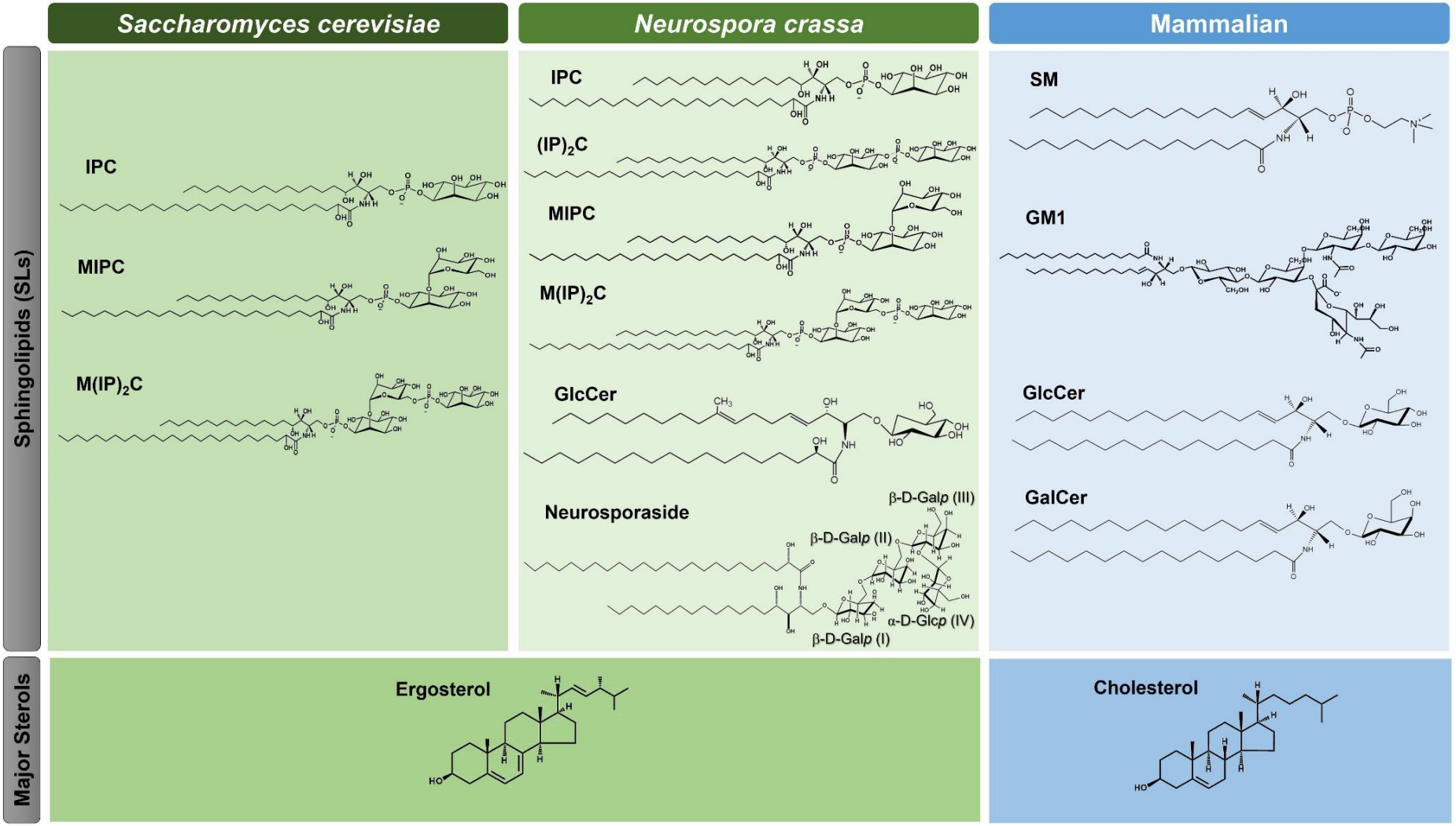

Figure 3 - Structures of main complex SLs and sterols found in the PM of fungi and mammals. Left: budding yeast S. cerevisiae; middle: filamentous fungus N. crassa; right: examples of different complex SLs found in mammalian cells PM. IPC – inositolphosphorylceramide; MIPC – mannosylinositolphosphorylceramide; $M(IP)_2C$ – mannosyldiinositolphosphorylceramide; $(IP)_2C$ – diinositolphosphorylceramide; GlcCer – glucosylceramide; GM1 – ganglioside GM1; SM – sphingomyelin and GalCer – galactosylceramide. See text for details.

1.3. Biophysical characterization of sphingolipid-enriched domains

1.3.1. Distinguishing between gel and liquid ordered phases

Lipids in lipid bilayers exist in different phases, called lamellar phases, and the most relevant are the liquid disordered (l_d), the gel or solid ordered and the liquid ordered (l_o) phases (Figure 4). In the l_o phase, the lipids have their chains in extended conformations and are tightly packed, but not as much as in the gel phase, diffusing laterally in the plane of the membrane slightly more slowly than in the l_d phase (Elson et al. 2010, de Almeida and Joly 2014). The lipid rafts, characterized by the tight packing of SLs and sterols are thought to be in a state resembling the l_o phase, coexisting with the surrounding disordered lipids (l_d phase) (Stradalova et al. 2009, Elson et al. 2010, de Almeida and Joly 2014, Sezgin et al. 2017). Membrane microdomains based on this type of liquid-liquid immiscibility have also been observed by fluorescence microscopy in yeast vacuoles (Rayermann et al. 2017). Ordered domains are frequently enriched in lipids with long and saturated hydrocarbon chains, while lipids with unsaturated chains tend to concentrate preferentially in more fluid domains. In fact, an l_o phase can be formed not only by a combination of many SLs with sterols, but also through the combination of certain glycerophospholipids, namely saturated and mono-unsaturated phosphatidylcholines, and sterols, as observed in artificial lipid mixtures (Marsh 2010). In the l_o phase, the extended chain conformation depends on the interactions between the phospholipid acyl chains with the sterol hydrophobic ring system and aliphatic chain (Meyer et al. 2014). Thus, it is not surprising that sterols differ on their ability to induce an l_o phase in the presence of different lipids (Khmelinskaia et al. 2020).

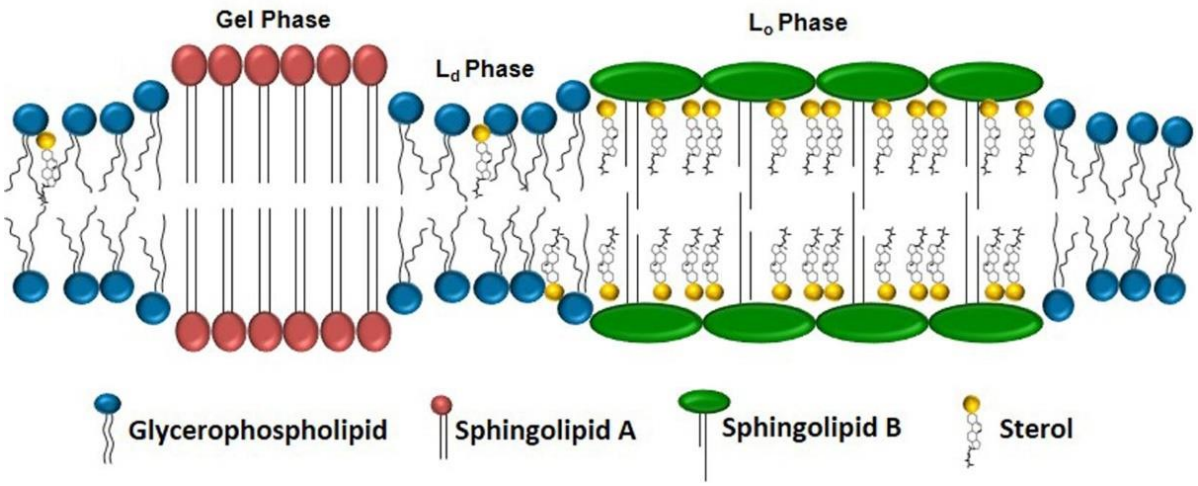

Figure 4 – Different lipid lamellar phases. Schematic representation of liquid disordered (l_d) phase, liquid ordered (l_o) phase and gel or solid ordered (s_o) phase (Marquês et al. 2015).

Due to their typically high main-phase transition temperature (T_m), isolated SLs will likely be in a highly ordered and rigid phase, such as the gel phase, rather than a fluid phase often attributed to biomembranes, whether at room temperature, at human body temperature or at the optimal growth temperature of several microorganisms (Marquês et al. 2015). The water content of the gel phase is usually low, depending, nonetheless, on the lipid headgroup size, polarity, and charge (Elson et al. 2010, Hartkamp et al. 2016). A slow rotation along the molecule long-axis occurs due to the organization of most of the hydrocarbon chains in an all-*trans* conformation (Elson et al. 2010, Goñi et al. 2014). In this phase, the average lipid cross-sectional area is minimal and the bilayer thickness is maximal, which results in closely packed lipids with strong van der Waals interactions between the hydrocarbon chains and H-bonds established by hydroxyl and/or amide groups of the SL between each other and the ester carbonyl group of glycerophospholipids for which they may compete with sterols OH-group (Meyer et al. 2014, Marques et al. 2018). This strong H-bonding network is responsible for further increasing the T_m of the SLEDs (Hartkamp et al. 2016, Marques et al. 2018) and is considered of importance for the lateral segregation of SLs and formation of ordered domains in fungi (Del Poeta et al. 2014). Moreover, the solubility of l_o-forming sterols is usually low both in the l_d and gel phases (Marsh 2010), although a gel phase stabilized by direct cholesterol-palmitoylceramide interactions in ternary lipid mixtures has been reported (Marsh 2010, Busto et al. 2014). The lateral diffusion in the gel phase is several orders of magnitude slower than in any of the fluid l_d or l_o phases (Elson et al. 2010).

1.3.2. Membrane model systems

The properties of membranes arise from the collective effects of a large number of weak non-covalent interactions which are challenging to study in chemically complex systems such as the biological membranes. Simpler systems are thus sometimes required. Membrane model systems are extensively used both in biophysical and biochemical studies. The chemically defined composition of these model systems makes them suitable to study specific interactions between different lipids. Although model systems do not exhibit all the complexity of a biological membrane, they effectively can mimic some of the relevant properties of those membranes. Membrane model systems may consist of pure lipids, lipid mixtures or lipid-protein mixtures. Different type of model systems can be used, lipid monolayers, black lipid membranes, liposomes (multilamellar vesicles (MLVs), unilamellar vesicles (large unilamellar vesicles (LUVs), small unilamellar vesicles (SUVs) and giant unilamellar vesicles (GUVs)), Figure 5) (Stillwell 2016).

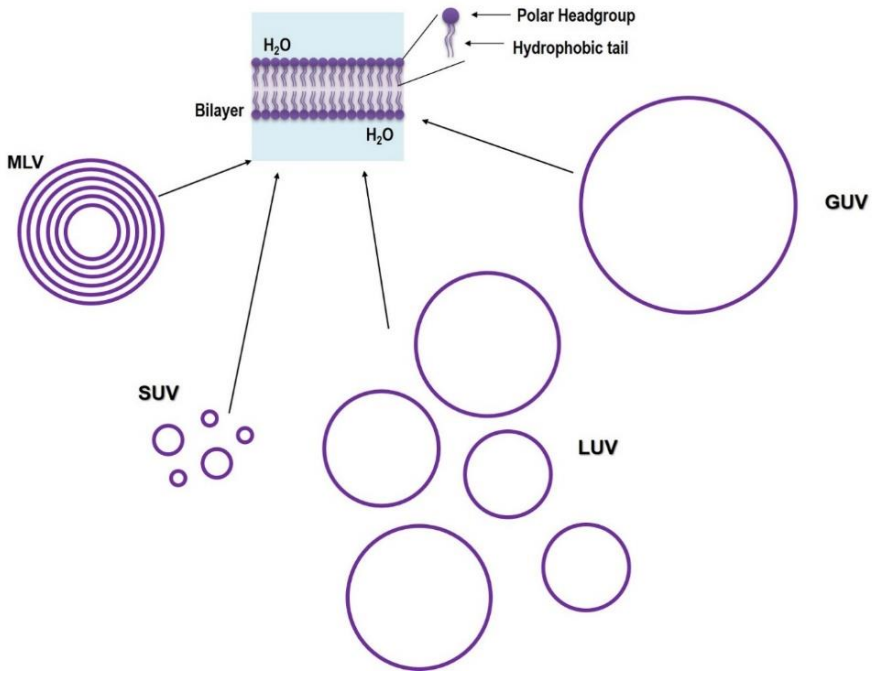

Figure 5 – Schematic representation of the structure of different type of vesicles based on (Loura and de Almeida 2004).

1.3.2.1. Liposomes

The term liposome can be defined as any lipid bilayer structure that encloses an aqueous volume. Liposomes are characterized by their lipid composition, average diameter and the extent of size heterogeneity (Szoka and Papahadjopoulos 1980). This type of model membranes is suitable for studies with incorporated proteins, and to encapsulate solutes to act as drug delivery systems.

1.3.2.1.1. Multilamellar vesicles

These vesicular structures, are spontaneously formed when phospholipids are dispersed in water (Mayer et al. 1986). MLVs consist of concentric bilayers of phospholipids with variable diameter (Figure 5). Since these model membranes are easy to prepare, giving reproducible properties, and can be prepared in large quantities and high concentrations, they are widely used in several biophysical studies. However, they also present disadvantages including the small aqueous space, which limit the use of these vesicles in studies involving trapping materials. The heterogeneity in size and number of layers might also be a disadvantage in photophysical studies, due to the associated increase in light scattering, especially for wavelength in the ultraviolet region (Castanho et al. 1997), being necessary to control the scattering in these samples. Furthermore, due to the concentric organization of the bilayers, only a small fraction of the lipids is available at the outer liposome surface, hindering or slowing the access of solutes and probes to the inner shells, which can be circumvented by the addition of the probes to the lipids before vesicle preparation. Despite some disadvantages, MLVs are, however, the model system of election for thermotropic studies of lipid mixtures due to the high reproducibility, easy preparation and high cooperativity in the phase transition (Marsh et al. 1977).

1.3.2.1.2. Unilamellar vesicles

The major advantage of this type of vesicles is the homogeneity in size and number of layers (forming a bilayer). These vesicles are classified according to their size, as briefly described below.

SUVs (Figure 5) are spherical vesicles that range in size from ~25 to ~50 nm diameter and are obtained by power sonication of MLVs (Huang 1969). Higher homogeneity in size can

be obtained by gel chromatography or centrifugation (Goormaghtigh et al. 1987). The small size of these vesicles leads, however, to a smaller radius of curvature compared to the one observed in biological membranes. In SUVs about ~60 to ~75% of the lipids are on the outside surface and this, in turn, introduces packing constraint in the lipid bilayer. Furthermore, the vesicles are not very stable and fusion to larger structures is a major problem. Other disadvantages are the small internal aqueous space, which makes these vesicles unsuitable for trapping solutes, and low cooperativity in the gel-fluid transition (Yeagle 2016).

LUVs (Figure 5) are also spherical vesicles, but with a diameter larger than ~50 nm and usually smaller than ~500 nm. There are several methods to prepare LUVs, but the most widely used is the extrusion of MLVs through polycarbonate filters with variable pore size (Mayer et al. 1986). The possibility to prepare vesicles of several lipids and lipid mixtures, with a wide range of concentrations and the absence of residual organic solvents or detergents constitute some of the major advantages of this method, however there are some disadvantages, since very high concentrations of lipid may clog the filter. LUVs are suitable for many studies, including trapping of solutes, transport studies and have great potential for the use as drug delivery systems, thus making them the model membranes of election.

GUVs (Figure 5) are simple model membrane systems of cell-size, reaching as high as 300 μm of diameter, which are instrumental to study the function of more complex biological membranes involving heterogeneities in lipid composition, shape, mechanical properties, and chemical properties (Bhatia et al. 2015). The size of GUVs and their curvature enable us to visualize these individually, using an optical microscope, and GUVs have found application in numerous biophysical contexts in which membrane composition, tension, and geometry is controlled and manipulated using microscopy techniques such as, membrane flickering analysis (Faucon et al. 1989, Méléard et al. 2011), micropipette aspiration (Kwok and Evans 1981, Henriksen and Ipsen 2004), or fluorescence imaging of lateral membrane organization (Dietrich et al. 2001). GUVs can be obtained either simply by hydration followed by deposition (Bhatia et al. 2015), or through electroformation in Platinum or Titanium GUV formation chamber (Ventura et al. 2021).

1.3.3. Lipid phase diagrams

When studying the lipid-lipid interactions, the phase transitions can be schematically represented by phase diagrams (Figure 6) (Heberle and Feigenson 2011). The higher the number of lipids included in the mixture, the more complex is the phase behaviour and usually there is a broad range of temperatures where two or more phases can coexist. To define the boundaries of a phase diagram, different techniques can be used in order to detect the lipid phase changes. These include differential scanning calorimetry, fluorescence spectroscopy and nuclear magnetic resonance (de Almeida et al. 2003, Goni et al. 2008, Engberg et al. 2016).

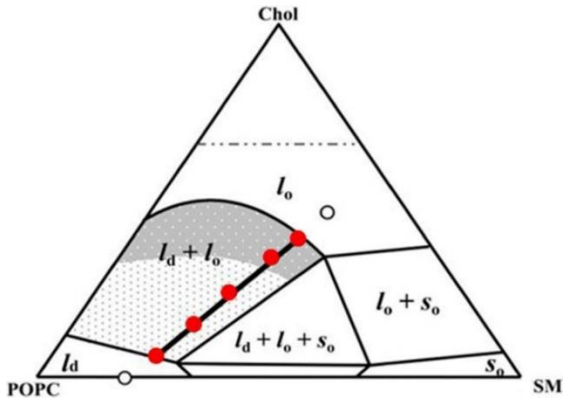

Figure 6 – Ternary phase diagram for the 1-palmitoyl-2-oleoyl-sn-glycero-3-phosphocholine (POPC)-SM-Cholesterol system at 23 °C. The thick black line represents the tie-line that includes the 1:1:1 POPC-SM-Cholesterol mixture (mol: mol: mol) which lays in the l_d/l_o phase coexistence region and has been considered a canonical mixture to study lipid rafts in mammalian PM models. The other lines represent phase coexistence boundaries. Note the tie-triangle where three-phases coexist. The grey shades correspond to regions of differently sized raft domains. l_d, liquid disordered; l_o, liquid ordered; s_o, solid ordered, the red points are examples of mixtures along the mentioned tie-line. The horizontal dot-dashed line represents the cholesterol solubility limit in phosphatidylcholine or SM membranes. Adapted from de Almeida et al 2005 (Sousa et al. 2021).

1.3.4. Liposomes as drug delivery systems

Drug delivery systems demonstrate how the pharmaceutical product is administered to the target site to provide therapeutic action.

Researchers believe that solely dependent on presently available antifungal compounds would not be sufficient to treat these fungal infections. The introduction of a whole new antifungal drug acting to the target sites must undergo a long process of discovery, various clinical testing and trials on animals and human, development and regulatory approval then

finally brought to the market. Hence, modifications of the existing drug delivery system have never left out and are being pursued innovatively. Applying the knowledge in pharmacodynamics and pharmacokinetic principles, novel advances in antifungal drug delivery systems have been produced and managed to conquer the issues of solubility, stability, bioavailability, safety and effectiveness present in conventional formulations and methods of administration. Vesicular system, nano-particulate based system, colloidal carriers and the miscellaneous drug delivery system are the four major groups of advances in delivering antifungal drugs (Chinnappan et al. 2020). The established therapeutic agents for antifungal therapy such as Amphotericin B (AmB), Nystatin (Nys) and azole drugs can be formulated into different carriers and delivery systems that specifically target the infected area and the illness level of the patient. Novel antifungal drug delivery systems have opened a new dimension in minimising the adverse effects of drugs.

Because liposomes have both lipophilic and hydrophilic characters, they increase the solubility of lipophilic drugs in aqueous body fluids and the hydrophilic drug penetration through phospholipid membranes, providing liposomes multi-functionality (Figure 7). Liposomes are biodegradable, biocompatible and have a higher protection against enzymes compared with other lipid formulations (Madni et al. 2014).

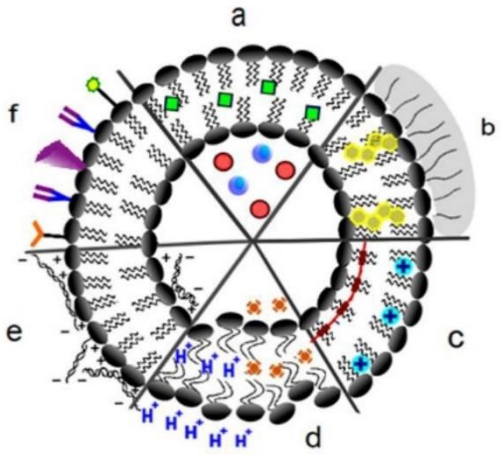

Figure 7 - Multi-functionality of liposomes as drug delivery systems: (a) Encapsulation of hydrophilic drug (red) and gas bubbles (blue) into an aqueous core and entrapment of lipophilic drug (green) inside the bilayer, (b) Stabilization of lipid bilayer with cholesterol (yellow) and attachment of hydrophilic polymer layer on the bilayer surface, (c) Liposome lipid bilayer is strengthened and stabilized by polymerization (red) or by incorporation of multivalent cations (blue), (d) bio-responsive destabilization of lipid bilayer in acidic pH (blue) or increased temperature achieved by magnetic agents (Blue), (e) negatively charged DNA molecules are attached to positively charged lipid molecules, (f) attachment of immunogenic or targeting ligands on the liposome surface (Madni et al. 2014).

1.4. Antifungal agents

1.4.1. Staurosporine

The emerging role of apoptosis as key regulator of fungal development suggests that it might be possible to develop new means of controlling fungal infections through the manipulation of some key components involved in the apoptotic cascade. In fungi, apoptotic-like cell death occurs naturally during the developmental process and reproduction and can be induced by environmental factors and exposure to toxic metabolites or abiotic factors. The core apoptotic process in fungi is similar to those in mammals, however, the apoptotic network is less complex (Sharon et al. 2009).

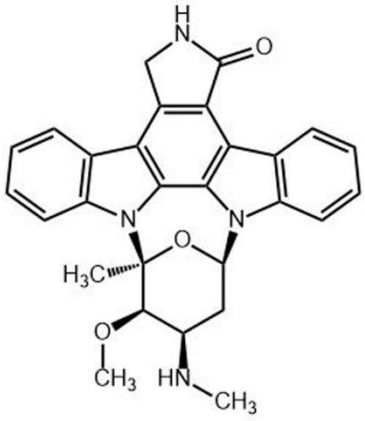

Figure 8 – Chemical structure of staurosporine.

The alkaloid staurosporine (STS, Figure 8) is well-known for its antifungal (Omura 1977, Park et al. 2006) and antitumoral characteristics (Correa et al. 2011), but also for being the most potent protein kinase inhibitor, with a half maximal inhibitory concentration (IC_{50}) *in vitro* in the nanomolar range (Tamaoki et al. 1986), and an inducer of programmed cell death in neuronal cells (*e.g.*, (Wiesner and Dawson 1996)), protozoans (*e.g.*, (Yin et al. 2010)) human macrophages (*e.g.*, (Dunai et al. 2012)) and in the filamentous fungus *Neurospora crassa* (Gescher 2000, Castro et al. 2010, Fernandes et al. 2011, Fernandes et al. 2013). STS-induced programmed cell death in filamentous fungus (Fernandes et al. 2011) is thus one of the many examples of important fungal physiological activities, such as cell proliferation or differentiation, sensing and signalling, that are usually found to be closely related to membrane composition and biophysical features, through their involvement with membrane microdomain

organization and lipid homeostasis (Malinsky and Opekarova 2016). Indeed, a gene expression (microarray) study for an STS challenge versus control (Fernandes et al. 2011) shows that there are important changes in the levels of mRNA coding for several enzymes of lipid metabolism and also of (signalling) proteins that interact with the membrane and may affect domain formation and properties (see annex Table S 1). The PM protein for which mRNA levels determined in the transcriptional profiling study are increased by a larger amount, attaining a 30-fold increase is ABC-3 (Fernandes et al. 2011). Moreover, this protein is responsible for most of the energy-dependent efflux of STS and a null-mutant of this ABC transporter (*abc3*) is extremely sensitive to STS and accumulates more STS than the *wt* strain (Fernandes et al. 2011).

1.4.2. Azoles – Ketoconazole

Ketoconazole (Ke) (Figure 9) has a long history of medical uses. It was approved by Food and Drug Administration (FDA) in 1981 as an antifungal drug and during the following decade was the only antifungal available for oral treatment of systemic fungal infections caused by pathogenic yeasts. Still in the 80's, Ke gained an interest as a potential anticancer agent. This effect led to the use of Ke in the treatment of prostatic cancer. Independent research proved that Ke was of value against Cushing's syndrome (Starosta and de Almeida 2020). Currently, this compound is regaining strong interest and new ketoconazole derivatives, such as diphenylphosphane (KeP), where acetyl group from the Ke molecule is replaced with – CH_2PPh_2 moiety, and the phosphane chalcogenides: oxide (KeOP), sulphide (KeSP) and selenide (KeSeP) (Figure 9), or complexes with several metal ions are under study (de Almeida et al. 2019, Starosta et al. 2020).

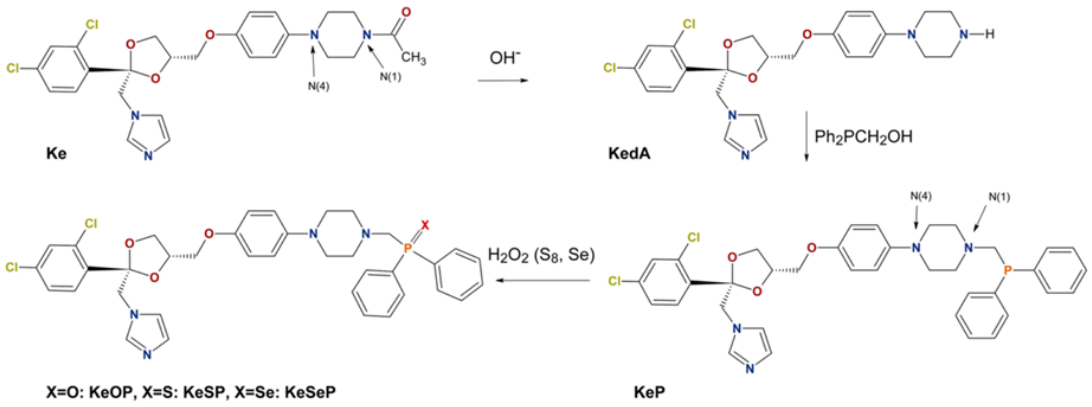

Figure 9 – Molecular schemes of ketoconazole (Ke) and its derivatives (de Almeida et al. 2019).

Our studies on their antifungal activity so far showed that these derivatives are promising antifungal agents towards *S. cerevisiae* and *C. albicans*, especially KeP and KeOP, in synergy with fluconazole. All the compounds share basically the same mode of action, inhibiting the cytochrome P450 14α-demethylase, azoles primary molecular target, as shown through docking calculations. However, differences in antifungal activity suggest that there may be additional modes of action or differential interactions with cellular components, such as drug efflux pumps (de Almeida et al. 2019, Starosta and de Almeida 2020).

1.4.3. Polyene antibiotic – Nystatin

Polyene macrolide antifungals present a very low antibacterial activity coupled with a potent broad-spectrum antifungal action, proving to be one of the most effective antifungal drug classes synthesized by bacteria, in this case *Streptomyces spp*. AmB and Nys (Figure 10) are two important members of this family. Despite its side effects and growing resistance to treatment, AmB is widely used to treat systemic fungal infections. Nys, which presents a higher antifungal activity, is restricted to topical and oral infections due to the lack of a formulation suitable for systemic use. The use of Nys as a viable pharmaceutical alternative to AmB-resistant infections hinges upon the development of an optimized drug carrier. An enhanced understanding of the mode of action of this polyene antifungal at the molecular level will certainly guide the design of alternative strategies to improve drug efficacy and reduce its toxicity (dos Santos et al. 2017).

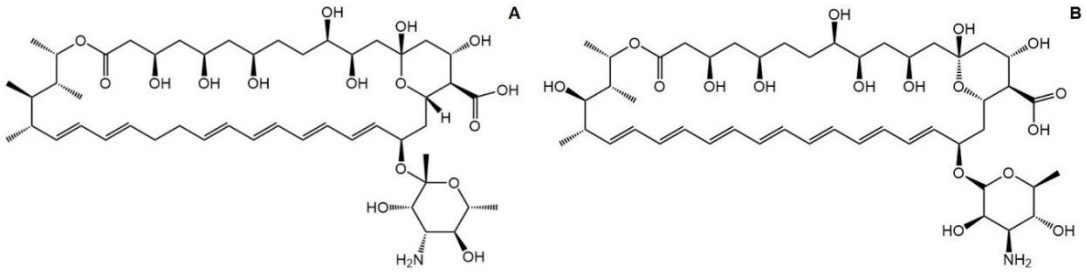

Figure 10 – Chemical structures of Nystatin A1 and Amphotericin B.

Polyene macrolides such as AmB and Nys (Figure 10) are amphipathic molecules, structurally characterized by a large lactone ring with multiple double bonds, targeting the membrane of sensitive organisms. Once in the membrane they can form small diameter channels (~0.6nm) that ultimately lead to cell death (van Hoogevest and de Kruijff 1978).

The formation of Nys active species depends both on the type of lipid and the presence of ordered gel domains in as much that: (i) only moderate membrane permeabilization is observed in fluid membranes; (ii) Nys interaction leading to pore formation occurred at the gel/fluid domain boundaries and (iii) gel domain properties and composition affected Nys membrane stabilization and Nys-induced membrane permeabilization. In summary, the work by dos Santos *et al.,* 2017 pinpoints that Nys-induced membrane permeabilization is related to its effects on membrane properties and organization, and this depends on membrane lipid composition and, thus, on the ability of Nys to interact differently with membranes displaying distinct membrane biophysical properties. This work further suggests that although ergosterol might remain one of the key factors in explaining Nys antifungal activity, other membrane properties need to be considered when addressing Nys molecular mode of action and cytotoxicity. A more comprehensive knowledge of Nys mode of action is pivotal for the development of lipid-based nanoparticles that can efficiently incorporate significant amounts of the antifungal and target lipid domains specific to fungal membranes, such as the SL-enriched sterol-free gel domains identified in yeast (Aresta-Branco et al. 2011, dos Santos et al. 2017).

CHAPTER II – BRIEF PRINCIPLES OF THE BIOPHYSICAL CHARACTERIZATION TECHNIQUES

In this chapter, the principles of the main characterization techniques used throughout this work will be concisely described. The techniques employed were essentially fluorescence based. Fluorescence Spectroscopy was used to assess the biophysical properties of fungal PM, both with membrane model systems and live fungal cells, and the existence of possible changes in those properties due to external drug stimuli, while Fluorescence Lifetime Imaging Microscopy (FLIM) was used to characterize the protein distribution/ organization along the PM.

2.1. Fluorescence Spectroscopy

Fluorescence spectroscopy is considered a primarily research tool comprising a set of techniques often employed in biochemistry and biophysics. The photophysical properties of fluorophores incorporated in the membrane can be either evaluated through steady-state and/ or time-resolved fluorescence, giving information on the physical features of a specific lipid environment (Sezgin and Schwille 2011).

In order to occur fluorescence emission, a fluorophore must enter in an excited state after light absorption that is represented by a transition from the fundamental electronic state (S_0) to a singlet electronic state of higher energy (*e.g.*, S_1 or S_2). Upon excitation, the energy absorbed by the fluorophore, can then be released through various processes, some of them represented by the Perrin-Jablonski diagram (Figure 11). The release of energy to the lowest excited state energy level (S_1) occurs usually through non-radiative processes. However, this internal conversion process may give place to a radiative process, by means of the emission of photons. Fluorescence corresponds to the radiative relaxation from S_1 to S_0 (Lakowicz 2006, Shanker and Bane 2008).

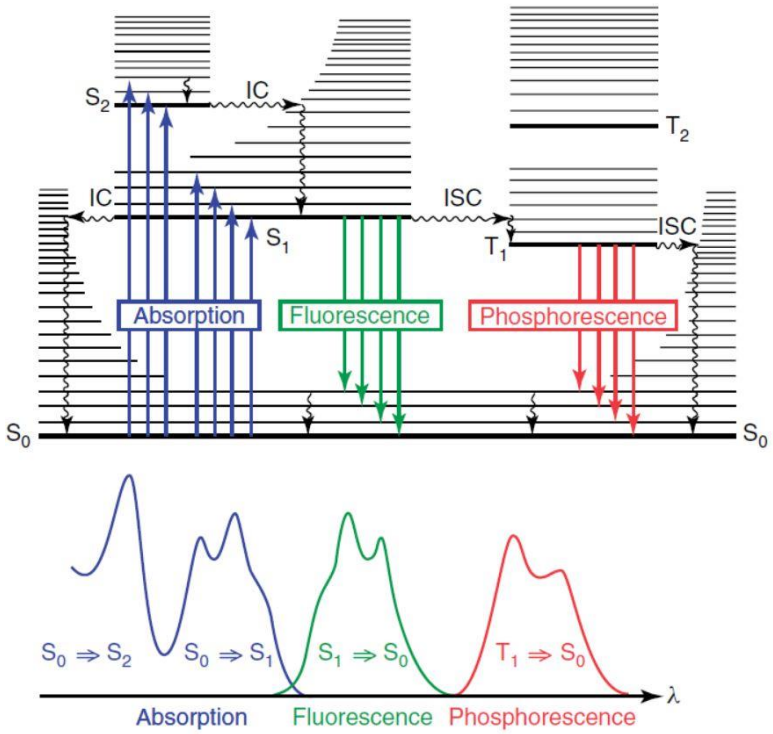

Figure 11 - Perrin – Jablonski diagram and relative positions of the absorption, fluorescence, and phosphorescence spectra. Straight arrows represent radiative processes, whereas wavy arrows stand for nonradiative ones. IC, internal conversion; ISC, intersystem crossing (Valeur 2009).

2.1.1. Fluorescence emission and excitation spectra

Once a fluorophore is excited at a fixed wavelength and the fluorescence intensity is collected at a higher range of wavelengths, an emission spectrum is obtained. While, the opposite process occurs in order to obtain an excitation spectrum, the fluorophore is excited within a range of wavelengths and the fluorescence intensity is collected at a fixed wavelength (Lakowicz 2006).

Fluorescence spectra are sensitive to changes in the medium and thus useful to study changes in the environment where the fluorophore is inserted (Lakowicz 2006). The solvent polarity has a large effect on the spectral properties of some fluorophores. As already mentioned, upon excitation, the fluorophore rapidly loses the excess of vibrational energy and relaxes to the level S_1, from where the emission occurs. This process, in which the maximum of fluorescence emission occurs at less energetic wavelengths, *i.e.* longer wavelengths, than that of absorption, leads to an energy gap between the absorption and the emission spectrum, denominated Stokes´ shift, Figure 12 (Shanker and Bane 2008). The effect of solvent polarity

displaces emission for even lower energy levels due to stabilization of the fluorophore in the excited state, lowering the energy of S_1 level (solvent relaxation). After returning to the ground state, the dipole alignment will no longer be optimal, being the energy in S_0 higher than in the initial state (before excitation). This results in a lower energy gap between S_1 and S_0 manifested by emission in longer wavelengths (red shift in emission) (Lakowicz 2006, Shanker and Bane 2008). However, excitation spectra are usually less sensitive because no solvent relaxation takes place during the extremely fast absorption process.

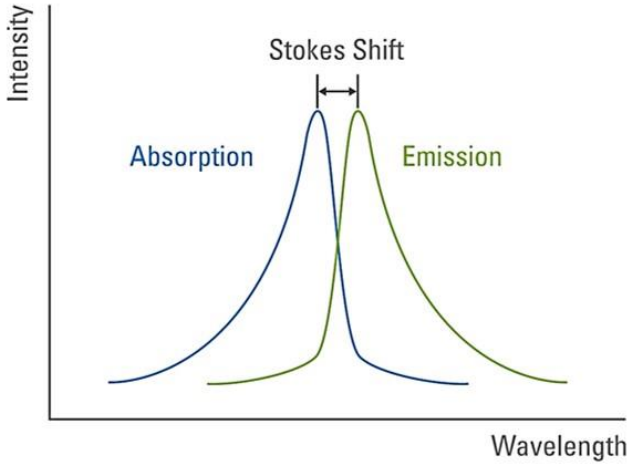

Figure 12 – Schematic representation of Stokes' shift. Strictly, the Stokes' shift should be given in wavenumber and not in wavelength, since the former is linearly related with the energy gap, and not the latter. However, because excitation and emission spectra are usually recorded in a wavelength scale, it is commonly represented as in this Figure.

2.1.2. Fluorescence anisotropy

Steady-state fluorescence anisotropy ($\langle r \rangle$) measurements are performed in spectrofluorometers equipped with polarizers, as exemplified in Figure 13.

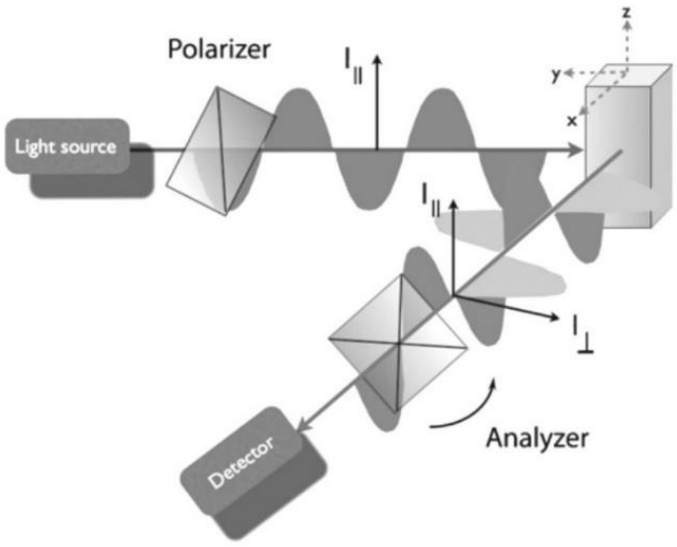

Figure 13 – Usual geometry of fluorescence anisotropy experiment.

Upon the continuous illumination of a fluorophore with a lamp emitting a constant flow of photons, the concentration of excited fluorophore remains constant, being thus in a steady-state. Steady-state fluorescence anisotropy is regularly used in membrane biophysics studies since it can sense the environment in which the fluorophore is inserted. This methodology consists in the measurement of depolarization of emitted light. When exciting with linearly polarized light, fluorophores presenting a parallel transition dipole with the electric vector of excitation will absorb the photons more efficiently. Then the emitted photons are detected after passing through another polarizer positioned in either a parallel or a perpendicular direction of the polarized light excitation (Shanker and Bane 2008, Borst and Visser 2010). The fluorescence anisotropy can be calculated using the intensities of the emitted light, through Equation 1:

$$r = \frac{(I_{VV} - G \times I_{VH})}{(I_{VV} + 2G \times I_{VH})}$$

Equation 1

where the different intensities (*I*), are the vertical and horizontal components of fluorescence emission in steady-state with vertical (I_{VV} and I_{VH}, respectively) and horizontal (I_{HV} and I_{HH}, respectively) excitation relatively to the emission axis. *G* factor can be determined by the I_{VH}/I_{HH} ratio and is used to correct the different sensitivity of the detector for the vertical and horizontal polarization (Lakowicz 2006).

As mentioned above, fluorescence anisotropy can be used to sense the surrounding environment in which the fluorophore is inserted. Hence, if the fluorophore is in a rigid environment, such as in a membrane in the gel phase, its rotational movement will be hindered and consequently the depolarization of light will be inefficient. In this case, the polarization of the emitted light will be intimately related with the polarization of the excitation light, and the fluorescence anisotropy will be high. However, if the fluorophore is in a more fluid environment, its rotation will be facilitated and there will be no preferential polarization orientation for the emitted light (Lakowicz 2006), and the anisotropy will be low.

In the case of spherical molecules, the anisotropy can be calculated through Equation 2 (Perrin's Equation),

$$\langle r \rangle = \frac{r_0}{\left(1 + \frac{\tau}{\varphi}\right)}$$

Equation 2

where r_0 is the expected value of $\langle r \rangle$ in the absence of rotation ($\cong 0.4$ for several fluorophores) and φ is the rotation correlation time of the fluorophore, which is in turn dependent on the hydrodynamic radius of the molecule, absolute temperature, and viscosity of the medium. If the emission is much faster than the fluorophore rotation, $\tau << \varphi$ and $\langle r \rangle \cong 0.4$; if the opposite occurs, $\tau >> \varphi$, then $\langle r \rangle \cong 0$. Hence, anisotropy is a measure of the amount of molecular rotation through the lifetime at the excited state of the molecule, thus being sensitive to the rigidity of the molecular environment, and to the fluorophore shape and size (Loura and de Almeida 2004).

Additionally, through time-dependent measurements of I_{VV} and I_{VH} the fluorescence anisotropy decay, $r(t)$, is obtained from which is possible to measure r_0, the rotational correlation time(s), as well as another parameter, the limiting anisotropy (r_∞). For many fluorophores, a single rotational correlation time is not sufficient to describe the fluorescence anisotropy decay. If the molecules can rotate over all orientations for long times, r_∞ will be zero. When $r_\infty \neq 0$, there are restrictions to the rotational movement of the molecule (more usual for fluorophores in the membrane in ordered phases) (Loura and de Almeida 2004, Bagulho et al. 2015).

2.1.3. Time-resolved Fluorescence

The average time a fluorophore spends in the excited state is very sensitive to the fluorophore dynamic microenvironment and can be accessed by measuring and analysing its fluorescence intensity decay (Shanker and Bane 2008) (examples obtained from live cultures are given in Figure 14).

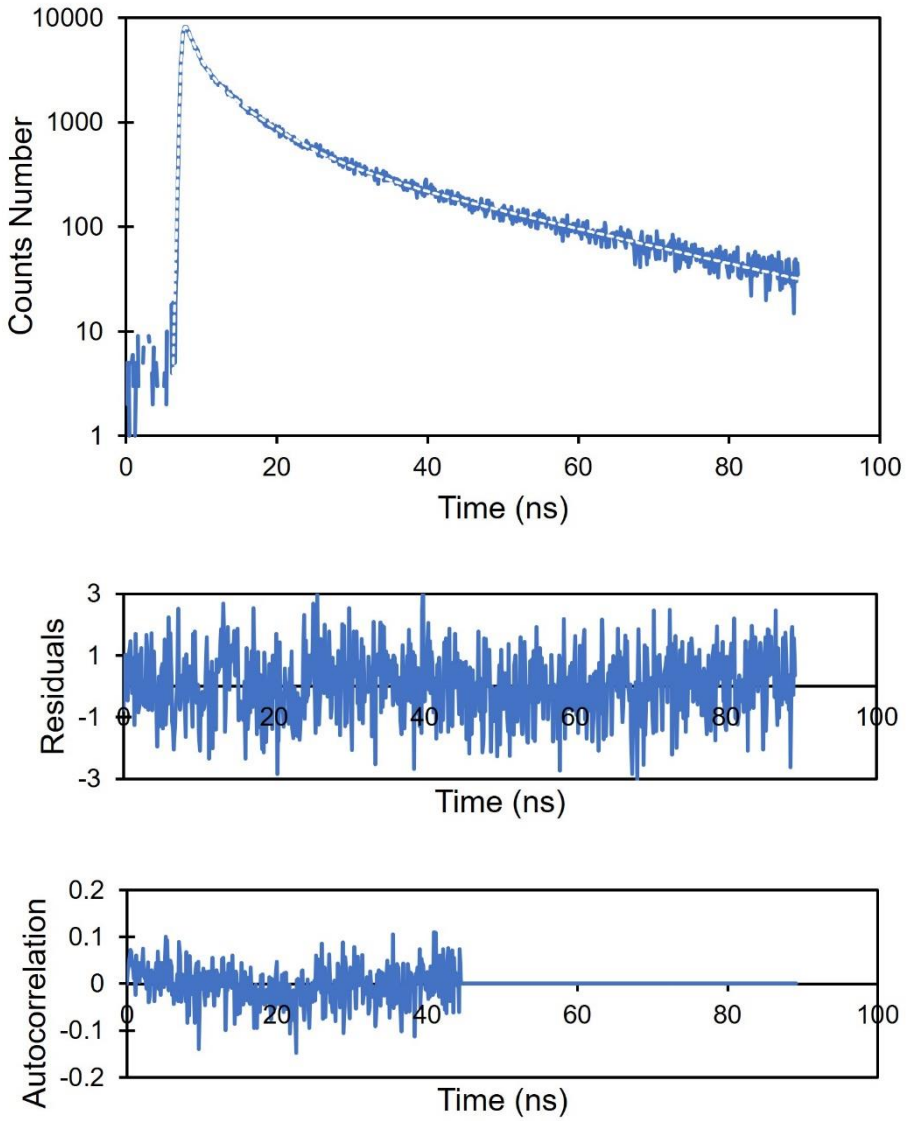

Figure 14 – Illustrative fluorescence intensity decay of t-PnA in a suspension of N. crassa wt conidia. Top panel: experimental decays and best fitting with a sum of exponentials (dashed white lines). Middle panel: random distribution of weighted residuals of the fitting. Bottom panel: Autocorrelation of the residuals.

In the simplest situation, fluorescence decays follow a first-order kinetics and are described by a mono-exponential decay law, Equation 3, where I_0 corresponds to the intensity at time 0.

$$I(t) = I_0 e^{\left(-\frac{t}{\tau}\right)}$$

Equation 3

The fluorescence (or excited state) lifetime is then the reciprocal of the decay rate constant. However, the fluorescence decay is usually more complex and is often described by a discrete sum of exponentials,

$$I(t) = \sum_{i=1}^{n} \alpha_i e^{\left(-\frac{t}{\tau_i}\right)}$$

Equation 4

or by a lifetime distribution. In Equation 4, α_i is the normalized pre-exponential factor or amplitude and τ_i the lifetime of decay component *i*. The intensity-weighted mean fluorescence lifetime of a fluorophore can be defined by Equation 5:

$$\langle \tau \rangle = \frac{\sum_{i=1}^{n} \alpha_i \tau_i^2}{\sum_{i=1}^{n} \alpha_i \tau_i}$$

Equation 5

and the amplitude-weighted mean fluorescence lifetime is obtained following Equation 6:

$$\tau_{av} = \sum_{i=1}^{n} \alpha_i \tau_i$$

Equation 6

The time-correlated single-photon counting (TCSPC) method, also known as single-photon timing is the most popular technique for lifetime determination. The principle of this technique is based in the probability of detecting a single photon at a time, t, after an excitation pulse, being proportional to the fluorescence intensity at that time (Lakowicz 2006). The time

between the excitation pulse and the emission of the photon is represented as a histogram (Figure 15).

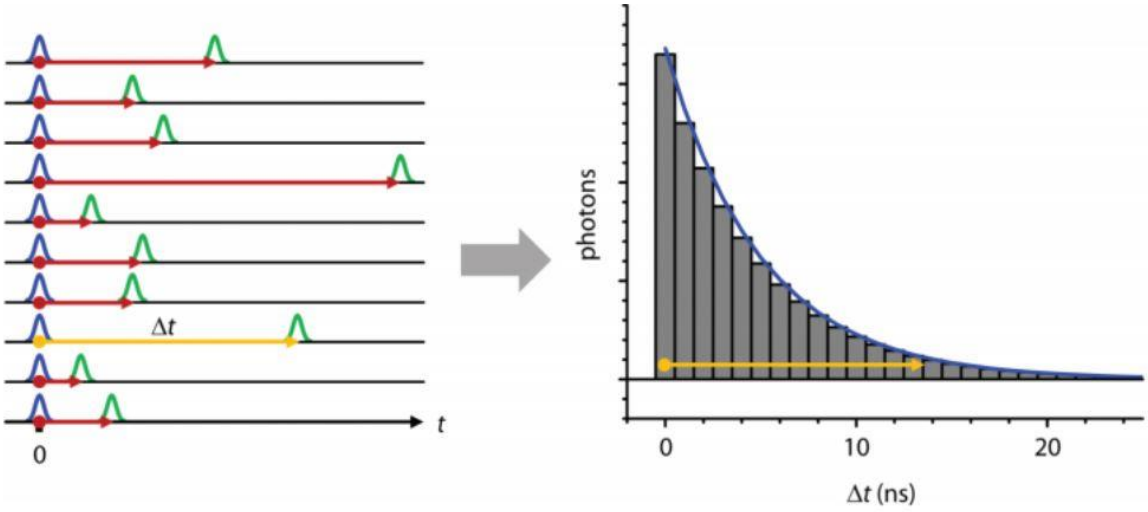

Figure 15 – Measurement of fluorescence lifetimes by time-correlated single photon counting: From histograms to decay curves (Klostermeier and Rudolph 2018).

Membrane probes often present multi-exponential decays even when in isotropic solutions or incorporated in single phase lipid bilayers without lipid domains (Wolf 1988, Mateo et al. 1993, Khmelinskaia et al. 2020). Nevertheless, the complexity of the fluorescence intensity decay, revealed by broad and multimodal lifetime distributions or by a relatively large number of discrete decay components, is an indication of heterogeneity and contains information about the biophysical properties and relative abundance of the lipid domains, which are responsible for the need of using a more complex model to describe the fluorescence intensity decay (Mateo et al. 1993, Castro et al. 2009, Aresta-Branco et al. 2011, Bastos et al. 2012a, Vecer et al. 2014).

2.1.3.1. Fluorescence Lifetime Imaging Microscopy

Fluorescence lifetime imaging is a fluorescence microscopy technique, which uses the detection of fluorescence lifetime instead of fluorescence intensities to obtain information on the environment of the fluorophore or the interaction of molecules labelled with a donor-acceptor pair via Förster resonance energy transfer (FRET) (Lakowicz 2006, Valeur and

Berberan-Santos 2012). Measurements in the time domain are single point measurements combining the TCSPC principle with a scanning method using for instance Confocal Laser Scanning Microscopes. This intuitive method provides a higher sensitivity since single photon counting detectors are used, a better time resolution can be obtained, and it provides more options for the analysis of multi-exponential fluorescence assays (Korte and Herrmann 2016). The later was the method used in this work.

The cuvette experiment *in vivo* is performed with cells in suspension and is quite similar to the acquisition of a fluorescence intensity decay for *in vitro* systems, such as a suspension of liposomes labelled with a certain membrane probe. Since cuvette experiments are performed in cellular suspensions, it is not possible to study a single cell. Thus, the typical number of cells used is on the order of 10^6-$10^7 mL^{-1}$. Therefore, the fluorescence decay obtained is an average of a large number of cells. Whereas this may be disadvantageous in some cases, it is a way of obtaining in one measurement an average over the variability that a biological sample always contains. However, identifying for example protein-protein interactions between two labelled protein species due to a drop in donor fluorescence lifetime will only give information that this process is occurring, but will not yield the membrane sites at which the interaction occurs. Therefore, FLIM techniques have been developed, which not only measure fluorescence lifetimes, but also allow visualizing their spatial distribution (Bastos et al. 2012a). It allows also to select a region of interest and recover the fluorescence intensity decay for the membrane probe or tagged protein located in that specific region. In the present study, for example, the PM of yeast cells was selected.

2.1.4. Membrane Probes

There are several fluorophores available for the study of membrane biophysical properties. The selection of those probes depends on the purpose of the study.

Some probes are used for labelling specific lipid molecules, others are sensitive to the hydration of the surrounding environment and there are also some probes that selectively partition into distinct membrane phases, being very useful for the study of membrane organization (Baumgart et al. 2007, Demchenko et al. 2009, Klymchenko and Kreder 2014).

In this work three different fluorescent probes were employed, to complement and corroborate the information gathered from each one alone. Hence, first it is deemed necessary to briefly introduce each fluorescent probe used.

Polyene fluorophores, such as *trans*-Parinaric Acid (*t*-PnA), shown in Figure 16, and Nys, have their chromophore buried in the hydrophobic core of the lipid bilayer, providing direct information on acyl chain packing, it presents a strongly allowed electronic transition that guarantees efficient absorption of light. However, they have a weak (forbidden) lowest energy transition that is the one responsible for fluorescence emission (Sklar et al. 1977a). For most fluorophores, as in the case of polyenes, nonradiative processes consist of intramolecular rotations, torsions, vibrations or isomerizations and intermolecular collisions (Berezin and Achilefu 2010, Aresta-Branco et al. 2011). They compete with the emission of fluorescence for the relaxation of the molecule into the electronic ground state. The reduction of the efficiency of such processes explains to a large extent why these molecules are weakly fluorescent in water, but their fluorescence quantum yield increases drastically upon incorporation in a membrane environment, one of the reasons why polyenes are often used as fluorescent membrane probes (Hudson and Cavalier 1988).

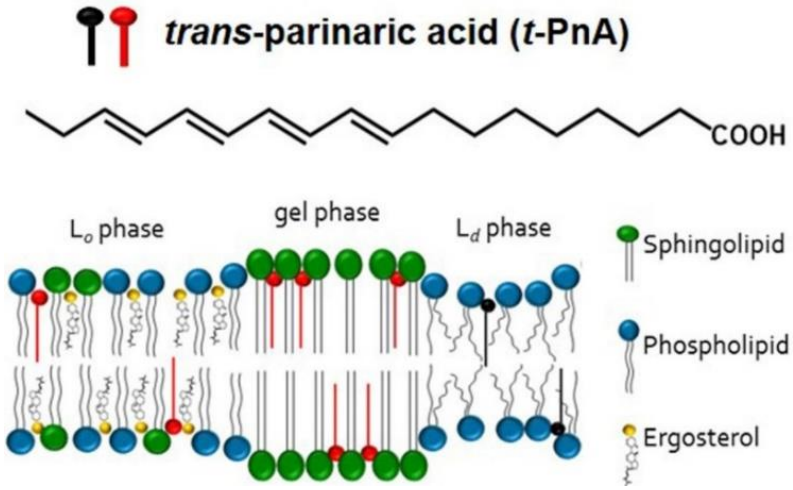

Figure 16 – Predicted location of the fluorescent probe, t-PnA in the different lamellar lipid phases. The polar headgroups of SLs and of phospholipids are represented in green and blue, respectively. Ergosterol (Lo-forming) is represented by a ring system. t-PnA that reports acyl chain packing, has preferential partition for gel phases (red) where it presents high quantum yield, but can be found also in Lo and Ld phases where it presents intermediate (red) and low quantum yield (black), respectively. In the ordered phases (gel and lo), t-PnA presents a long component in its fluorescence decay, which is absent in the disordered phase, hence, the red and black colour, respectively. The long component becomes very long in the presence of gel domains and can be used as a fingerprint for this phase. See text for details.

Although fluorescence lifetimes are typically in the nanosecond or sub-nanosecond timescale, in the case of *t*-PnA because fluorescence emission corresponds to a forbidden electronic transition, its intrinsic fluorescence lifetime, that is, in the absence of any competing processes, is very long (ca. 100 ns) (Sklar et al. 1977a). *t*-PnA is one of the few probes known to partition preferentially into gel domains (and thus labelling yeast SLEDs), where it displays a markedly increased quantum yield as compared to fluid membranes (Mateo et al. 1993, Reyes Mateo et al. 1995, de Almeida et al. 2009, Aresta-Branco et al. 2011, Bento-Oliveira et al. 2020). This increase occurs due to a reduction in the efficiency of nonradiative decay processes in the more rigid environment, leading also to an increase in the fluorescence lifetime of *t*-PnA. In membranes, this increase is associated to the appearance of a long lifetime component, in the order of tenths of nanoseconds, which therefore is a fingerprint for the presence of ordered domains (Mateo et al. 1993, Reyes Mateo et al. 1995, de Almeida et al. 2009). Since this component is due to the conjugated tetraene fluorophore of *t*-PnA, which is buried in the hydrophobic core of the lipid bilayer, Figure 16, it provides information on the chain packing, reflecting directly the rigidity of these ordered domains (Sklar et al. 1977a, Sklar et al. 1977b, de Almeida et al. 2009, Aresta-Branco et al. 2011). Hence, the long lifetime component obtained for *t*-PnA is usually used to support the identification of the ordered phase, which can be safely assigned to a gel phase when longer than 30 ns (Silva et al. 2007, Castro et al. 2009, González-Ramírez et al. 2019). This criterion was established based on results on multiple model systems, many of which performed at room temperature (ca. 23 °C) (de Almeida et al. 2009). Long lifetime component values between 20 and 30 ns are generally attributed to the presence of a l_o phase, but they have been found in the gel phase of phosphatidylcholines near the gel/fluid phase transition (Mateo et al. 1993).

The fluorescent probe 1,6-diphenyl-1,3,5-hexatriene (DPH) (Figure 17), a rod-shaped molecule which incorporates parallel to the acyl chains of the phospholipids, displays a close to equal partition among the different membrane lipid phases (l_d, l_o and gel) (Florine-Casteel and Feigenson 1988, Davenport 1997) reporting on the global order of both plasma and intracellular membranes (de Almeida et al. 2003, Folmer et al. 2008, Aresta-Branco et al. 2011). DPH is also located in the hydrophobic core of the lipid bilayer.

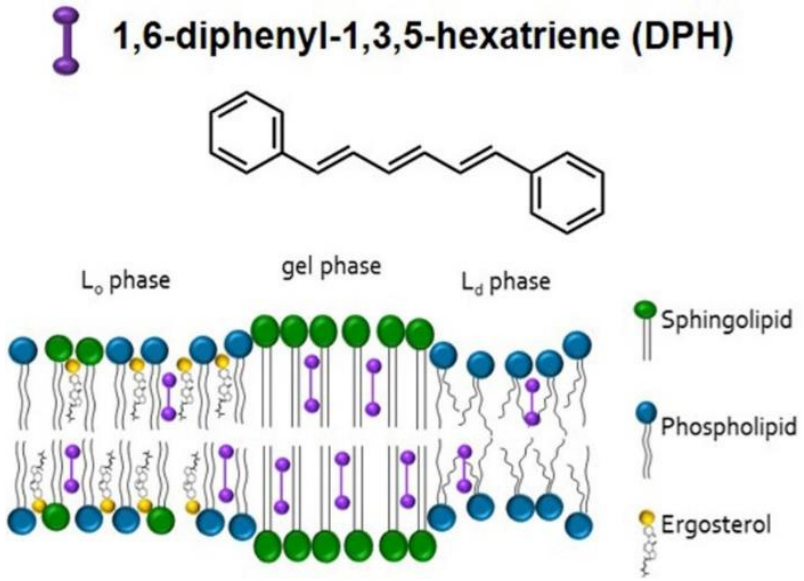

Figure 17 – Predicted location of the fluorescent probe, DPH in the different lamellar lipid phases. The polar headgroups of SLs and of phospholipids are represented in green and blue, respectively. Ergosterol (Lo-forming) is represented by a ring system. DPH reports the global order of the membrane in the hydrophobic core.

DPH, presents a high quantum yield in hydrophobic environments and negligible fluorescence in water, and a lifetime sensitive to environmental properties (Parasassi et al. 1991, Baumgart et al. 2007), though to a much smaller extent than *t*-PnA. Hence, DPH is a very sensitive probe to evaluate biophysical membrane properties, such as membrane fluidity through its steady-state fluorescence anisotropy (de Almeida et al. 2003, de Almeida et al. 2005, Aresta-Branco et al. 2011, do Canto et al. 2016). Steady-state fluorescence polarization studies of membranes using DPH as a probe have shown that the transition between the gel and liquid-crystalline phases can be followed by changes in polarization (Parasassi et al. 1991). Despite its non-preferential partition to distinct lipid phases, this probe shows a higher steady-state fluorescence anisotropy and lifetime values in l_o and gel phases, compared to the l_d phase (Carreira 2019).

Contrary to DPH and *t*-PnA chromophore, 4-(2-(6-(dibutylamino)-2-naphthalenyl)ethenyl)-1-(3-sulfopropyl)-pyridinium (di-4-ANEPPS) (Figure 18), presents a superficial location in the membrane, which makes it useful for characterizing properties at the membrane/water interfacial region. For that reason, also is a probe particularly responsive to changes in hydration patterns and membrane dipole potential due to its electrochromic properties; additionally, its emission spectrum presents a strong blue-shift with increasing concentrations of both ergosterol and cholesterol (Santos et al. 2017). ANEP (aminonaphthylethenylpyridinium) dyes undergo a charge transfer process upon excitation,

and consequently in their fluorescence spectra, in response to changes in the surrounding electric field (Loew 1996). This optical response is sufficiently fast (~10%/ 100mV, (Loew et al. 1992)) to detect transient potential changes in excitable cells, including single neurons, cardiac cells, and intact tissue preparations. Furthermore, the charge transfer occurs parallel to the membrane normal. Therefore, these dyes display a membrane potential-dependent shift in their excitation spectra, thus permitting the quantitation of membrane potential using excitation ratio measurements (Montana et al. 1989).

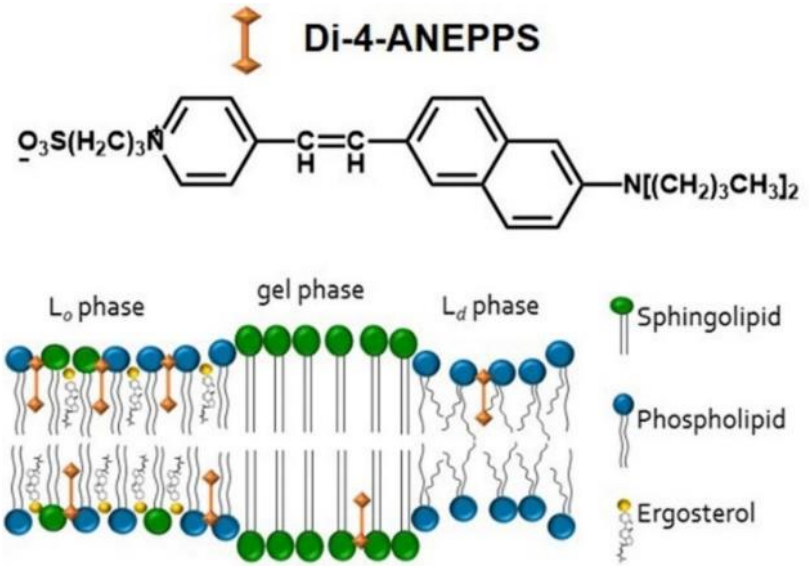

Figure 18 – Predicted location of the fluorescent probe, di-4-ANEPPS in the different lamellar lipid phases. The polar headgroups of SLs and of phospholipids are represented in green and blue, respectively. Ergosterol (l_o-forming) is represented by a ring system. Di-4-ANEPPS presents sensitivity to polarity and hydration patterns in the headgroup region, and membrane dipole potential; partition and fluorescence quantum yield favourable to sterol-rich domains.

CHAPTER III – TECHNIQUES AND EXPERIMENTAL PROCEDURES

3.1. Microbiological Techniques

In this chapter, the microbiological techniques and procedures applied throughout the development of this Ph.D. project will be briefly described. Standard procedures were employed for growth and handling of both *Neurospora crassa* (Davis 1970), and *Saccharomyces cerevisiae* (Branco et al. 2004, Matias et al. 2007) strains, all the necessary adaptations for the specific strains and cultures were performed.

3.1.1. *Neurospora crassa* strains, growth conditions and replicates

The three *N. crassa* strains, the *wild-type* (*wt*) (FGSC 2489), a mutant strain devoid of cell wall (*slime*) (FGSC 4761) and a null-mutant of the ABC transporter (*abc3*) (FGSC 14572) used were obtained from the Fungal Genetics Stock Centre (McCluskey 2003). STS, CAS: 62996-74-1, was obtained from LC-Laboratories (MA, USA).

For both *wt* and *abc3* strains the handling procedure was similar, each biological replicate was grown in solid Vogel's Minimal Medium (MMV) during 7 days at 30 ºC, under controlled light conditions, in a different culture flask, to obtain biologically independent conidial suspensions. To this end, 25 mL of sterile water were added to the culture flask which was re-caped and shaken to dislodge the conidia. The conidia obtained were then filtered through a funnel with a four-layered cheesecloth into a sterile flask. An aliquot was observed under an optical microscope and cells were counted with a hemocytometer to ensure that the spectroscopic determinations were always made with the same number of conidia per mL of suspension (Santos et al. 2017). In order to preserve the *wt* and *abc3* strains in a stock at - 80 ºC, 25 mL of sterile fat milk was added to the prepared conidial suspensions, which was then re-caped and shaken to dislodge the conidia. The conidia obtained were filtered through a funnel with a four-layered cheesecloth into a sterile flask and divided into 1 mL aliquots with glass beads (90-150 μm, Sigma).

In the case of *N. crassa slime* mutant, Supplemented Vogel's Medium (SeM) containing 2% mannitol (*w/v*), 0.75% yeast extract (*w/v*) and 0.75 % nutrient broth (*w/v*) was used. The initial procedure was slightly different. Independent cultures were grown in liquid SeM during 3 days at 30 ºC under constant agitation, 150 rpm, after which an aliquot was observed, and cells counted as described above. Each suspension was kept in glycerol and stored in aliquots

of 1 mL at −80 °C, when necessary and before each experiment the stored *slime* stock was activated on a 30 °C water bath during 30 min.

3.1.1.1. Establishing Neurospora crassa growth profile

N. crassa wt, *abc3* or *slime* at ~1.5×10^6 cell/mL were grown at 30 °C in MMV or SeM for 14–16 h (*wt* and *slime*) and 22 h (*abc3*). Growth profile was monitored by following the absorbance of the liquid cultures at 690 nm (A_{690}) to avoid interference of culture media and cellular components (namely, carotenes). Morphological alterations were inspected under a transmission microscope Axiovert 100 A with an Adaptor Tube Soligor® for Canon A640 - PowerShot Digital Camera, used to record the observations made with a magnification of 100×, taking 50 μL aliquots at different time points. The images shown are representative of each culture condition/strain.

3.1.1.2. Isolation of Neurospora crassa wt cell wall

N. crassa wt at 1.5×10^6 cell/mL were grown in MMV for 5 h at 30 °C and 150 rpm. Cells were washed twice with PBS (10 mM phosphate buffered saline pH 7.4, 0.138 M NaCl, 0.0027 M KCl) by centrifugation at 10,000 *g* for 2 min. Afterwards, one volume of glass beads was added to the pellet. Solutions of 100 mM Na_2ATP and 100 mM PMSF, were added to the suspension at final concentrations of 4 mM and 6 mM, respectively. The suspension was stirred for 90 s. The homogenate was decanted and reserved. The glass beads were then washed with a solution of 300 mM D-Sorbitol, 3 mM HEPES, 0.3 mM Na_2EDTA, pH 7.5, 6 mM Na_2ATP and 0.06 mM PMSF, and the solution obtained was added to the previous homogenate. The suspension was centrifuged at 2,083 *g* for 10 min. The pellet is rich in cell wall and nuclei (cell wall rich fraction), while the other membranes remain in the supernatant (membrane rich fraction). The pellet was resuspended in PBS and again centrifuged at 2,083 *g* for 10 min, after which it was resuspended in PBS (Bowman and Bowman 2007).

3.1.1.3. Fluorescence spectroscopy of Staurosporine in Liposomes

Liposome (multilamellar vesicles) suspensions of 3 mM lipid were used. This high lipid concentration was used to ensure that even a weak interaction with the membrane could be perceived. Three different lipid compositions were prepared: DPPC (1,2-dipalmitoyl-*sn*-glycero-3-phosphocholine), POPC (1-palmitoyl-2-oleoyl-*sn*-glycero-3-phosphocholine) (Table 2), and a binary mixture of DPPC/ Cholesterol (1:1 mol:mol), corresponding to gel, l_d and l_o phase membranes, respectively (de Almeida and Joly 2014). Cholesterol was chosen instead of ergosterol because ergosterol absorbs light in the same range as STS and, as it corresponds to 50 mol% of the lipid, is present in a much higher concentration (1.5 mM vs. 12.5 µM), precluding reliable measurements of STS fluorescence.

To prepare the liposome suspensions, lipid stock solutions were added to a glass tube and the solvent was slowly vaporized by a mild flow of nitrogen, forming a thin layer of lipid. The lipid was hydrated through the addition of 1 mL of PBS previously heated above the T_m of the lipids. The samples were then progressively vortex-stirred and submitted to at least 5 freeze/thaw cycles. Afterwards, STS was added to the prepared multilamellar vesicles suspensions to a final concentration of 12.5µM, and the suspension was incubated at room temperature (23 ± 2 °C). After 1 h, the liposome suspensions were analysed by steady-state and time-resolved fluorescence spectroscopy, taking advantage of the intrinsic fluorescence of the drug, using excitation and emission wavelengths of 290 and 377 nm, respectively, and bandwidth of 1.5 nm in spectral acquisition and 3 nm in anisotropy measurements. STS in PBS was used as control. Liposome suspensions without STS were used as blanks. Both steady-state and time-resolved fluorescence measurements were performed with a Horiba Jobin-Yvon Spex Fluorolog 3.22, at 30 °C in a temperature-controlled sample compartment under magnetic stirring. For time-resolved measurements by the SPT technique, a nanoLED N-280 was used for excitation at 279 nm; emission was collected at 377 nm with a bandwidth between 5 and 7 nm. The other experimental conditions and data analysis follow the procedure described below for the studies with cell suspensions (section 3.2).

3.1.1.4. Staurosporine challenge in cells

N. crassa wt and *abc3* conidia were grown in liquid MMV, while *slime* was grown in liquid SeM, at a starting concentration of 10^7 conidia/mL, at 30 °C and 150 rpm. After 2 or 5 h of growth, each culture was submitted to a 12.5 µM STS challenge and cells were further incubated for 1 h. STS in PBS was prepared fresh from a stock solution. The molar absorption coefficient of STS in methanol was determined and found to be, $\varepsilon_{(292\ nm,\ methanol)}$ of 3.1×10^3 $M^{-1}cm^{-1}$. In parallel, 3 or 6 h grown cultures of *wt* were challenged with 12.5 µM STS during 15 min, under the same conditions. The same volume of PBS was added to control cultures. This 1 h delay ensured that the total growth time of the controls was similar in both sets of experiments, *i.e.*, 3 and 6 h or 3 h 15 min and 6 h 15 min, respectively. Cells were washed by centrifugation at 10,000 *g* for 2 min and resuspended in PBS.

3.1.1.5. SDS-Page and Western Blot

N. crassa at a starting concentration of 10^7 conidia/mL was grown in 10 mL liquid MMV at 30 °C and 150 rpm, followed by the addition of 12.5 µM STS or same volume of dimethylsulfoxide (DMSO), and incubated under the same conditions. Cells were collected by fast filtration. Total protein extracts were obtained from disruption with zirconia beads in a FastPrep-24 (MP Biomedicals). SDS-PAGE and western blot using an antibody against ABC-3 protein were performed as described in Fernandes et al. (Fernandes et al. 2011).

3.1.2. *Saccharomyces cerevisiae* strains, growth conditions and replicates

3.1.2.1. Materials and strains

Table 1 lists the *S. cerevisiae* strains used throughout this work. The *wt, ipt1*Δ and *scs7*Δ strains were transformed using the lithium acetate procedure (Gietz et al. 1992), with the integrative plasmid Ylp211-CAN1-GFP (*URA3*) or Ylp128-PMA1-mRFP (*LEU2*) kindly provided by Dr. Guido Grossmann and Professor Widmar Tanner (University of Regensburg, Germany).

Table 1 – Saccharomyces cerevisiae strains used in this work, genotype description and growth media.

Strains	Genotype	Source	Growth media
wild-type (*wt*; BY4741)	MATa; his3Δ1; leu2Δ0; met15Δ0; ura3Δ0	EUROSCARF (Frankfurt, Germany)	Synthetic Complete Medium (SC)
***ipt1*Δ**	BY4741; YMR272c::KanMX4		SC
***wt*-Can1p-GFP**	BY4741; Ylp211CAN::GFP	This study	SC *ura-*
***wt*-Pma1p-mRFP**	BY4741; Ylp128PMA1:mRFP		SC *leu-*
***ipt1*Δ-Can1p-GFP**	BY4741; YMR272c::KanMX4; Ylp211CAN::GFP		SC *ura-*
***ipt1*Δ-Pma1p-mRFP**	BY4741; YMR272c::KanMX4; Ylp128PMA1::mRFP		SC *leu-*
***scs7*Δ**	BY4741; MATa; *his3*Δ1; *leu2*Δ0; *met15*Δ0; *ura3*Δ0; YMR272c::KanMX4	EUROSCARF (Frankfurt, Germany)	SC
***scs7*Δ-Can1p-GFP**	YMR272c::KanMX4; Ylp211CAN::GFP	This study	SC *ura-*
***scs7*Δ-Pma1p-mRFP**	YMR272c::KanMX4; Ylp128PMA1::mRFP	This study	SC *leu-*
***sur1*Δ:*csg2*Δ**	BY4741*; MATa his3*Δ1 *leu2*Δ0 *met15*Δ0 *ura3*Δ0 *sur1*Δ::UraMX; *csg2*Δ::KanMX	Gifts from Prof. Andreas Conzelmann (University of Fribourg, Switzerland)	SC
***sur1*Δ:*csh1*Δ**	BY4741*; MATa his3*Δ1 *leu2*Δ0 *met15*Δ0 *ura3*Δ0 *sur1*Δ::UraMX; *csh1*Δ::KanMX		SC

Yeast extract, bactopeptone, yeast nitrogen base, and bacto-agar were purchased from Difco (Hampton, NH, USA). Amino acids, nucleotides and glucose used in the synthetic complete (SC) medium, sucrose, and organic solvents (of analytical grade for lipid extraction and spectroscopic grade for lipids and probes stock solutions) were obtained from Merck (Darmstadt, Germany). *t*-PnA was purchased from Santa Cruz Biotech. (Santa Cruz, CA, USA), DPH and di-4-ANEPPS were obtained from Invitrogen (Carlsbad, CA, USA) and Ludox (TM-50 colloidal silica, 50 wt.% suspension in water) acquired from Sigma-Aldrich (St. Louis, MO, USA). Solvents/ co-solvents such as ethanol, methanol and glycerol were spectroscopic grade and purchased from Merck and Scharlau. All other reagents were of the highest purity available.

The polyene antibiotic Nys, CAS: 1400-61-9, was obtained from Alfa Aesar (Karlsruhe, Germany) and was stored at -20 °C in the dark.

Table 2 – Structure and T_m of the lipids used in the studies.

Lipids	Structure	T_m (°C)	References
DPPC	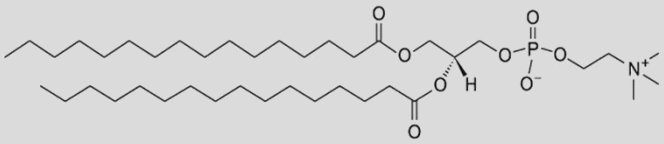	+41.3	(Biltonen and Lichtenberg 1993)
POPC	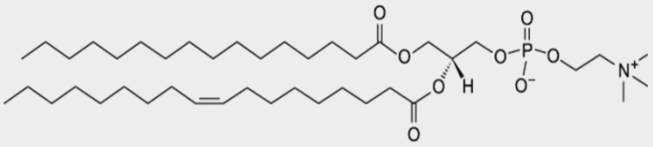	-3	(Litman et al. 1991, Koynova and Caffrey 1998)

The fluorescent probes were quantified spectrophotometrically using the respective molar absorption coefficients: *t*-PnA, $\varepsilon_{ethanol}^{299.4\,nm}$ = 89,000 $M^{-1}cm^{-1}$; DPH, $\varepsilon_{methanol}^{350\,nm}$ = 88,000 $M^{-1}cm^{-1}$ and di-4-ANEPPS, $\varepsilon_{methanol}^{497\,nm}$.= 42,000 $M^{-1}cm^{-1}$ (Johnson and Spence 2010).

The cuvettes used in the fluorescence spectroscopy were Hellma Analytics quartz (Suprasil®) cells with 4 mm (excitation) versus 10 mm (emission) of optical path and were purchased from VWR International.

3.1.2.2. Media and growth conditions

S. cerevisiae cells were grown at 30 °C and 160 rpm overnight in SC medium (2 % (*w/v*) glucose, 0.68 % (*w/v*) yeast nitrogen base and amino acid composition given in (Branco et al. 2004)), except when specifically stated, and reinoculated at an A_{600nm} of ca. 0.15. Upon reaching an A_{600nm} of 0.6, which occurs after 5-6 h of growth, *i.e.* in the mid-exponential phase, cells were harvested.

3.1.2.3. Rouser method for phosphate dosing

Phospholipid quantification was performed following the Rouser method (Rouser et al. 1970), in which released inorganic phosphate reacts with ammonium molybdate to form a complex with a strong blue color. The following volumes of 0.5 mM Na_2HPO_4 were added to

glass vials in triplicate for the standard curve: 0, 20, 40, 60, 80, 100, 120 and 140 µL (these values change according to the necessity) and left to dry at 170 °C in a heat block (Techne, Dri-block® DB3A). Separately, adequate volumes of the sample (in this case 100 µL) were added in triplicate to the glass vials and dried under a nitrogen stream. Then, 300 µL of 70 % perchloric acid were added to all the vials at 170 °C in the heat block for 45 min to digest the samples and release the inorganic phosphate. Once, the glass vials were at room temperature, 1 mL of water, 400 µL of ammonium molybdate (1.25 %) and 400 µL of ascorbic acid (5 %) were added in this order to all the vials and well-mixed. Then, the glass vials were heated in a thermostatic water bath (Bioblock scientific, polystat 33) for 5 min at 100 °C. After quickly cooling the glass vials with running tap water, the absorbance was read at 797 nm, within one hour.

3.1.2.4. Fluorescence intensity and lifetime imaging by confocal microscopy

3.1.2.4.1. Yeast living cells tagged with GFP and mRFP

FLIM measurements as well as confocal images of harvested *S. cerevisiae wt* and *ipt1*Δ cells with GFP-tagged Can1p and mRFP-tagged Pma1p were performed on a time-resolved confocal fluorescence microscope, model MicroTime 200, from PicoQuant GmbH (Berlin, Germany), with details of the equipment setup described in (Francisco et al. 2019).

The point-spread function of the setup was measured using fluorescent beads of size 100 nm, which afforded a lateral resolution of about 400 nm. Intensity images were obtained concomitantly with FLIM measurements. GFP and mRFP were excited at 480 nm using a pulsed-laser diode and detected by a SPAD using a longpass filter above 510 nm. The images were obtained with a scanning resolution of 0.156 µm/pixel. All images were acquired with an excitation power of ca. 0.54 kW/cm^2 and further processed by creating a mask in which the cell membrane regions were visually selected using the region-of-interest (ROI) tools of SymPhoTime program, version 5.3.2.2. The fluorescence decays corresponding to the regions identified as cell membranes were obtained from the histograms of photon arrival times concerning only the pixels contained in these regions. Analysis of FLIM data was performed using the software from PicoQuant, SymPhoTime 64, (version 2.5), considering the convolution of the fluorescence decays with the instrument response function (IRF). The time distribution of photon counts in each pixel retrieved from the regions of interest were combined

into a single decay curve which was further analysed by using a nonlinear least-squares iterative procedure, to fit a sum of 2 exponentials, judging the fitting quality from the distribution of the residuals and reduced χ^2 value. The intensity-weighted mean fluorescence lifetime $\langle\tau\rangle$ and the amplitude-weighted mean fluorescence lifetime, τ_{av}, were calculated using Equation 5 and Equation 6 from Chapter II. The results are averaged over more than 200 cells from 4 independent experiments.

Confocal images were used to assess the distribution of Can1p-GFP and Pma1p-mRFP in the PM of yeast living cells. For numerical data extraction a line profile of the fluorescence intensity of the PM was obtained using Image Pro-Plus v6.0 and the fluorescence heterogeneity, *i.e.*, the fraction of pixels which have intensity higher or lower than the average plus or minus 10 %, respectively (or plus or minus the standard deviation – both calculations yield the same relative results when comparing proteins or strains). It reflects to which extent the fluorescence intensity is concentrated in specific pixels and is independent on the total fluorescence intensity. The heterogeneity was determined for the PM of each cell. For each transformed yeast strain, 4 independent experiments were performed, and more than 190 cells were analysed.

3.1.2.5. Azoles – Minimal inhibitory concentration determination

The following strains of *S. cerevisiae* were used: BY4741 (*wt*, ACC Y00000; MATa; his3Δ1; leu2Δ0; met15Δ0; ura3Δ0), *erg6*Δ (ACC Y00568; BY4741 isogenic with YML008c::kanMX4), W303 (*wt* towards AD1-8; MATα; leu2-3,112 trp1-1 can1-100 ura3-1 ade2-1 his3-11,15 AD1-8 (W303 isogenic with pdr1-3, ura3, his1, yor1Δ::hisG, snq2Δ::hisG, pdr5Δ::hisG, pdr10Δ::hisG, pdr11Δ::hisG, ycf1Δ::hisG, pdr3Δ::hisG, pdr15Δ::hisG). BY4741 and *erg6*Δ were acquired from EUROSCARF, Frankfurt, Germany; W303 and AD1-8 were kind gifts from Prof. A. Goffeau, Chaire Internationale Blaise Pascal, Lab. Genet. Mol., École Normale Supérieure, Paris, and Prof. M. Ghislain, Université Catholique de Louvain, Faculté des sciences Agronomiques, Louvain-la-Neuve, Belgium. Visible turbid overnight cultures of *S. cerevisiae* strains were prepared and diluted to $A_{600} \approx 0.1$ in fresh Yeast Extract – Peptone - Dextrose (YPD) medium. The cultures were transferred to 96 microtiter well plates containing aliquots of serially diluted antifungal drugs (Ke and its derivatives: KeP, KeOP, KeSP, KeSeP (Figure 9), prepared from DMSO stock solutions and drug-free controls. The yeast cultures

were statically incubated at 30 °C for 48 hours with compounds (Bojsen et al. 2014). The dose-response curves were analysed with GraphPad Prism 5 software (San Diego, USA) or a microplate reader ASYS UVM (Biogenet). All values presented are the mean of at least three independent experiments.

3.2. Fluorescence spectroscopy measurements in Neurospora crassa and Saccharomyces cerevisiae

N. crassa wt at 1.5×10^7 cell/mL were grown in liquid MMV and/or in liquid SeM for 2 and 5 h at 30 °C and 150 rpm. Cells were washed twice by centrifugation at 10,000 *g* for 2 min and resuspended in 10 mM PBS pH 7.4. *Slime* strain was grown in liquid SeM at 10^7 cells/mL at 30 °C and 150 rpm for 2 or 5 h. The washing procedure was the same as for *wt* strain, except that the rate of centrifugation was reduced to 7,500 *g*.

The fluorescence probes (*t*-PnA and DPH (2 μM), di-4-ANEPPS (1 μM)) were added to the cells and incubated for 10 min (unless otherwise stated) in a heating block at 30 °C. The same labelling conditions were applied to the cell wall and membrane-enriched fractions obtained through the procedure described in the previous section.

For fluorescence measurements in *S. cerevisiae wt*, harvested cells were washed twice at 2,700 *g* with sterile water and then suspended in 100 mM NaH_2PO_4, 100 mM NaCl, 1 mM EDTA, pH 7.4 to a final cell concentration of 2.43×10^7 cell/mL (A_{600} = 0.826). The probe *t*-PnA was added to a final concentration of 2 μM and incubated for 5 min (Aresta-Branco et al. 2011), at 30 °C, and di-4-ANEPPS was added to a final concentration of 1 μM and incubated at 24 °C for 10 min.

Both steady-state and time-resolved fluorescence measurements were performed with a Horiba Jobin-Yvon Spex Fluorolog 3.22, at 30 °C in a temperature-controlled sample compartment under magnetic stirring. For *N. crassa* steady-state anisotropy measurements, the excitation and emission wavelengths were 320 nm and 404 nm for *t*-PnA, 360 nm and 425 nm for DPH, and 486 nm and 634 nm for di-4-ANEPPS. The slits used in spectra acquisition were 2 nm for *t*-PnA and DPH, and 4 nm for di-4-ANEPPS. For *S. cerevisiae* steady-state anisotropy measurements, the excitation and emission wavelengths were also 320 and 404 nm for *t*-PnA, and 475 and 613 nm for di-4-ANEPPS. The slits used in spectra acquisition were 2 nm for *t*-

PnA, and 4 nm for di-4-ANEPPS. An adequate blank, with the addition of the solvent without the probe in study, was subtracted from each intensity reading.

The membrane dipole potential was measured through the excitation ratio intensities at 420 nm and 520 nm of di-4-ANEPPS with emission at 635 nm for *N. crassa*. Starke and Peterkovic found that this ratio and the membrane dipole potential had an approximately linear relationship (Starke-Peterkovic et al. 2005). The R_{ex} can be linearly related with the membrane dipole potential under the conditions met in the study described in Chapter V (Loew 1996, Clarke and Kane 1997, Vitha and Clarke 2007, Haldar et al. 2012), hence the excitation spectra were acquired with the emission wavelength of 635 nm, which is in the red edge of the spectrum, allowing to rule out the membrane fluidity effects, and as referred in Chapter V there were no shifts observed in the spectra upon the STS challenge. Thus, the dipole potential (ψ_d) in mV was calculated from R_{ex} using the linear relationship corrected for our conditions described by Equation 7,

$$\psi_d/mV = 154.19.\, R_{ex} + 68.705$$

Equation 7

following a procedure analogous to the one found in (de Matos et al. 2021).
This relation was obtained using the data from mixtures of POPC/cholesterol and POPC/ergosterol, in the same conditions of the known ψ_d/mV (Haldar et al. 2012, Khmelinskaia et al. 2020).

The slits for anisotropy measurements were 4 nm for *t*-PnA and DPH and 8 nm for di-4-ANEPPS. An adequate blank, with the addition of the solvent without the probe in study, was subtracted from each intensity reading.

For time-resolved measurements by the single photon counting technique, a nanoLED N-320 was used for excitation of *t*-PnA, and emission wavelength was 404 nm; nanoLED N-370 plus a UGI-370 band pass filter was used for the excitation of DPH, and emission wavelength was set to 450 nm; nanoLED N-460 was used for the excitation of di-4-ANEPPS, and emission detected at 634 nm and 613 nm, for *N. crassa* and *S. cerevisiae*, respectively. Ludox® was used as the scatterer to obtain the instrumental response function. An adequate blank, with the addition of the solvent without the probe in study, was performed and measured as described below. The program TRFA data processor version 1.4 (Minsk, Belarus) was used for the analysis of the experimental fluorescence decays. Regarding *N. crassa*, the time scales

used were 0.1114129 ns/channel for *t*-PnA and 0.055517 ns/channel for both DPH and di-4-ANEPPS. The sample decays were always acquired first, with 20,000 counts on the peak channel, and afterwards the blank decays were acquired with the same accumulation time used for the sample. The prompt (scatter) was acquired with 50,000 counts on the peak channel, at the end of each replicate (sample and respective blank). In the case of *S. cerevisiae*, the time scale used for *t*-PnA was of 0.2231209 ns/channel and for di-4-ANEPPS the time scale was the same as for *N. crassa*. The total number of channels that Horiba Jobin-Yvon Spex Fluorolog 3.22 allowed were 1024 channels. In the specific case of *t*-PnA labelling *S. cerevisiae* cells, a global analysis method was applied to completely separate probe emission from the autofluorescence of the cells (Aresta-Branco et al. 2011). The details of this global analysis method can be found in (Bastos et al. 2012a). The quality of the fit was judged by a reduced χ^2 value close to 1 and random distribution of weighted residuals and residuals autocorrelation (see Figure 14 for an example).

3.3. Statistical analysis

The results are presented as mean ± standard deviation (S.D.), unless stated otherwise, and the sample dimension and number of biologically independent replicates are given with the results. The statistical significance was determined using Student's *t*-test. Mean values were considered significantly different for *p* values below or equal to 0.05. For multiple comparisons, the Bonferroni correction was taken in consideration.

CHAPTER IV – REORGANIZATION OF PLASMA MEMBRANE LIPID DOMAINS DURING CONIDIAL GERMINATION

N. crassa, a filamentous fungus, in the unicellular conidial stage has ideal features to study SLEDs, which are implicated in fundamental cellular processes ranging from antifungal resistance to apoptosis. Several changes in lipid metabolism and in the membrane composition of *N. crassa* occur during spore germination. However, the biophysical impact of those changes was unknown. Thus, a biophysical study of *N. crassa* PM, particularly SLEDs, and their dynamics along conidial germination is prompted.

Two *N. crassa* strains, *wt* and *slime*, which is devoid of cell wall, were studied. Conidial growth of *N. crassa wt* from a dormancy state to an exponential phase was accompanied by membrane reorganization, namely an increase of membrane fluidity, occurring faster in a supplemented medium (SeM) than in Vogel's minimal medium (MMV). Gel-like domains, likely enriched in SLs, were found in both *N. crassa* strains, but were particularly compact, rigid and abundant in the case of *slime* cells, even more than in budding yeast *S. cerevisiae wt*. In *N. crassa*, our results suggest that the melting of SLEDs occurs near growth temperature (30°C) for *wt*, but at higher temperatures for *slime*. Regarding biophysical properties strongly affected by ergosterol, the PM of *slime* conidia lays in between those of *N. crassa wt* and *S. cerevisiae wt* cells. The differences in biophysical properties found in this work, and the relationships established between membrane lipid composition and dynamics, give new insights about the PM organization and structure of *N. crassa* strains during conidial growth.

4.1. Results

4.1.1. *Neurospora crassa wt* and *slime* cells growth profile

In order to characterize the growth behaviour under the conditions used for the ensuing biophysical studies, *N. crassa wt* conidia was grown in liquid MMV and liquid SeM and *slime* conidia was grown in liquid SeM, as shown in Figure 19. The growth curves showed the usual behaviour comprising a latency (*lag*) phase of ca. 6 h, with similar duration for all the conditions tested, followed by an exponential (*log*) phase of growth.

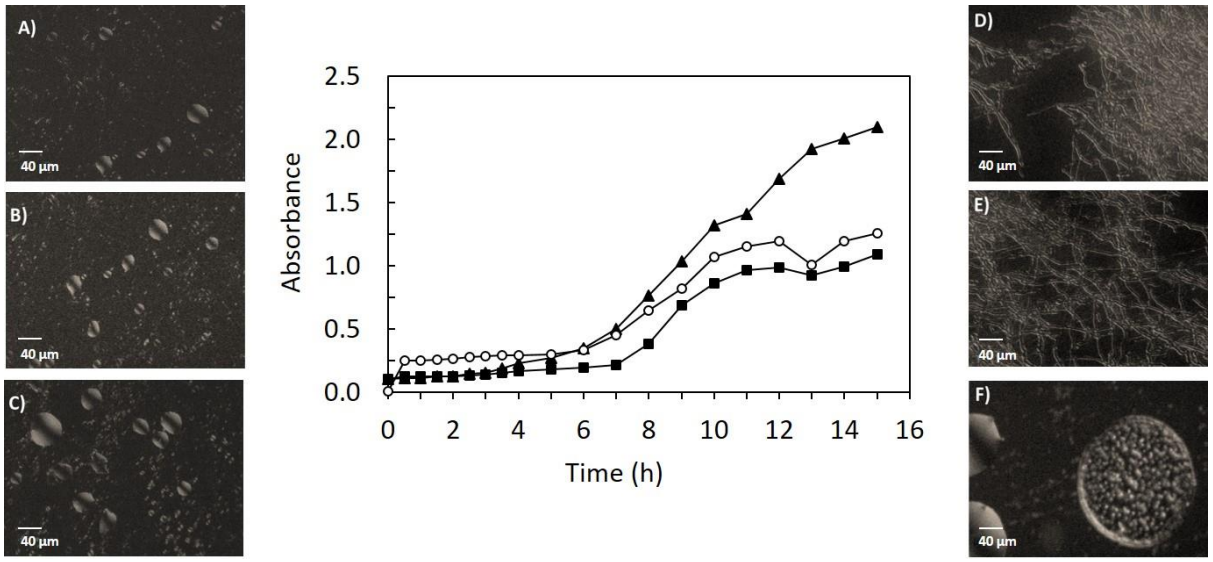

Figure 19 - Central panel: the growth profiles at 30 °C of N. crassa wt in MMV (circle), wt in SeM (square) and slime strain in SeM (triangle) obtained from absorbance at 690 nm, n ≥ 3 (according to Materials and Methods, Chapter III). Left and right panels: transmission microscopy images for N. crassa wt and slime cells at different phases of growth. wt cells in MMV at 5 h (A) and 12 h (D) of growth; wt cells in SeM at 5 h (B) and 12 h (E) of growth; slime cells at 5 h (C) and 12 h (F) growth, with a magnification of 100×.

In SeM, *N. crassa wt* cells have a generation time of 1.462 ± 0.008 h, growing more rapidly than *slime* cells which have a generation time of 2.04 ± 0.35 h. *Wt* cells in MMV grow much slower than in SeM, with a generation time of 2.46 ± 0.18 h, probably due to the richer composition of SeM. The slower growth obtained for *slime* cells is probably due to their different organization when compared to *wt* cells, as *slime* grow with spherical shape and micronuclei, as could be observed from (Figure 19C, F), in agreement with previous reports (Scarborough 1985). These observations led us to develop further experiments in the *lag* phase, because the conidial organization (Figure 19A, B, C) at this stage should be more similar for both *wt* and *slime*, minimizing any interference due to mycelium formation (Figure 19D, E).

4.1.2. Labelling of *Neurospora crassa* conidia membrane with *t*-PnA and di-4-ANEPPS

4.1.2.1. Influence of the cell wall on the photophysical parameters of the probes

Starting with a *wt* conidial suspension, two fractions were separated by centrifugation, one enriched in cell wall (plus nuclei) and the other one enriched in the other cellular membranes (including PM) (Bowman and Bowman 2007). We found that the fluorescence

anisotropy of the probes in the membrane-enriched fraction was similar to the one measured in *wt* intact conidial suspensions, *i.e.*, a high value of ~0.30 typical of ordered domains, whereas in the cell wall-enriched fraction the fluorescence anisotropy of the probe was much lower, close to zero in the case of *t*-PnA (Figure 20).

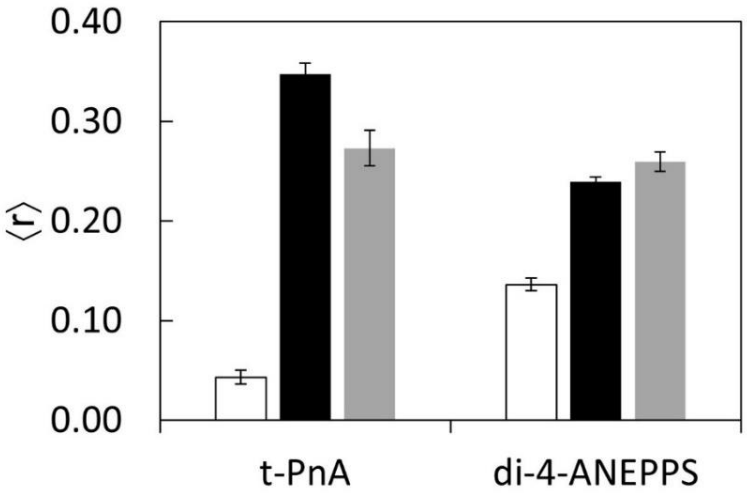

Figure 20 – The influence of the cell wall on the photophysical parameters of the probes labelling the membrane of N. crassa conidia is negligible. Steady-state fluorescence anisotropy of t-PnA and di-4-ANEPPS in two cellular sub-fractions of N. crassa wt conidia grown in MMV for 5 h at 30 ℃. Pellet, cell wall-enriched fraction (white); Supernatant, membrane-enriched fraction (black), wt intact conidial suspensions (grey), after incubation with probes for 10 minutes, at 30 ℃. The values are the mean ± S.D. of at least three independent experiments, n ≥ 3.

4.1.2.2. Time evolution of fluorescence parameters of the probes upon addition to Neurospora crassa conidial suspensions

The results concerning kinetics of probe incorporation showed a similar kinetic behaviour in *wt* and *slime* strains, Figure 21A. The initial rates were slightly faster for germination times of 5 h as compared to 2 h. After 10 minutes of probe incorporation, the kinetic curves for the cultures with 5 h germination overlap with those obtained for the 2 h germination cultures and reached a plateau. Thus, this was considered the optimal probe incorporation time, for which there is neither an influence of an eventual difference in the dynamics of endocytic processes nor a significant probe distribution among intracellular membranes, because if this took place, it would have led to more complex incorporation

kinetics. The information retrieved from Figure 21A was then taken into consideration for the following experiments.

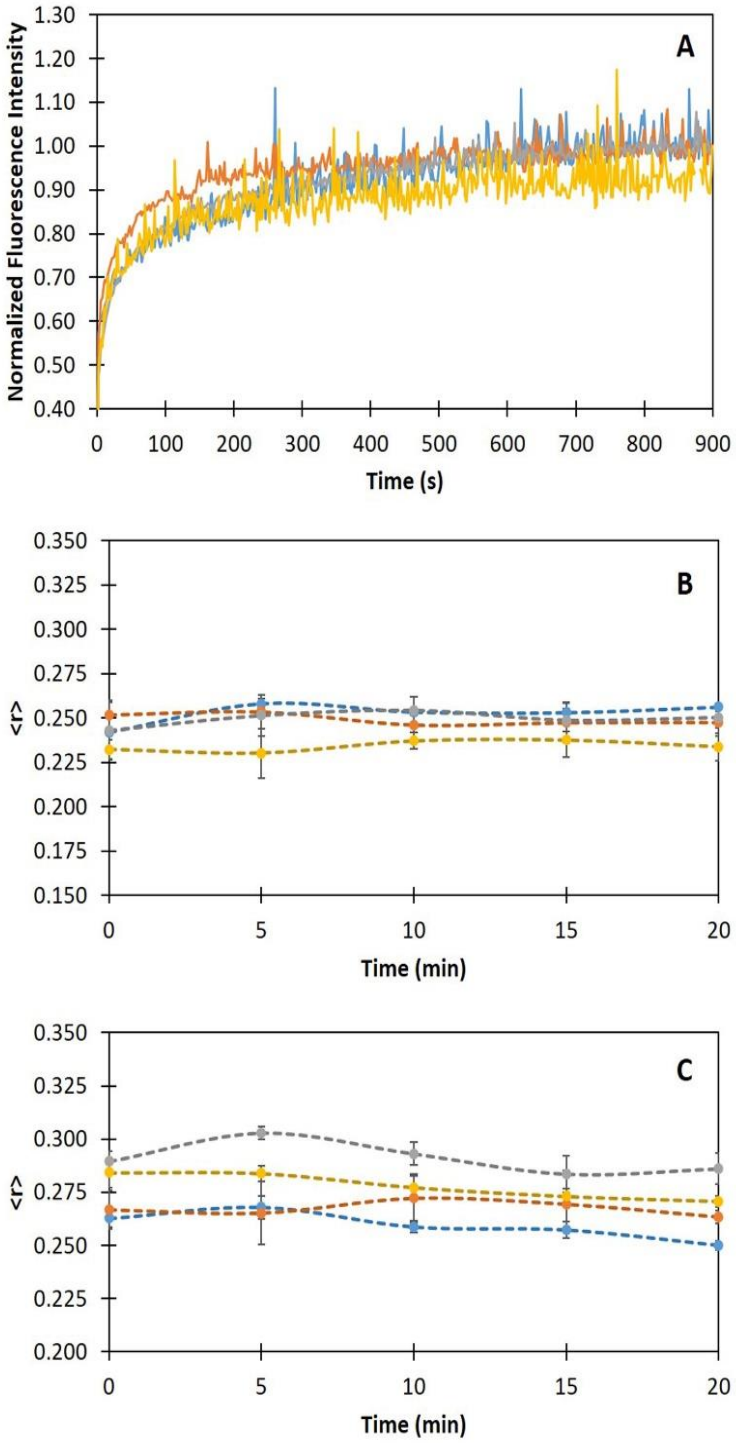

Figure 21 – Time evolution of fluorescence parameters of the probes upon addition to N. crassa conidial suspensions (A) Incorporation kinetics of di-4-ANEPPS; (B) Steady-state fluorescence anisotropy of di-4-ANEPPS and (C) t-PnA, incubation time (0 – 20 min.) at 30 ℃. Strain and germination time: slime 2 h (blue) and slime 5 h (orange) in SeM; wt 2 h (grey) and wt 5 h (yellow) in MMV. The values are the mean ± S.D. of at least three independent experiments, n ≥ 3. The lines in (B) and (C) are merely to guide the eye.

The fluorescence anisotropy of both di-4-ANEPPS and *t*-PnA display a high initial value, measured immediately after probe addition, and therefore corresponds to probe located in the PM. This value does not suffer significant changes with time (0 – 20 minutes, Figure 21B and C) and is comparable with the one obtained afterwards for the membrane and presented in the results ahead, hence confirming that the probes are reporting mainly the PM properties.

4.1.3. Establishing *Neurospora crassa* plasma membrane biophysical properties using fluorescence spectroscopy

The biophysical properties of *N. crassa* PM were studied using the fluorescence probes *t*-PnA, DPH and di-4-ANEPPS, to retrieve complementary information on membrane biophysical properties, in order to obtain a comprehensive characterization of lipid domains. The results below are usually presented in the order *slime* (SeM) – black, *wt* (SeM) – grey, *wt* (MMV) – white, to facilitate comparison between the two strains grown in the same medium, and between the *wt* grown in MMV with *wt* grown in SeM.

4.1.3.1. The plasma membrane of Neurospora crassa contains sphingolipid-enriched highly ordered domains

The PM of *N. crassa wt* cells grown in SeM and MMV media, and of *slime* cells grown in SeM were labelled with *t*-PnA, and the fluorescence intensity decay of the probe was obtained (Figure 22). A long lifetime component of *t*-PnA of about 25 ns was found for *wt* cells at 2 and 5 h growth in both culture media, while for *slime* cells this lifetime component reached a value of ca. 39 ns (Figure 22A). The long lifetime component of *t*-PnA can be used to identify the ordered phase, which can be assigned to a gel (solid ordered) phase when longer than 30 ns (Aresta-Branco et al. 2011, Bastos et al. 2012a, Vecer et al. 2014). When between 20 and 30 ns, it is usually attributed to the presence of a l_o phase, but this criterion was established based on results of model systems most of which performed at room temperature, *i.e.* 23 ± 2 °C (de Almeida et al. 2009). Therefore, in the case of the PM of *slime* cells it can be inferred that gel

domains are present. This gel lipid phase is not commonly found in living cells (de Almeida and Joly 2014), especially in eukaryotic cells, under physiological conditions (usually taken as the optimal growth temperature, ca. 28–30 °C for *N. crassa* and *S. cerevisiae*). The amplitude of this lifetime component was larger than 10 % (Figure 22C), and the contribution to the total fluorescence intensity decay was very significant, yielding a long mean fluorescence lifetime value of ~25 ns (Figure 22D), which is among the longest found in living cells labelled with *t*-PnA (Aresta-Branco et al. 2011, Bastos et al. 2012a).

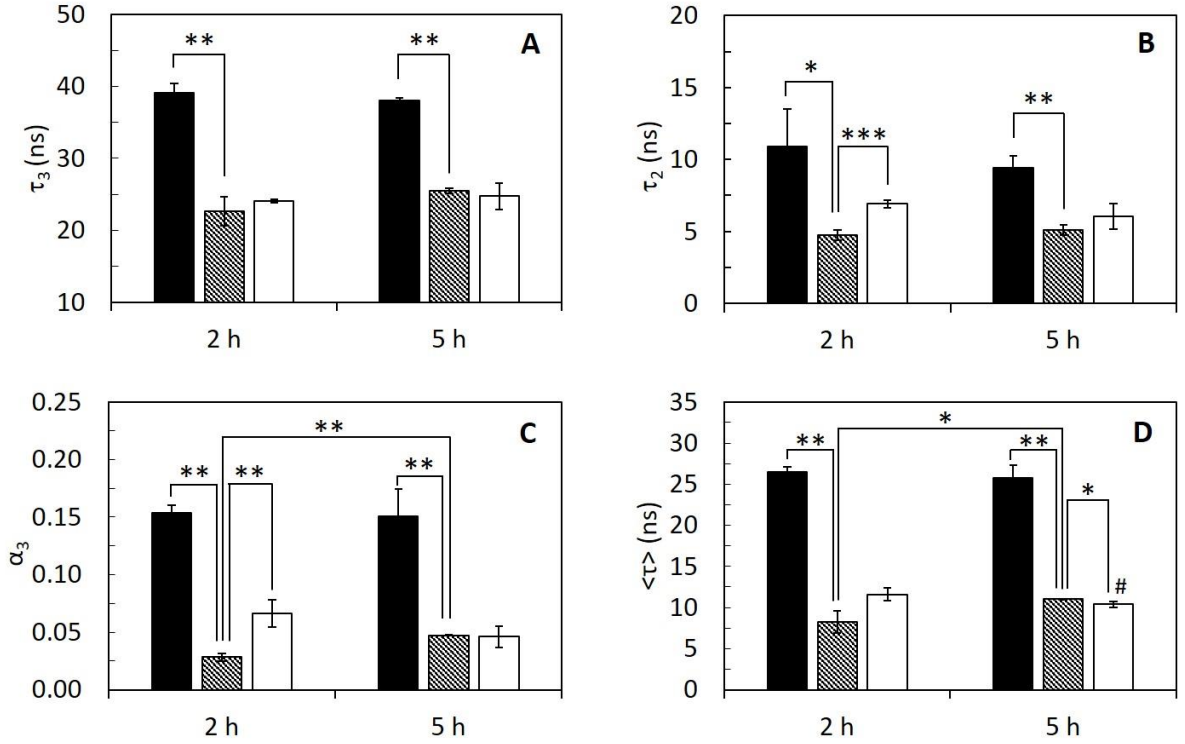

Figure 22 - Time-resolved fluorescence spectroscopic parameters of t-PnA in the PM of N. crassa conidia at 30 °C. (A) The long lifetime component, τ_3, (B)medium lifetime component, τ_2, (C) normalized amplitude of the long component, α_3, and (D) mean fluorescence lifetime, ⟨τ⟩, of t-PnA were obtained from the fluorescence intensity decay of the probe at 30 °C. Slime cells (black), wt in SeM (grey pattern) and wt in MMV (white). The values are the mean ± S.D. of at least three independent experiments, n ≥ 3 (according to Materials and Methods, Chapter III). $^{\#}p < 0.05$ vs. wt in MMV 2 h; $^{*}p < 0.05$; $^{**}p < 0.01$; $^{***}p < 0.001$.

Regarding *wt* cells, the long lifetime component of *t*-PnA obtained was much shorter than that in *slime* cells and its amplitude was clearly below 10 %. Thus, the mean fluorescence lifetime of *t*-PnA in *wt* cells was between one half and one third of the one observed for *slime* cells. This difference is in agreement with the different SL profiles reported for these two strains, namely that the PM of *wt* cells is rich in the SL $(IP)_2C$, whereas that of *slime* cells has

a higher amount of another SL, probably IPC (Lester et al. 1974), which having a smaller headgroup allows a tighter packing of lipid acyl chains. Although all the fluorescent dyes used in this study are lipophilic and well-established as *bona fide* membrane probes, the control experiments described in the beginning of this chapter show that the probes do not display significant interaction with the cell-wall that could contribute to the differences observed between *slime* and *wt* cells.

Although the nature of the ordered domain in *wt* conidia is less obvious than in *slime*, an important fact should be considered, *wt* conidia have very low/undetectable ergosterol levels (Bianchi and Turian 1967). Later in this work (section 4.1.3.3), experimental evidence supporting the lack of ergosterol in *N. crassa wt* conidial membrane will be shown. Thus, it should not be possible to encounter sterol-enriched l_o domains in the PM of these cells. The most likely interpretation for this result is the presence of domains which are close to their transition temperature, *i.e.*, either fluid phase domains/heterogeneities (Bunge et al. 2008) still retaining considerable order or density fluctuations which are known to persist or increase in intensity and frequency close to the gel/fluid transition temperature (de Almeida and Joly 2014), or gel domains but with a lower compactness than the typical gel phase formed by a saturated phospholipid in model systems. It is also important to note that the presence of membrane proteins can reduce the maximum packing of the lipid acyl chain. In such a crowded environment, the long lifetime component of *t*-PnA may be shortened even in highly ordered membrane regions (Aresta-Branco et al. 2011, Bagulho et al. 2015).

For *S. cerevisiae wt* cells at 30 °C, all the parameters obtained from the fluorescence intensity decay of *t*-PnA (Table 3) were higher than those obtained for *N. crassa wt* cells, namely the long lifetime component which was about 38 ns for *S. cerevisiae wt* cells and 26.5 ns for *N. crassa wt* cells. This difference in the long lifetime component of *t*-PnA may be explained, at least in part, by the fact that the prevailing acyl chains in inositol-based SLs are 24:0-OH and 22:0-OH for *N. crassa wt* cells (Lester et al. 1974), *i.e.* slightly shorter than for *S. cerevisiae wt* cells (26:0-OH) (Dickson and Lester 2002, Dickson 2008, Pedroso et al. 2009). When comparing *slime* cells with *S. cerevisiae wt* cells, however, the situation is reversed, *i.e.*, the long lifetime component of *t*-PnA obtained for the PM of *slime* cells (~39 ns) is similar to the one found for the budding yeast, and the mean fluorescence lifetimes are also quite comparable (25.8 ± 1.6 ns and 26.7 ± 1.2 ns, respectively).

Table 3 - Fluorescence spectroscopy parameters of t-PnA and di-4-ANEPPS in S. cerevisiae after a 5 h growth (mid-exponential phase) (Santos et al. 2017).

Probes	α_1	τ_1 (ns)	α_2	τ_2 (ns)	α_3	τ_3 (ns)	α_4	τ_4 (ns)	τ_{av} (ns)	$\langle\tau\rangle$ (ns)	$\langle r\rangle$	λ_{max} (nm)
***t*-PnA**	0.20 ± 0.06	1.11 ± 0.25	0.50 ± 0.03	4.61 ± 0.21	0.13 ± 0.03	16.48 ± 2.38	0.15 ± 0.04	38.13 ± 1.11	10.10 ± 0.50	26.60 ± 1.20	0.285 ± 0.009	404 ± 1
di-4-ANEPPS	0.31 ± 0.05	0.46 ± 0.13	0.51 ± 0.09	2.13 ± 0.19	0.18 ± 0.06	3.71 ± 0.38	-	-	1.88 ± 0.18	2.55 ± 0.06	0.294 ± 0.001	613 ± 5

Previously, we have suggested that the main SL component of the highly ordered gel domains in *S. cerevisiae* could be IPC (Aresta-Branco et al. 2011), due to the high gel/fluid transition temperature reported for this lipid (Bjorkbom et al. 2010, Klose et al. 2010). This hypothesis is further sustained by the previous suggestion in this work that the putative IPC-enrichment of the PM of *slime* cells could explain the longer fluorescence lifetime of *t*-PnA in this mutant strain as compared to *N. crassa wt*.

The steady-state fluorescence anisotropy of *t*-PnA was also determined in *N. crassa wt* and *slime* cells (Figure 23). In this case, the behaviour of *N. crassa* cells in all conditions tested was similar, and the values were quite high and close to 0.3 especially for 2 h of growth. Such high values corroborate the existence of a significant fraction of highly-ordered membrane domains which seemed to decrease from 2 h to 5 h of growth. The major differences were observed for *slime* and *wt* cells in SeM, and were, in fact, significant for the latter. However, in the case of *slime* neither the long fluorescence lifetime component nor the amplitude changed significantly between 2 h and 5 h, and in the case of *wt* cells grown in SeM they increased, in contrast with the fluorescence anisotropy. This indicates that growth time and medium may lead to the appearance of different types of ordered domains, and in fact it is known that growth conditions can affect the phospholipid composition of *N. crassa* (Hubbard and Brody 1975).

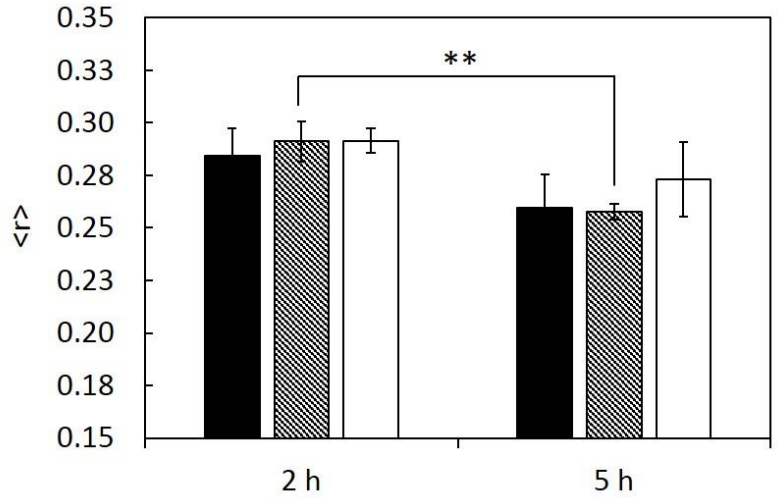

*Figure 23 - The t-PnA steady-state fluorescence anisotropy in the PM of N. crassa conidia at 30 ºC. Slime cells (black), wt in SeM (grey pattern) and wt in MMV (white). The values are the mean ± S.D. of at least three independent experiments, n ≥ 3 (according to Materials and Methods, Chapter III). **p <0.01.*

Despite the much shorter values of the long lifetime component of *t*-PnA in *N. crassa wt* cells when compared to *slime* cells (Figure 22A), the anisotropy values were similar in all situations and very close to 0.3, which is a value typical of gel or solid ordered phases (de Almeida et al. 2003, Marques et al. 2015). Hence, the fluorescence anisotropy results favour the assignment of *t*-PnA long lifetime component in *wt* cells also to SL-enriched gel-like domains. In this case the values found were identical to those obtained for *S. cerevisiae wt* cells at 30 °C (Table 3).

For a binary mixture of POPC/Phytoceramide (PhyCer), corresponding to a PhyCer mole fraction of 65 % the maximum fluorescence anisotropy value obtained was ~0.25 at 30 °C (Marques et al. 2015). For this composition, the bilayer is made mostly of highly ordered and tightly packed POPC/PhyCer complexes. This value of fluorescence anisotropy obtained in a model system is lower than in the PM of living *N. crassa wt* and *slime* cells probed in the present work, which points again to the existence of gel-like ordered domains. In addition, the POPC/PhyCer binary system fails to completely mimic the biophysical properties of those domains in *N. crassa*. Interestingly, the fluorescence anisotropy values found at 24 °C for living *S. cerevisiae* cells are much more similar to the maximum value obtained in the POPC/PhyCer binary mixture at this temperature, indicating that the gel domains in fungi are more thermally stable than the PhyCer domains characterized in (Marques et al. 2015), probably due to the presence of SLs with higher transition temperature, such as IPC (Bjorkbom et al. 2010, Klose et al. 2010).

4.1.3.2. Global fluidity of Neurospora crassa plasma membrane

In order to understand the whole cell membrane behaviour, *N. crassa* cells were also labelled with DPH, a probe that is sensitive to membrane global properties, rather than to a particular kind of domain. As can be seen in Figure 24, the steady-state anisotropy of DPH was smaller in *slime* cells until 5 h of growth, when compared with *wt* cells. Thus, for *slime* cells much higher fluorescence anisotropy for *t*-PnA than for DPH (Figure 23 and Figure 24), *i.e.*, a behaviour typical of the presence of a gel phase, was observed. This happens because, even in presence of a small amount of gel domains, due to its preferential partition and increased quantum yield in this phase, most of *t*-PnA emission arises from the probe being located in such domains, with a typical fluorescence anisotropy ≥ 0.3. In the case of DPH, however, most of the probe will also be located in other domains which when comprising the majority of the membrane, are responsible for a marked decrease of DPH anisotropy. The steady-state anisotropy of DPH for *wt* cells in SeM showed the same trend of variation as the one observed for the anisotropy of *t*-PnA, *i.e.*, a decrease with incubation time, although the effect was much more pronounced for DPH, and again opposite to the one observed for *t*-PnA mean fluorescence lifetime. This is consistent with the known distribution of the probes among ordered and disordered domains (de Almeida et al. 2009). If the global fluidity of the membrane increases, *e.g.*, by raising the unsaturation degree of glycerophospholipids, from 0 to 5 h of growth, and new gel domains are being formed, this can explain the 12 % decrease in *t*-PnA fluorescence anisotropy, and the 30 % decrease found for DPH fluorescence anisotropy. In fact, this difference obtained for *wt* cells in SeM at 5 h growth is a strong indication of the presence of a small amount of gel domains.

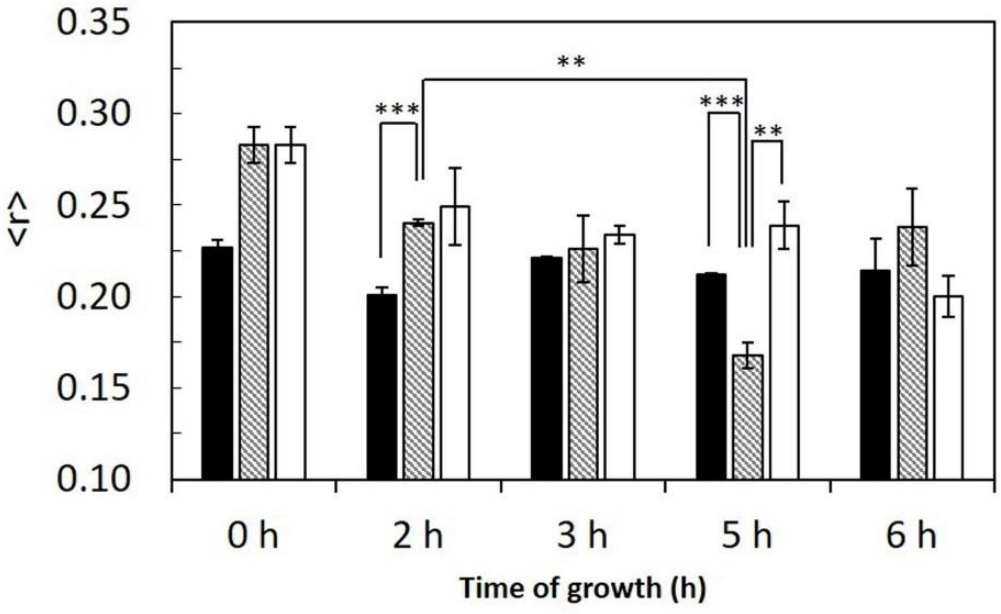

*Figure 24 - Global order of the cell membrane system of N. crassa strains assessed through the steady-state fluorescence anisotropy of DPH at 30 ºC. The linear correlation coefficient of ⟨r⟩ as a function of time for the slime strain is only R^2 = 0.192 but for wt in MMV is R^2 = 0.839 and for wt in SeM (0 – 5 h) is R^2 = 0.985. To obtain the anisotropy values for t = 0 h, conidia stored in sterile water at 4 ºC were resuspended in PBS at 30 ºC and immediately labelled with DPH as described for the other samples. Slime cells (black), wt in SeM (grey pattern) and wt in MMV (white). The values are the mean ± S.D. of at least three independent experiments, n ≥ 3 (according to Materials and Methods, Chapter III). **p <0.01; ***p <0.001.*

In the case of *wt* cells in MMV, the changes observed for consecutive growth culture times are smaller, as for the parameters presented above for *t*-PnA. However, the value for 6 h growth is clearly different from that obtained for 2 h growth and there is a reasonable degree of correlation, *i.e.*, it is clear that also in MMV, the membrane fluidity is increasing, although at a slower rate than in the richer medium, SeM. This is probably due to a higher proportion of polyunsaturated fatty acids acylating glycerophospholipids, as suggested above. Such effect was observed in germinating *N. crassa* ascospores, where saturated 18:0 and 16:0 acyl chains are progressively replaced with polyunsaturated ones, namely 18:2 and 18:3, whereas the monounsaturated 18:1 remains practically unchanged during the first 6 h of germination (Goodrich-Tanrikulu et al. 1998).

The steady-state fluorescence anisotropy of DPH incorporated into *S. cerevisiae wt* membranes has been measured in several laboratories, under different conditions, including different temperatures (Folmer et al. 2008, Córcoles-Sáez et al. 2016). The values are always much lower than those here presented for the *N. crassa wt* cells, even when measured at 24 °C. DPH anisotropy in *S. cerevisiae wt* cells, in the mid-exponential and stationary phases of the

growth curve, was 0.146 ± 0.003 and 0.147 ± 0.003, respectively. Although still lower, these values are much closer to those measured in *N. crassa* for the *slime* than for the *wt* conidia, reflecting that the biophysical properties of the PM of *S. cerevisiae wt* are closer to those of the *slime* strain, as observed using *t*-PnA.

The PM of *N. crassa wt* cells growing in SeM undergoes a rearrangement involving an increase of the ordered domains (Figure 19C), concomitant with a higher membrane fluidization during growth (Figure 24). Concurrently, *slime* cells exhibit more rigid gel domains, yet the global fluidity of the membrane was smaller than *N. crassa wt* cells at 2 h growth but not at 5 h. When compared to *S. cerevisiae wt*, the gel domains in *N. crassa wt* are less rigid, but the global fluidity smaller. Previously, we have compared *S. cerevisiae* intact *wt* cells with several mutant strains, and with enzymatically generated cell-wall-less spheroplasts, and we also observed in every case the same reverse relation between global membrane order measured through DPH fluorescence anisotropy and the packing of the gel domains reported by *t*-PnA fluorescence lifetime (Aresta-Branco et al. 2011). To explain this, we put forward the hypothesis that a different organization of the lipids due to a more marked segregation of lipid rendered the gel domains more rigid, and the remainder of the membrane more SL-depleted and, therefore, more fluid. This PM reorganization may also be related with the asymmetry between outer and inner leaflets, since DPH will report both, whereas *t*-PnA reflects preferentially domains rich in SLs, which are mainly localized in the outer leaflet. In the case of *slime* cells, for example, cell-wall absence is possibly compensated through a more rigid membrane mostly in the outer leaflet, which could explain the larger difference between *t*-PnA and DPH anisotropy for shorter growth times (Figure 23, Figure 24).

4.1.3.3. Surface dipolar and hydration properties of the plasma membrane of Neurospora crassa

To further clarify the results above and obtain a more accurate picture of *N. crassa* PM, conidia cells were labelled with the probe, di-4-ANEPPS, that belongs to the class of potential sensitive (Loew 1996) naphtylstyryl dyes, recognizably responsive to ergosterol- and cholesterol-enriched lipid domains (Bastos et al. 2012b). The fluorescence parameters of di-4-ANEPPS depend, at least, on two inter-related factors, on ergosterol content and on the hydration of the membrane.

It has been consistently reported that *N. crassa* conidia contains a negligible amount of ergosterol, and that ergosterol is detected in significant amounts only when mycelium is formed (Bianchi and Turian 1967, Kushwaha et al. 1976, Renaud et al. 1978). As can be observed in Figure 25 (see also annex Table S 3), the emission of di-4-ANEPPS incorporated in the PM of *N. crassa wt* cells had its maximum at λ_{max} ~635 nm, pointing to a very small amount or even absence of ergosterol. In fact, in pure phospholipid bilayers either in the fluid 1,2-dioleoyl-*sn*-glycero-3-phosphocholine (DPPC) or in the gel phase, the λ_{max} is ca. 630 nm, and the presence of sterols shifts the value to shorter wavelengths (Bastos et al. 2012b). For *S. cerevisiae wt* cells the emission spectrum of di-4-ANEPPS had its maximum at 613 nm (Figure 25B). This value is consistent with the well-known presence of high levels of ergosterol in this organism (Gaspar et al. 2007, Ejsing et al. 2009, Pedroso et al. 2009, Klose et al. 2012) and, comparing with results in model systems, the same λ_{max} is observed for POPC with 20% mole fraction of ergosterol (Bastos et al. 2012b).

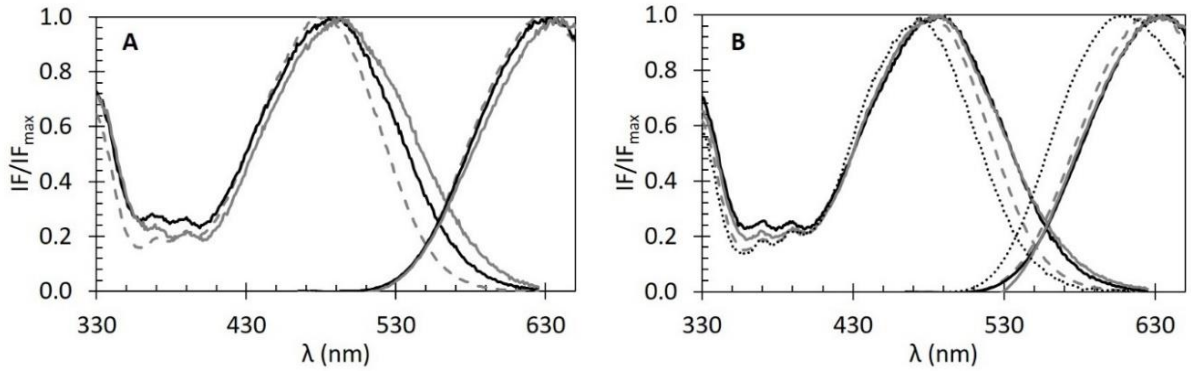

Figure 25 - Normalized excitation (λ_{em} = 635 nm) and emission spectra (λ_{exc} = 450 nm) of di-4-ANEPPS in N. crassa cells at 30 ºC after 2 h growth, wt in MMV (black line), wt in SeM (grey line), slime (grey dashed line) (A); N. crassa cells at 5 h growth, wt in MMV (black line), wt in SeM (grey line), slime (grey dashed line) and S. cerevisiae wt (black dotted line) (B). The represented spectra are the median of at least three independent experiments, n ≥ 3 (according to Materials and Methods, Chapter III).

There was a small red shift between *N. crassa wt* cells growing in MMV when compared to *wt* cells growing in SeM, more visible on the excitation spectra at 2 h growth than at 5 h growth. This shift is consistent with the very small levels of ergosterol previously found in *N. crassa wt* conidia germinated in MMV for 2 h (Bianchi and Turian 1967). Our results indicate that the PM of *N. crassa wt* has a slightly higher proportion of ergosterol at 2 h growth in SeM than in MMV. According to these results the minimum sterol seems to be attained in SeM at 2 h incubation, while it has been shown that this occurs latter in MMV (Bianchi and Turian 1967). This would also be in agreement with the faster growth rate in SeM. However,

there were no differences in the spectra obtained for *N. crassa wt* cells in both media at 5 h growth, which suggests a progression to a similar sterol profile. This is in agreement with the similar results obtained for the fluorescence intensity decay of *t*-PnA in *N. crassa wt* cells grown in MMV and SeM for 5 h (Figure 22), but is opposed with the variation observed for DPH fluorescence anisotropy (Figure 24), again pointing to the existence of different types of domains, rearranging during germination, and thus originating diverse trends for different fluorescence parameters and/or probes. However, a small blue shift between *N. crassa wt* cells in MMV and *slime* cells, occurred at both 2 h and 5 h growth. In this respect the PM of *slime* cells seems more alike that of *S. cerevisiae wt* cells (Figure 25B) than *N. crassa wt* cells, as also reported by *t*-PnA and DPH.

The ratio of the di-4-ANEPPS fluorescence intensity produced by excitation at 420 nm to that produced by excitation at 520 nm (IF_{420}/IF_{520}) is known to be, under certain circumstances, linearly related to the membrane dipole potential (Clarke and Kane 1997, Vitha and Clarke 2007). Although in our experiments these conditions were generally met (Wang 2012), we still prefer to restrict the discussion to a qualitative level, given the complexity of living organism membranes. Thus, the IF_{420}/IF_{520} ratio was calculated and is shown for *N. crassa* cells in different conditions (Figure 26). For *N. crassa wt* cells in SeM the IF_{420}/IF_{520} ratio increased between 2 h and 5 h of growth. In contrast, no changes in IF_{420}/IF_{520} were found for *N. crassa wt* cells in MMV or for *slime* cells. Still, the following comparisons are worth noting: in *N. crassa wt* cells in SeM at 2 h growth, IF_{420}/IF_{520} was ~23 % smaller, when compared with *N. crassa wt* cells growing in MMV; for *slime* cells at 2 h growth IF_{420}/IF_{520} was ~39 % higher when compared to *N. crassa wt* cells in SeM. When analysing only the results for 5 h growth, there were no differences in IF_{420}/IF_{520} between *N. crassa wt* cells growing in MMV and SeM, but IF_{420}/IF_{520} was still ~22% smaller than for *slime* cells. This is consistent with the information obtained directly through the observation of di-4-ANEPPS spectra, and *t*-PnA fluorescence.

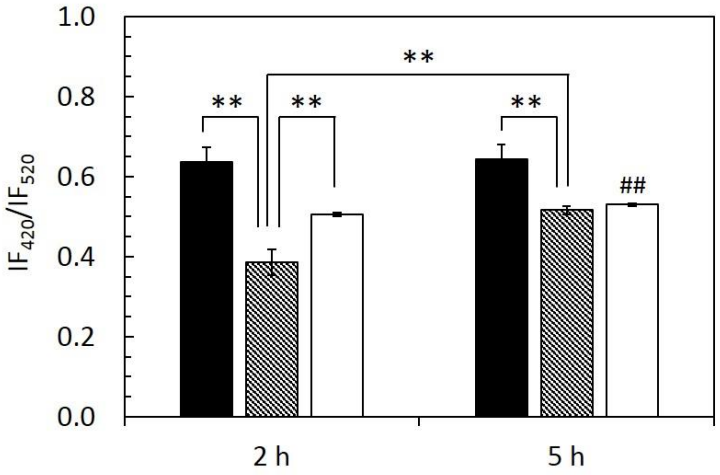

*Figure 26 - Ratio of di-4-ANEPPS fluorescence intensity produced by excitation at 420 nm to that produced by excitation at 520 nm, IF_{420}/IF_{520} in N. crassa cells at 30 ºC. Slime cells (black), wt in SeM (grey pattern) and wt in MMV (white). The values are the mean ± S.D. of at least three independent experiments, n ≥ 3 (according to Materials and Methods, Chapter III). **p <0.01; ## vs. wt in MMV 2 h.*

The low values observed for IF_{420}/IF_{520} in *N. crassa wt* conidia are consistent with very low levels of ergosterol, and with higher ergosterol content for *slime* strain. Even for this strain, IF_{420}/IF_{520} values, however, were still smaller than those found in *S. cerevisiae wt* cells for which an IF_{420}/IF_{520} of 0.93 ± 0.09 was obtained. Although, from studies in model systems, it is known that the ability of ergosterol to increase the membrane dipole potential is much lower than that of cholesterol, there is still a ~10 to 20% increase from POPC vesicles to POPC/ergosterol 3:2 vesicles (Haldar et al. 2012), and in DPPC bilayers, in the gel phase, with a lower value of IF_{420}/IF_{520} than POPC, ergosterol at the same molar ratio induces an increase in the membrane dipole potential of ca. 20-30% (Khmelinskaia et al. 2020). Noteworthy, is that in any of the biological systems addressed in the present work, the membrane dipole potential is smaller than in model systems containing cholesterol (Khmelinskaia et al. 2014), which is known to have much stronger effect on this biophysical parameter than ergosterol (Haldar et al. 2012).

The fluorescence intensity decay of di-4-ANEPPS was also measured. As can be seen in Figure 27A, the long lifetime component of di-4-ANEPPS in *N. crassa wt* cells in MMV was longer both after 2 and 5 h growth when compared to *N. crassa wt* cells in SeM, suggesting a lower degree of hydration for the former. For the *slime* cells the long lifetime component of di-4-ANEPPS was also longer than in *N. crassa wt* cells grown in SeM. From the observation of the mean fluorescence lifetime alone (Figure 27C), a considerable difference of ca. 24 % is

noted between *slime* cells and *wt* cells in SeM. At least two factors account for the variations in di-4-ANEPPS fluorescence lifetime, which are not completely independent. The presence of ergosterol *per se* increases the fluorescence lifetime, even when maintaining all other lipids constant, but also the bilayer hydration, dipolar relaxation and microviscosity contribute to the observed lifetime value. Altogether, the higher contribution of the long lifetime component for the fluorescence decay and longer mean fluorescence lifetime are consistent with the presence of higher levels of ergosterol and a more rigid membrane surface. This could be anticipated taking into account that this is a cell wall-less strain which would have somehow to rely solely on its PM as a barrier from the environmental conditions and their variations, in opposition to the cell walled *wt*. These fluorescence lifetime values also corroborate a lower hydration of the PM indicated by the blue shifted emission and the presence of more ordered domains (as reported by *t*-PnA) in *N. crassa slime* and *wt* conidia in SeM. This can be due either to the presence of SLs with smaller headgroup (Aresta-Branco et al. 2011), as already invoked in the case of *slime* cells to explain the much longer lifetime of *t*-PnA (Figure 19), or to a different PE/PC ratio, which is also known to increase *e.g.*, along conidial growth (Beck and Greenawalt 1977), because these phospholipids also have very different extents of hydration at the headgroup level. In PE/PC monolayers, an increase in PE proportions leads to larger values of the membrane dipole potential, (Lairion and Disalvo 2004) as observed for the *R* parameter of di-4-ANEPPS in *N. crassa wt* cells at 5 h growth vs. 2 h growth (Figure 26). A comparison of the fluorescence decay parameters obtained for *S. cerevisiae wt* cells (Table 3) with those obtained for *N. crassa wt* conidia (Figure 27), showed that, excluding the short component (~0.5 ns), all lifetime values obtained for *S. cerevisiae wt* cells, including the average lifetimes, are clearly longer, which confirms the absence of ergosterol in *N. crassa wt* conidia.

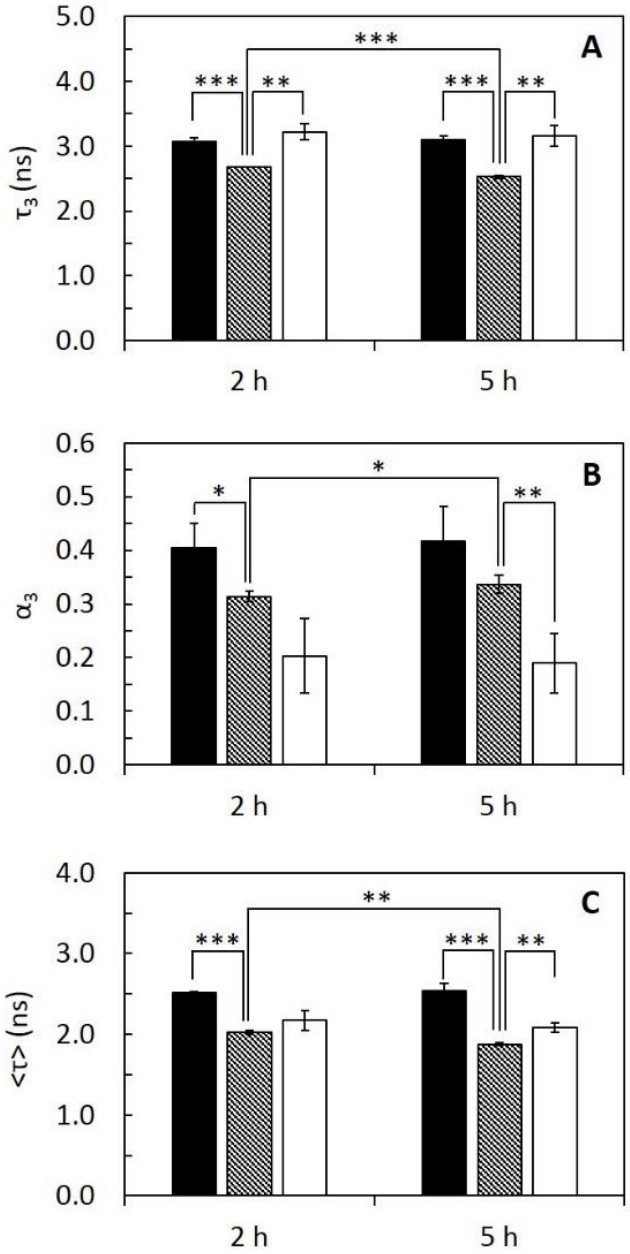

*Figure 27 - The long lifetime component (A), normalized amplitude (B) and mean fluorescence lifetime (C) of di-4-ANEPPS in N. crassa cells. Values were obtained from the fluorescence intensity decay of the probe at 30 ºC. Slime cells (black), wt in SeM (grey pattern) and wt in MMV (white). The values are the mean ± S.D. of at least three independent experiments, n ≥ 3 (according to Materials and Methods, Chapter III). *p < 0.05; **p < 0.01 and ***p < 0.001.*

The steady-state fluorescence anisotropy of di-4-ANEPPS (Figure 28) also pointed to a more fluid membrane at the membrane/water interface, when comparing *N. crassa wt* cells growing in SeM with *wt* cells in MMV, at both 2 h and 5 h growth, while for *slime* cells the results point to a lower membrane surface fluidity, as already reported by the results obtained with *t*-PnA and DPH. This further supports that the properties of the PM of *N. crassa* cells are

dependent on the growth media used and on the development of the conidia. The value for the steady-state fluorescence anisotropy of di-4-ANEPPS in *S. cerevisiae wt* cells was higher than the value obtained for *N. crassa* cells (Table 3), which also corroborates the low amount or even the absence of ergosterol in the PM of *N. crassa* conidia.

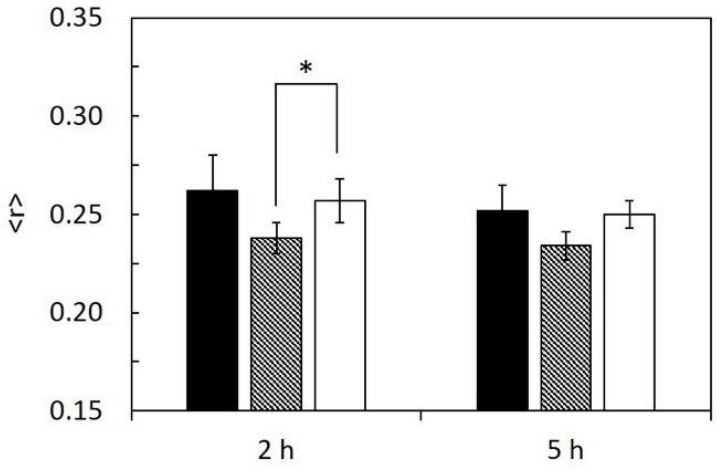

*Figure 28 - Steady-state fluorescence anisotropy of di-4-ANEPPS in N. crassa cells at 30 ºC. Slime cells (black), wt in SeM (grey pattern) and wt in MMV (white). The values are the mean ± S.D. of at least three independent experiments, n ≥ 3 (according to Materials and Methods, Chapter III). *p <0.05.*

4.2. Discussion

Understanding the biophysical properties of SLEDs is crucial, as it is known that the proper organization of this important lipid class is essential in several vital functions in eukaryotic cells. Filamentous fungi, such as *N. crassa* possess cerebrosides, and thus their composition in SLs shares similarities with both higher eukaryotes and pathogenic fungi (Gaspar et al. 2007, Ejsing et al. 2009, Klose et al. 2012). The characterization of lipid organization in fungi under different conditions *e.g.* growth media and growth phase may also be relevant in the context of antifungal therapies (Marquês et al. 2015). The work presented here is the first thorough characterization of *N. crassa wt* conidia PM biophysical properties. The only previous study that could be found was performed using *N. crassa* mycelium and was restricted to the use of a spin-probe in a single growth condition (Juretić 1977).

The trends of the several photophysical parameters of the different probes overtime and in the two-growth media, together with the known changes in SL composition of the PM, are globally interpreted in a consistent way, assigning the observed changes to PM domain

dynamics. However, it cannot be completely ruled-out that there may be an influence of inner membranes in the measured values, and that the differences encountered may be partially due to different rates of endocytosis. However, such influence, if existent, should be small compared to the other effects considered above, as explained in Figure 21. For the incubation times used in this study (5–10 min), endocytosis seems to occur to a negligible extent, in agreement with a study of endocytic processes in *N. crassa* conidia (Palma-Guerrero et al. 2009). In that study, the authors used the fluorescent marker FM4-64, which is specific for endocytosis due to its faster labelling of endosomes and belongs to the same chemical family of di-4-ANEPPS. Only after a period of 15 min, a clear but still incipient labelling of endosomes could be observed (Palma-Guerrero et al. 2009).

The studies here described were performed in *N. crassa wt* cells in different culture conditions, namely the growth media and growth phase, to evaluate how much the membrane biophysical properties of *N. crassa* are dynamic and relate with their cellular state. The growth rate and the generation time of *N. crassa* cells were determined to be faster for *slime* cells when compared with *wt* cells in both culture media. However, as previously described by other Authors, *slime* cells were not able to form hyphae and develop mycelium (Scarborough 1985). As *slime* cells grow, the PM radius of curvature increases, and their shape remains unchanged. In *N. crassa wt* cells, however, huge morphological changes take place during hyphae and mycelium formation (see *e.g.*, Figure 19) and cell shape suffers a transition from round to tubular, with a concomitant decrease in the PM radius of curvature in certain regions of the membrane that have to be highly curved to stabilize the non-round morphology of the cells. This is consistent with the fact that the PE/PC ratio increases during *N. crassa* conidial germination (Beck and Greenawalt 1977). In fact, the PE/PC ratio is considered an essential parameter in the maintenance of the optimal yeast PM curvature (de Kroon 2007). Regarding *N. crassa wt* cells only the richer medium, SeM, led to faster growth during the exponential phase. It is interesting to note that the duration of the latency state is similar for *N. crassa wt* cells in both media and to *slime* cells, but the metabolic changes taking place during this stage, at least those reflected directly on PM behaviour, are not entirely parallel.

The characterization of *N. crassa* membrane through the use of three membrane probes pertaining to different families of chromophores, commonly used due to their preferences for different parts of the membrane and sensitivity to changes in diverse biophysical properties was carried out in the *lag* phase (Figure 19). This was due to the importance of that growth phase/stage, in which there is a preparation of the conidia to the *log* phase, including a high

rate of membrane biogenesis well before morphological changes take place, *i.e.* prior to *wt* cells acquiring the mycelial structure (Beck and Greenawalt 1977).

The conidial growth of *N. crassa* from a dormancy state to a *log* phase was accompanied by membrane reorganization, namely an increase of membrane fluidity, which occurs more rapidly in SeM than in MMV. Concomitantly, most biophysical parameters determined for the PM were significantly different for *wt* cells in SeM between 2 h and 5 h growth, including the abundance of ordered domains reported by *t*-PnA (Figure 22; see also annex Table S 2 and Table S 3) or the surface polarity properties reported by di-4-ANEPPS (*e.g.*, Figure 26 and Figure 27). Noteworthy, most *t*-PnA fluorescence parameters were not significantly different between *N. crassa wt* conidia grown in SeM and in MMV, indicating that the PM ordered domains should be mainly attributed to the presence of SLs, *i.e.*, the lipids with high gel/fluid transition temperature, since the *wt* conidia grown in MMV are known to be essentially devoid of ergosterol (Bianchi and Turian 1967), and therefore unable to form l_o domains.

In this study *slime* cells were used, with two main aims, first to verify that in a general way the fluorescence properties of the probes used were sufficiently analogous so that any possible artifacts due to the presence of the cell wall could be excluded, as done previously in intact cells of *S. cerevisiae* vs. spheroplasts (Aresta-Branco et al. 2011), and second to explore which changes on the membrane biophysical properties could result from the absence of the cell wall. In general, although many significant differences were observed between the fluorescence properties of the probes in *N. crassa wt* and *slime* conidial suspensions, the overall range of parameters was not drastically different and falls well within the range retrieved for the PM of other cellular systems devoid of cell wall, including mammalian cells (Bastos et al. 2012a) and yeast spheroplasts (Aresta-Branco et al. 2011). Therefore, the fluorescence parameters of the probe were reporting the PM properties in both cell walled and cell wall-less cells. As stated above, the PM of *N. crassa wt* cells contains ordered domains but *slime* cells contain even more compact and ordered lipid domains, a fact that we could assign to the differences in SL composition reported for these two strains (Lester et al. 1974). In biological terms, it is reasonable to attribute those differences to an adaptation to the absence of cell wall in *slime* cells. The viability of the cell wall-less cells possibly relied on a more rigid and gel-like outer membrane surface, where most SLs are located, giving rise to the longer lifetime component obtained for *t*-PnA. Both *t*-PnA and DPH results strongly suggest that the lipids comprising the membrane of *N. crassa slime* cells have a very high mean transition temperature, when compared with *wt* cells and with model systems such as POPC/PhyCer

liposomes. In fact, as already discussed, the value of the long lifetime component of *t*-PnA, together with its anisotropy values (Figure 23) and the anisotropy values obtained for DPH (Figure 24) in *N. crassa wt* cells, all suggest the existence of a transition temperature for SL-rich domains near the growth temperature of 30 °C. To confirm that a gel/fluid transition occurs in the vicinity of growth temperature, we measured the long lifetime component of *t*-PnA at 26 °C and obtained values of 37.1 ns and 33.3, for 5 h and 2 h growth, respectively, clearly above the 30 ns threshold (see Annex Table S 5). Those lifetime values are also much longer than the one obtained at 30 °C (24.0 ns). Such drastic change in a narrow temperature range is a very strong indication of a neighbouring gel/l_d transition. Moreover, the values measured at 26 °C are quite similar to the ones obtained at 30 °C for *slime* conidia, and also for *S. cerevisiae wt* cells, where the existence of SL-enriched gel domains in its PM was previously established. To further confirm that there were no transitions involving l_o domains we also measured the fluorescence intensity decay of di-4-ANEPPS at 26 °C. In this case we obtained a long lifetime component of 3.09 ns (to compare with a value of 3.16 ± 0.16 ns measured at 30 °C). Contrary to *t*-PnA, which has a fluorescence behaviour very sensitive to the presence, packing and order of gel domains, di-4-ANEPPS is a probe that reports adequately on l_o domains. The invariance of its fluorescence lifetime (in opposition to *t*-PnA) is further evidence of the absence of l_o domains in *N. crassa* conidial membrane.

A comparison of biophysical properties of the PM *N. crassa* cells with *S. cerevisiae* cells, allowed to evaluate the impact of ergosterol concentration on PM properties. *S. cerevisiae wt* cells PM contains high levels of ergosterol which represents approximately 80 % of total sterols and an ergosterol/phospholipid molar ratio that may reach values close to 1 (Ejsing et al. 2009, Pedroso et al. 2009), while as already mentioned *N. crassa* conidia are practically devoid of ergosterol (Bianchi and Turian 1967). These differences were corroborated by di-4-ANEPPS maximum emission wavelength, that was ~613 nm for *S. cerevisiae wt* cells, while for *N. crassa wt* cells was ~635 nm (Figure 25). The global fluidity of the PM of *N. crassa* approaches that of *S. cerevisiae* as the growth time increases (Figure 24), which probably coincides with the appearance of significant amounts of ergosterol in the PM of *N. crassa*. The formation of l_o domains is triggered by the higher levels of ergosterol and a replacement of gel domains by more fluid, yet mechanically resistant, domains start occurring, decreasing the passive permeability, due to a higher thickness than that of disordered domains, and thus an ability to selective segregate lipids and proteins.

4.3. Conclusions

N. crassa wt conidial PM displays a main transition temperature very close to the optimal growth temperature, which is also known to happen in other organisms, such as bacteria (Stockton et al. 1975) or even in the case of human brain lipids (Ginsberg et al. 1993), reinforcing the notion that such may be a quite ubiquitous biophysical property of PM lipids (Mouritsen 2005).

This study also allowed to better understand the PM organization and structure of *N. crassa*, as well as to establish relationships between its lipid composition and its dynamics during conidial growth. With the results obtained it is possible to infer that the PM of both *N. crassa wt* and *slime* conidia has ordered SLEDs. These domains are different from those usually known as lipid rafts, since they cannot be enriched in ergosterol, which in *N. crassa* cells is present in very low amounts during most of the conidial stage. It could also be determined that the absence of ergosterol had a profound impact on membrane properties, as the gel-like nature of those domains led to a higher global membrane order when compared to the PM of *S. cerevisiae* cells, which contains a large fraction of l_o-like ergosterol-enriched domains. The absence of ergosterol was also responsible for a very low membrane dipole potential in *N. crassa* conidia. The absence of cell wall in *slime* strain led to concomitant peculiarities in its PM that could be related to its impaired development, keeping conidial-type morphology, and had a curious parallel with the biophysical properties of the PM of *S. cerevisiae*, which does not form hyphae and mycelium as well.

Finally, this work paves the way for future studies using *N. crassa* to address the modes of action of compounds with antifungal properties, and important biological processes, such as cell proliferation, senescence (Stancevic and Kolesnick 2010, Huang et al. 2012) and adaptation (Pedroso et al. 2009), all intimately related with membrane lipid composition and their biophysical properties.

CHAPTER V – CHANGES IN THE BIOPHYSICAL PROPERTIES OF THE CELL MEMBRANE ARE INVOLVED IN THE RESPONSE OF *NEUROSPORA CRASSA* TO STAUROSPORINE

As mentioned previously, *N. crassa* is a non-pathogenic filamentous fungus widely used as a multicellular eukaryotic model. Recently, the biophysical properties of the PM of *N. crassa* conidia were thoroughly characterized. They evolve during conidial germination at a speed that depends on culture conditions, suggesting an important association between membrane remodelling and the intense membrane biogenesis that takes place during the germinative process. STS is a drug used to induce programmed cell death in various organisms. In *N. crassa*, STS up-regulates the expression of the ABC transporter ABC-3, which localizes at the PM and pumps STS out. To understand the role of PM biophysical properties in the fungal drug response, *N. crassa* was subjected to STS treatment during early and late conidial development stages. Following 1 h treatment with STS, there is an increase in the abundance of the more ordered, SLEDs in the PM of conidia. This leads to higher fluidity in other membrane regions. The global order of the membrane remains thus practically unchanged. Significant changes in SLEDs were also observed after 15 min challenge with STS, but they were essentially opposite to those verified for the 1 h treatment, suggesting different types of drug responses. STS effects on membrane properties that are more dependent on ergosterol levels also depend on the developmental stage. There were no alterations on 2 h-grown cells, clearly contrasting to what happens at longer growth times. In this case, the differences were more marked for longer STS treatment, and rationalized considering that the drug prevents the increase in the ergosterol/glycerophospholipid ratio that normally takes place at the late conidial stage/transition to the mycelial stage. This could be perceived as a drug-induced development arrest after 5 h growth, involving ergosterol, and pointing to a role of lipid rafts possibly related with an up-regulated expression of the ABC-3 transporter. Overall, our results suggest the involvement of membrane ordered domains in the response mechanisms to STS in *N. crassa*.

5.1. Results

5.1.1. Staurosporine-Lipid Interactions

To study a possible interaction of STS with membrane lipids, three different model systems were used, covering the three lipid bilayer phases thought to represent the most important types of lipid domains in fungal PM (Rosetti et al. 2017): gel [composed of DPPC,

with a T_m value 41.5 ºC (Huang and Li 1999)], l_d [composed of POPC, T_m ca. -3 ºC (Koynova and Caffrey 1998)], and l_o [composed of a binary mixture of DPPC/cholesterol, which is l_o at both room temperature and 30 ºC (de Almeida et al. 2007)]. Moreover, due to STS intrinsic fluorescence, this study could be performed without resorting to externally added labels.

Different photophysical parameters of STS were measured. The steady-state fluorescence anisotropy reflects the rotational mobility of the drug, which should be significantly restricted upon membrane adsorption or incorporation. The fluorescence intensity decay allows computing the amplitude-weighted and intensity-weighted mean fluorescence lifetime, after analysis using Equation 4 with a bi-exponential model (n = 2) and Equation 5 and Equation 6. Those two parameters reflect the microenvironment of the probe: the contribution of each of them to the total decay can change with the solvent polarity and specific interactions, or with the pathways the excited fluorophore follows to return to the ground state, which depend on collisions with other molecules, vibrations and torsions (Berezin and Achilefu 2010).

None of the STS parameters analysed were significantly altered by the presence of any of the model systems used (Figure 29). These results show that STS does not interact directly with the membrane lipids. The variations detected in the conidial PM (next section) must therefore arise from active membrane reorganization and/ or lipid composition alterations actively performed by the cell.

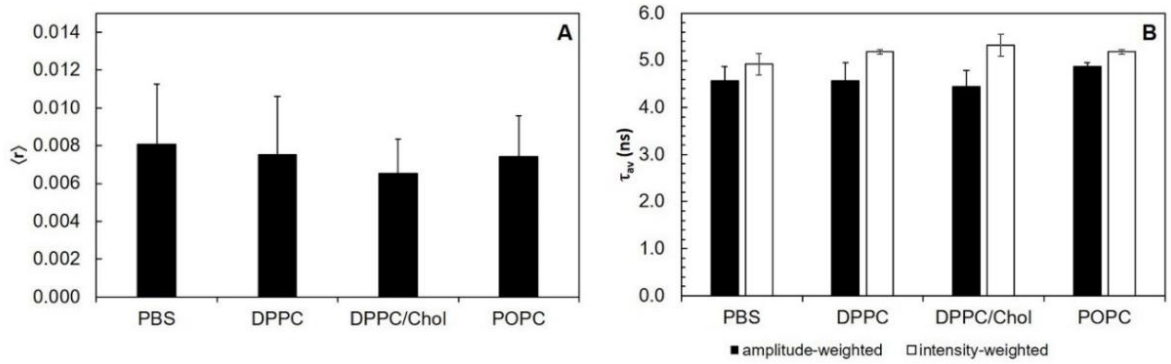

Figure 29 – STS does not interact with lipid bilayers: the intrinsic fluorescence properties of STS are similar in PBS and in the presence of different lipid phases. (A) steady-state fluorescence anisotropy; (B) amplitude-weighted (black bars) and intensity-weighted (white bars) mean fluorescence lifetime. The results represent the mean ± S. D. of at least three independent experiments, n ≥ 3.

5.1.2. ABC-3 expression at the plasma membrane: Influence of germination and STS exposure time

The expression of membrane proteins, such as the ones from the ATP Binding Cassette (ABC) transporter family, is an important part of antifungal drug response. These are primary active transporters involved in the modulation of absorption, metabolism and toxicity of pharmaceutical drugs (Glavinas et al. 2004). From this family, the ABC-3 transporter of *N. crassa*, homologous to the human P-glycoprotein 1 (Cannon et al. 2009), is responsible for the STS efflux (Fernandes et al. 2011). As mentioned above, this is the single protein whose levels of mRNA showed by far, for specific conditions, the largest increase (Fernandes et al. 2011). Therefore, we chose to study in more detail the expression of this protein at the PM because it is expected to observe very clear trends that can be used in combination with our previous biophysical study along conidial germination to choose a feasible number of experimental conditions that clearly complement each other as far as STS physiological response of *N. crassa* conidia is concerned.

In Figure 30, the Western blots for ABC-3 are shown for different growth times and different STS time exposure. However, we used only one concentration of STS. Previous studies from Castro *et al.* 2010, show that the concentration and incubation times used here ensure high survival rates and noticeable physiological effects. Hence, the concentration of STS used in the previous work by Fernandes *et al.* 2011 for most of the experiments was already 12.5 μM. Moreover, there were practical reasons to choose this concentration. Lower values of STS would yield low absorbance or fluorescence intensity values, which would introduce larger uncertainty in the study of STS intracellular accumulation (Fernandes et al. 2011). Larger concentration values could interfere with the fluorescence studies using *t*-PnA, since there is a large overlap between the absorption and emission spectra of this membrane probe and those of STS. As detailed below, *t*-PnA is an essential probe in membrane biophysical studies because of its unique sensitivity to acyl chain packing in the most ordered lipid domains, *i.e.*, to study the important PM SLEDs.

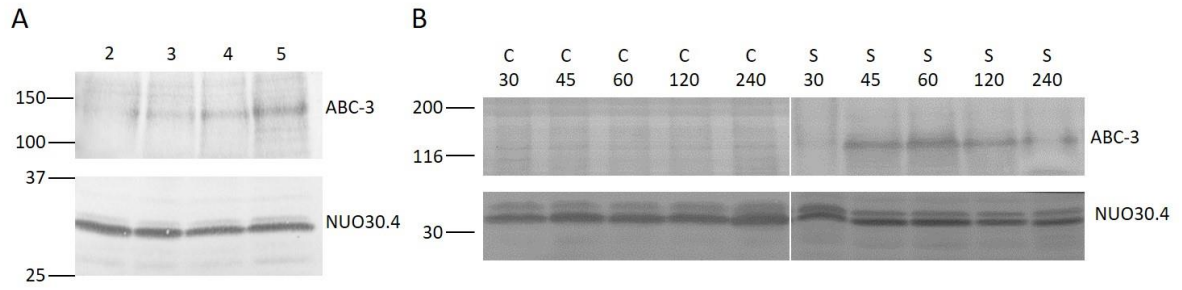

Figure 30 – Western blots of total protein extracts from N. crassa cells, using antiserum against the 130 kDa ABC-3 and the constitutive 30.4 kDa subunit of complex I (NUO30.4), as control for loading. (A) N. crassa was grown for the indicated times in hour and subsequently exposed to 12.5 μM STS for 1 h. (B) N. crassa was grown for 5 h and subsequently incubated with 12.5 μM STS (S) or DMSO as control (C) for the indicated times in min. Standard molecular weights (kDa) are indicated on the left of each blot.

STS at a concentration of 12.5 μM induces ABC-3 expression after 1 h of incubation but much more markedly in 5 h-grown cells than in 2 or 3 h-grown cells (Figure 30A), and the expression is only detected after 45 min (Figure 30B), which means that after 15 min exposure there is practically no overexpression at the PM.

5.1.3. Biophysical changes of plasma membrane lipids upon Staurosporine challenge

To assess the influence of germination time and duration of STS stimulus, comparison will be attempted for the four combinations of 2 and 5 h growth plus 1 h drug challenge and 3 and 6 h plus 15 min drug challenge, and respective controls. To facilitate the analysis of the results, they are presented as *N. crassa* cells in the absence (full pattern) and in the presence of STS (stripped pattern) with incubation time of 1 h (black coloured) and of 15 min (grey coloured). These two growth times allow comparison of the fungal drug responses at the early vs. late conidial stages of development, ensuring at the same time complementary information regarding the expression of ABC-3 at the PM. The STS treatment times were chosen taking into account the data presented in Figure 30B, where it is possible to observe the highest levels of protein ABC-3 expression between the STS incubation times of 45 min and 60 min, thus we have chosen the STS 1 h treatment. For a more complete study we decided to perform a 15 min treatment with STS, to ensure that the increase of ABC-3 expression levels at the PM were still undetectable, even for a growth time of 5 h. This allows assessing if we can distinguish a fast

vs. a slow response to the drug in terms of membrane biophysical properties in conditions where the expression of large membrane proteins such as ABC transporters are unchanged or not.

5.1.4. Packing and order of the acyl chains

The fluorescence intensity decay of *t*-PnA can be used to identify the presence of ordered domains. These can be attributed to a gel phase in the presence of a very long lifetime component in the fluorescence decay (Aresta-Branco et al. 2011, Bastos et al. 2012a, Vecer et al. 2014) or to a l_o phase (de Almeida et al. 2009). In *N. crassa* conidia, the very low levels of ergosterol impede the formation of detectable amounts of l_o domains by *t*-PnA (Santos et al. 2017). The lifetime value of the long component is related to the packing efficiency of the acyl chains. In turn, the amplitude of the long lifetime component is related to the relative abundance of those ordered domains.

Commencing with the 1 h challenge, STS did not have a major impact on the long lifetime component of *t*-PnA (Figure 31A and Table S 6). This parameter increased from ~20 ns at 2 h to ~25 ns at 5 h growth, and was independent of the presence of STS, reflecting the presence of ordered domains as reported previously by us (Santos et al. 2017). These are SLEDs that are not highly rigid gel, because their melting temperature is very close to *N. crassa* growth temperature. However, significant effects were observed for the relative abundance of the SLEDs, since the amplitude associated with the long lifetime component increased in the presence of STS at 5 h of growth (Figure 31C). Regarding the mean fluorescence lifetimes of *t*-PnA, the general trend is to observe an increase of their values induced by STS (Figure 31B, D).

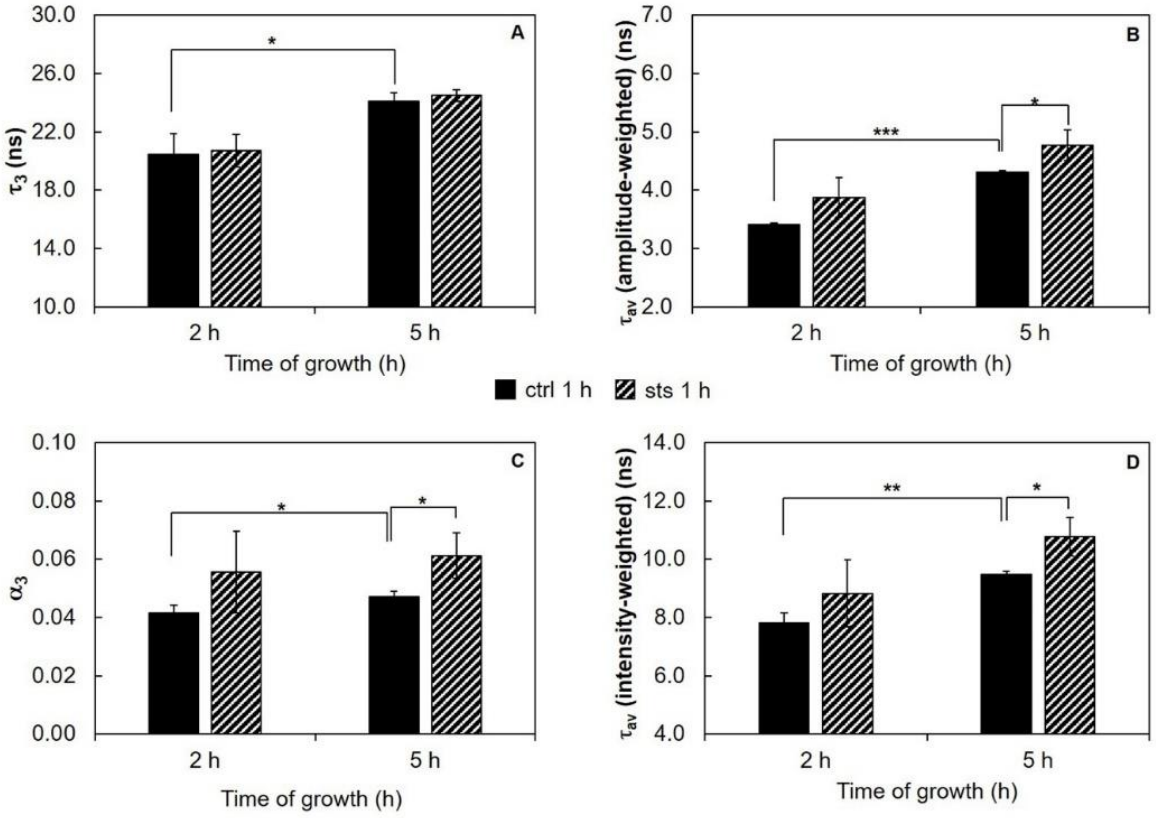

*Figure 31 – Time-resolved fluorescence spectroscopic parameters of t-PnA in the PM of N. crassa conidia. (A) The long lifetime component, τ_3, (B) amplitude-weighted mean fluorescence lifetime, τ_{av} (amplitude-weighted), (C) normalized amplitude of the long component, α_3, and (D) intensity-weighted mean fluorescence lifetime, τ_{av} (intensity-weighted), of t-PnA were obtained from the fluorescence intensity decay of the probe at 30 ºC. The results present the mean ± S.D. of at least three independent experiments, n ≥ 3. *p < 0.05, **p <0.01, ***p < 0.001.*

The ordering or disordering effects of STS in the membrane were also assessed. The steady-state fluorescence anisotropy values of DPH in the controls were similar to previously reported (Santos et al. 2017). DPH, not being sensitive to any particular kind of domain, gives a view of the PM global order. The values of steady-state fluorescence anisotropy of DPH decrease from 2 to 5 h of growth (these results are presented in the next chapter together with those for the mutant *abc3* in Figure 42), showing a fluidization of the PM along germination. For *wt* cells, STS did not have any significant effect on this parameter, suggesting that the effects sensed by *t*-PnA fluorescence intensity decays are localized into specific membrane domains, since the global properties of the membrane remain essentially unchanged.

Wt cells were also subjected to a 15 min challenge. In these conditions, the long lifetime component of *t*-PnA (Figure 32A and Table S 7) showed only a change on the 3 h grown cells, increasing ca. 8 % from ~24 ns in the control to ~26 ns in the presence of STS, *i.e.*, the drug is inducing tighter packing of the acyl chains in the more ordered domains. The amplitude

(Figure 32C) associated with this long lifetime component presents the opposite behaviour, decreasing with the addition of STS. This is also reflected in the amplitude-weighted mean fluorescence lifetime (Figure 32B) but not on the intensity-weighted mean fluorescence lifetime (Figure 32D). In the case of 6 h-grown cells, there were no significant changes, but in this case the long lifetime is already very high, even in the control situation. What is clear is that after 3 h growth a 15 min challenge with STS induces a rearrangement of SLEDs. Considering the steady-state fluorescence anisotropy of DPH (not shown), no significant changes induced by STS could be perceived, as observed for the 1 h stimulus.

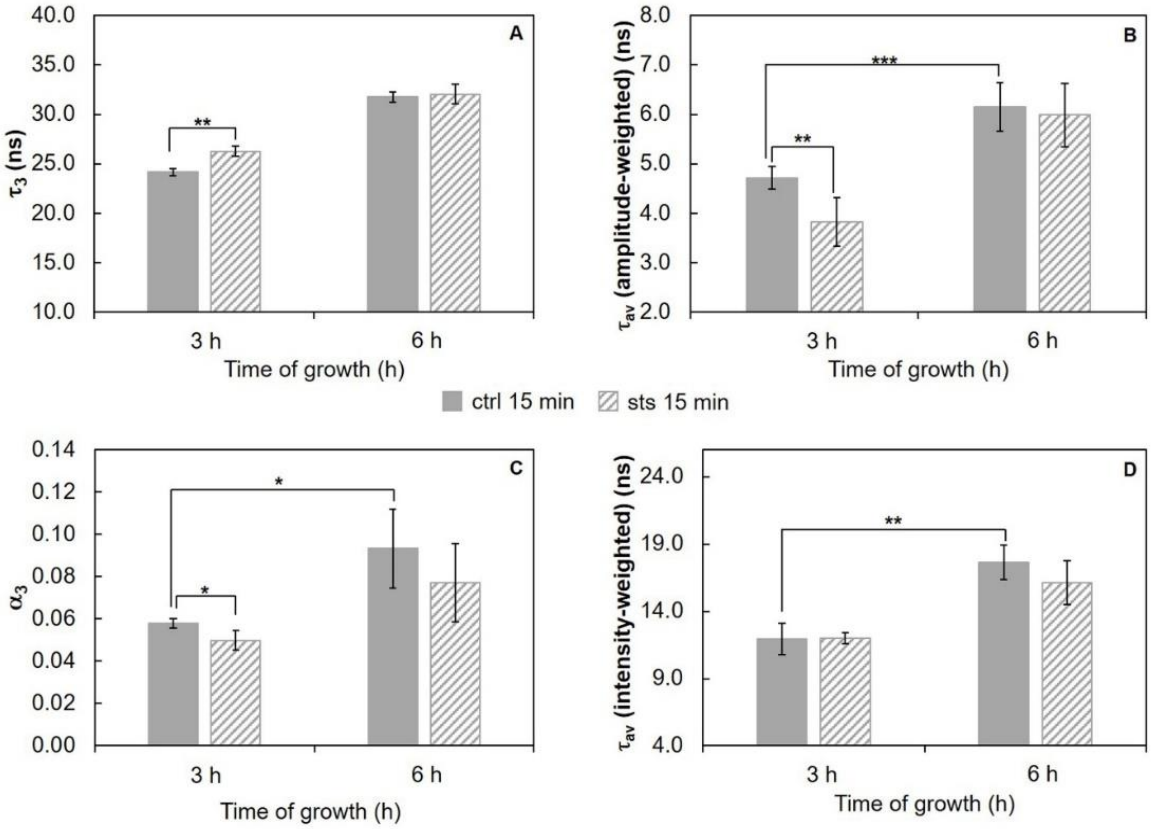

*Figure 32 – Time-resolved fluorescence spectroscopic parameters of t-PnA in the PM of N. crassa conidia. (A) The long lifetime component, τ_3, (B) amplitude-weighted mean fluorescence lifetime, τ_{av} (amplitude-weighted), (C) normalized amplitude of the long component, α_3, and (D) intensity-weighted mean fluorescence lifetime, τ_{av} (intensity-weighted), of t-PnA were obtained from the fluorescence intensity decay of the probe at 30 ºC. The results present the mean ± S.D. of at least three independent experiments, n ≥ 3. *p < 0.05, **p <0.01, ***p < 0.001.*

5.1.5. Polarity changes at the lipid/water interface

To evaluate if STS can affect *N. crassa* PM polarity properties, conidia were labelled with di-4-ANEPPS, a probe from the class of potential sensitive naphtylstyryl dyes, extremely responsive to either ergosterol- or cholesterol-enriched lipid domains (Loew 1996, Bastos et al. 2012b, Mariana et al. 2017). STS did not shift the emission or the excitation spectra of di-4-ANEPPS (Figure 33A, see also Figure S 1, Table S 8, Table S 9 and Table S 10). However, the intensities of emission and excitation bands presented consistent variations that matched the trend of the amplitude-weighted mean fluorescence lifetime (Figure 33B). At 5 h growth, a significant decrease in the amplitude-weighted mean fluorescence lifetime with the addition of STS was observed. This decrease at 5 h of growth is contrary to the behaviour of *t*-PnA fluorescence intensity decays (Figure 31), implying that di-4-ANEPPS is probably reporting the PM surface behaviour of different domains than *t*-PnA.

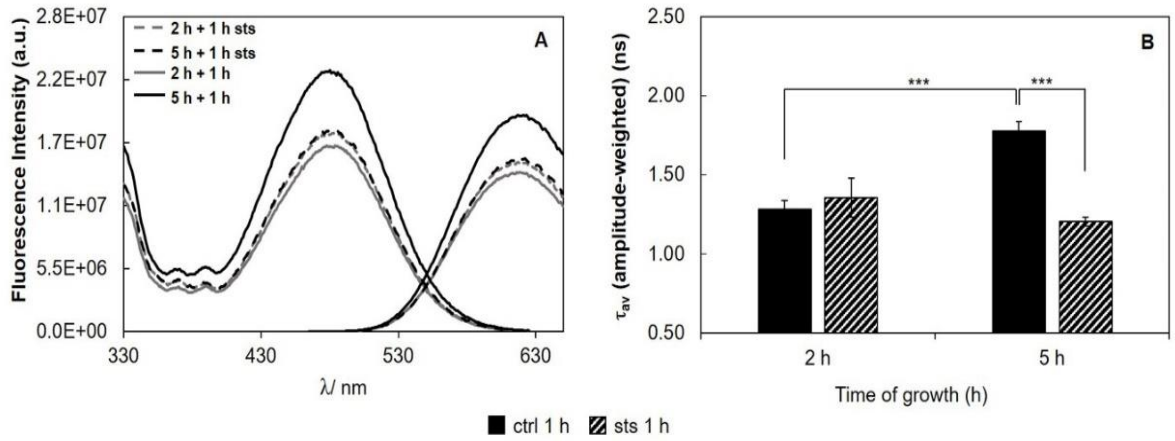

*Figure 33 – Di-4-ANEPPS fluorescence properties in N. crassa cells, at 30 ºC, (A) fluorescence excitation (λ_{em} = 635 nm) and emission spectra (λ_{exc} = 450 nm), (B) amplitude-weighted mean fluorescence lifetime of di-4-ANEPPS. The results present the mean ± S.D. of at least three independent experiments, n ≥ 3. ***p < 0.001.*

As a measure of the membrane dipole potential, the ratio of the di-4-ANEPPS fluorescence intensity by excitation at 420 nm to that produced by excitation at 520 nm (R_{ex} = IF_{420}/IF_{520}) was calculated (Figure 34). On 5 h-grown cells, STS significantly decreased R_{ex}, from ~0.65 to ~0.61. This behaviour corroborates the results of Figure 33, where both the steady-state fluorescence intensity and amplitude-weighted mean fluorescence lifetime of di-4-ANEPPS show similar trends. We can now suggest that these differences may be due to larger ergosterol content, since despite the absence of shifts of the spectra whether in the

absence or in the presence of STS, this sterol is known to increase all the other photophysical parameters of di-4-ANEPPS (Bastos et al. 2012b).

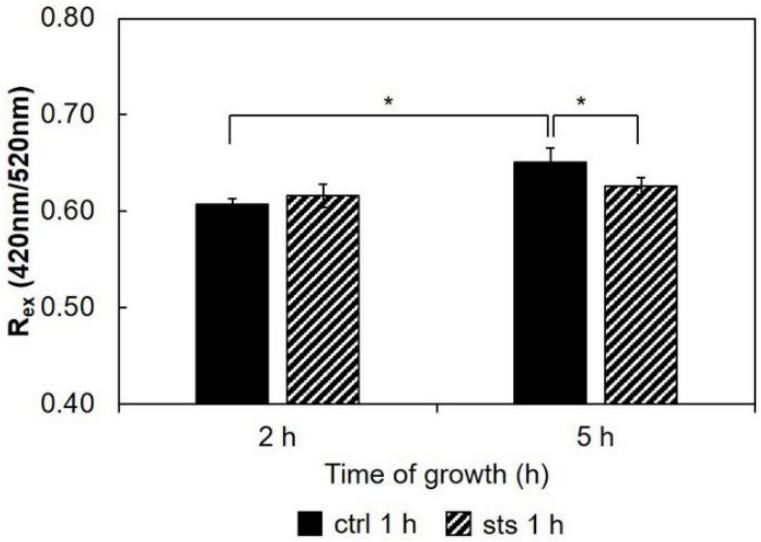

*Figure 34 – Ratio of di-4-ANEPPS fluorescence intensity produced by excitation at 420 nm to that produced by excitation at 520 nm, R_{ex} (420 nm/520 nm) cells, at 30 ºC. The results present the mean ± S.D. of at least three independent experiments, n ≥ 3. *p < 0.05.*

Regarding the 15 min stimulus (Figure 35), the effect of STS on the steady-state fluorescence intensity and amplitude-weighted mean fluorescence lifetime of di-4-ANEPPS is similar to the one obtained for 1 h stimulus (Figure 33), however, less pronounced at both growth times.

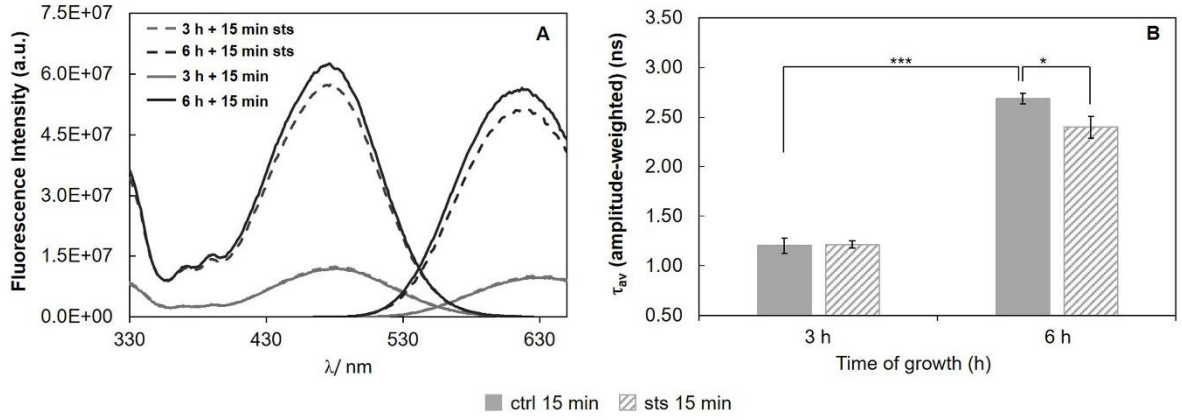

*Figure 35 – Di-4-ANEPPS fluorescence properties in N. crassa cells, at 30 ºC, (A) fluorescence excitation (λ_{em} = 635 nm) and emission spectra (λ_{exc} = 450 nm), (B) amplitude-weighted mean fluorescence lifetime of di-4-ANEPPS. The results present the mean ± S.D. of at least three independent experiments, n ≥ 3. *p < 0.05, ***p < 0.001.*

Considering the ratio, $R_{ex} = IF_{420}/IF_{520}$, for the 15 min STS challenge (Figure 36), there were no significant changes induced by STS at both growth times. Nonetheless, note that the ratio at 6 h growth is ca. 0.9. Regarding the control, this value is considerably higher than that observed for any of the shorter growth times (Figure 34 and (Santos et al. 2017)), again reflecting the change in membrane composition. This abrupt change coincides with the transition from the conidial to mycelial stage, where a marked increase of ergosterol content occurs.

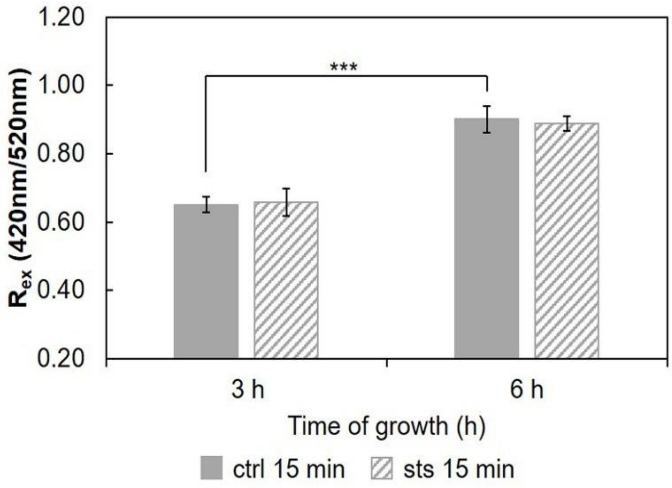

*Figure 36 – Ratio of di-4-ANEPPS fluorescence intensity produced by excitation at 420 nm to that produced by excitation at 520 nm, R_{ex} (420 nm/520 nm) in cells, at 30 ºC. The results present the mean ± S.D. of at least three independent experiments, $n \geq 3$. ***$p < 0.001$.*

STS does not interact directly with membrane lipids (Section 5.1.1). Thus, the differences observed in the membrane dipole potential, namely the increase with growth time and the decrease at 5 h growth upon incubation with STS relative to the control, can be also explained by the sterol content (Renaud et al. 1978). The 1 h treatment with the drug probably hampers the development of the fungus, and the change of growth phase from latency (*lag*) to exponential (*log*), when mycelium forms, preventing the rise in ergosterol content and membrane dipole potential.

5.2. Discussion

As mentioned above, studies in *N. crassa* conidia showed that it is possible to establish relationships between lipid composition and dynamics during conidial growth (Santos et al. 2017). In this work, this relationship was further exploited by studying the influence of an STS challenge. The effects of STS were particularly noticeable for the 1 h treatment of conidia germinated for 5 h. These are the conditions for which ABC-3 protein reaches its maximum levels at the PM. At that time point, the process of STS driven programmed cell death is at its early stage: reactive oxygen species had formed, glutathione efflux is at its maximum, but the integrity of the membrane is not yet affected (Fernandes et al. 2013).

The intracellular accumulation of STS over time was thoroughly studied (Fernandes et al. 2011). There is a higher accumulation of STS at 15 min than at 1 h probably due to STS export through ABC-3. However, we observe much stronger changes in membrane properties (related to ergosterol content) reported by di-4-ANEPPS for the 1 h treatment than for the 15 min, interestingly, when we confront the results of *t*-PnA fluorescence intensity decay for the two STS challenge times, it is possible to observe an opposite behaviour for most of the changing parameters. Altogether, these results suggest a different response for the shorter and longer STS treatments. Upon 15 min treatment with STS the significant changes reported by *t*-PnA are observed only in 3 h-grown cells. There is an increase in the acyl chain packing of the more ordered domains, possibly associated with the increment of the levels of SLs with smaller headgroups (*e.g.*, ceramides, which are known to increase in certain apoptotic routes), which induce tighter packing of the lipid acyl chains (Lester et al. 1974). Although the increase in the value of τ_3 seems modest (ca. 2 ns), and the significance is $p < 0.05$, once this value is converted to the rate constant for nonradiative processes, k_{nr}, concerning the long-lived excited state *t*-PnA molecules, these values become $(2.86 \pm 0.08) \times 10^7$ s^{-1} and $(3.19 \pm 0.06) \times 10^7$ s^{-1}, respectively for the control and treated cells, *i.e.*, the effect surpasses 10 %, and the statistical significance is $p < 0.01$). The constant k_{nr} is directly related to the molecular motions and collisions responsible for the non-emissive relaxation of the excited probe molecules, and thus to the motions of the surrounding lipid acyl chains, reflecting the acyl chain packing of the lipids under physiological conditions, provided that probe molecules are highly diluted in the membrane, which is the case under our experimental conditions. This stronger segregation of SLs contributes to a decrease in their abundance (α_3). Both these alterations suggest an increased SL catabolism, which might be associated with the initiation of proapoptotic

signalling. For the 1 h STS challenge, an increase in the SLED abundance (α_3) is observed instead for both growth times, without any change in the acyl chain packing.

On another hand, there were no changes in the photophysical properties of di-4-ANEPPS at the early conidial stage (shorter growth times), in clear contrast to what happens for longer growth times, at which the fungus has larger ability to express the STS exporter ABC-3. Being a very large transmembrane protein, from a major family that has been associated to lipid metabolism and transport (Li and Prinz 2004), and to SLEDs and/ or lipid rafts (Hinrichs et al. 2004, Modok et al. 2004), it is conceivable that ABC-3 expression induces changes on the membrane organization, especially in ordered domains, *i.e.*, those reported, on one hand, by *t*-PnA (abundance increase) and on the other hand by di-4-ANEPPS, which abundance seems to be decreasing, since the increase of ergosterol levels is being limited by the treatment with STS. STS does not induce a marked expression of ABC-3 in 2 h-grown *N. crassa* conidia. The hypothetical involvement of membrane domains containing ABC-3 in the observed biophysical changes is therefore consistent with the fact that these changes are minor in 2 h-grown cells and upon short STS incubations when compared with the 5 h-grown cells, along with 1 h STS incubation.

Genes related to ion channel activity and ion pumps (Na^+-K^+ ATPase) are overexpressed in *N. crassa* conidia upon STS stimulus (Nagata et al. 2008, Fernandes et al. 2011). Thus, membrane dipole potential variations (Figure 37), which are known to be intimately related with sterol composition and levels, might also be due to changes in lipid rafts that modulate ion channel activity (Ostroumova et al. 2015).

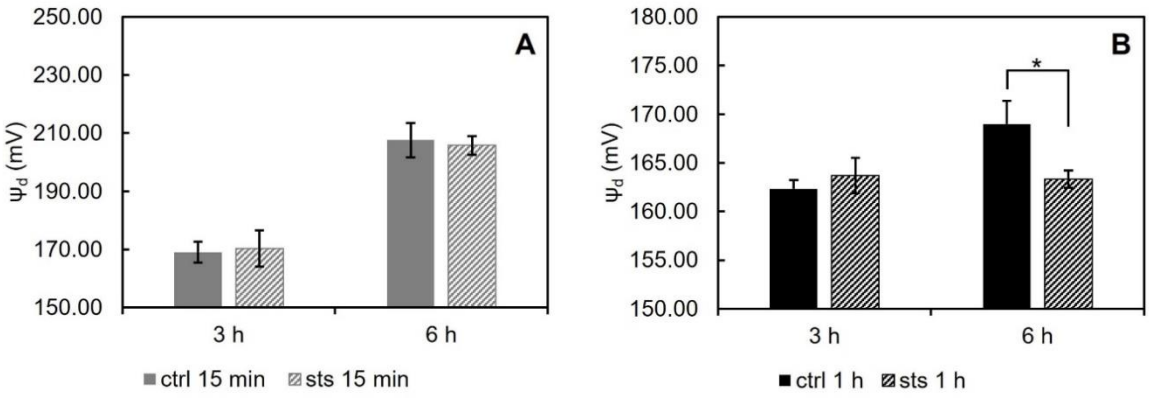

*Figure 37 – Dipole potential of wt N. crassa conidia (ψ_d) in mV obtained through Equation 7 (see Chapter III). The values represent the mean ± S.D. of at least three independent experiments, $n \geq 3$. *$p < 0.05$.*

It is known that, depending on the membrane composition, the magnitude of the dipole potential can range from ca. 200 to 400 mV (Ostroumova et al. 2015). The dipole potential of DPPC bilayers (one of the model systems used in this work) is 243 ± 4 mV (Peterson et al. 2002), and the dipole potential of neutral dioleoylphosphatidylethanolamine membranes is 220 ± 5 mV (Pickar and Benz 1978, Cseh and Benz 1998). However, *N. crassa wt* membrane dipole potential seems to be in a slightly lower range, as can be observed in Figure 37. Nevertheless, when we compare our results of membrane dipole potential measured through the excitation intensity ration (R_{ex}) at 420nm/ 520nm for di-4-ANEPPS in *N. crassa wt* with the ones obtained by Khmelinskaia, *et al.* 2014 (Khmelinskaia et al. 2014) in single-phase liposomes, it is possible to affirm that our values are in majority within the range found for gel phased liposomes (Khmelinskaia et al. 2014). The known lipid composition of *N. crassa* in the conidial and in the mycelium stages (Bianchi and Turian 1967, Lester et al. 1974, Kushwaha et al. 1976, Renaud et al. 1978) suggest that, during culture growth and development, the ratio PE/PC increases, which might also contribute to the increase in dipole potential, in addition to the aforementioned ergosterol.

For the membrane dipole potential, the effects of 1 h STS treatment and 5 h growth (the only case where they are significant) also correspond to a reversal of changes that occur between 5 h (+1 h) and shorter culture growth times.

To evaluate to what extent the amplitude-weighted mean fluorescence lifetime of di-4-ANEPPS is indeed related to ergosterol levels, measures of that parameter (in the absence of STS) from this and previous work (Santos et al. 2017) were plotted against total time of growth (black points) and compared with the ergosterol/glycerophospholipid ratios (blue points) (Bianchi and Turian 1967, Kushwaha et al. 1976) (Figure 38). The overall trend of di-4-ANEPPS amplitude-weighted mean fluorescence lifetime correlates remarkably with what happens for ergosterol/glycerophospholipid ratios, both departing from a small value that further decreases, to increase exponentially upon starting of the exponential phase. In this figure it can also be more easily observed how STS prevents the marked increase observed upon transition to the *log* phase of di-4-ANEPPS. The amplitude-weighted mean fluorescence lifetime of di-4-ANEPPS for STS treated cells (red triangles) is represented considering that growth stopped upon the addition of the drug. These points have a similar trend as the controls (black points) and are reasonably well described by the polynomial curve obtained from the fit to the controls. These effects can thus be putatively thought of as the result of a growth arrest or a slow-down in the development of the fungus. Despite the induction of a number of classical apoptotic markers, including caspase-like activity and surface binding of annexin V, in other

organisms, such as *Leishmania donovani*, STS does not cause cell death but causes cell cycle arrest (Foucher et al. 2013). This arrest can be a direct consequence of the signalling pathways induced by STS but might also be due to the targeting of energetic and metabolic resources for the synthesis of ABC-3 and other proteins involved in drug resistance mechanisms.

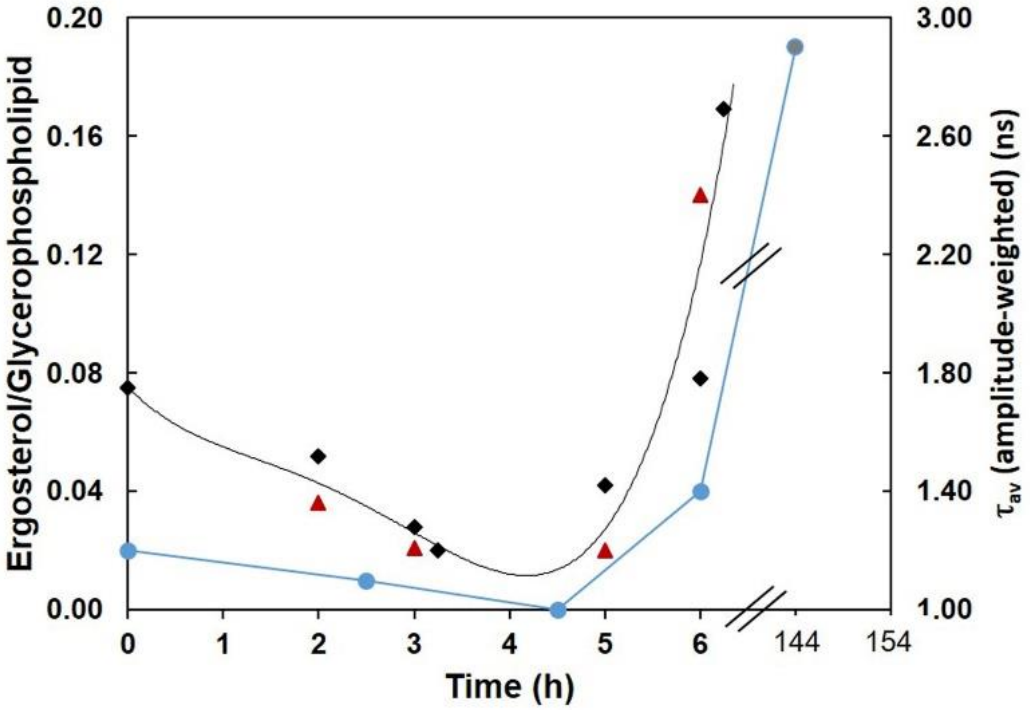

Figure 38 – Ergosterol/Glycerophospholipid ratio (Bianchi and Turian 1967, Kushwaha et al. 1976) (blue), and amplitude-weighted mean fluorescence lifetime of di-4-ANEPPS at 30 ºC, in the absence (CTRL, black) or in the presence of STS (red) vs. time of growth (this work and (Santos et al. 2017). The last blue data point corresponds to the composition of mycelium (6 days growth). The lines are merely to guide the eye.

5.3. Conclusions

This work clearly demonstrates that filamentous fungi response to STS involves changes of PM biophysical properties even though the drug does not interact directly with membrane lipids. SLEDs and SL metabolism and/or traffic to the PM seem to be involved in both fast and slow responses to the drug, by different mechanisms. Furthermore, ergosterol and possibly ergosterol-enriched domains may be crucial for the transition to the exponential phase and mycelium formation. Investigation on the relationships between drug export and sterol levels/enriched domains and membrane biophysical properties is worth pursuing in the context

of antifungal resistance and eventually other drug resistance situations, such as drug resistant cancer cell lines expressing proteins of the ABC-3 family, like the P-glycoprotein.

CHAPTER VI – BIOPHYSICAL IMPACT OF A STAUROSPORINE CHALLENGE IN THE PLASMA MEMBRANE OF HIGH DRUG-SENSITIVITY *NEUROSPORA CRASSA* STRAINS

In order to follow up the work presented in the previous chapter, and with the intent to further deepen our knowledge about *N. crassa* membrane biophysical properties and antifungal drug response, it was decided to perform further steady-state and time-resolved fluorescence spectroscopy studies in the *N. crassa abc3* mutant, which as mentioned above is devoid of the multidrug-resistance protein ABC-3, analogous to the human P-glycoprotein 1, known to be an STS exporter, intimately involved in SL transport, and upon challenge with STS, overexpressed. The changes of membrane biophysical properties upon treatment with STS was also explored in the *slime* strain, devoid of cell wall and with more rigid and abundant SLEDs.

6.1. Results and Discussion

6.1.1. *Neurospora crassa abc3* mutant strain growth profile

The growth curve of the *N. crassa abc3* mutant presented a *lag* phase of ca. 8 h followed by an exponential (*log)* phase (Figure 39), similarly to the growth curves of *wt* and *slime* strains (Santos et al. 2017). Hence, we focused the biophysical studies on the conidial stage (*lag* phase), performing 1 h incubations with STS after 2 h of growth, which leads to a small expression level of the ABC-3 transporter protein on the *wt*, and after 5 h of growth, which leads to a much higher level of protein expression (Santos et al. 2018).

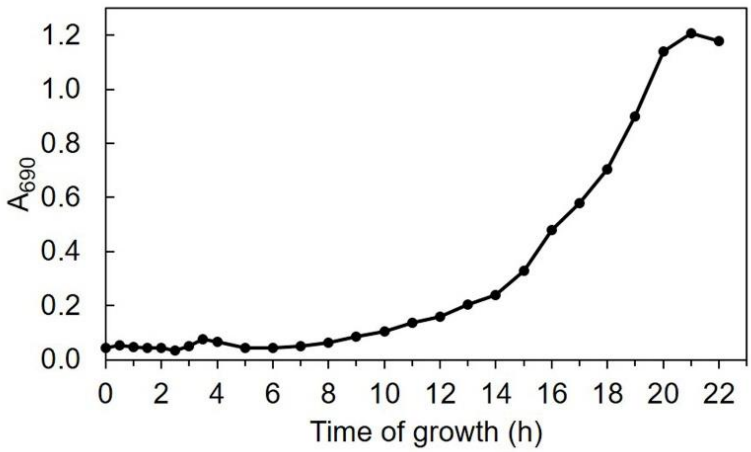

Figure 39 – Growth profile at 30 ºC of N. crassa abc3 mutant strain in MMV, obtained from absorbance at 690 nm, n ≥ 3.

N. crassa abc3 mutant cells have a generation time of 2.750 ± 0.004 h, while *wt* strain in the same culture medium presented a generation time of 2.46 ± 0.18 h (Santos et al. 2017), meaning that *wt* grows more rapidly than *abc3* in the same growth medium. As in our previous studies (Santos et al. 2017), the ensuing experiments were developed in the *lag* phase, during which all the strains present a conidial organization, minimizing possible interference of mycelium formation, either due to excessive turbidity of the samples, difficulty in maintaining a suspension, or large differences in lipid composition, namely the increase of ergosterol levels.

6.1.2. Establishing *Neurospora crassa abc3* mutant strain plasma membrane biophysical properties using fluorescence spectroscopy

To facilitate comparison, the biophysical results obtained in conidial suspensions will be presented as: *wt* (grey), *abc3* (light grey), *slime* (black); absence of STS (full pattern), presence of STS (stripped pattern).

Before proceeding to the effects of STS challenge, it is important to establish the general biophysical properties of the *abc3* PM in the same growth conditions as previously done for the *wt*. Since the expression of *abc3* is low in the absence of STS stimulus (Fernandes et al. 2011), the expectation is that minute differences will be encountered, if any. The *N. crassa abc3* PM was studied using the fluorescence probes di-4-ANEPPS, *t*-PnA, and DPH, as previously done for *wt* and *slime* (Santos et al. 2017).

The excitation spectra of di-4-ANEPPS in cells after 3 h of growth showed no deviation between *abc3* and *wt* strains (Figure 40A). However, when incorporated in the PM of *abc3*, the emission of di-4-ANEPPS had, a blue shift of ~3 nm in relation to the *wt* value, which indicates a lower ergosterol level in the *abc3* mutant at 3 h of growth.

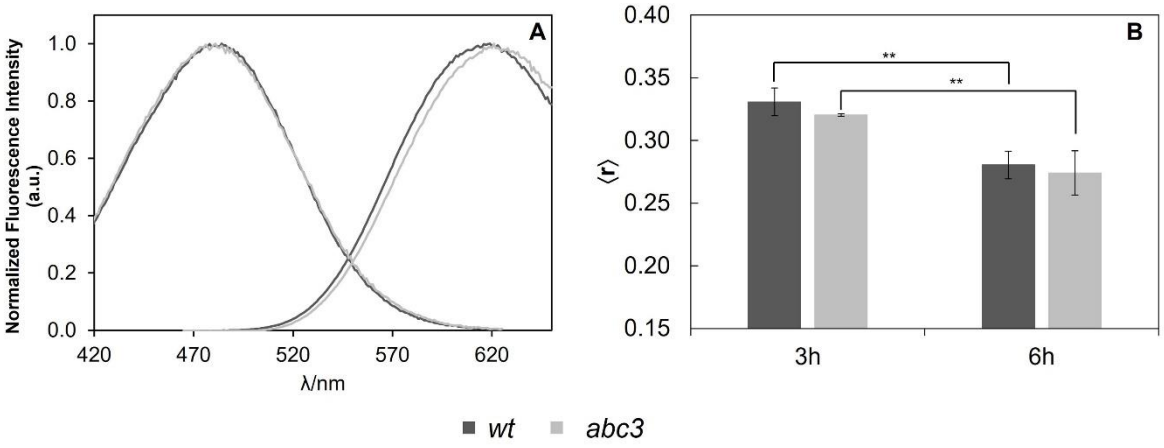

Figure 40 – A) Fluorescence excitation (λ_{em} = 635 nm) and emission spectra (λ_{exc} = 450 nm) of di-4-ANEPPS in N. crassa cells, at 3 h of growth, at 30 ºC. B) The t-PnA steady-state fluorescence anisotropy in the PM of N. crassa conidia, at 30 ºC, at the indicated times of growth. The values are the mean ± S.D. of at least three independent experiments, n ≥ 3.

The steady-state fluorescence anisotropy of *t*-PnA was also determined in *abc3* and *wt* cells (Figure 40B). In this case, the behaviour was similar for both strains, and the values were high and close to 0.3, especially at 3 h of growth. The major difference was observed with time of growth, being the values at 3 h of 0.331 and 0.320, for *wt* and *abc3*, respectively, and at 6 h of 0.281 and 0.274, respectively. Such high values corroborate the existence of a significant fraction of highly ordered membrane domains, which decrease with growth time. Comparing these values with the ones obtained previously at 2 and 5 h of growth for the *wt* (Santos et al. 2017), there is a sequential decrease in the anisotropy values from 2 h to 6 h of growth.

The long lifetime component of *t*-PnA is usually used to identify the existence of an ordered phase, as already detailed in previous chapters. We found a long lifetime component of *t*-PnA of ca. 20 and 22 ns at 3 and 6 h of growth, respectively, for *abc3* cells, pointing to the existence of ordered domains in the *abc3* conidial PM. Since these values are clearly below 30 ns, the question arises of whether these are l_o domains or another type of heterogeneity. However, as stated before, the absence or very low levels of ergosterol preclude the formation of l_o domains. For *wt* cells, a similar value of the long lifetime component was obtained at 3 h; at 6 h the value was slightly longer, ca. 24 ns (Figure 41A). The amplitude was clearly below 10 % (Figure 41C). The intensity-weighted mean fluorescence lifetime of *t*-PnA obtained (Figure 41D) was very similar in both strains at 6 h of growth, but slightly shorter in *abc3* cells at 3 h of growth.

6.1.3. *Neurospora crassa* plasma membrane biophysical properties change upon challenging with staurosporine

Following the general characterization of *abc3* PM biophysical properties and after establishing that STS does not interact directly with membrane lipids (Santos et al. 2018), it is possible to analyse the outcomes of STS challenge in such properties, not only for *abc3* and compare them with those occurring for the *wt* strain.

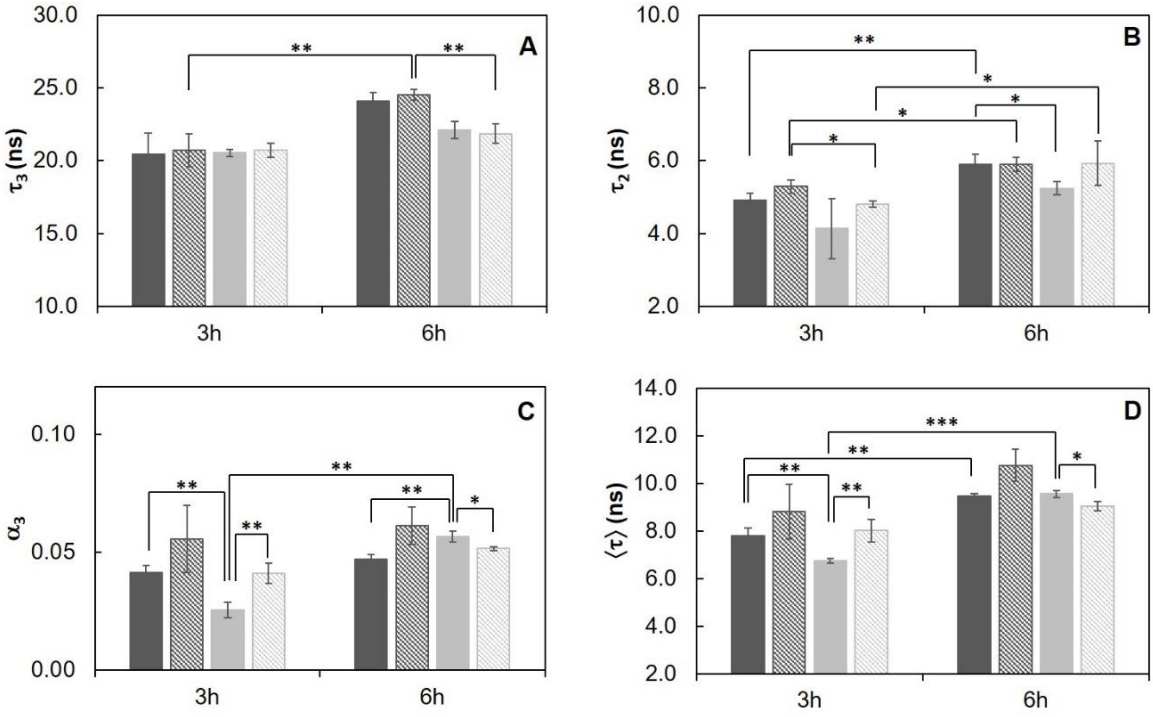

Figure 41 – Time-resolved fluorescence spectroscopic parameters of t-PnA in the PM of N. crassa conidia, at 30 ºC. ***(A)*** *The long lifetime component, τ_3,* ***(B)*** *medium lifetime component, τ_2,* ***(C)*** *normalized amplitude of the long component, α_3, and* ***(D)*** *mean fluorescence lifetime, $\langle\tau\rangle$, of t-PnA were obtained from the fluorescence intensity decay of the probe at 30 ºC, at 3 or 6 h of growth, as indicated. The values are the mean ± S.D. of at least three independent experiments, n ≥ 3. * p < 0.05, ** p <0.01, *** p < 0.001.*

STS did not have an impact on the long lifetime component of *t*-PnA (Figure 41A). This parameter increased from ~20 ns in both strains at 3 h to ~25 ns in *wt* or ~22 ns in *abc3* at 6 h of growth, independently of the presence of STS. However, significant effects were observed for the relative abundance of the SLEDs, *i.e.*, the amplitude of the long lifetime component. In general, the trend is to observe an increase of its mean value, only significant in

abc3. The exception is *abc3* at 6 h for which a decrease is observed. The more general behaviour can be interpreted in the framework of general stress responses that lead often to increased SL levels.

In order to understand the whole cell membrane behaviour, *N. crassa* cells were labelled with DPH and the steady-state fluorescence anisotropy measured (Figure 42). *Wt* showed the same trend of variation as the one observed for the anisotropy of *t*-PnA (Figure 40B), *i.e.*, a decrease with growth time, although the effect was much more pronounced for DPH (Figure 42), and again opposite to the observed for the mean fluorescence lifetime of *t*-PnA (Figure 41D). STS treatment did not have any statistically significant effect. The steady-state fluorescence anisotropy of DPH for *abc3* cells was ca. 0.24 at 3 h of growth with or without STS, while at 6 h of growth, the anisotropy value of the control decreased to ~0.18.

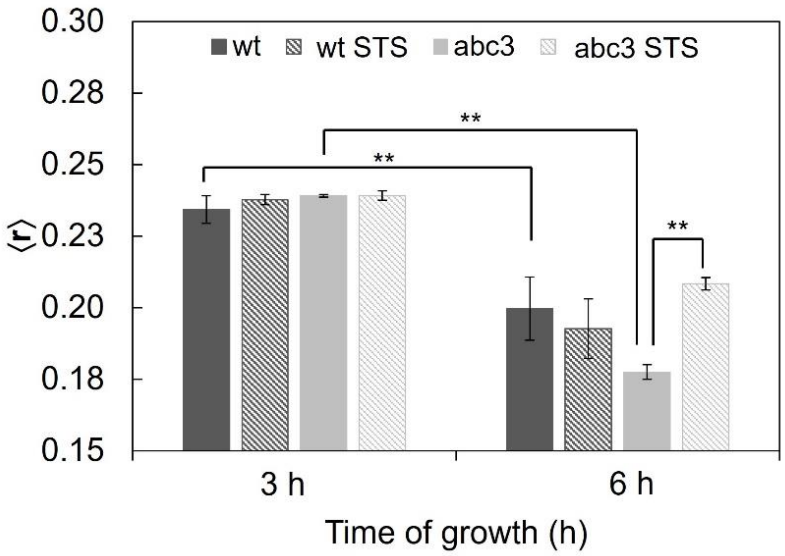

*Figure 42 - Steady-state fluorescence anisotropy of DPH in the PM of N. crassa conidia, at 30 ºC of the wt or abc3 mutant, after 1 h incubation in the absence or presence of 12.5 μM STS. The values are the mean ± S.D. of at least three independent experiments, n ≥ 3. **p < 0.01.*

Thus, concerning the *abc3* mutant, for 3 h growth, DPH steady-state fluorescence anisotropy reports no statistically significant effect of STS. For 6 h of growth, the anisotropy value of the control decreased, following the general trend already reported for the *wt*, with the PM becoming more fluid along the germination process. However, for this growth time, upon STS challenge, the DPH anisotropy of *abc3* undergoes a marked increase to ~0.21. For this growth time, *abc3* cells present a trend quite different from the *wt* cells, since the membrane

of the mutant cells becomes much more rigid with the STS challenge, in fact recovering from a control situation of higher fluidity, attaining a membrane fluidity that is between the control for 3 and 6 h of growth. This increased rigidity of the membrane as a whole is a biophysical response observed only for the mutant that is unable to efficiently export the drug.

Finally, the effect of STS on *slime* cells was also studied. This strain is devoid of cell-wall and its PM is markedly different from the *wt*, in several biophysical properties, namely the packing of SL domains (Santos et al. 2017). The presence of STS on the conidial PM of *slime* at 3 h of growth led to a notorious decrease in the medium lifetime component of *t*-PnA, while at 6 h of growth no differences could be observed between both conditions. The long lifetime component of *t*-PnA (Figure 43C) showed a similar variation at 3 h of growth and, in addition, a strikingly marked decrease of its amplitude. At 6 h growth on the other hand, the gel domains are already less compact and have a very small amplitude already in the control. Previously it was reported that for 5 h growth, both the amplitude and lifetime of the long component was similar to the one at 2 h in that work, and with the one at 3 h in the present work. There is thus major reorganization of the SL domains between 5 h and 6 h growth. For 5 h growth + 1 h challenge the STS challenge further induces a shortening in the value of this component. At this point it is still unclear why the SLEDs almost vanish in *slime* conidia between 5 h and 6 h and also why STS has a similar effect when added to cells grown for 2 h. However, the morphology of conidia is very similar in *slime* and in the *wt* until 5 h, time at which *slime* is already starting to grow exponentially, forming very large polynucleated conidia due to its inability to mycellize.

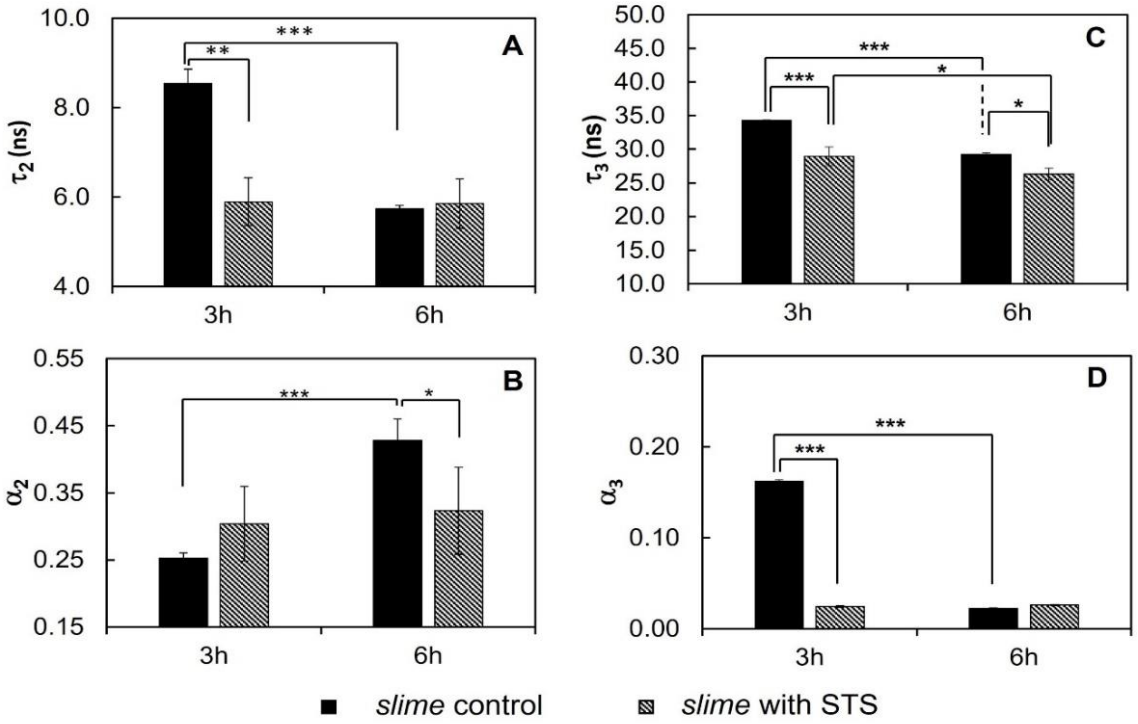

Figure 43 – Fluorescence spectroscopic parameters of t-PnA obtained in the PM of N. crassa slime, at 30 ºC. ***(A)*** *The medium lifetime component, τ_2,* ***(B)*** *normalized amplitude of the medium lifetime component, α_2,* ***(C)*** *long lifetime component, τ_3,* ***(D)*** *normalized amplitude of the long component, α_3, were obtained from the fluorescence intensity decay of t-PnA. The values are the mean ± S.D. of at least three independent experiments, $n \geq 3$. * $p < 0.05$, ** $p < 0.01$, *** $p < 0.001$.*

The steady-state fluorescence anisotropy of DPH (Figure 44A) presents a decrease upon the STS challenge, which at 3 h reflects mainly the strong decrease in packing density and abundance of SL-enriched gel-like domains, and at 6 h is probably due to a global fluidization of the whole membrane since SLEDs are already scarce in the control.

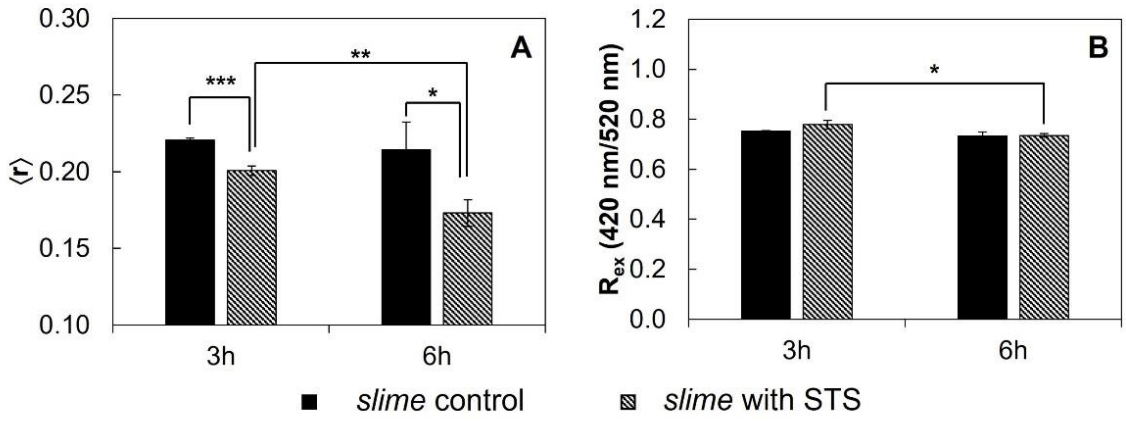

*Figure 44 – Fluorescence spectroscopic parameters obtained in the PM of N. crassa slime, at 30 ºC. (A) Steady-state fluorescence anisotropy of DPH and (B) Ratio of di-4-ANEPPS fluorescence intensity produced by excitation at 420 nm to that produced by excitation at 520 nm, IF_{420}/IF_{520}. The values are the mean ± S.D. of at least three independent experiments, n ≥ 3. * p < 0.05, ** p <0.01, *** p < 0.001.*

6.2. Conclusions

In general, the lipid domain organization and biophysical properties of both *wt* and *abc3* strains are similar. The small differences noted maybe related to the slower growth rate of *abc3*, which may be due to a slower rate of membrane biogenesis or some of its components as compared to the *wt*. In fact, at 3 h, it appears that *abc3* has smaller relative amounts of both ergosterol and complex SLs in its PM. Since SL domains are already present in latent spores and start to reorganize at shorter incubation times, assuming that glycerophospholipid synthesis occurs at similar rates in both strains, the net abundance of SLEDs will be smaller in *abc3*. In *wt* membrane fluidization occurs in part at the expense of SL domains which become less abundant than in *abc3* at 6 h growth. However, these domains are more rigid, a typical feature of membrane response/remodelling, as previously noted for both *S. cerevisiae* and *N. crassa*, denoting a lesser ability of *abc3* to finely tune the SL content of its PM. Overall, there are no differences in the membrane order of the PM reported by either a probe that is based towards the more ordered domains (*t*-PnA) or one that is reporting on the global properties of the membrane (DPH – Figure 42). Considering the increase in abundance and probably in rigidity of the SLEDs from 3 to 6 h in this mutant, the larger decrease in membrane fluidity as compared to *wt* is again consistent with lower ergosterol levels in the mutant, concomitant with higher glycerophospholipid/ergosterol ratio and/or higher unsaturation ratio in *abc3*, or a higher

PE/PC ratio. These changes would compensate a possible smaller headgroup of PM SLs, which in turn would justify the stronger packing in these domains for *abc3* at 6 h growth. Lower ergosterol levels in the PM of the mutant could be related with slower growth, since it is known that for the *wt* after 5 h growth ergosterol levels start to increase markedly, and it is feasible that for the same growth time, *abc3* conidia did not reach the same development stage yet.

ABC transporters are ubiquitous in all three phyla of life. They share the same core structure consisting of two transmembrane regions and two soluble nucleotide binding domains. The first ones bind and translocate substrates across lipid bilayers while the second ones bind and hydrolyse ATP. ABC transporters can function as exporters (*i.e.,* removing substrates from the cytoplasm) or importers (*i.e.*, translocating substrates into the cytoplasm) (Neumann et al. 2017). The null-mutant of the ABC transporter (*abc3*) is extremely sensitive to STS, accumulates more STS than the *wt* and is defective in energy-dependent export of the drug, indicating that ABC-3 protein is the first described STS transporter (Fernandes et al. 2011). This protein analogous to the human P-glycoprotein 1, which family in humans is responsible for several functions, such as removal of cholesterol and phospholipids onto high density lipids, drug resistance, surfactant protection and N-retinydilester-PE efflux (Glavinas et al. 2004).

Considering that we know already that STS does not interact directly with membrane lipids (Santos et al. 2018), it is possible to interpret the influence of an STS challenge in the biophysical properties of both *wt* and *abc3* mutant in terms of changes in lipid composition/ membrane reorganization. The general trend observed was an increase in the relative abundance of the SLEDs. This result can be due to stress responses, which often lead to an increase in the SL levels, namely of ceramides (Lester et al. 1974). Regarding the whole cell membrane behaviour, *wt* labelled with DPH presented the same variation profile as the one observed for the anisotropy of *t*-PnA, a decrease with growth time, being more pronounced for DPH (Figure 42) and opposite to the observed for the mean fluorescence lifetime of *t*-PnA. At 6 h growth *abc3* cells present the opposite trend of the *wt* cells, increasing with the STS challenge, in fact recovering from a control situation of higher fluidity. An exceptional behaviour occurred also for *abc3* at 6 h in the relative abundance of SLEDs, where a decrease was observed. This could be related to the higher sensitivity of *abc3* cells to STS and/or their inability to efficiently export the drug. In the *wt*, the biophysical changes induced by STS can be rationalized by a growth arrest and an increase in ABC-3 expression, a protein of a family that has been associated to membrane ordered domains, either SL-enriched or raft-like. In the

6 h-grown *abc3* mutant, the PM global fluidity is lower than for the *wt* (control). In the presence of the drug, the intracellular level of STS remains high in *abc3* cells even after 1 h of addition of the drug, and higher than for the *wt* at 15 min (Fernandes et al. 2011). However, there is a strong decrease in global membrane fluidity (increased DPH anisotropy) in the mutant cells upon STS 1 h challenge, attaining a value that is intermediate between its control values for 2 h and 5 h growth. In the absence of the drug exported, the growth arrest might be more drastic, and senescence or cell death cannot be ruled out.

In *N. crassa slime*, STS induces a large membrane reorganization, leading to a decrease in global membrane rigidity at the expense of ordered domains. A similar compensation mechanism has been observed in *S. cerevisiae* for mutants possessing less ordered domains than the *wt* (Aresta-Branco et al. 2011).

CHAPTER VII – TACKLING A POSSIBLE RELATIONSHIP BETWEEN YEAST PLASMA MEMBRANE BIOPHYSICAL PROPERTIES AND ANTIFUNGAL SENSITIVITY

The relevance of $M(IP)_2C$ synthesis, the terminal complex SL class in the yeast *S. cerevisiae*, for the lateral organization of the PM was investigated by fluorescence microscopy. Specifically, we addressed how changing the complex SL profile in the PM could influence the membrane compartments (MC) containing either the arginine/ H^+-symporter Can1p (MCC) or the PM H^+-ATPase Pma1p (MCP). To achieve these goals, *wt*, *ipt1*Δ cells, which are unable to synthesize $M(IP)_2C$ accumulating MIPC and *scs7*Δ cells, which lacks the gene coding for a SL fatty acyl 2-hydroxylase that catalyses the 2-hydroxylation of the very long chain fatty acid 2-OH-C26:0, were compared. Can1p and Pma1p were tagged with GFP and *m*RFP, respectively, in the three yeast strains, to evaluate their lateral organization using confocal fluorescence intensity and fluorescence lifetime imaging. In these cells lacking $M(IP)_2C$, a clear alteration in Pma1p membrane distribution, but no significant changes in Can1p distribution, were observed. Thus, this work strongly supports the involvement of SL domains in the formation and stability of the MCP, possibly being enriched in this compartment.

Additionally, it is shown that new derivatives of Ke tested first in this work, especially KeP and KeOP, proved to be promising antifungal compounds.

Finally, the results regarding the antifungal activity of Nys and Ke against different SL-biosynthetic mutant strains of *S. cerevisiae ipt1*Δ, *scs7*Δ, *sur1*Δ:*csg2*Δ and *sur1*Δ:*csh1*Δ, obtained at 24 h and 48 h, shown to be promising for a better understanding of the antifungal drug mode of action and resistance.

7.1. Results and Discussion

7.1.1. The lateral organization of Pma1p but not Can1p is dependent on the sphingolipid profile

In order to evaluate the impact of changing SL composition of *S. cerevisiae* PM in the organization of MCC and MCP, the time-resolved fluorescence properties of Can1p tagged with GFP (Can1p-GFP) and Pma1p tagged with mRFP (Pma1p-mRFP) were studied by FLIM in living *wt*, *ipt1*Δ and *scs7*Δ cells. As already mentioned, Can1p is found in MCC domains that co-localize with ergosterol staining by filipin, whereas Pma1p is the hallmark of MCP

which seems to be intimately related with SLs, but with no direct evidence for SL enrichment (Athanasopoulos et al. 2019).

The fluorescence decay parameters of the proteins mentioned above were collected for *wt*, *ipt1*Δ and *scs7*Δ cells (Figure 45). The decays are bi-exponential as expected when exciting GFP using a wavelength outside the absorption band of the protonated form and detecting above 500 nm (Cotlet et al. 2001, Heikal et al. 2001, Suhling et al. 2002). Moreover, the lifetime and amplitude values obtained for each component of the fluorescence decay are in line with those reported in the literature (Cotlet et al. 2001, Heikal et al. 2001, Suhling et al. 2002). The mean fluorescence lifetime obtained for GFP suggests that the protein is close to a medium with high refractive index (Suhling et al. 2001) as anticipated considering the membrane location of Can1p.

For Can1p-GFP no differences were found between *wt* cells and *ipt1*Δ and *scs7*Δ cells. On the contrary, for Pma1p-mRFP there were significant differences in the fluorescence decay parameters for both strains studied. It was possible to observe (Figure 45B) a significant decrease in the amplitude-weighted mean fluorescence lifetime, from 1.80 ± 0.02 ns to 1.75 ± 0.03 ns for *wt* and *ipt1*Δ cells respectively, and in the intensity-weighted mean fluorescence lifetime, from 2.09 ± 0.04 ns to 1.93 ± 0.07 ns for *wt* and *ipt1*Δ cells, respectively. *Scs7*Δ showed a similar behaviour as the one presented by *ipt1*Δ (Figure 45), corroborating the importance of the SL profile and of gel domains in the organization of Pma1p. This corresponds to, approximately, a 6 % variation. This alteration reflects a different environment surrounding the protein in the strains, which could be related to changes in the membrane refractive index, or to alterations in the pH or local ion concentration in the vicinity of the protein. Considering, *e.g.*, that the refractive index of a lipid membrane varies with the length and packing of the lipid hydrophobic chains (Petrov et al. 1999) and also with polar headgroup chemistry (Kienle et al. 2014), the change obtained in the mean fluorescence lifetime is particularly relevant since it would represent a variation equivalent to ~0.03 in terms of refractive index, or an increase of 20 % (*v/v*) of glycerol in a water/glycerol mixture for a GFP in solution (Suhling et al. 2001), which, in turn, is also comparable *e.g.*, to a change of about 6 carbons in the length of a fatty acid chain monolayer (Petrov et al. 1999).

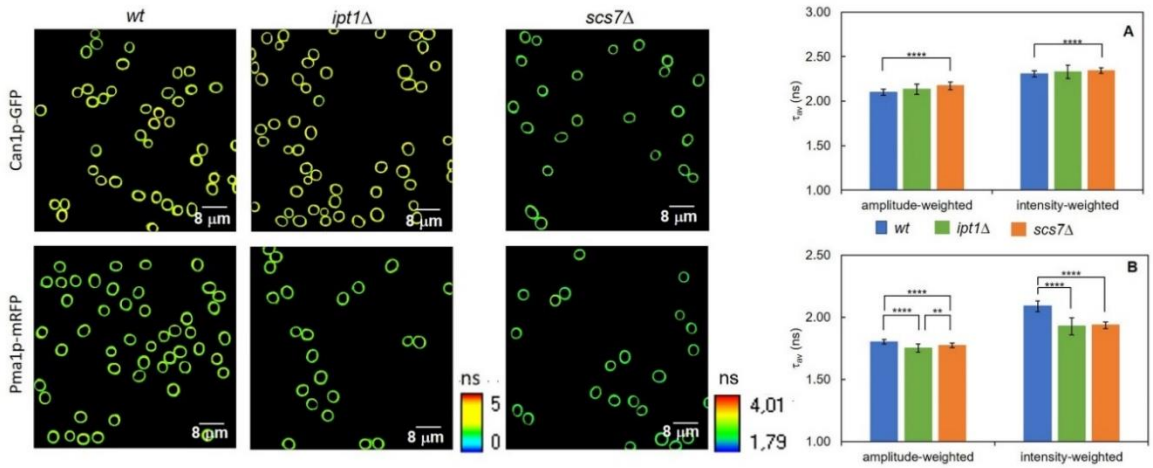

*Figure 45 - The lack in M(IP)$_2$C leads to a change in the microenvironment surrounding Pma1p but not Can1p. Representative FLIM images of ROI comprising S. cerevisiae wt, ipt1Δ and scs7Δ cells PM. Amplitude-weighted and intensity-weighted mean fluorescence lifetime for S. cerevisiae cells. (A) wt-Can1p-GFP, ipt1Δ-Can1p-GFP and scs7Δ-Can1p-GFP cells and (B) wt-Pma1p-mRFP, ipt1Δ-Pma1p-mRFP and scs7Δ-Pma1p-mRFP cells. The values are the mean ± S.D. of three independent biological replicates with a total of ca. 200 cells analysed for each strain. ** p ≤ 0.01; **** p ≤ 0.0001.*

The heterogeneity of Can1p and Pma1p distribution on the PM of *S. cerevisiae* was also assessed to further evaluate the possible influence of the complex SLs in the yeast membrane compartments, MCC and MCP. The distribution heterogeneity was determined by confocal fluorescence microscopy (Malinska et al. 2003, Grossmann et al. 2007), as described in the experimental section. These fusion proteins have been used previously to visualize and detect alterations in both membrane compartments in *S. cerevisiae* (Malinska et al. 2003, Grossmann et al. 2007), or similar proteins, *e.g.*, Pma-1-GFP in other fungi such as *N. crassa* (Fajardo-Somera et al. 2013) or Pma1p tagged with hemagglutinin in *C. neoformans* (Farnoud et al. 2014).

In Figure 46, representative confocal images for the three strains labelled with either Pma1p-mRFP or Can1p-GFP are shown, as well as values obtained for the heterogeneity of their distribution in the PM for all the replicates. The fact that the heterogeneity values for Can1p and Pma1p distribution in the PM of *wt* cells are very similar, 0.68 ± 0.10 and 0.66 ± 0.12 respectively, can be due to the reported complementarity of the two membrane compartments. The heterogeneity of Can1p distribution is only slightly—if at all—affected by 3 % in *ipt1*Δ cells relatively to *wt* cells (Figure 46A). In contrast, the heterogeneity of Pma1p distribution in the PM is 15 % higher in *ipt1*Δ cells than in *wt* cells (Figure 46B), a prominent change between strains especially when compared to the one found for Can1p. Interestingly, the quantification of fluorescence intensity at the PM (see annex Figure S 2), reveals that

Can1p-GFP has slightly higher average intensity in *ipt1*Δ PM than in the *wt*, whilst for Pma1p-mRFP, the intensity is significantly weaker in *ipt1*Δ cells. This difference in fluorescence intensity between strains indicates a change in the amount of protein at the PM, since the fluorescence quantum yield of Pma1p-RFP is only marginally lower in *ipt1*Δ cells, according to the measured amplitude-weighted mean fluorescence lifetimes (see annex Table S 11) and pinpoints a potential defect in Pma1p accumulation at the PM in *ipt1*Δ cells. The mechanism underlying the lower Pma1p-mRFP levels at the PM of *ipt1*Δ cells can be related to alterations in the protein traffic or turnover or protein expression levels.

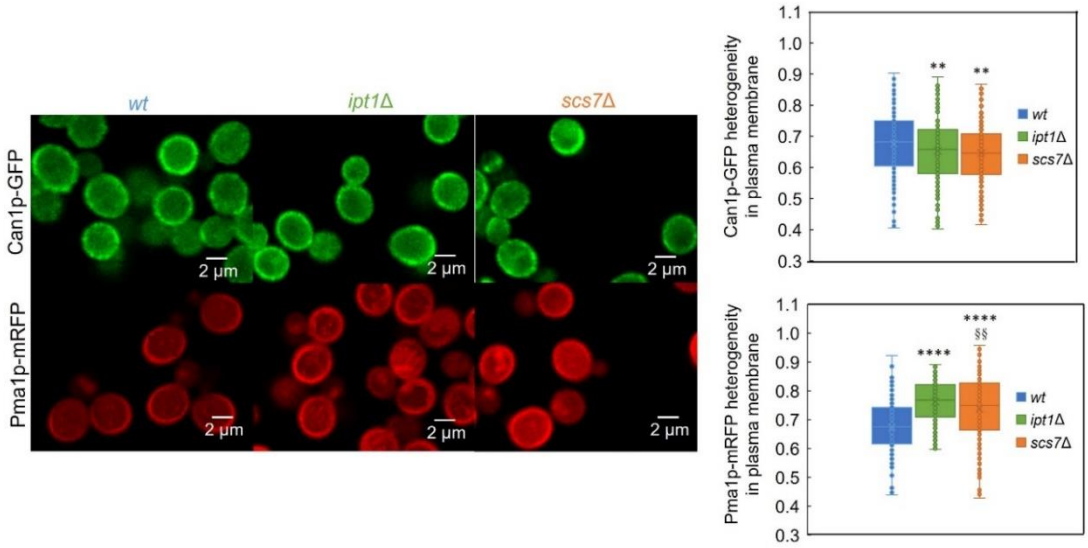

*Figure 46 – MCP distribution in the PM is different in wt, ipt1Δ and scs7Δ cells. The heterogeneity of Can1p-GFP and Pma1p-mRFP distribution along the PM was determined for wt, ipt1Δ and scs7Δ cells as described in the experimental procedures. The values are the median ± S.D. of at least four biological replicates with a total of at least 190 cells analysed per replicate. **, p ≤ 0.01; ****, p ≤ 0.0001 (wt vs. ipt1Δ or scs7Δ cells); §§, p ≤ 0.01 (ipt1Δ vs. scs7Δ cells). On the left, representative confocal fluorescence images of living S. cerevisiae cells expressing either Can1p-GFP or Pma1p-mRFP, as indicated, are shown.*

7.1.2. Antifungal sensitivity of yeast *Saccharomyces cerevisiae* and the involvement of lipids of plasma membrane domains

7.1.2.1. Ketoconazole and its diphenylphosphane derivatives

To study the antifungal activity of the Ke and its diphenylphosphane derivatives KeP, KeOP, KeSP and KeSeP, we chose *S. cerevisiae*, which is generally considered a non-pathogenic organism, but currently recognized as a potentially important agent causing

opportunistic infections against immunocompromised patients (Pérez-Torrado and Querol 2016). In order to assess whether all the Ke derivatives share the mechanism of action with the parent compound, or if they might present different or additional modes of action, the inhibitory concentration MIC_{50} (Table 4) was determined on the basis of the dose-response curves (data not shown) in a 48 h assay against *S. cerevisiae wt* strain BY4741 and the deletion mutant *erg6*Δ, which lacks the gene coding for the S-adenosylmethionine: 24-methyltransferase (Gaber et al. 1989), accumulating cholesta-5,7,24-trienol and zymosterol instead of ergosterol (Guan et al. 2009). There are several studies reporting that the *ERG6* gene deletion may increase the resistance of *S. cerevisiae* cells to azole compounds (Anderson et al. 2003, Kapitzky et al. 2010, Konecna et al. 2016). As explained in Chapter I (section 1.4.2), this family of antifungal compounds inhibits the synthesis of ergosterol by targeting the enzyme the cytochrome P450 14α-demethylase.

We first studied Ke, and a MIC_{50} of 0.865 μM was determined against *wt* cells, whereas this compound showed no activity against the mutant cells. Thus, under our conditions, deletion of *ERG6* gene renders *S. cerevisiae* cells resistant to Ke. The value determined for the *wt* strain is in very good agreement with previous studies carried out under similar condition (48 h, 30 °C) (*e.g.* (Parker et al. 2008)).

Table 4 – Antifungal activity expressed as MIC_{50} values [μM] of Ke and its derivatives against S. cerevisiae cells at 48 h (de Almeida et al. 2019).

***S. cerevisiae* strains**	**Ke**	**KeP**	**KeOP**	**KeSP**	**KeSeP**
***wt* (BY4741)**	0.865	9.023	0.00416	> 200	1.244
***erg6*Δ**	> 200	0.654	0.00482	> 200	0.578
***wt* (W303)**	6.25	12.5	3.13	> 200	50
ADI-8*	0.02	0.2	0.05	0.2	0.2

Regarding the Ke derivatives, they exhibit clearly distinct behaviour from the parent compound, and notably, they were all active against the resistant strain to similar or even greater extent as they were against the *wt* strain (except KeSP, which was also inactive against *wt* cells). These results strongly suggest that the Ke derivatives may present different or additional modes of action underlining their antifungal activity, or override mechanism of drug resistance operative against Ke, since not only they are active against yeast cells that are resistant to azole compounds, and shown to be Ke resistant in this study, but also the behaviour in relation both to the parent compound and between the two strains can change. For KeP, the *wt* cells are less sensitive (MIC_{50} 9.023 μM) than for Ke, while *erg6*Δ cells are very sensitive, presenting a MIC_{50} value (0.654 μM) which is even smaller than the one found for the parent

compound against the *wt*. KeSeP and KeOP are active against both strains with similar MIC_{50} values (Table 4). Finally, as mentioned above, KeSP is inactive against both *S. cerevisiae* strains. KeOP, on the other hand, presents very high activity (MIC_{50} values on the nM range) against both *wt* and *erg6*Δ cells.

The lack of activity of KeSP is somewhat surprising, as it contrasts markedly with the behaviour exhibited by the two other calchogenide derivatives, KeOP and KeSeP. We have, thus, hypothesized that this compound could be more efficiently exported by PM pumps. To test this hypothesis, we measured the activity of the compounds against a strain that lacks all the major ABC transporters in *S. cerevisiae* responsible for drug export, which is in general very susceptible to most xenobiotic compounds (Holmes et al. 2016). As control, we have also used the respective *wt* strain, W303. As with BY4741, W303 cells are susceptible to Ke and its derivatives, except for KeSP. This suggests that the inactivity of this compound against *S. cerevisiae* is a general trend, as it was observed in two different genetic backgrounds. On another hand, the MIC_{50} values are always considerably higher for W303 cells than for BY4741. This result is not unexpected, since it has been previously reported that, when grown in YPD medium, as in this study, BY4741 cells are more sensitive to Hygromycin B than W303, and they also differ in alkali-metal cation tolerance and PM potential, and in other important physiological parameters, as consequence of their different genome (Petrezselyova et al. 2010, Ralser et al. 2012). Notwithstanding, it is noteworthy that for both *wt* strains; the order of MIC_{50} values for the different compounds tested is almost the same, the only difference being between KeSeP and KeP, which are the second and third most active against BY4741 and in reverse order for W303 cells.

Regarding the strain lacking the major PM drug exporters, AD1-8, it is clear that all the compounds show much higher antifungal activity. The most striking result is the one for KeSP which displays a MIC_{50} value that is similar to KeP and KeSeP and is more than 3 orders of magnitude lower than against the W303 cells, the *wt* with the same genetic background. The most active derivative is, again, KeOP. These results strongly suggest that the inactivity of KeSP is due to a very efficient efflux of this compound by *S. cerevisiae*.

7.1.2.2. Nystatin and Ketoconazole antifungal activity against cells with different sphingolipid profile

For these experiments several mutant strains were used, *ipt1*Δ, as previously mentioned is devoid of *IPT1* encoding gene being unable to synthesize $M(IP)_2C$ accumulating MIPC; *scs7*Δ, which presents a sterol profile similar to the *wt*, however lacks the gene encoding for a SL fatty acyl 2-hydroxylase that catalyses the 2-hydroxylation of the very long chain fatty acid 2-OH-C26:0, the most predominant fatty acid species in *S. cerevisiae* SLs; both *sur1*Δ:*csg2*Δ and *sur1*Δ:*csh1*Δ, lack MIPC synthases, being unable to synthesize MIPC, accumulating IPC.

One major goal of this work was to assess the influence of SL structure and biophysical properties on the sensitivity to antifungal compounds. To this end, we used two drugs, Nys and Ke, pertaining to the two major classes of antifungals, the polyenes and the azoles. In Table 5, it is possible to observe that, in general, both compounds are more efficient at 48 h. For *sur1*Δ:*csg2*Δ, however, Ke treatments showed to be more efficient at 24 h. Overall, the MIC_{50} values for *sur1*Δ:*csg2*Δ are higher than for *wt*, except for Ke 24 h, and the other strains, which means the sensitivity towards both Nys and Ke decreased when compared with the other strains. The mutants present a smaller abundance of gel domains, in case of *ipt1*Δ, a small difference that is not significant (Bento-Oliveira et al. 2020), *scs7*Δ a small but significant difference (Aresta-Branco et al. 2011), as well as the double mutants, (unpublished results obtained in the lab, data not shown. The strain presenting lower relative abundance of gel domains is the double mutant, *sur1*Δ:*csg2*Δ. Moreover, all the mutants present stronger hydrophobic packing in the SLEDs. Although many factors come to play, the combined effect of more rigid and less abundant gel domains seems to correlate with an increased resistance towards Nys, particularly for the shorter incubation time (with the notable exception of the double mutant *sur1*Δ:*csh1*Δ). Nys is active on ordered membranes, but there may be a threshold of rigidity above which the drug starts to interact less favourably with the membrane. On another hand, if the SLEDs in the PM outer leaflet are important for Nys incorporation in the PM, a reduced abundance of these domains will also lead to a lower Nys partition, and a higher concentration of the polyene is required to achieve the necessary concentration at the membrane to form active pores. For 48 h, all strains are similarly sensitive to this polyene drug, except for the double mutant with the lowest gel domain relative abundance, which remains less sensitive.

The differences found for the efficiency of the two antifungal drugs, between the 24h and the 48 h assays, in the case of *wt*, are possibly related to the different mode of action. Nys mode of action implies direct permeabilization of the PM, whereas the effects of Ke inhibition of ergosterol synthesis should be more noticed at longer times, which may be required for shortage of ergosterol pools and accumulation of toxic sterols.

The increased sensitivity of all the mutants to Ke for 24 h incubation suggests that altered membrane properties may render these strains more susceptible to the alterations in sterol profile induced by the drug. However, the mechanism behind this remains unknown. For example, it can be due to a less efficient expression of drug export pumps at the PM. Nonetheless, taking into account the results from the previous section, for *ipt1*Δ and generalizing to the other SL-mutant strains, the different hydrophobic packing (and abundance) of the SLEDs has consequences in the MCP organization. As mentioned above, Pma1p plays crucial roles in cell homeostasis, namely, the maintenance of pH and ion balance and of the transmembrane potential at the PM (Malinsky and Opekarova 2016, Athanasopoulos et al. 2019, Santos et al. 2020), which in turn are required for proper transport of many molecules at the PM, namely the arginine/ H^+ symport at the MCC. Considering that cell death by the action of Ke and other azoles results from alterations in membrane organization, but also due to accumulation of toxic sterol intermediates, leading to severe membrane stress, which among other consequences, leads to malfunction of the vacuolar H^+-ATPase and cation homeostasis imbalance (Zhang et al. 2010, Shapiro et al. 2011), it is feasible to anticipate that cells with impaired MCP and altered Pma1p activity can more readily be affected by those drugs, even when the accumulated toxic sterols are still at lower concentrations, compared to the *wt* cells, with a properly functioning MCP.

Table 5 – Antifungal activity expressed as MIC_{50} values [μM] of Nys and Ke against several S. cerevisiae strains.

	Drugs	*wt*	*ipt1*Δ	*scs7*Δ	*sur1*Δ:*csh1*Δ	*sur1*Δ:*csg2*Δ	Incubation time with drug (h)
MIC_{50}, μM	Nys	1.81 ± 0.04	5.08 ± 0.07	12.19 ± 0.10	1.74 ± 0.03	11.8 ± 0.08	24
		1.73 ± 0.03	1.38 ± 0.085	1.54 ± 0.11	1.15 ± 0.04	12.1 ± 0.09	48
	Ke	110.9 ± 0.24	0.139 ± 0.02	0.14 ± 0.02	0.143 ± 0.05	8.46 ± 0.04	24
		0.92 ± 0.05	0.137 ± 0.042	0.10 ± 0.03	0.137 ± 0.04	10.8 ± 0.016	48

7.2. Conclusions

There are still many unaddressed questions regarding lipid–protein interactions in the PM of fungi. Disclosing the mechanism of membrane compartments formation, their lipid composition and interrelations will hopefully lead to significant advances in membrane biology, but their investigation is also driven by the importance of some of these compartments in the pathogenicity of clinically relevant fungal species.

A direct correlation between SL polar headgroup and protein distribution was demonstrated (Bento-Oliveira et al. 2020). Pma1p distribution is more heterogeneous in *ipt1*Δ cells, whereas Can1p distribution, if affected at all, becomes slightly more homogeneous. This suggests that $M(IP)_2C$ is directly involved in the organization of MCP, but possibly not of MCC. The concomitant alteration in the rigidity of gel-like domains and Pma1p distribution supports a close communication between gel-like domains and MCP. On the other hand, MCC and ergosterol-enriched domains did not undergo any noticeable changes upon a major alteration of complex SL profile, which corroborates that MCC and ergosterol co-localize, further supporting that $M(IP)_2C$ is not an important constituent of ergosterol-enriched domains.

The antifungal activity of the Ke derivatives was tested against different strains of *S. cerevisiae wt*, *erg6*Δ, *W303* and *AD1-8* with different degrees of resistance to the parent drug. The new Ke derivatives proved to be promising antifungal compounds, especially KeP and KeOP, which presented in general the higher antifungal activity.

Finally, interesting results were obtained regarding the antifungal activity of Nys and Ke against different SL-biosynthetic mutant strains of *S. cerevisiae* at 24 h and 48 h. Although the differences encountered are probably multifactorial and pleiotropic effects cannot be ruled-out, the general trends observed suggest that SL structure and SLEDs, and their influence on membrane compartmentalization are features that should deserve more attention in the pursue of a better understanding of antifungal drug mode of action and resistance, and in the development of more effective therapies against fungal infections.

CHAPTER VIII – CONCLUDING REMARKS AND FUTURE PERSPECTIVES

8.1. Sphingolipid-enriched domains in the plasma membrane of fungi: from biophysics to biology

8.1.1. Biophysical properties of sphingolipid-enriched domains

In *S. cerevisiae*, it was found that the PM of *wt* intact cells contains highly ordered gel domains, since a *t*-PnA lifetime component clearly longer than 30 ns was detected (41.0 ns) (Aresta-Branco et al. 2011). The assignment of the long lifetime component to PM lipid domains was confirmed in PM suspensions and liposomes reconstituted from PM lipids, that is, in the absence of proteins, where even longer lifetime components were obtained (46.0 ns and 50 ns, respectively) (Table 6) (Aresta-Branco et al. 2011).

Table 6 – Long component lifetime (τ_{long}) and normalized amplitude (α_{long}) of t-PnA labelling fungal living cells, isolated PM or reconstituted membranes.

Strains	Biological or reconstituted membranes	Growth conditions	Measurement conditions	τ_{long} (ns)	α_{long}	References
***S. cerevisiae wt* (BY4741; Y00000)**	Intact cells grown to a mid-exponential phase	SC at 30 °C	100 mM $NaH_2PO_4.H_2O$, 100 mM NaCl, 1 mM EDTA, pH 7.4 at 24 °C	40.9 ± 0.8	0.12 ± 0.01	(Aresta-Branco et al. 2011)
			100 mM $NaH_2PO_4.H_2O$, 100 mM NaCl, 1 mM EDTA, pH 7.4 at 30 °C	38.1 ± 1.1	0.15 ± 0.04	(Santos et al. 2017)
	Spheroplasts		100 mM $NaH_2PO_4.H_2O$, 100 mM NaCl, 1 mM EDTA, pH 7.4 at 24 °C	41.4 ± 0.8	0.07 ± 0.02	(Aresta-Branco et al. 2011)
	PM			46.6 ± 2.9	0.4 ± 0.1	
	PM lipids			49.7 ± 0.6	0.32 ± 0.03	
***S. cerevisiae erg6*Δ (Y00568)**	Intact cells grown to a mid-exponential phase			40.7 ± 0.6	0.083 ± 0.007	
***S. cerevisiae per1*Δ (Y05768)**				43.2 ± 0.9	0.123 ± 0.005	
***S. cerevisiae scs7*Δ (Y00858)**				45.7 ± 0.2	0.077 ± 0.003	
***S. cerevisiae ipt1*Δ (Y04007)**				45.1 ± 2.4	0.1 ± 0.01	(Bento-Oliveira et al. 2020)

***S. cerevisiae wt* (RH1800)**	Intact cells grown to an early *log* phase	SC at 25 °C	10 mM MES pH 6.0 at 23 °C	54.6	0.34 ± 0.02	(Vecer et al. 2014)
***S. cerevisiae* (RH3804; lcb1-100)**				54.8	0.09 ± 0.01	
***S. cerevisiae wt* (RH1800)**		Control - SC at 30 °C		57.1	0.35 ± 0.06	
		A = (Myriocin treatment, 2 h incubation with 5 μM solution, at 30 °C)		58.3	0.12 ± 0.06	
		A + DHS 20 μM (2 h incubation, at 30 °C)		57.9	0.42 ± 0.12	
***S. cerevisiae wt* (BY4742)**	Intact cells grown to a stationary phase	YPD at 30 °C	10 mM MES pH 6.0 at 23 °C	57.9	0.43	(Herman et al. 2015)
		YPD at 30 °C + 5 μM DM-11		53.6	0.12	
		YPD at 30 °C + 1.5 μM ODDC		58.9	0.04	
***S. cerevisiae cox7*Δ (BY4742)**		YPD at 30 °C		55.5	0.23	
***S. cerevisiae atp1*Δ (BY4742)**		YPD at 30 °C		55.8	0.20	
C. neoformans* var. *grubii* serotype A strain H99 *(wt)	Intact cells	DMEM, pH 7.2 at 37 °C, 5 % CO_2	-	40.5 ± 4.4	-	(Singh et al. 2012)
Δ*smt1* mutant derived from H99				22.2 ± 1.1	-	
Δ*gcs1* mutant derived from H99				22.7 ± 1.1	-	
***N. crassa wt* (FGSC 2489)**	Conidial suspensions (*lag phase*)	5 h MMV at 26 °C	10mM PBS, pH 7.4 at 30 °C	37.1 ± 0.5	0.076 ± 0.004	(Santos et al. 2017)
		5 h MMV at 30 °C		24.0 ± 0.2	0.051 ± 0.006	
		6 h 15min MMV at 30 °C		31.8 ± 0.5	0.09 ± 0.02	(Santos et al. 2018)
		5 h MMV + 1 h STS at 30 °C		24.5 ± 0.4	0.061 ± 0.008	
		5 h MMV + 1 h Control at 30 °C		24.1 ± 0.6	0.047 ± 0.002	
		5 h SeM at 30 °C		25.5 ± 0.3	0.047 ± 0.001	(Santos et al. 2017)
***N. crassa slime* (FGSC 4761)**	Conidial suspensions (*lag phase*)			38.0 ± 0.4	0.15 ± 0.02	

To better understand the nature of the highly rigid domains, *t*-PnA time-resolved fluorescence was also measured in cellular suspensions of *S. cerevisiae* single deletion mutants, either of the SL or the ergosterol biosynthetic pathways (Figure 47), for which the major lipid alterations has been previously determined relatively to *wt*. Those changes were much more pronounced in the SL or in the sterol profile, respectively. *Erg6*Δ cells are defective in the *ERG6* gene that encodes for the Δ(24)-sterol C-methyltransferase in the ergosterol biosynthetic pathway. This enzyme catalyses the conversion of zymosterol to fecosterol through methylation at C-24, thus *ERG6* gene deletion leads to the accumulation of zymosterol and cholesta-5,7,24-trienol instead of ergosterol (Heese-Peck et al. 2002, Guan et al. 2009). Regarding the SL profile, *erg6*Δ presents minor differences when compared to the *wt*, such as a slightly lower amount of IPCs (Swain et al. 2002, Guan et al. 2009). No alteration in the rigidity of SLEDs was observed in *erg6*Δ cells, which strongly suggested that ergosterol is not a major component of the gel domains (τ_{long} ~ 41 ns as for the *wt*; Table 6) (Aresta-Branco et al. 2011). This interpretation was confirmed using *wt* PM suspensions, where partial ergosterol removal by methyl-β-cyclodextrin did not affect the long lifetime component of *t*-PnA (Aresta-Branco et al. 2011).

For *scs7*Δ and *ipt1*Δ cells, the opposite was observed, that is, a significant increase in the rigidity of the gel domains took place (Table 6). When compared to the *wt*, in both these strains there are major differences in the SL profile, but the ergosterol levels remain approximately the same (Leber et al. 1997, Uemura et al. 2014). Although a different structural change in the SLs is at play in *ipt1*Δ and *scs7*Δ cells, the same trend in the fluorescence behaviour of *t*-PnA was observed, pointing to a similar reorganization of SLEDs (Bento-Oliveira et al. 2020). In *ipt1*Δ yeast cells, MIPC is accumulated instead of $M(IP)_2C$, as they lack the inositolphosphotransferase that catalyses the addition of an inositol phosphate group to MIPC (Figure 47) (Leber et al. 1997). The absence of a second inositol phosphate group renders the polar headgroup of MIPC both smaller and less charged, which results in less electrostatic repulsion between the SL molecules and/or steric hindrance at the headgroup level. This allows a tighter packing of the molecules in the SLEDs and a more rigid environment at the hydrophobic core of the membrane (Bento-Oliveira et al. 2020). A similar explanation has also been formulated to rationalize the tighter packing in gel domains found at the PM of *scs7*Δ cells, which completely lack the 2-OH group in the SL acyl chain (Haak et al. 1997, Aresta-Branco et al. 2011) (Figure 47). Actually, several studies show that the gel formed by SL species hydroxylated in both the fatty acyl chain and the LCB, the most abundant in *wt* cells,

is not as stable as the gel formed by SL species hydroxylated only in either one of them (Marques et al. 2018). The result obtained with *scs7*Δ cells indicated that the highly rigid domains detected in yeast PM were, in fact, SLEDs, later confirmed with the studies using *ipt1*Δ cells (Bento-Oliveira et al. 2020). Between these two works, a study was carried out to obtain more direct evidence for the SL-enriched character of the gel domains using multiple approaches (Vecer et al. 2014). First, in a SL-deficient *S. cerevisiae* strain, *lcb1-100*, no significant variations in the packing of SLEDs were detected in comparison to *wt* cells. However, the normalized amplitude decreased drastically, as shown in Table 6 (from 0.34 in *wt* to 0.09 in *lcb1-100*). A similar behaviour was observed between control cells and cells treated with the serine-palmitoyl transferase inhibitor Myriocin (Figure 47), an alteration that was reverted with the external addition of dihydrosphingosine (DHS) (Vecer et al. 2014). This study thus provided important evidence for both the SL-enriched nature of the highly rigid domains and the use of the normalized amplitude as a measure of their relative abundance in living yeast cells.

More recently, the membrane biophysical properties of the filamentous fungus *N. crassa* started to be studied in detail. The PM of *N. crassa* also contains SL-enriched highly ordered domains. A long lifetime component of ca. 25 ns was found for *t*-PnA labelled *wt* conidia in two different growth media, while for a mutant devoid of cell wall, *slime*, this lifetime reached a value of ca. 38 ns, all these values at 30 °C (Table 6). Hence, in the case of the PM of *slime* cells, gel domains are unequivocally present (Santos et al. 2017). On another hand, in the case of *wt* cells, the long lifetime component of *t*-PnA was much shorter (< 30 ns), and its amplitude clearly below 10 %. This difference can be rationalized in terms of the different SL profiles in these two *N. crassa* strains. In *wt*, $(IP)_2C$ is dominant, while in the case of *slime* higher levels of IPC have been reported (Lester et al. 1974). By having a smaller and less charged headgroup, IPC might promote a tighter packing of the lipids in SLEDs. As compared to, for example, $M(IP)_2C$, $(IP)_2C$ lacks the mannosyl sugar, decreasing the extent of H-bonding at the membrane surface, still retaining a double negative charge, increasing electrostatic repulsion when compared to MIPC. In fact, the difference between the long lifetime component of *t*-PnA in *N. crassa wt* conidia and in *S. cerevisiae wt* cells, at least in part, is likely due to their different sphingolipidome. An important factor may be the shorter acyl chains in the complex SLs of *N. crassa* (Figure 3, Figure 47). In addition, the presence of $(IP)_2C$ and GlcCer in the outer leaflet of the PM of *N. crassa* and also Neurosporaside, though at lower amounts (~4x less) (Costantino et al. 2011), which are not found in *S. cerevisiae*, may account for the differences observed. These differences can result from the individual structure

of these lipids, but also from the broader sphingolipidome in *N. crassa*, which may cause the domains to be more heterogeneous and the packing among SLs less efficient.

Because in *wt N. crassa* the value of long lifetime component of *t*-PnA was below 30 ns, further confirmation that it corresponds to SL-enriched gel domains was required. First, it should be recalled that in *N. crassa* conidia, the ergosterol levels are too low to justify the formation of l_o domains. Second, fluorescence anisotropy measurements carried out with *t*-PnA and DPH (Santos et al. 2017), also indicated the presence of gel domains. The fluorescence anisotropy values were too high for a membrane devoid of both gel and l_o domains, and the anisotropy was much higher for *t*-PnA than DPH which is explained by the presence of gel domains for which *t*-PnA has a strong preference, but not DPH (*e.g.* (Silva et al. 2007, Castro et al. 2009, Marques et al. 2015, dos Santos et al. 2017)). To confirm this hypothesis, the long lifetime component of *t*-PnA was also measured at 26 °C and a value of ca. 37 ns was obtained (Santos et al. 2017), clearly above the 30 ns threshold (Table 6). This lifetime value was much longer than the one obtained at 30 °C (25 ns). Such a drastic change in a narrow temperature range is a strong indication of a neighbouring gel/ l_d phase transition. For DPPC (T_m ~ 42 °C), the long lifetime component distribution is centred at 37 ns at 20 °C, but closer to the transition temperature, at 41 °C it is centred around 29 ns, decreasing drastically to 20 ns at 42 °C, accompanied by a strong reduction in the abundance of gel domains, as determined by time-resolved fluorescence anisotropy measurements (Mateo et al. 1993). Moreover, the value measured at 26 °C is quite similar to the ones obtained at 30 °C for *slime* conidia, and for *S. cerevisiae wt* cells, where the existence of SL-enriched gel domains in the PM was previously established (Aresta-Branco et al. 2011). Therefore, in *N. crassa* conidia at 30 °C, the SLs are responsible for the presence of heterogeneity in the PM and the formation of lipid aggregates that are more rigid than the bulk membrane. The long lifetime component becomes longer than 30 ns at 30 °C for 6 h 15 min germination in MMV (Table 6).

To gain insight into the biophysics behind the formation of gel domains in fungi, artificial mixtures of POPC and PhyCer were characterized (Marques et al. 2015). The PhyCer used had a non-hydroxylated acyl chain. The long lifetime component of *t*-PnA and other photophysical properties of both *t*-PnA and DPH for the molar ratio POPC/PhyCer 3:1, were quite similar to those found in *S. cerevisiae wt* cells. However, they were closer to the values found in *scs7*Δ cells, which also lack the 2-OH group in the acyl chain (Aresta-Branco et al. 2011). Thus, this binary mixture mimics very well the hydrophobic packing of the gel domains in *S. cerevisiae* with the same hydroxylation pattern (Marques et al. 2018). At a POPC/PhyCer molar proportion of 3:1, highly compact and stable stoichiometric complexes are formed due

to the presence of the extra hydroxyl group in the LCB, phytosphingosine (Marques et al. 2015). It is thus possible that the stability of gel domains in yeast when compared to other organisms is also due to the formation of complexes between SLs and glycerophospholipids in the PM. However, the mixture fails to completely mimic the biophysical properties of those domains in *N. crassa*, which is possibly related to its more complex sphingolipidome.

The thermal stability of yeast gel domains was studied in liposome-reconstituted lipids extracted from the *S. cerevisiae* isolated PM, revealing a high melting temperature of yeast PM gel domains (Aresta-Branco et al. 2011). Another interesting observation was that the melting profile of SLEDs (beginning after 42 °C and ending only at about 60 °C) was notably identical to the one observed for liposomes prepared with IPC purified from yeast (Klose et al. 2010) and more thermally stable than a synthetic IPC with sphingosine and a C16:0 acyl chain (palmitoylceramide backbone) (Bjorkbom et al. 2010).

The presence of gel domains was also detected in *C. neoformans*, where the long lifetime component of *t*-PnA fluorescence intensity decay in *wt* cells is ca. 40.5 ns. Interestingly, for the two mutants in the GlcCer synthesis pathway Δ*smt1* and Δ*gcs1*, the long lifetime component values were drastically reduced below 30 ns (Table 6) (Singh et al. 2012). In the mutant Δ*gcs1*, the gene *GCS1*, that encodes for the enzyme glucosylceramide synthase, has been deleted. Thus, these cells are not able to produce glucosylceramide from C9-methyl ceramide. On the other hand, C9-methyl ceramide is produced by methylation at position C-9 of the LCB in ceramide. This reaction is catalysed by C-methyltransferase, encoded by a gene that is deleted in the mutant Δ*smt1*, which synthesizes only unmethylated GlcCer (Singh et al. 2012). This points to an important structural role of glucosylceramides in the formation and stability of gel domains in *C. neoformans*.

The works described above helped in the elucidation of the gel nature of the highly rigid domains found in fungal PM and consistently supported that they are SL-enriched and that their packing and thermal stability are highly dependent on the structure of complex SLs.

8.2. Possible physiological roles of sphingolipid-enriched domains

Following the discovery of SLEDs, their physiological relevance became a pressing question, motivating several studies aiming at finding an association between these domains and different cellular processes involving the fungal PM and the plethora of functions attributed

to SLs (Breslow and Weissman 2010, Dickson 2010, Mota Fernandes and Del Poeta 2020). The higher order and the ability to undergo a well-defined gel/fluid phase transition seem to be important features that differentiate SLEDs from other lipid domains (Aresta-Branco et al. 2011, Vecer et al. 2014), making them, for example, more responsive to thermal stress (Dickson 2008, Marques et al. 2018).

The PM organization in yeast is deeply affected by depolarization, a subject reviewed in detail elsewhere (Malinsky et al. 2016). The strong connection between the transmembrane potential of the fungal PM and the organization of membrane compartments and of the SLEDs was shown with multiple protocols, namely depolarization attained by external stimuli, such as electric fields and chemical agents, for example, DM-11 and ODDC (Malinsky et al. 2016). DM-11 is an ionophore that makes the PM permeable to electrical stimuli and inhibits the PM H^+-ATPase activity, whereas ODDC is an ionophore with antimicrobial properties that binds to negatively charged cell surfaces and induces the permeabilization of the PM. Both these ionophores markedly decrease the abundance of gel domains in the PM (from 0.43 (*wt*) to ca. 0.12 (with DM-11) and 0.04 (with ODDC)) (Table 6). However, the long lifetime component of *t*-PnA that decreases with the addition of DM-11 is essentially unchanged with the addition of ODDC (Herman et al. 2015). A reduction of the relative abundance of the gel domains, but not of their rigidity, was also observed in respiratory deficient strains (*cox7*Δ and *atp1*Δ), when compared to *wt* cells (Table 6) (Herman et al. 2015). In the same work, the authors used other methods to achieve membrane depolarization and, while in a few cases a small reduction in the long lifetime component of *t*-PnA could be noted, the constant observation was a drastic reduction of the relative abundance of gel domains (Herman et al. 2015).

The results above are of unquestionable physiological relevance, as they show that SL segregation into SLEDs in yeast depends on energy supply and transmembrane potential, that is, SLEDs are actively maintained in the membranes of living yeast cells and their modulation does not require changes in membrane composition (Malinsky and Opekarova 2016). Also, during the depolarization of the yeast PM, gel domains are dissipated, indicating that these lipid domains can quickly and reversibly respond to stress situations and environmental changes (Grossmann et al. 2007, Herman et al. 2015, Marques et al. 2015, Malinsky et al. 2016). Thus, one possible role of SLEDs is to sense, resist and/or respond to environmental stress.

A decrease in the abundance of SLEDs was reported for cells that lack one of the enzymes necessary for ergosterol synthesis (*erg6*Δ mutant) or SLs acyl chain 2-hydroxylation (*scs7*Δ mutants), and in both cases was accompanied by an increased global membrane order (as well as in spheroplasts, as will be discussed below), underpinning a possible general

adaptation mechanism involving SLEDs (Table 6; (Aresta-Branco et al. 2011)). This increase in the order of fluid domains in cells with impaired SL or sterol metabolism (or cell wall) was interpreted as resulting from a more homogeneous distribution of the SLs in the membrane, which increases the order of the fluid regions, an effect that largely compensates for the decrease in the order resulting from a diminished relative abundance of the gel domains (Aresta-Branco et al. 2011). The significant reduction in the abundance of gel domains at the PM of intact *wt S. cerevisiae* cells invoked by cell depolarization using DM-11 or ODDC (Table 6) is accompanied by the homogenous dispersion of specific MCC H^+-symporters (Grossmann et al. 2007) and an increase in the order of fluid domains in the PM of *S. cerevisiae* (Herman et al. 2015). It was proposed that ergosterol is released from a specific pool in the MCC, ensuring the stabilization of SLs in more disordered regions of the PM (Malinsky et al. 2016), contributing further to the observed global rigidification of the membrane.

SLEDs have been associated with *S. cerevisiae* cellular adaptation to hydrogen peroxide (H_2O_2) (Marques et al. 2018). *S. cerevisiae* cells, when adapted to H_2O_2, have reduced levels of the hydroxylated very long-chain fatty acid 2-OH-C26:0, the major acyl chain in the complex SLs of *wt* budding yeast, as compared to non-adapted cells (Pedroso et al. 2009). This sphingolipidome alteration is accompanied by a decrease in the permeability to H_2O_2, alterations of the membrane order (Folmer et al. 2008), and an increase in *t*-PnA quantum yield (Pedroso et al. 2009).

Moreover, in model systems, we found the lowest values of IF_{420}/IF_{520} in lipid bilayers in the gel phase (Khmelinskaia et al. 2014, Khmelinskaia et al. 2020), which are another indication of the presence of gel domains in fungal PM. Finally, 2-hydroxylated fatty acids are able to decrease membrane dipole potential, as measured by di-4-ANEPPS excitation intensity ratio, in either l_d, l_o or gel membranes (Khmelinskaia et al. 2014). Such result is of particular interest and should be further exploited, as fungal SL are highly hydroxylated, as compared to their most common mammalian counterparts (Marques et al. 2018). Therefore, it can be hypothesized that the SL hydroxylation pattern in fungi may contribute, in addition to the presence of ergosterol *versus* cholesterol, for the low membrane dipole potential in the PM of fungi. In *N. crassa* conidia, which are practically devoid of ergosterol, the SL hydroxylation may be of particular relevance. This is a subject that undoubtedly deserves further investigation.

Conidial cell death in *N. crassa* caused by heat shock and/or analogue-induced glucose deprivation was concomitant with an increase in phytoceramides production, correlating SLs with cell death in this fungus, although gel domains were not directly addressed in this study

(Plesofsky et al. 2008). More recently, it was shown that SLEDs abundance is increased in *N. crassa* conidia PM following 1 h challenge with STS, a drug used in several organisms to induce programmed cell death, after 5 h germination (Table 6). This change was accompanied by an increased fluidity in other membrane regions (Santos et al. 2018), again correlating a higher abundance of SLEDs with a lower global membrane order in fungi, and therefore suggesting an involvement of gel domains in the response of *N. crassa* to STS.

Since the lateral diffusion in the gel phase is much slower than in less ordered phases, and discontinuous gel domains strongly hinder long range diffusion of membrane components in the fluid phase (Almeida et al. 1992, Ratto and Longo 2002, van 't Klooster et al. 2020), SLEDs might be important diffusion barriers for both lipids and proteins in fungal membranes (de Almeida and Joly 2014). In this way, they would contribute to the larger immobility or characteristic slower diffusion of proteins in the PM of fungi (Malinsky et al. 2013, Khan et al. 2015) when compared to the PM of animal cells (Valdez-Taubas and Pelham 2003, Bianchi et al. 2018). This guarantees a polarized distribution and stable spatiotemporal compartmentalization of proteins and lipids along the fungal PM (Marques et al. 2015).

Recently, it was reported that proteins of the MCP are surrounded (periprotein lipidome) by more SLs and less ergosterol when compared to MCC proteins, indicating that proteins in the MCP would diffuse even more slowly due to their surrounding lipid environment (van 't Klooster et al. 2020). Moreover, SLs play an important role in cell division, most likely at a late stage of cytokinesis and certainly in cell separation (Epstein et al. 2012). Additionally, there is evidence for the need of an integral SL biosynthesis pathway for the formation of diffusion barriers in the cortical endoplasmic reticulum at the bud neck, specifically necessary for the separation of mother and daughter cell components during budding (Clay et al. 2014).

SLEDs are also thought to be relevant for trafficking and signalling of certain proteins. Glycosylphosphatidylinositol (GPI) anchors in yeast have mostly a (phyto)ceramide backbone, rather than being diacylglycerol-based as typically found in mammals, thus having the same hydrophobic backbone as the SLs. When one of the enzymes involved in the remodelling of GPI-anchors is deleted as in *per1*Δ cells, the GPI anchor remains with an unsaturated acyl chain at the *sn*-2 position and the ceramide-type anchor is not inserted. Moreover, this deletion leads to more rigid SLEDs (Table 6; (Aresta-Branco et al. 2011)). These results indicate that SLEDs might contain a significant amount of GPI-anchored proteins, suggesting a role of these highly ordered domains in GPI-anchored proteins trafficking and signalling. It is also known that SLs stabilize the association of GPI-anchored proteins with membranes and are required for

trafficking from the endoplasmic reticulum to the Golgi (Heese-Peck et al. 2002, Watanabe et al. 2002, Gaigg et al. 2005). Moreover, the vesicles that transport GPI-anchored proteins from the endoplasmic reticulum to the Golgi are ceramide-enriched (Watanabe et al. 2002) and may already contain gel domains. Interestingly, the transport of GPI-anchored proteins is different between mammals and fungi (Muñiz and Riezman 2016, Lopez et al. 2019), which may be justified by the fact that SLEDs are only found in fungi and not mammals.

SLEDs may play a crucial role in the maintenance of transmembrane proton gradient and ion homeostasis. In fact, evidence suggesting that Pma1p is associated with SLEDs has been accumulating. SLs with very long-chain fatty acids that typically form gel domains are required for Pma1p oligomerization (Bagnat et al. 2001, Lee et al. 2002, Wang and Chang 2002), traffic (Bagnat et al. 2001), stability at the PM (Wang and Chang 2002) and degradation (Gaigg et al. 2006). In *C. neoformans*, alteration of the SL biosynthesis pathway affects Pma1p function and cell growth (Farnoud et al. 2014, Munshi et al. 2018). In *S. cerevisiae ipt1*Δ cells, the alteration of SL profile simultaneously affected the SLEDs rigidity (Table 6) and the distribution and environment of Pma1p (Bento-Oliveira et al. 2020), which in turn might interfere with Pma1p normal functioning (Kane 2016), and consequently with nutrient uptake by H^+-symporters at the MCC. Accordingly, SLEDs might be relevant for adapting the PM permeability when facing depolarization-induced stress (as described above), in a quicker and less energy-consuming manner than through active ion transport, and also for regulating membrane global order and protein distribution.

Finally, SLEDs may play a role in GPI-anchored proteins sorting to the cell wall (Gow et al. 2017), or in PM stabilization, when the cell wall is damaged or removed. These domains become less abundant in *S. cerevisiae* spheroplasts obtained from *wt* cells by cell wall enzymatic removal (Table 6; (Aresta-Branco et al. 2011)), but the membrane becomes globally less fluid. Lipid and protein compartmentalization on the membrane is interconnected with the cell wall and is sensitive to cell wall stress (de Almeida 2018), further suggesting that SLEDs may be involved in the response to alterations in the cell wall. Sur7p, for instance, is a transmembrane protein involved in SL metabolism that is stabilized in the MCC, due to interactions between the cell wall and the PM (Young et al. 2002). Also, in *S. cerevisiae*, MIPC and/or ergosterol defective strains with hyperactivated cell wall integrity pathway, exhibit cell wall defects that are sensed by proteins located at the MCW, such as Wsc1 and 2 (Tanaka and Tani 2018). *N. crassa slime* strain lacks cell wall and has SLEDs with much tighter packing and higher melting temperature than the *wt* (Table 6) (Santos et al. 2017). Altogether, these studies point to different possible connections between the cell wall and the SLEDs in yeasts

and filamentous fungi. In *N. crassa slime*, STS induces a large membrane reorganization, leading to a decrease in global membrane rigidity at the expense of ordered domains. A similar increase in global fluidity has been observed in *S. cerevisiae* for mutants possessing less abundant SLEDs than the *wt* (Aresta-Branco et al. 2011), as well as for *S. cerevisiae* spheroplasts, as described above.

Finally, the lipid domain organization and biophysical properties of both *wt* and *abc3* strains are similar. The small differences observed maybe due to the slower growth rate of *abc3*. In fact, at 3 h, it appears that *abc3* has smaller relative amounts of both ergosterol and complex SLs in its PM. Since SL domains are already present in latent spores and start to reorganize at shorter incubation times, assuming that glycerophospholipid synthesis occurs at similar rates in both strains, the net abundance of SLEDs will be smaller in *abc3*. At 6 h growth *abc3* cells present the opposite trend of the *wt* cells, increasing membrane rigidity with the STS challenge, in fact recovering from a control situation of higher fluidity compared to the *wt*. An exceptional behaviour occurred also for *abc3* at 6 h in the relative abundance of SLEDs, where a decrease was observed. This could be related to the higher sensitivity of *abc3* cells to STS and/or their inability to efficiently export the drug. To fully interpret the specific behaviour of *abc3* mutant strain at 6 h it will be crucial to analyse the relative fractions of cells that are undergoing cell death and apoptosis under the STS challenge (future work).

8.3. Antifungal activity and sphingolipid-enriched domains

SLs, in particular gel domains rich in SLs, are important parts of the fungal PM and, considering that they are not found in mammalian PM under physiological conditions, they emerge as elements that may contribute for the specific action of antifungal agents on fungi *vs.* mammalian PM.

It was recently shown that Nys, a polyene antifungal drug, has a strong pore-forming activity in membranes containing gel domains and lacking any sterols, and that Nys-membrane interactions are highly dependent on the composition and properties of gel domains (dos Santos et al. 2017). These observations challenged the current understanding of Nys mode of action at the time, which implicated a strong dependence on the presence of sterols. This polyene antifungal agent contains a tetraene motif identical to *t*-PnA, which has a preferential partition towards gel domains. In fact, the membrane/water partition coefficients of Nys measured in

liposomes composed by either POPC/SM or POPC/DPPC are higher towards these gel-containing membranes (dos Santos et al. 2017) as opposed to fluid POPC membranes (Coutinho and Prieto 2003), which clearly shows the preference of this antifungal for gel-containing membranes.

Nys at 10 μg/mL inhibits the growth of *wt S. cerevisiae* cells, whereas *ipt1*Δ cells are, under certain conditions, resistant to this antifungal agent. In this work, we report a MIC_{50} for 24 h incubation that is ~5-fold for *ipt1*Δ than for the *wt*. The impact of $M(IP)_2C$ depletion in the properties of gel domains, but not in ergosterol-enriched domains (Bento-Oliveira et al. 2020), together with the ability of Nys to form active pores in the absence of any sterol, as long as a gel phase is present (dos Santos et al. 2017), supports the hypothesis that SLEDs are a target for polyene antifungal drugs in the PM of fungi. In *wt* yeast cells depolarized with the uncoupling agent p-trifluoromethoxycarbonylcyanide phenylhydrazone (FCCP), Nys effects are almost suppressed completely (Komor et al. 1979). Considering that Nys might preferentially target SL-enriched gel domains in the PM of fungi, the resistance phenotype observed upon FCCP uncoupling might be explained by the great decrease in the abundance of gel domains as a result of membrane depolarization using ionophores (Table 6) (Herman et al. 2015). Alternatively, and in line with the model of a mode of action of polyene drugs largely dependent on membrane sterols, it has been previously suggested that the reduced vulnerability of fungi towards polyenes upon cell depolarization can be a cause of decreased sterol accessibility, possibly due to the decline in local sterol accumulation in depolarized PMs (Malinsky et al. 2016). It is also possible that both mechanisms are taking place.

Syringomycin E is another agent that forms channels in the membrane and causes K^+ efflux and Ca^{2+} influx (Zhang and Takemoto 1989, Takemoto et al. 1991). Its activity is also highly dependent on the SL composition of the PM in yeast. As in the case of Nys, in *wt* a sensitivity phenotype is observed, whereas *ipt1*Δ cells, where MIPC accumulates and $M(IP)_2C$ is absent, display a higher resistance (Stock et al. 2000). However, higher levels of MIPC, when $M(IP)_2C$ is still produced, do not change the sensitivity phenotype (Stock et al. 1999). The hydroxylation pattern of SLs in yeast also seems to be important for the fungicidal activity of syringomycin E. In fact, yeast *scs7*Δ cells are also less susceptible to the action of this antifungal than *wt* cells (Hama et al. 2000). In these cells, where $M(IP)_2C$ is present, though lacking a hydroxyl group at C-2 position of the fatty acid (Figure 47), SLEDs are also more rigid than in *wt* (Marques et al. 2018) (Table 6) and in this case higher resistance to syringomycin E is also obtained (Hama et al. 2000), just as in *ipt1*Δ cells.

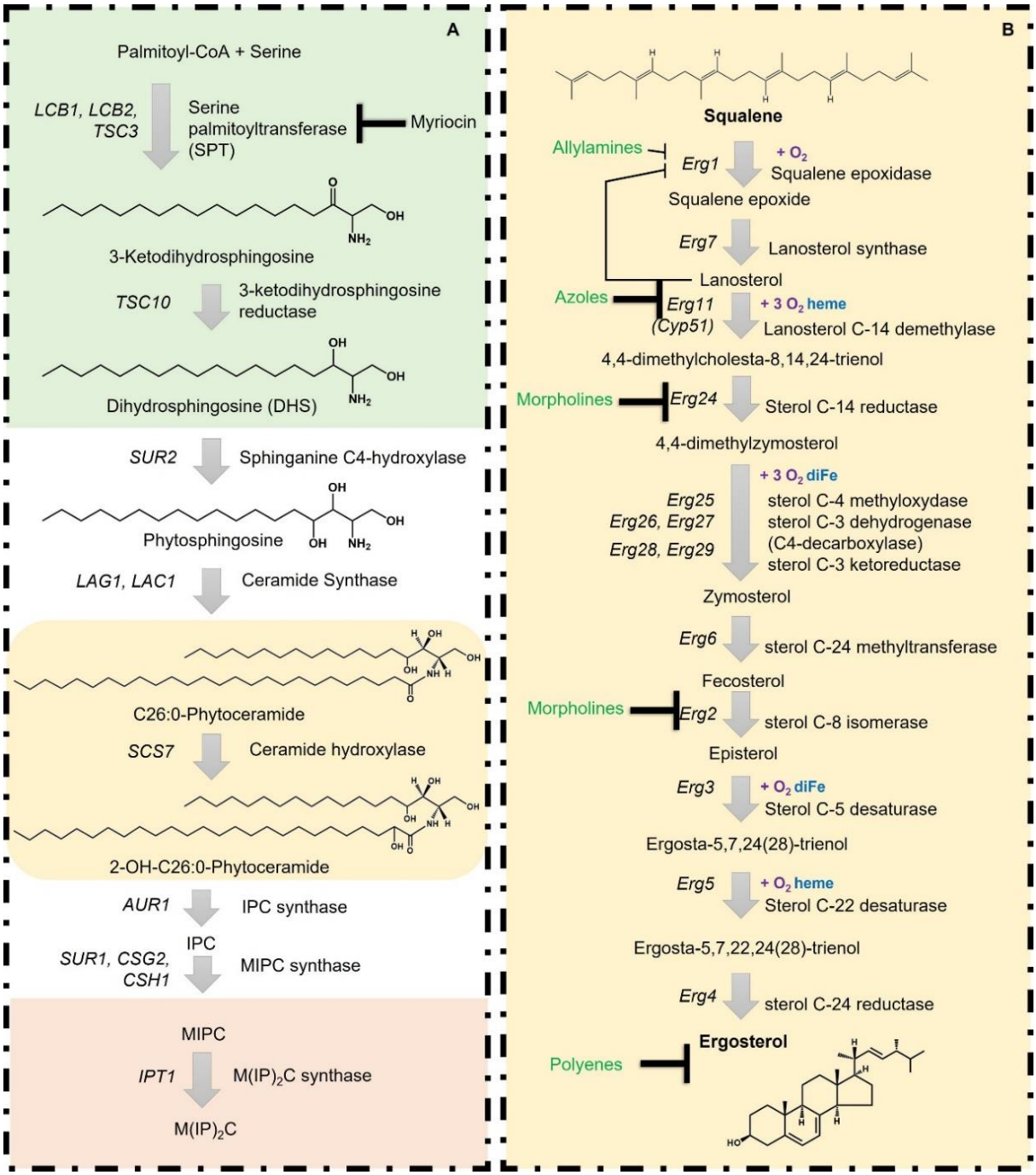

Figure 47 – A) Schematic and simplified representation of the complex SL biosynthetic pathway in S. cerevisiae. The scheme highlights the reaction catalysed by SPT, which is inhibited by myriocin and can be bypassed by the addition of DHS, and the reactions catalysed by Scs7p and Ipt1p. B) Late Ergosterol biosynthetic pathway in S. cerevisiae, which ends with ergosterol biosynthesis, and mainly takes place in the endoplasmic reticulum. Enzymes, intermediates, inhibitors and requirements of oxygen, heme and iron are indicated.

In summary, the lack of $M(IP)_2C$ seems to render the PM of yeast cells more resistant to the action of antifungal agents that need to insert into the membrane and subsequently assemble into active pores in order to become active. The absence of $M(IP)_2C$ (*ipt1*Δ cells) leads to an increase in the rigidity of gel domains (Bento-Oliveira et al. 2020) (Table 6), which, to some extent, can hinder membrane insertion of those antifungals that may target SL-enriched gel domains. Recently, we have shown that the absence of $M(IP)_2C$ alters Pma1p distribution (Bento-Oliveira et al. 2020), thus the organization of MCP. Despite the fact that particular SLs in the PM of fungi might constitute the specific binding sites of some antifungal agents, the requirement of intact MCP/ SLED cannot be ruled out as an important feature for antifungals to trigger their toxic effects.

Regarding, Nys the results of antifungal activity obtained against different SL-biosynthetic mutant strains of *S. cerevisiae* at 24 h and 48 h, were interesting, being the behaviour of some mutant strains different between 24 h and 48 h. Hence, is still necessary to further study these strains in order to confirm and interpret the behaviour observed.

The importance of PM SLs for the action of plant defensins has also been well demonstrated for *N. crassa* (Ferket et al. 2003, Thevissen et al. 2003, Park et al. 2005). Mutants of *N. crassa* chemically induced by ethylmethanesulphonate were studied and selected regarding their resistance towards radish plant defensin RsAFP2. Among the mutants produced, some exhibited increased resistance against several plant defensins including DmAMP1 and RsAFP2 (Ferket et al. 2003). Lipid analysis by high-performance thin layer chromatography revealed altered profiles of both IPC-based SLs, and neutral lipids, including putative glycosylceramides and sterylglucosides (Ferket et al. 2003). An altered balance of neutral and negatively charged SLs may have an impact on PM net surface charge and charge distribution, and thus influence the interaction of antimicrobial peptides with the membrane (Huber et al. 2019), which frequently has an important electrostatic component. The cationic *Penicillium chrysogenum* antifungal protein B, interacts much more promptly with liposomes prepared from lipid extracts of the Δ*lac* strain of *N. crassa* than with the *wt* or Δ*gcs1* (Huber et al. 2019). The mutant strain Δ*lac* accumulates negatively charged SLs and the liposomes prepared from its lipid extracts exhibit a zeta-potential of - 39 mV, whereas that of *wt* and Δ*gcs1* derived liposomes was −34 mV and −29 mV, respectively (Huber et al. 2019). Of special relevance in *N. crassa* was also the fatty acyl chain of GlcCer. In the mutant strains there is a significant structural change of the acyl chain, both in unsaturation and length. Instead of a E-Δ(3)-unsaturated, 2-hydroxy-(3E)-octadecenoyl chain (C18:1), found in *wt* GlcCer, in the

mutants GlcCer presented a saturated, 2-hydroxy-16:0 acyl chain (Ferket et al. 2003, Park et al. 2005). Although no biophysical characterization is available regarding these mutants of *N. crassa*, the Δ*gcs1* and Δ*smt1* strains of *C. neoformans* were shown to contain profoundly altered gel domains as compared to the *wt* (Table 6) (Singh et al. 2012), which corroborates the role played by this kind of domains in the interaction of plant defensins with the PM. In agreement, it has been shown that the absence of the fatty acid E-Δ(3)-unsaturation in GlcCer renders different fungal species more tolerant against AFP, an antimicrobial peptide produced by *Aspergillus giganteus* (Paege et al. 2019). Therefore, despite the fact that the mechanisms of action are still under clarification, the structure of fungal GlcCers, which has consequences in the properties of ordered domains, seems to affect the sensitivity of fungal species to antimicrobial peptides.

Alterations in SLEDs also have an impact on the action of other antifungal agents for which the PM is not a direct target. Miconazole pertains to the class of azole antimycotics and its mode of action concerns the inhibition of two cytochrome P450 enzymes implicated in the biosynthesis of ergosterol (Kelly et al. 1997). Thus, ultimately, azoles inhibit the production of this sterol and lead to the accumulation of toxic intermediates. Though miconazole has an intracellular target, its action against the *ipt1*Δ mutant strain is severely decreased. This strain is more resistant to miconazole than *wt* (Tanaka and Tani 2018) at least one order of magnitude higher (Francois et al. 2009). The authors observed that the intracellular accumulation of miconazole was significantly lower in the mutant strain (Francois et al. 2009). Thus, it seems that its action may be controlled by altering PM properties and organization. In this case, the alterations in yeast PM led to an impaired miconazole uptake that can be justified by an increased export of the drug or a less permeable membrane.

The antifungal activity of the new Ke derivatives was tested against different strains of *S. cerevisiae wt*, *erg6*Δ, *W303* and *AD1-8* with different degrees of resistance to the parent drug. The new Ke derivatives proved to be promising antifungal compounds, especially KeP and KeOP, which presented in general the higher antifungal activity.

Ke, as Nys, was also studied against different SL-biosynthetic mutant strains of *S. cerevisiae* at 24 h and 48 h and the results were also curious. The differences found for the efficiency of both Ke and Nys, between the 24 h and the 48 h assays, in case of *wt*, are possibly related to the different mode of action. Nys mode of action implies direct permeabilization of the PM, whereas the effects of Ke inhibition of ergosterol synthesis should be more noticed at

longer times, which may require for shortage of ergosterol pools and accumulation of toxic sterol intermediates.

Finally, and although the differences encountered for both Ke and Nys are probably multifactorial and pleiotropic effects cannot be ruled-out, the general trends observed suggest that SL structure and SLEDs, and their influence on membrane compartmentalization are features that should deserve more attention in the pursue of a better understanding of antifungal drug mode of action and resistance, and in the development of more effective therapies against fungal infections.

CHAPTER IX – REFERENCES

Almeida, P. F. F., Vaz, W. L. C. and Thompson, T. E. (1992). "Lateral Diffusion and Percolation in 2-Phase, 2-Component Lipid Bilayers - Topology of the Solid-Phase Domains Inplane and Across the Lipid Bilayer." Biochemistry **31**(31): 7198-7210.

Anderson, J. B., Sirjusingh, C., Parsons, A. B., Boone, C., Wickens, C., Cowen, L. E. and Kohn, L. M. (2003). "Mode of selection and experimental evolution of antifungal drug resistance in Saccharomyces cerevisiae." Genetics **163**(4): 1287-1298.

Aresta-Branco, F., Cordeiro, A. M., Marinho, H. S., Cyrne, L., Antunes, F. and de Almeida, R. F. (2011). "Gel domains in the plasma membrane of Saccharomyces cerevisiae: highly ordered, ergosterol-free, and sphingolipid-enriched lipid rafts." Journal of Biological Chemistry **286**(7): 5043-5054.

Athanasopoulos, A., Andre, B., Sophianopoulou, V. and Gournas, C. (2019). "Fungal plasma membrane domains." FEMS Microbiology Reviews **43**(6): 642-673.

Bagnat, M., Chang, A. and Simons, K. (2001). "Plasma membrane proton ATPase Pma1p requires raft association for surface delivery in yeast." Molecular Biology of the Cell **12**(12): 4129-4138.

Bagulho, A., Vilas-Boas, F., Pena, A., Peneda, C., Santos, F. C., Jerónimo, A., de Almeida, R. F. M. and Real, C. (2015). "The extracellular matrix modulates H2O2 degradation and redox signaling in endothelial cells." Redox Biology **6**: 454-460.

Bastos, A. E., Marinho, H. S., Cordeiro, A. M., de Soure, A. M. and de Almeida, R. F. (2012b). "Biophysical properties of ergosterol-enriched lipid rafts in yeast and tools for their study: characterization of ergosterol/phosphatidylcholine membranes with three fluorescent membrane probes." Chemistry and Physics of Lipids **165**(5): 577-588.

Bastos, A. E., Scolari, S., Stockl, M. and Almeida, R. F. (2012a). Applications of fluorescence lifetime spectroscopy and imaging to lipid domains in vivo. Methods in Enzymology. **504:** 57-81.

Baumgart, T., Hunt, G., Farkas, E. R., Webb, W. W. and Feigenson, G. W. (2007). "Fluorescence probe partitioning between Lo/Ld phases in lipid membranes." Biochimica et Biophysica Acta (BBA) - Biomembranes **1768**(9): 2182-2194.

Beck, D. P. and Greenawalt, J. W. (1977). "Composition And Synthesis Of Cellular Lipids In Neurospora-Crassa During Cellular Differentiation." Journal of Bacteriology **131**(1): 188-193.

Bento-Oliveira, A., Santos, F. C., Marquês, J. T., Paulo, P. M. R., Korte, T., Herrmann, A., Marinho, H. S. and de Almeida, R. F. M. (2020). "Yeast sphingolipid-enriched domains and membrane compartments in the absence of mannosyldiinositolphosphorylceramide." Biomolecules **10**(6): 871.

Berezin, M. Y. and Achilefu, S. (2010). "Fluorescence Lifetime Measurements and Biological Imaging." Chemical reviews **110**(5): 2641-2684.

Bhatia, T., Husen, P., Brewer, J., Bagatolli, L. A., Hansen, P. L., Ipsen, J. H. and Mouritsen, O. G. (2015). "Preparing giant unilamellar vesicles (GUVs) of complex lipid mixtures on demand: Mixing small unilamellar vesicles of compositionally heterogeneous mixtures." Biochimica et Biophysica Acta (BBA) - Biomembranes **1848**(12): 3175-3180.

Bianchi, D. E. and Turian, G. (1967). "Lipid Content Of Conidia Of Neurospora Crassa." Nature **214**(5095): 1344-&.

Bianchi, F., Syga, Ł., Moiset, G., Spakman, D., Schavemaker, P. E., Punter, C. M., Seinen, A.-B., van Oijen, A. M., Robinson, A. and Poolman, B. (2018). "Steric exclusion and protein conformation determine the localization of plasma membrane transporters." Nature Communications **9**(1): 501.

Biltonen, R. L. and Lichtenberg, D. (1993). "The use of differential scanning calorimetry as a tool to characterize liposome preparations." Chemistry and Physics of Lipids **64**(1): 129-142.

Bjorkbom, A., Ohvo-Rekila, H., Kankaanpaa, P., Nyholm, T. K., Westerlund, B. and Slotte, J. P. (2010). "Characterization of membrane properties of inositol phosphorylceramide." Biochimica et Biophysica Acta (BBA) - Biomembranes **1798**(3): 453-460.

Bojsen, R., Regenberg, B. and Folkesson, A. (2014). "Saccharomyces cerevisiae biofilm tolerance towards systemic antifungals depends on growth phase." BMC Microbiology **14**: 305.

Bolard, J. (1986). "How do the polyene macrolide antibiotics affect the cellular membrane properties?" Biochimica et Biophysica Acta (BBA) - Reviews on Biomembranes **864**(3-4): 257-304.

Borkovich, K. A., Alex, L. A., Yarden, O., Freitag, M., Turner, G. E., Read, N. D., Seiler, S., Bell-Pedersen, D., Paietta, J., Plesofsky, N., Plamann, M., Goodrich-Tanrikulu, M., Schulte, U., Mannhaupt, G., Nargang, F. E., Radford, A., Selitrennikoff, C., Galagan, J. E., Dunlap, J. C., Loros, J. J., Catcheside, D., Inoue, H., Aramayo, R., Polymenis, M., Selker, E. U., Sachs, M. S., Marzluf, G. A., Paulsen, I., Davis, R., Ebbole, D. J., Zelter, A., Kalkman, E. R., O'Rourke, R., Bowring, F., Yeadon, J., Ishii, C., Suzuki, K., Sakai, W. and Pratt, R. (2004). "Lessons from the Genome Sequence of Neurospora crassa: Tracing the Path from Genomic Blueprint to Multicellular Organism." Microbiology and Molecular Biology Reviews **68**(1): 1-108.

Borst, J. W. and Visser, A. J. W. G. (2010). "Fluorescence lifetime imaging microscopy in life sciences." Measurement Science and Technology **21**(10): 102002.

Botstein, D. and Fink, G. R. (2011). "Yeast: An Experimental Organism for 21st Century Biology." Genetics **189**(3): 695-704.

Bowman, E. J. and Bowman, B. J. (2007, September 2007). "How to prepare vacuolar membranes and other membrane fractions." Neurospora - Neurospora Protocol Guide, from https://www.fgsc.net/Neurospora/NeurosporaProtocolGuide.htm.

Branco, M., Pedros, N., Sousa, A., Marinho, H. S., Cyrne, L. and Antunes, F. (2004). Regulation of the permeability of biomembranes to H2O2: Implications for redox compartmentalization.

Branco, M. R., Marinho, H. S., Cyrne, L. and Antunes, F. (2004). "Decrease of H2O2 Plasma Membrane Permeability during Adaptation to H2O2 in Saccharomyces cerevisiae." Journal of Biological Chemistry **279**(8): 6501-6506.

Braun, E. L., Natvig, Donald O., Werner-Washburne, Margaret, Nelson, Mary Anne (2004). "Genomics in Neurospora crassa: From One-Gene-One-Enzyme to 10,000 Genes." Fungal Genomics **3 e 4**: 295-313.

Breslow, D. K. and Weissman, J. S. (2010). "Membranes in balance: mechanisms of sphingolipid homeostasis." Molecular Cell **40**(2): 267-279.

Bunge, A., Müller, P., Stöckl, M., Herrmann, A. and Huster, D. (2008). "Characterization of the Ternary Mixture of Sphingomyelin, POPC, and Cholesterol: Support for an Inhomogeneous Lipid Distribution at High Temperatures." Biophysical Journal **94**(7): 2680-2690.

Busto, J. V., Elting, A., Haase, D., Spira, F., Kuhlman, J., Schafer-Herte, M. and Wedlich-Soldner, R. (2018). "Lateral plasma membrane compartmentalization links protein function and turnover." The EMBO Journal **37**(16).

Busto, J. V., Garcia-Arribas, A. B., Sot, J., Torrecillas, A., Gomez-Fernandez, J. C., Goni, F. M. and Alonso, A. (2014). "Lamellar Gel (L-beta) Phases of Ternary Lipid Composition Containing Ceramide and Cholesterol." Biophysical Journal **106**(3): 621-630.

Cannon, R. D., Lamping, E., Holmes, A. R., Niimi, K., Baret, P. V., Keniya, M. V., Tanabe, K., Niimi, M., Goffeau, A. and Monk, B. C. (2009). "Efflux-mediated antifungal drug resistance." Clinical Microbiology Reviews **22**(2): 291-321, Table of Contents.

Carlile, M. J., Watkinson, S. C. and Gooday, G. W. (2001). 2 - Fungal Diversity. The Fungi. M. J. Carlile, S. C. Watkinson and G. W. Gooday. London, Academic Press**:** 11-84.

Carreira, A. C. (2019). Sphingosine-induced alterations in membrane biophysical properties: biological relevance in the pathophysiology of human disease. Doctoral, Universidade de Lisboa.

Carreira, A. C., Santos, T. C., Lone, M. A., Zupančič, E., Lloyd-Evans, E., de Almeida, R. F. M., Hornemann, T. and Silva, L. C. (2019). "Mammalian sphingoid bases: Biophysical, physiological and pathological properties." Progress in Lipid Research **75**: 100988.

Carreira, A. C., Ventura, A. E., Varela, A. R. P. and Silva, L. C. (2015). "Tackling the biophysical properties of sphingolipids to decipher their biological roles." Biological Chemistry **396**(6-7): 597-609.

Case, M. E., Griffith, J., Dong, W., Tigner, I. L., Gaines, K., Jiang, J. C., Jazwinski, S. M., Arnold, J. and Georgia Centenarian, S. (2014). "The aging biological clock in Neurospora crassa." Ecology and Evolution **4**(17): 3494-3507.

Castanho, M. A. R. B., Santos, N. C. and Loura, L. M. S. (1997). "Separating the turbidity spectra of vesicles from the absorption spectra of membrane probes and other chromophores." European Biophysics Journal **26**(3): 253-259.

Castro, A., Lemos, C., Falcao, A., Fernandes, A. S., Glass, N. L. and Videira, A. (2010). "Rotenone enhances the antifungal properties of staurosporine." Eukaryotic Cell **9**(6): 906-914.

Castro, B. M., Silva, L. C., Fedorov, A., de Almeida, R. F. and Prieto, M. (2009). "Cholesterol-rich fluid membranes solubilize ceramide domains: implications for the structure and dynamics of mammalian intracellular and plasma membranes." The Journal of Biological Chemistry **284**(34): 22978-22987.

Chakrabarti, A. (2011). "Drug resistance in fungi – an emerging problem." Regional Health Forum **15**(1): 97-103.

Chinnappan, S., Yi, C. L., Chen, C. J., Hsia, T. W. and Qi, Y. H. (2020). "Recent Advances in Delivery of Antifungal Agents – A Review." Journal of Young Pharmacists **12**(3): 193-196.

Clarke, R. J. and Kane, D. J. (1997). "Optical detection of membrane dipole potential: Avoidance of fluidity and dye-induced effects." Biochimica et Biophysica Acta (BBA) - Biomembranes **1323**(2): 223-239.

Clay, L., Caudron, F., Denoth-Lippuner, A., Boettcher, B., Frei, S. B., Snapp, E. L. and Barral, Y. (2014). "A sphingolipid-dependent diffusion barrier confines ER stress to the yeast mother cell." Elife **3**.

Córcoles-Sáez, I., Hernández, M. L., Martínez-Rivas, J. M., Prieto, J. A. and Randez-Gil, F. (2016). "Characterization of the S. cerevisiae inp51 mutant links phosphatidylinositol 4,5-bisphosphate levels with lipid content, membrane fluidity and cold growth." Biochimica et Biophysica Acta (BBA) - Molecular and Cell Biology of Lipids **1861**(3): 213-226.

Correa, H., Aristizabal, F., Duque, C. and Kerr, R. (2011). "Cytotoxic and antimicrobial activity of pseudopterosins and seco-pseudopterosins isolated from the octocoral Pseudopterogorgia elisabethae of San Andres and Providencia Islands (Southwest Caribbean Sea)." Marine Drugs **9**(3): 334-343.

Costantino, V., Mangoni, A., Teta, R., Kra-Oz, G. and Yarden, O. (2011). "Neurosporaside, a tetraglycosylated sphingolipid from Neurospora crassa." Journal of Natural Products **74**(4): 554-558.

Cotlet, M., Hofkens, J., Maus, M., Gensch, T., Van der Auweraer, M., Michiels, J., Dirix, G., Van Guyse, M., Vanderleyden, J., Visser, A. J. W. G. and De Schryver, F. C. (2001). "Excited-State Dynamics in the Enhanced Green Fluorescent Protein Mutant Probed by Picosecond Time-Resolved Single Photon Counting Spectroscopy." The Journal of Physical Chemistry B **105**(21): 4999-5006.

Coutinho, A. and Prieto, M. (2003). "Cooperative Partition Model of Nystatin Interaction with Phospholipid Vesicles." Biophysical Journal **84**(5): 3061-3078.

Cseh, R. and Benz, R. (1998). "The Adsorption of Phloretin to Lipid Monolayers and Bilayers Cannot Be Explained by Langmuir Adsorption Isotherms Alone." Biophysical Journal **74**(3): 1399-1408.

Davenport, L. (1997). [24] Fluorescence probes for studying membrane heterogeneity. Methods in Enzymology, Academic Press. **278:** 487-512.

Davis, R. H. (2000). Neurospora: Contributions of a Model Organism, Oxford University Press.

Davis, R. H., de Serres, Frederick J. (1970). "[4] Genetic and microbiological research techniques for Neurospora crassa." Methods in Enzymology **17**: 79-143.

de Almeida, R. F., Borst, J., Fedorov, A., Prieto, M. and Visser, A. J. (2007). "Complexity of lipid domains and rafts in giant unilamellar vesicles revealed by combining imaging and microscopic and macroscopic time-resolved fluorescence." Biophysical Journal **93**(2): 539-553.

de Almeida, R. F., Fedorov, A. and Prieto, M. (2003). "Sphingomyelin/phosphatidylcholine/cholesterol phase diagram: boundaries and composition of lipid rafts." Biophys J **85**(4): 2406-2416.

de Almeida, R. F. and Joly, E. (2014). "Crystallization around solid-like nanosized docks can explain the specificity, diversity, and stability of membrane microdomains." Frontiers in Plant Science **5**: 72.

de Almeida, R. F., Loura, L. M., Fedorov, A. and Prieto, M. (2005). "Lipid rafts have different sizes depending on membrane composition: a time-resolved fluorescence resonance energy transfer study." J Mol Biol **346**(4): 1109-1120.

de Almeida, R. F., Loura, L. M. and Prieto, M. (2009). "Membrane lipid domains and rafts: current applications of fluorescence lifetime spectroscopy and imaging." Chemistry and Physics of Lipids **157**(2): 61-77.

de Almeida, R. F. M. (2018). "A route to understanding yeast cellular envelope – plasma membrane lipids interplaying in cell wall integrity." The FEBS Journal.

de Almeida, R. F. M., Fedorov, A. and Prieto, M. (2003). "Sphingomyelin/phosphatidylcholine/cholesterol phase diagram: boundaries and composition of lipid rafts." Biophysical Journal **85**(4): 2406-2416.

de Almeida, R. F. M., Santos, F. C., Marycz, K., Alicka, M., Krasowska, A., Suchodolski, J., Panek, J. J., Jezierska, A. and Starosta, R. (2019). "New diphenylphosphane derivatives of ketoconazole are promising antifungal agents." Scientific Reports **9**(1): 16214.

de Kroon, A. I. P. M. (2007). "Metabolism of phosphatidylcholine and its implications for lipid acyl chain composition in Saccharomyces cerevisiae." Biochimica et Biophysica Acta (BBA) - Molecular and Cell Biology of Lipids **1771**(3): 343-352.

de Matos, A. M., Blázquez-Sánchez, M. T., Sousa, C., Oliveira, M. C., de Almeida, R. F. M. and Rauter, A. P. (2021). "C-Glucosylation as a tool for the prevention of PAINS-induced membrane dipole potential alterations." Scientific Reports **11**(1): 4443.

Deacon, J. (2005). Introduction: The Fungi and Fungal Activities. Fungal Biology**:** 1-15.

Del Poeta, M., Nimrichter, L., Rodrigues, M. L. and Luberto, C. (2014). "Synthesis and biological properties of fungal glucosylceramide." Plos Pathogens **10**(1): e1003832-e1003832.

Demchenko, A. P., Mely, Y., Duportail, G. and Klymchenko, A. S. (2009). "Monitoring biophysical properties of lipid membranes by environment-sensitive fluorescent probes." Biophysical Journal **96**(9): 3461-3470.

Dickson, R. C. (2008). "Thematic Review Series: Sphingolipids. New insights into sphingolipid metabolism and function in budding yeast." Journal of Lipid Research **49**(5): 909-921.

Dickson, R. C. (2010). "Roles for sphingolipids in Saccharomyces cerevisiae." Advances in Experimental Medicine and Biology **688**: 217-231.

Dickson, R. C. and Lester, R. L. (2002). "Sphingolipid functions in Saccharomyces cerevisiae." Biochimica et Biophysica Acta (BBA) - Molecular and Cell Biology of Lipids **1583**(1): 13-25.

Dietrich, C., Bagatolli, L. A., Volovyk, Z. N., Thompson, N. L., Levi, M., Jacobson, K. and Gratton, E. (2001). "Lipid rafts reconstituted in model membranes." Biophysical Journal **80**(3): 1417-1428.

do Canto, A., Robalo, J. R., Santos, P. D., Carvalho, A. J. P., Ramalho, J. P. P. and Loura, L. M. S. (2016). "Diphenylhexatriene membrane probes DPH and TMA-DPH: A comparative molecular dynamics simulation study." Biochimica et Biophysica Acta (BBA) - Biomembranes **1858**(11): 2647-2661.

dos Santos, A. G., Marquês, J. T., Carreira, A. C., Castro, I. R., Viana, A. S., Mingeot-Leclercq, M. P., de Almeida, R. F. M. and Silva, L. C. (2017). "The molecular mechanism of Nystatin action is dependent on the membrane biophysical properties and lipid composition." Physical Chemistry Chemical Physics **19**(44): 30078-30088.

Dujon, B. (2015). "Basic principles of yeast genomics, a personal recollection." FEMS Yeast Research **15**(5).

Dunai, Z. A., Imre, G., Barna, G., Korcsmaros, T., Petak, I., Bauer, P. I. and Mihalik, R. (2012). "Staurosporine induces necroptotic cell death under caspase-compromised conditions in U937 cells." Plos One **7**(7): e41945.

Ejsing, C. S., Sampaio, J. L., Surendranath, V., Duchoslav, E., Ekroos, K., Klemm, R. W., Simons, K. and Shevchenko, A. (2009). "Global analysis of the yeast lipidome by quantitative shotgun mass spectrometry." Proceedings of the National Academy of Sciences **106**(7): 2136-2141.

Elson, E. L., Fried, E., Dolbow, J. E. and Genin, G. M. (2010). "Phase separation in biological membranes: integration of theory and experiment." Annual Review of Biophysics **39**: 207-226.

Engberg, O., Yasuda, T., Hautala, V., Matsumori, N., Nyholm, Thomas K. M., Murata, M. and Slotte, J. P. (2016). "Lipid Interactions and Organization in Complex Bilayer Membranes." Biophysical Journal **110**(7): 1563-1573.

Epstein, S., Castillon, G. A., Qin, Y. and Riezman, H. (2012). "An essential function of sphingolipids in yeast cell division." Molecular Microbiology **84**(6): 1018-1032.

Fajardo-Somera, R. A., Bowman, B. and Riquelme, M. (2013). "The Plasma Membrane Proton Pump PMA-1 Is Incorporated into Distal Parts of the Hyphae Independently of the Spitzenkörper in Neurospora crassa." Eukaryotic Cell **12**(8): 1097-1105.

Fajardo-Somera, R. A., Bowman, B. and Riquelme, M. (2013). "The plasma membrane proton pump PMA-1 is incorporated into distal parts of the hyphae independently of the Spitzenkorper in Neurospora crassa." Eukaryot Cell **12**(8): 1097-1105.

Farnoud, A. M., Mor, V., Singh, A. and Del Poeta, M. (2014). "Inositol phosphosphingolipid phospholipase C1 regulates plasma membrane ATPase (Pma1) stability in Cryptococcus neoformans." FEBS Letters **588**(21): 3932-3938.

Faucon, J. F., Mitov, M. D., Méléard, P., Bivas, I. and Bothorel, P. (1989). "Bending elasticity and thermal fluctuations of lipid membranes. Theoretical and experimental requirements." Journal de Physique **50**(17): 2389-2414.

Ferket, K. K. A., Levery, S. B., Park, C., Cammue, B. P. A. and Thevissen, K. (2003). "Isolation and characterization of Neurospora crassa mutants resistant to antifungal plant defensins." Fungal Genetics and Biology **40**(2): 176-185.

Fernandes, A. S., Castro, A. and Videira, A. (2013). "Reduced glutathione export during programmed cell death of Neurospora crassa." Apoptosis **18**(8): 940-948.

Fernandes, A. S., Goncalves, A. P., Castro, A., Lopes, T. A., Gardner, R., Glass, N. L. and Videira, A. (2011). "Modulation of fungal sensitivity to staurosporine by targeting proteins identified by transcriptional profiling." Fungal Genetics and Biology **48**(12): 1130-1138.

Florine-Casteel, K. and Feigenson, G. W. (1988). "On the use of partition coefficients to characterize the distribution of fluorescent membrane probes between coexisting gel and fluid lipid phases: an analysis of the partition behavior of 1,6-diphenyl-1,3,5-hexatriene." Biochimica et Biophysica Acta (BBA) - Biomembranes **941**(1): 102-106.

Folmer, V., Pedroso, N., Matias, A. C., Lopes, S. C., Antunes, F., Cyrne, L. and Marinho, H. S. (2008). "H2O2 induces rapid biophysical and permeability changes in the plasma membrane of Saccharomyces cerevisiae." Biochimica et Biophysica Acta (BBA) - Biomembranes **1778**(4): 1141-1147.

Foucher, A. L., Rachidi, N., Gharbi, S., Blisnick, T., Bastin, P., Pemberton, I. K. and Spath, G. F. (2013). "Apoptotic marker expression in the absence of cell death in staurosporine-treated Leishmania donovani." Antimicrobial Agents and Chemotherapy **57**(3): 1252-1261.

Francisco, A. P., Botequim, D., Prazeres, D. M. F., Serra, V. V., Costa, S. M. B., Laia, C. A. T. and Paulo, P. M. R. (2019). "Extreme Enhancement of Single-Molecule Fluorescence from Porphyrins Induced by Gold Nanodimer Antennas." The Journal of Physical Chemistry Letters **10**(7): 1542-1549.

Francois, I. E., Bink, A., Vandercappellen, J., Ayscough, K. R., Toulmay, A., Schneiter, R., van Gyseghem, E., Van den Mooter, G., Borgers, M., Vandenbosch, D., Coenye, T., Cammue, B. P. and Thevissen, K. (2009). "Membrane rafts are involved in intracellular miconazole accumulation in yeast cells." Journal of Biological Chemistry **284**(47): 32680-32685.

Gaber, R. F., Copple, D. M., Kennedy, B. K., Vidal, M. and Bard, M. (1989). "The yeast gene ERG6 is required for normal membrane function but is not essential for biosynthesis of the cell-cycle-sparking sterol." Molecular and Cellular Biology **9**(8): 3447-3456.

Gaigg, B., Timischl, B., Corbino, L. and Schneiter, R. (2005). "Synthesis of sphingolipids with very long chain fatty acids but not ergosterol is required for routing of newly synthesized plasma membrane ATPase to the cell surface of yeast." Journal of Biological Chemistry **280**(23): 22515-22522.

Gaigg, B., Toulmay, A. and Schneiter, R. (2006). "Very long-chain fatty acid-containing lipids rather than sphingolipids per se are required for raft association and stable surface transport of newly synthesized plasma membrane ATPase in yeast." Journal of Biological Chemistry **281**(45): 34135-34145.

Galagan, J. E. e. a. (2003). "The genome sequence of filamentous fungus Neurospora crassa." Nature **422**: 859-868.

Gaspar, M. L., Aregullin, M. A., Jesch, S. A., Nunez, L. R., Villa-García, M. and Henry, S. A. (2007). "The emergence of yeast lipidomics." Biochimica et Biophysica Acta (BBA) - Molecular and Cell Biology of Lipids **1771**(3): 241-254.

Gescher, A. (2000). "Staurosporine analogues - pharmacological toys or useful antitumour agents?" Critical Reviews in Oncology/Hematology **34**(2): 127-135.

Gietz, D., St Jean, A., Woods, R. A. and Schiestl, R. H. (1992). "Improved method for high efficiency transformation of intact yeast cells." Nucleic Acids Research **20**(6): 1425-1425.

Ginsberg, L., Atack, J. R., Rapoport, S. I. and Gershfeld, N. L. (1993). "Evidence for a membrane lipid defect in Alzheimer disease." Mol Chem Neuropathol **19**(1-2): 37-46.

Glavinas, H., Krajcsi, P., Cserepes, J. and Sarkadi, B. (2004). "The role of ABC transporters in drug resistance, metabolism and toxicity." Current Drug Delivery **1**(1): 27-42.

Goffeau, A., Barrell, B. G., Bussey, H., Davis, R. W., Dujon, B., Feldmann, H., Galibert, F., Hoheisel, J. D., Jacq, C., Johnston, M., Louis, E. J., Mewes, H. W., Murakami, Y., Philippsen, P., Tettelin, H. and Oliver, S. G. (1996). "Life with 6000 genes." Science **274**(5287): 546-&.

Goni, F. M., Alonso, A., Bagatolli, L. A., Brown, R. E., Marsh, D., Prieto, M. and Thewalt, J. L. (2008). "Phase diagrams of lipid mixtures relevant to the study of membrane rafts." Biochimica et Biophysica Acta (BBA) - Molecular and Cell Biology of Lipids **1781**(11-12): 665-684.

Goñi, F. M., Sot, J. and Alonso, A. (2014). "Biophysical properties of sphingosine, ceramides and other simple sphingolipids." Biochemical Society Transactions **42**(5): 1401-1408.

González-Ramírez, E. J., Artetxe, I., García-Arribas, A. B., Goñi, F. M. and Alonso, A. (2019). "Homogeneous and Heterogeneous Bilayers of Ternary Lipid Compositions Containing Equimolar Ceramide and Cholesterol." Langmuir **35**(15): 5305-5315.

Goodrich-Tanrikulu, M., Howe, K., Stafford, A. and Nelson, M. A. (1998). "Changes in fatty acid composition of Neurospora crassa accompany sexual development and ascospore germination." Microbiology-Uk **144**: 1713-1720.

Goormaghtigh, E., Brasseur, R., Huart, P. and Ruysschaert, J. M. (1987). "Study of the adriamycin-cardiolipin complex structure using attenuated total reflection infrared spectroscopy." Biochemistry **26**(6): 1789-1794.

Gournas, C., Gkionis, S., Carquin, M., Twyffels, L., Tyteca, D. and André, B. (2018). "Conformation-dependent partitioning of yeast nutrient transporters into starvation-protective membrane domains." Proceedings of the National Academy of Sciences **115**(14): E3145-E3154.

Gow, N. A. R., Latge, J. P. and Munro, C. A. (2017). "The Fungal Cell Wall: Structure, Biosynthesis, and Function." Microbiology Spectrum Journal **5**(3).

Grossmann, G., Opekarova, M., Malinsky, J., Weig-Meckl, I. and Tanner, W. (2007). "Membrane potential governs lateral segregation of plasma membrane proteins and lipids in yeast." The EMBO Journal **26**(1): 1-8.

Grossmann, G., Opekarova, M., Malinsky, J., Weig-Meckl, I. and Tanner, W. (2007). "Membrane potential governs lateral segregation of plasma membrane proteins and lipids in yeast." Embo Journal **26**(1): 1-8.

Guan, X. L., Souza, C. M., Pichler, H., Dewhurst, G., Schaad, O., Kajiwara, K., Wakabayashi, H., Ivanova, T., Castillon, G. A., Piccolis, M., Abe, F., Loewith, R., Funato, K., Wenk, M. R. and Riezman, H. (2009). "Functional Interactions between Sphingolipids and Sterols in Biological Membranes Regulating Cell Physiology." Molecular Biology of the Cell **20**(7): 2083-2095.

Haak, D., Gable, K., Beeler, T. and Dunn, T. (1997). "Hydroxylation of Saccharomyces cerevisiae ceramides requires Sur2p and Scs7p." Journal of Biological Chemistry **272**(47): 29704-29710.

Haldar, S., Kanaparthi, R. K., Samanta, A. and Chattopadhyay, A. (2012). "Differential effect of cholesterol and its biosynthetic precursors on membrane dipole potential." Biophysical Journal **102**(7): 1561-1569.

Hama, H. (2010). "Fatty acid 2-Hydroxylation in mammalian sphingolipid biology." Biochimica et Biophysica Acta (BBA) - Molecular and Cell Biology of Lipids **1801**(4): 405-414.

Hama, H., Young, D. A., Radding, J. A., Ma, D., Tang, J., Stock, S. D. and Takemoto, J. Y. (2000). "Requirement of sphingolipid alpha-hydroxylation for fungicidal action of syringomycin E." FEBS Letters **478**(1-2): 26-28.

Hannun, Y. A. and Obeid, L. M. (2018). "Sphingolipids and their metabolism in physiology and disease." Nature Reviews Molecular Cell Biology **19**(3): 175-191.

Hanson, B. and Brody, S. (1979). "Lipid And Cell-Wall Changes In An Inositol-Requiring Mutant Of Neurospora-Crassa." Journal of Bacteriology **138**(2): 461-466.

Hanson, B. A. and Lester, R. L. (1980). "The Extraction Of Inositol-Containing Phospholipids And Phosphatidylcholine From Saccharomyces-Cerevisiae And Neurospora-Crassa." Journal of Lipid Research **21**(3): 309-315.

Hartkamp, R., Moore, T. C., Iacovella, C. R., Thompson, M. A., Bulsara, P. A., Moore, D. J. and McCabe, C. (2016). "Investigating the Structure of Multicomponent Gel-Phase Lipid Bilayers." Biophysical Journal **111**(4): 813-823.

Heberle, F. A. and Feigenson, G. W. (2011). "Phase separation in lipid membranes." Cold Spring Harbor Perspectives in Biology **3**(4): a004630.

Heese-Peck, A., Pichler, H., Zanolari, B., Watanabe, R., Daum, G. and Riezman, H. (2002). "Multiple functions of sterols in yeast endocytosis." Molecular Biology of the Cell **13**(8): 2664-2680.

Heikal, A. A., Hess, S. T. and Webb, W. W. (2001). "Multiphoton molecular spectroscopy and excited-state dynamics of enhanced green fluorescent protein (EGFP): acid–base specificity." Chemical Physics **274**(1): 37-55.

Henriksen, J. R. and Ipsen, J. H. (2004). "Measurement of membrane elasticity by micro-pipette aspiration." The European Physical Journal E **14**(2): 149-167.

Herman, P., Vecer, J., Opekarova, M., Vesela, P., Jancikova, I., Zahumensky, J. and Malinsky, J. (2015). "Depolarization affects the lateral microdomain structure of yeast plasma membrane." The FEBS Journal **282**(3): 419-434.

Hinrichs, J. W. J., Klappe, K., Hummel, I. and Kok, J. W. (2004). "ATP-binding Cassette Transporters Are Enriched in Non-caveolar Detergent-insoluble Glycosphingolipid-enriched Membrane Domains (DIGs) in Human Multidrug-resistant Cancer Cells." Journal of Biological Chemistry **279**(7): 5734-5738.

Holmes, A. R., Cardno, T. S., Strouse, J. J., Ivnitski-Steele, I., Keniya, M. V., Lackovic, K., Monk, B. C., Sklar, L. A. and Cannon, R. D. (2016). "Targeting efflux pumps to overcome antifungal drug resistance." Future Medicinal Chemistry **8**(12): 1485-1501.

Huang, C.-h. and Li, S. (1999). "Calorimetric and molecular mechanics studies of the thermotropic phase behavior of membrane phospholipids." Biochimica et Biophysica Acta (BBA) - Reviews on Biomembranes **1422**(3): 273-307.

Huang, C. (1969). "Studies on phosphatidylcholine vesicles. Formation and physical characteristics." Biochemistry **8**(1): 344-352.

Huang, X., Liu, J. and Dickson, R. C. (2012). "Down-Regulating Sphingolipid Synthesis Increases Yeast Lifespan." PLoS Genet **8**(2): e1002493.

Hubbard, S. C. and Brody, S. (1975). "Glycerophospholipid variation in choline and inositol auxotrophs of Neurospora crassa. Internal compensation among zwitterionic and anionic species." Journal of Biological Chemistry **250**(18): 7173-7181.

Huber, A., Oemer, G., Malanovic, N., Lohner, K., Kovács, L., Salvenmoser, W., Zschocke, J., Keller, M. A. and Marx, F. (2019). "Membrane Sphingolipids Regulate the Fitness and Antifungal Protein Susceptibility of Neurospora crassa." Frontiers in Microbiology **10**: 605.

Hudson, B. and Cavalier, S. (1988). Studies of Membrane Dynamics and Lipid-Protein Interaction with Parinaric Acid. Spectroscopic Membrane Probes. M. Loew. Boca Raton, USA**:** 43-62.

Johnson, I. and Spence, M. T. Z. (2010). The Molecular Probes Handbook - A Guide to Fluorescent Probes and Labeling Technologies, Invitrogen**:** 965.

Juretić, D. (1977). "The effect of phosphatidylcholine depletion on biochemical and physical properties of a Neurospora crassa membrane mutant." Biochimica et Biophysica Acta (BBA) - Biomembranes **469**(2): 137-150.

Kane, P. M. (2016). "Proton Transport and pH Control in Fungi." Advances in Experimental Medicine and Biology **892**: 33-68.

Kapitzky, L., Beltrao, P., Berens, T. J., Gassner, N., Zhou, C., Wüster, A., Wu, J., Babu, M. M., Elledge, S. J., Toczyski, D., Lokey, R. S. and Krogan, N. J. (2010). "Cross-species chemogenomic profiling reveals evolutionarily conserved drug mode of action." Molecular Systems Biology **6**(1): 451.

Kelly, S. L., Lamb, D. C., Baldwin, B. C., Corran, A. J. and Kelly, D. E. (1997). "Characterization of Saccharomyces cerevisiae CYP61, Sterol Δ22-Desaturase, and Inhibition by Azole Antifungal Agents." Journal of Biological Chemistry **272**(15): 9986-9988.

Khan, A., McQuilken, M. and Gladfelter, A. S. (2015). "Septins and Generation of Asymmetries in Fungal Cells." Annual Review of Microbiology **69**: 487-503.

Khmelinskaia, A., Ibarguren, M., de Almeida, R. F., Lopez, D. J., Paixao, V. A., Ahyayauch, H., Goni, F. M. and Escriba, P. V. (2014). "Changes in membrane organization upon spontaneous insertion of 2-hydroxylated unsaturated fatty acids in the lipid bilayer." Langmuir **30**(8): 2117-2128.

Khmelinskaia, A., Marques, J. M. T., Bastos, A. E. P., Antunes, C. A. C., Bento-Oliveira, A., Scolari, S., Lobo, G., Malho, R., Herrmann, A., Marinho, H. S. and de Almeida, R. F. M. (2020). "Liquid-Ordered Phase Formation by Mammalian and Yeast Sterols: A Common Feature With Organizational Differences." Frontiers in Cell and Developmental Biology **8**: 15.

Khurana, V. and Lindquist, S. (2010). "Modelling neurodegeneration in Saccharomyces cerevisiae: why cook with baker's yeast?" Nature Reviews Neuroscience **11**(6): 436-449.

Kienle, D. F., de Souza, J. V., Watkins, E. B. and Kuhl, T. L. (2014). "Thickness and refractive index of DPPC and DPPE monolayers by multiple-beam interferometry." Analytical and Bioanalytical Chemistry **406**(19): 4725-4733.

Klose, C., Ejsing, C. S., Garcia-Saez, A. J., Kaiser, H. J., Sampaio, J. L., Surma, M. A., Shevchenko, A., Schwille, P. and Simons, K. (2010). "Yeast lipids can phase-separate into micrometer-scale membrane domains." Journal of Biological Chemistry **285**(39): 30224-30232.

Klose, C., Surma, M. A., Gerl, M. J., Meyenhofer, F., Shevchenko, A. and Simons, K. (2012). "Flexibility of a Eukaryotic Lipidome – Insights from Yeast Lipidomics." Plos One **7**(4): e35063.

Klostermeier, D. and Rudolph, M. G. (2018). Biophysical Chemistry, CRC Press.

Klymchenko, A. S. and Kreder, R. (2014). "Fluorescent probes for lipid rafts: from model membranes to living cells." Chemistry & Biology **21**(1): 97-113.

Komor, E., Weber, H. and Tanner, W. (1979). "Greatly decreased susceptibility of nonmetabolizing cells towards detergents." Proceedings of the National Academy of Sciences **76**(4): 1814-1818.

Konecna, A., Toth Hervay, N., Valachovic, M. and Gbelska, Y. (2016). "ERG6 gene deletion modifies Kluyveromyces lactis susceptibility to various growth inhibitors." Yeast **33**(12): 621-632.

Korte, T. and Herrmann, A. (2016). Fluorescence Lifetime Imaging Microscopy by TCSPC (TD-FLIM). Practical Manual for Fluorescence Microscopy Techniques. Berlin, Germany, PicoQuant GmbH.

Koynova, R. and Caffrey, M. (1998). "Phases and phase transitions of the phosphatidylcholines." Biochimica et Biophysica Acta (BBA) - Reviews on Biomembranes **1376**(1): 91-145.

Kushwaha, S. C., Kates, M., Kramer, J. K. G. and Subden, R. E. (1976). "Lipid-Composition Of Neurospora-Crassa." Lipids **11**(10): 778-780.

Kwok, R. and Evans, E. (1981). "Thermoelasticity of large lecithin bilayer vesicles." Biophysical journal **35**(3): 637-652.

Lairion, F. and Disalvo, E. A. (2004). "Effect of Phloretin on the Dipole Potential of Phosphatidylcholine, Phosphatidylethanolamine, and Phosphatidylglycerol Monolayers." Langmuir **20**(21): 9151-9155.

Lakowicz, J. R. (2006). Principles of Fluorescence Spectroscopy, Springer.

Leber, A., Fischer, P., Schneiter, R., Kohlwein, S. D. and Daum, G. (1997). "The yeast mic2 mutant is defective in the formation of mannosyl-diinositolphosphorylceramide." FEBS Letters **411**(2-3): 211-214.

Lee, M. C., Hamamoto, S. and Schekman, R. (2002). "Ceramide biosynthesis is required for the formation of the oligomeric H+-ATPase Pma1p in the yeast endoplasmic reticulum." Journal of Biological Chemistry **277**(25): 22395-22401.

Lester, R. L. and Dickson, R. C. (2001). "High-Performance Liquid Chromatography Analysis of Molecular Species of Sphingolipid-Related Long Chain Bases and Long Chain Base Phosphates in Saccharomyces cerevisiae after Derivatization with 6-Aminoquinolyl-N-hydroxysuccinimidyl Carbamate." Analytical Biochemistry **298**(2): 283-292.

Lester, R. L., Smith, S. W., Wells, G. B., Rees, D. C. and Angus, W. W. (1974). "Isolation And Partial Characterization Of 2 Novel Sphingolipids From Neurospora-Crassa - Di(Inositolphosphoryl)Ceramide And (Gal)3glu Ceramide." Journal of Biological Chemistry **249**(11): 3388-3394.

Li, Y. and Prinz, W. A. (2004). "ATP-binding cassette (ABC) transporters mediate nonvesicular, raft-modulated sterol movement from the plasma membrane to the endoplasmic reticulum." Journal of Biological Chemistry **279**(43): 45226-45234.

Litman, B. J., Lewis, E. N. and Levin, I. W. (1991). "Packing characteristics of highly unsaturated bilayer lipids: Raman spectroscopic studies of multilamellar phosphatidylcholine dispersions." Biochemistry **30**(2): 313-319.

Loew, L. M. (1996). "Potentiometric dyes: Imaging electrical activity of cell membranes." Pure and Applied Chemistry **68**(7): 1405-1409.

Loew, L. M., Cohen, L. B., Dix, J., Fluhler, E. N., Montana, V., Salama, G. and Wu, J. Y. (1992). "A Naphthyl Analog Of The Aminostyryl Pyridinium Class Of Potentiometric Membrane Dyes Shows Consistent Sensitivity In A Variety Of Tissue, Cell, And Model Membrane Preparations." Journal of Membrane Biology **130**(1): 1-10.

Lopez, S., Rodriguez-Gallardo, S., Sabido-Bozo, S. and Muñiz, M. (2019). "Endoplasmic Reticulum Export of GPI-Anchored Proteins." International Journal of Molecular Sciences **20**(14): 3506.

Loura, L. M. S. and de Almeida, R. F. M. (2004). Tópicos de Biofísica de Membranas. Lisboa, LIDEL - Edições Técnicas, lda.

Luque, E. M., Gutierrez, G., Navarro-Sampedro, L., Olmedo, M., Rodriguez-Romero, J., Ruger-Herreros, C., Tagua, V. G. and Corrochano, L. M. (2012). "A Relationship between Carotenoid Accumulation and the Distribution of Species of the Fungus Neurospora in Spain." Plos One **7**(3).

Madni, A., Sarfraz, M., Rehman, M., Ahmad, M., Akhtar, N., Ahmad, S., Tahir, N., Ijaz, S., Al-Kassas, R. and Löbenberg, R. (2014). "Liposomal drug delivery: a versatile platform for challenging clinical applications." Journal of Pharmaceutical Sciences **17**(3): 401-426.

Malinska, K., Malinsky, J., Opekarova, M. and Tanner, W. (2003). "Visualization of protein compartmentation within the plasma membrane of living yeast cells." Molecular Biology of the Cell **14**(11): 4427-4436.

Malinsky, J. and Opekarova, M. (2016). "New Insight Into the Roles of Membrane Microdomains in Physiological Activities of Fungal Cells." International Review of Cell and Molecular Biology **325**: 119-180.

Malinsky, J., Opekarova, M., Grossmann, G. and Tanner, W. (2013). "Membrane microdomains, rafts, and detergent-resistant membranes in plants and fungi." Annual Review of Plant Biology **64**: 501-529.

Malinsky, J., Tanner, W. and Opekarova, M. (2016). "Transmembrane voltage: Potential to induce lateral microdomains." Biochimica et Biophysica Acta (BBA) - Molecular and Cell Biology of Lipids **1861**(8 Pt B): 806-811.

Mannhaupt, G., Montrone, C., Haase, D., Mewes, H. W., Aign, V., Hoheisel, J. D., Fartmann, B., Nyakatura, G., Kempken, F., Maier, J. and Schulte, U. (2003). "What's in the genome of a filamentous fungus? Analysis of the Neurospora genome sequence." Nucleic Acids Research **31**(7): 1944-1954.

Mariana, A., Francesco, R., Martin, H., Christian, E. and Erdinc, S. (2017). "Laurdan and Di-4-ANEPPDHQ probe different properties of the membrane." Journal of Physics D: Applied Physics **50**(13): 134004.

Marquês, J. T., Antunes, C. A. C., Santos, F. C. and de Almeida, R. F. M. (2015). Chapter Three - Biomembrane Organization and Function: The Decisive Role of Ordered Lipid Domains. Advances in Planar Lipid Bilayers and Liposomes. C. V. K. Aleš Iglič and R. Michael, Academic Press. **Volume 22:** 65-96.

Marques, J. T., Cordeiro, A. M., Viana, A. S., Herrmann, A., Marinho, H. S. and de Almeida, R. F. (2015). "Formation and Properties of Membrane-Ordered Domains by Phytoceramide: Role of Sphingoid Base Hydroxylation." Langmuir **31**(34): 9410-9421.

Marques, J. T., Marinho, H. S. and de Almeida, R. F. M. (2018). "Sphingolipid hydroxylation in mammals, yeast and plants - An integrated view." Progress in Lipid Research **71**: 18-42.

Marsh, D. (2010). "Liquid-ordered phases induced by cholesterol: A compendium of binary phase diagrams." Biochimica et Biophysica Acta (BBA) - Biomembranes **1798**(3): 688-699.

Marsh, D., Watts, A. and Knowles, P. F. (1977). "Cooperativity of the phase transition in single- and multibilayer lipid vesicles." Biochimica et Biophysica Acta (BBA) - Biomembranes **465**(3): 500-514.

Maschmeyer, G., Haas, A. and Cornely, O. A. (2007). "Invasive aspergillosis: epidemiology, diagnosis and management in immunocompromised patients." Drugs **67**(11): 1567-1601.

Mateo, C. R., Brochon, J. C., Lillo, M. P. and Acuna, A. U. (1993). "Lipid Clustering in Bilayers Detected by the Fluorescence Kinetics and Anisotropy of Trans-Parinaric Acid." Biophysical Journal **65**(5): 2237-2247.

Matias, A. C., Pedroso, N., Teodoro, N., Marinho, H. S., Antunes, F., Nogueira, J. M., Herrero, E. and Cyrne, L. (2007). "Down-regulation of fatty acid synthase increases the resistance of Saccharomyces cerevisiae cells to H2O2." Free Radical Biology and Medicine **43**(10): 1458-1465.

Mayer, L. D., Bally, M. B., Hope, M. J. and Cullis, P. R. (1986). "Techniques for encapsulating bioactive agents into liposomes." Chemistry and Physics of Lipids **40**(2-4): 333-345.

Mayer, L. D., Hope, M. J. and Cullis, P. R. (1986). "Vesicles of variable sizes produced by a rapid extrusion procedure." Biochimica et Biophysica Acta (BBA) - Biomembranes **858**(1): 161-168.

McCluskey, K. (2003). "The Fungal Genetics Stock Center from molds to molecules." Advances in Applied Microbiology **52**: 245-262.

Méléard, P., Pott, T., Bouvrais, H. and Ipsen, J. H. (2011). "Advantages of statistical analysis of giant vesicle flickering for bending elasticity measurements." The European Physical Journal E **34**(10): 116.

Meyer, T., Baek, D. J., Bittman, R., Haralampiev, I., Müller, P., Herrmann, A., Huster, D. and Scheidt, H. A. (2014). "Membrane properties of cholesterol analogs with an unbranched aliphatic side chain." Chemistry and Physics of Lipids **184**: 1-6.

Modok, S., Heyward, C. and Callaghan, R. (2004). "P-glycoprotein retains function when reconstituted into a sphingolipid- and cholesterol-rich environment." Journal of Lipid Research **45**(10): 1910-1918.

Montana, V., Farkas, D. L. and Loew, L. M. (1989). "Dual-wavelength ratiometric fluorescence measurements of membrane potential." Biochemistry **28**(11): 4536-4539.

Mota Fernandes, C. and Del Poeta, M. (2020). "Fungal sphingolipids: role in the regulation of virulence and potential as targets for future antifungal therapies." Expert Review of Anti-infective Therapy: 1-10.

Mouritsen, O. G. (2005). Life - as a Matter of Fat Heidelberg, Springer.

Muñiz, M. and Riezman, H. (2016). "Trafficking of glycosylphosphatidylinositol anchored proteins from the endoplasmic reticulum to the cell surface." Journal of Lipid Research **57**(3): 352-360.

Munshi, M. A., Gardin, J. M., Singh, A., Luberto, C., Rieger, R., Bouklas, T., Fries, B. C. and Del Poeta, M. (2018). "The Role of Ceramide Synthases in the Pathogenicity of Cryptococcus neoformans." Cell Reports **22**(6): 1392-1400.

Nagata, T., Iizumi, S., Satoh, K. and Kikuchi, S. (2008). "Comparative molecular biological analysis of membrane transport genes in organisms." Plant Molecular Biology **66**(6): 565-585.

Nakashima, H. and Onai, K. (1996). "The circadian conidiation rhythm in Neurospora crassa." Seminars in Cell & Developmental Biology **7**(6): 765-774.

Neumann, J., Rose-Sperling, D. and Hellmich, U. A. (2017). "Diverse relations between ABC transporters and lipids: An overview." Biochimica et Biophysica Acta - Biomembranes **1859**(4): 605-618.

Omura, S., Iwai, Yuzuru, Hirano, Atsushi, Nakagawa, Akira, Awaya, Juichi, Tsuchiya, Hisae, Takahashi, Yoko, Masuma, Rokurou (1977). "A new alkaloid am-2282 of streptomyces origin taxonomy, fermentation, isolation and preliminary characterization." The Journal of Antibiotics **XXX**(4): 275-282.

Ostroumova, O. S., Efimova, S. S. and Malev, V. V. (2015). "Modifiers of membrane dipole potentials as tools for investigating ion channel formation and functioning." International Review of Cell and Molecular Biology **315**: 245-297.

Paege, N., Warnecke, D., Zäuner, S., Hagen, S., Rodrigues, A., Baumann, B., Thiess, M., Jung, S. and Meyer, V. (2019). "Species-Specific Differences in the Susceptibility of Fungi to the Antifungal Protein AFP Depend on C-3 Saturation of Glycosylceramides." mSphere **4**(6): e00741-00719.

Palma-Guerrero, J., Huang, I. C., Jansson, H. B., Salinas, J., Lopez-Llorca, L. V. and Read, N. D. (2009). "Chitosan permeabilizes the plasma membrane and kills cells of Neurospora crassa in an energy dependent manner." Fungal Genetics and Biology **46**(8): 585-594.

Parasassi, T., De Stasio, G., Rusch, R. M. and Gratton, E. (1991). "A photophysical model for diphenylhexatriene fluorescence decay in solvents and in phospholipid vesicles." Biophysical Journal **59**(2): 466-475.

Park, C., Bennion, B., Francois, I. E., Ferket, K. K., Cammue, B. P., Thevissen, K. and Levery, S. B. (2005). "Neutral glycolipids of the filamentous fungus Neurospora crassa: altered expression in plant defensin-resistant mutants." Journal of Lipid Research **46**(4): 759-768.

Park, H. J., Lee, J. Y., Hwang, I. S., Yun, B. S., Kim, B. S. and Hwang, B. K. (2006). "Isolation and Antifungal and Antioomycete Activities of Staurosporine from Streptomyces roseoflavus Strain LS-A24." Journal of Agricultural and Food Chemistry **54**(8): 3041-3046.

Parker, J. E., Merkamm, M., Manning, N. J., Pompon, D., Kelly, S. L. and Kelly, D. E. (2008). "Differential azole antifungal efficacies contrasted using a Saccharomyces cerevisiae strain humanized for sterol 14 alpha-demethylase at the homologous locus." Antimicrobial Agents and Chemotherapy **52**(10): 3597-3603.

Pedroso, N., Matias, A. C., Cyrne, L., Antunes, F., Borges, C., Malho, R., de Almeida, R. F. M., Herrero, E. and Marinho, H. S. (2009). "Modulation of plasma membrane lipid profile and microdomains by H2O2 in Saccharomyces cerevisiae." Free Radical Biology and Medicine **46**(2): 289-298.

Pérez-Torrado, R. and Querol, A. (2016). "Opportunistic Strains of Saccharomyces cerevisiae: A Potential Risk Sold in Food Products." Frontiers in Microbiology **6**(1522).

Peterson, U., Mannock, D. A., Lewis, R. N. A. H., Pohl, P., McElhaney, R. N. and Pohl, E. E. (2002). "Origin of membrane dipole potential: Contribution of the phospholipid fatty acid chains." Chemistry and Physics of Lipids **117**(1): 19-27.

Petrezselyova, S., Zahradka, J. and Sychrova, H. (2010). "Saccharomyces cerevisiae BY4741 and W303-1A laboratory strains differ in salt tolerance." Fungal Biology **114**(2): 144-150.

Petrov, J. G., Pfohl, T. and Möhwald, H. (1999). "Ellipsometric Chain Length Dependence of Fatty Acid Langmuir Monolayers. A Heads-and-Tails Model." The Journal of Physical Chemistry B **103**(17): 3417-3424.

Pickar, A. D. and Benz, R. (1978). "Transport of oppositely charged lipophilic probe ions in lipid bilayer membranes having various structures." The Journal of Membrane Biology **44**(3): 353-376.

Plesofsky, N. S., Levery, S. B., Castle, S. A. and Brambl, R. (2008). "Stress-induced cell death is mediated by ceramide synthesis in Neurospora crassa." Eukaryotic Cell **7**(12): 2147-2159.

Ralser, M., Kuhl, H., Ralser, M., Werber, M., Lehrach, H., Breitenbach, M. and Timmermann, B. (2012). "The Saccharomyces cerevisiae W303-K6001 cross-platform genome sequence: insights into ancestry and physiology of a laboratory mutt." Open Biology **2**(8): 120093.

Ratto, T. V. and Longo, M. L. (2002). "Obstructed diffusion in phase-separated supported lipid bilayers: A combined atomic force microscopy and fluorescence recovery after photobleaching approach." Biophysical Journal **83**(6): 3380-3392.

Rayermann, S. P., Rayermann, G. E., Cornell, C. E., Merz, A. J. and Keller, S. L. (2017). "Hallmarks of Reversible Separation of Living, Unperturbed Cell Membranes into Two Liquid Phases." Biophysical Journal **113**(11): 2425-2432.

Regional Committee for the Western, P. (2019). Antimicrobial resistance. Manila, WHO Regional Office for the Western Pacific.

Renaud, R. L., Subden, R. E., Pierce, A. M. and Oehlschlager, A. C. (1978). "Sterol Composition Of Neurospora-Crassa." Lipids **13**(1): 56-58.

Reyes Mateo, C., Ulises Acuña, A. and Brochon, J. C. (1995). "Liquid-crystalline phases of cholesterol/lipid bilayers as revealed by the fluorescence of trans-parinaric acid." Biophysical Journal **68**(3): 978-987.

Rosetti, C. M., Mangiarotti, A. and Wilke, N. (2017). "Sizes of lipid domains: What do we know from artificial lipid membranes? What are the possible shared features with membrane rafts in cells?" Biochimica et Biophysica Acta (BBA) - Biomembranes **1859**(5): 789-802.

Rouser, G., Fleischer, S. and Yamamoto, A. (1970). "Two dimensional thin layer chromatographic separation of polar lipids and determination of phospholipids by phosphorus analysis of spots." Lipids **5**(5): 494-496.

Santos, F. C., Fernandes, A. S., Antunes, C. A., Moreira, F. P., Videira, A., Marinho, H. S. and de Almeida, R. F. (2017). "Reorganization of plasma membrane lipid domains during conidial germination." Biochimica et Biophysica Acta (BBA) - Molecular and Cell Biology of Lipids **1862**(2): 156-166.

Santos, F. C., Lobo, G. M., Fernandes, A. S., Videira, A. and de Almeida, R. F. M. (2018). "Changes in the Biophysical Properties of the Cell Membrane Are Involved in the Response of Neurospora crassa to Staurosporine." Frontiers in Physiology **9**(1375).

Santos, F. C., Marquês, J. T., Bento-Oliveira, A. and de Almeida, R. F. M. (2020). "Sphingolipid-enriched domains in fungi." FEBS Letters **594**(22): 3698-3718.

Sarmento, M. J., Ricardo, J. C., Amaro, M. and Sachl, R. (2020). "Organization of gangliosides into membrane nanodomains." FEBS Letters **594**(22): 3668-3697.

Scarborough, G. A. (1985). "A variant of the cell wall-less fz;sg;os-1 strain of Neurospora crassa with altered morphology and improved growth." Experimental Mycology **9**(3): 5-78.

Schmit, J. C. and Brody, S. (1976). "Biochemical genetics of Neurospora crassa conidial germination." Bacteriological Reviews **40**(1): 1-41.

Schuberth, C. and Wedlich-Söldner, R. (2015). "Building a patchwork — The yeast plasma membrane as model to study lateral domain formation." Biochimica et Biophysica Acta (BBA) - Molecular Cell Research **1853**(4): 767-774.

Sezgin, E., Levental, I., Mayor, S. and Eggeling, C. (2017). "The mystery of membrane organization: composition, regulation and roles of lipid rafts." Nature Reviews Molecular Cell Biology **18**(6): 361-374.

Sezgin, E. and Schwille, P. (2011). "Fluorescence techniques to study lipid dynamics." Cold Spring Harbor Perspectives in Biology **3**(11): a009803.

Shanker, N. and Bane, S. L. (2008). Basic Aspects of Absorption and Fluorescence Spectroscopy and Resonance Energy Transfer Methods. Methods in Cell Biology, Academic Press. **84:** 213-242.

Shapiro, R. S., Robbins, N. and Cowen, L. E. (2011). "Regulatory circuitry governing fungal development, drug resistance, and disease." Microbiology and Molecular Biology Reviews **75**(2): 213-267.

Sharon, A., Finkelstein, A., Shlezinger, N. and Hatam, I. (2009). "Fungal apoptosis: function, genes and gene function." FEMS Microbiology Reviews **33**(5): 833-854.

Silva, L. C., de Almeida, R. F. M., Castro, B. M., Fedorov, A. and Prieto, M. (2007). "Ceramide-domain formation and collapse in lipid rafts: Membrane reorganization by an apoptotic lipid." Biophysical Journal **92**(2): 502-516.

Singh, A. and Del Poeta, M. (2016). "Sphingolipidomics: An Important Mechanistic Tool for Studying Fungal Pathogens." Frontiers in Microbiology **7**(501).

Singh, A., Wang, H., Silva, L. C., Na, C., Prieto, M., Futerman, A. H., Luberto, C. and Del Poeta, M. (2012). "Methylation of glycosylated sphingolipid modulates membrane lipid topography and pathogenicity of Cryptococcus neoformans." Cellular Microbiology **14**(4): 500-516.

Sklar, L. A., Hudson, B. S., Petersen, M. and Diamond, J. (1977a). "Conjugated polyene fatty acids on fluorescent probes: spectroscopic characterization." Biochemistry **16**(5): 813-819.

Sklar, L. A., Hudson, B. S. and Simoni, R. D. (1977b). "Conjugated Polyene Fatty-Acids as Fluorescent-Probes - Synthetic Phospholipid Membrane Studies." Biochemistry **16**(5): 819-828.

Sousa, C., Santos, F. C., Bento-Oliveira, A., Mestre, B., Silva, L. C. and de Almeida, R. F. M. (2021). Biophysical Analysis of Lipid Domains in Mammalian and Yeast Membranes by Fluorescence Spectroscopy. Lipid Rafts: Methods in Molecular Biology. E. Bieberich. New York, NY, Humana. **2187:** 247-269.

Spira, F., Mueller, N. S., Beck, G., von Olshausen, P., Beig, J. and Wedlich-Soldner, R. (2012). "Patchwork organization of the yeast plasma membrane into numerous coexisting domains." Nature Cell Biology **14**(6): 640-648.

Stancevic, B. and Kolesnick, R. (2010). "Ceramide-rich platforms in transmembrane signaling." FEBS Lett **584**(9): 1728-1740.

Starke-Peterkovic, T., Turner, N., Else, P. L. and Clarke, R. J. (2005). "Electric field strength of membrane lipids from vertebrate species: membrane lipid composition and Na+-K+-ATPase molecular activity." American Journal of Physiology-Regulatory, Integrative and Comparative Physiology **288**(3): R663-R670.

Starosta, R. and de Almeida, R. F. M. (2020). "Luminescence properties of the antifungal agent ketoconazole and its diphenylphosphane derivatives." Journal of Luminescence **220**: 116956.

Starosta, R., de Almeida, R. F. M., Puchalska, M., Bialonska, A., Panek, J. J., Jezierska, A., Szmigiel, I., Suchodolski, J. and Krasowska, A. (2020). "New anticandidal Cu(i) complexes with neocuproine and ketoconazole derived diphenyl(aminomethyl)phosphane: luminescence properties for detection in fungal cells." Dalton Transactions **49**(25): 8528-8539.

Stillwell, W. (2016). An Introduction to Biological Membranes - Composition, Structure and Function. San Diego, Elsevier Science.

Stock, S. D., Hama, H., DeWald, D. B. and Takemoto, J. Y. (1999). "SEC14-dependent secretion in Saccharomyces cerevisiae. Nondependence on sphingolipid synthesis-coupled diacylglycerol production." Journal of Biological Chemistry **274**(19): 12979-12983.

Stock, S. D., Hama, H., Radding, J. A., Young, D. A. and Takemoto, J. Y. (2000). "Syringomycin E inhibition of Saccharomyces cerevisiae: requirement for biosynthesis of sphingolipids with very-long-chain fatty acids and mannose- and phosphoinositol-containing head groups." Antimicrobial Agents and Chemotherapy **44**(5): 1174-1180.

Stockton, G. W., Johnson, K. G., Butler, K. W., Polnaszek, C. F., Cyr, R. and Smith, I. C. (1975). "Molecular order in Acholeplasma laidlawii membranes as determined by deuterium magnetic resonance of biosynthetically-incorporated specifically-labelled lipids." Biochim Biophys Acta **401**(3): 535-539.

Stradalova, V., Stahlschmidt, W., Grossmann, G., Blazikova, M., Rachel, R., Tanner, W. and Malinsky, J. (2009). "Furrow-like invaginations of the yeast plasma membrane correspond to membrane compartment of Can1." Journal of Cell Science **122**(Pt 16): 2887-2894.

Suhling, K., Davis, D., Petrasek, Z., Siegel, J. and Phillips, D. (2001). Influence of the refractive index on EGFP fluorescence lifetimes in mixtures of water and glycerol, SPIE.

Suhling, K., Siegel, J., Phillips, D., French, P. M. W., Lévêque-Fort, S., Webb, S. E. D. and Davis, D. M. (2002). "Imaging the Environment of Green Fluorescent Protein." Biophysical Journal **83**(6): 3589-3595.

Swain, E., Baudry, K., Stukey, J., McDonough, V., Germann, M. and Nickels, J. T. (2002). "Sterol-dependent regulation of sphingolipid metabolism in Saccharomyces cerevisiae." Journal of Biological Chemistry **277**(29): 26177-26184.

Szoka, F., Jr. and Papahadjopoulos, D. (1980). "Comparative properties and methods of preparation of lipid vesicles (liposomes)." Annual Review of Biophysics and Bioengineering **9**: 467-508.

Takagi, H. (2019). "Metabolic regulatory mechanisms and physiological roles of functional amino acids and their applications in yeast." Bioscience, Biotechnology, and Biochemistry **83**(8): 1449-1462.

Takagi, H., Hashida, K., Watanabe, D., Nasuno, R., Ohashi, M., Iha, T., Nezuo, M. and Tsukahara, M. (2015). "Isolation and characterization of awamori yeast mutants with L-leucine accumulation that overproduce isoamyl alcohol." Journal of Bioscience and Bioengineering **119**(2): 140-147.

Takemoto, J. Y., Zhang, L., Taguchi, N., Tachikawa, T. and Miyakawa, T. (1991). "Mechanism of action of the phytotoxin syringomycin: a resistant mutant of Saccharomyces cerevisiae reveals an involvement of Ca2+ transport." Microbiology **137**(3): 653-659.

Tamaoki, T., Nomoto, H., Takahashi, I., Kato, Y., Morimoto, M. and Tomita, F. (1986). "Staurosporine, a potent inhibitor of phospholipidCa++dependent protein kinase." Biochemical and Biophysical Research Communications **135**(2): 397-402.

Tanaka, S. and Tani, M. (2018). "Mannosylinositol phosphorylceramides and ergosterol coodinately maintain cell wall integrity in the yeast Saccharomyces cerevisiae." The FEBS Journal **285**(13): 2405-2427.

Tani, M. (2016). "Structure-Function Relationship of Complex Sphingolipids in Yeast." Trends in Glycoscience and Glycotechnology **28**(164): E109-E116.

Thevissen, K., Ferket, K. K., François, I. E. and Cammue, B. P. (2003). "Interactions of antifungal plant defensins with fungal membrane components." Peptides **24**(11): 1705-1712.

Uemura, S., Shishido, F., Tani, M., Mochizuki, T., Abe, F. and Inokuchi, J.-i. (2014). "Loss of hydroxyl groups from the ceramide moiety can modify the lateral diffusion of membrane proteins in S. cerevisiae." Journal of Lipid Research **55**(7): 1343-1356.

Valdez-Taubas, J. and Pelham, H. R. (2003). "Slow diffusion of proteins in the yeast plasma membrane allows polarity to be maintained by endocytic cycling." Current Biology **13**(18): 1636-1640.

Valeur, B. (2009). Molecular Fluorescence. Digital Encyclopedia of Applied Physics**:** 477-531.

Valeur, B. and Berberan-Santos, M. (2012). Molecular Fluorescence: Principles and Applications. Weinheim, Germany, Wiley-VCH.

van 't Klooster, J. S., Cheng, T.-Y., Sikkema, H. R., Jeucken, A., Moody, D. B. and Poolman, B. (2020). "Membrane Lipid Requirements of the Lysine Transporter Lyp1 from Saccharomyces cerevisiae." Journal of Molecular Biology **432**(14): 4023-4031.

van 't Klooster, J. S., Cheng, T. Y., Sikkema, H. R., Jeucken, A., Moody, B. and Poolman, B. (2020). "Periprotein lipidomes of Saccharomyces cerevisiae provide a flexible environment for conformational changes of membrane proteins." Elife **9**.

van Hoogevest, P. and de Kruijff, B. (1978). "Effect of amphotericin B on cholesterol-containing liposomes of egg phosphatidylcholine and didocosenoyl phosphatidylcholine. A refinement of the model for the formation of pores by amphotericin B in membranes." Biochimica et Biophysica Acta (BBA) - Biomembranes **511**(3): 397-407.

van Meer, G., Voelker, D. R. and Feigenson, G. W. (2008). "Membrane lipids: where they are and how they behave." Nature Reviews Molecular Cell Biology **9**(2): 112-124.

Vecer, J., Vesela, P., Malinsky, J. and Herman, P. (2014). "Sphingolipid levels crucially modulate lateral microdomain organization of plasma membrane in living yeast." FEBS Letters **588**(3): 443-449.

Ventura, A. E., Santos, T. C. B., Marquês, J. T., de Almeida, R. F. M. and Silva, L. C. (2021). Biophysical Analysis of Lipid Domains by Fluorescence Microscopy. Lipid Rafts: Methods and Protocols. E. Bieberich. New York, NY, Springer US**:** 223-245.

Vitha, M. F. and Clarke, R. J. (2007). "Comparison of excitation and emission ratiometric fluorescence methods for quantifying the membrane dipole potential." Biochimica et Biophysica Acta (BBA) - Biomembranes **1768**(1): 107-114.

W.K.Ng, A. and M.Wasan, K. (2003). "Development of liposomal polyene antibiotics: an historical perspective." Journal of Pharmaceutical Sciences **6**(1): 67-83.

Walther, T. C., Brickner, J. H., Aguilar, P. S., Bernales, S., Pantoja, C. and Walter, P. (2006). "Eisosomes mark static sites of endocytosis." Nature **439**(7079): 998-1003.

Wang, L. (2012). "Measurements and implications of the membrane dipole potential." Annual Review of Biochemistry **81**: 615-635.

Wang, Q. and Chang, A. (2002). "Sphingoid base synthesis is required for oligomerization and cell surface stability of the yeast plasma membrane ATPase, Pma1." Proceedings of the National Academy of Sciences **99**(20): 12853-12858.

Watanabe, R., Funato, K., Venkataramam, K., Futerman, A. H. and Riezman, H. (2002). "Sphingolipids are required for the stable membrane association of glycosylphosphatidylinositol-anchored proteins in yeast." Journal of Biological Chemistry **277**(51): 49538-49544.

Wiesner, D. A. and Dawson, G. (1996). "Staurosporine induces programmed cell death in embryonic neurons and activation of the ceramide pathway." Journal of Neurochemistry **66**(4): 1418-1425.

Wisplinghoff, H., Bischoff, T., Tallent, S. M., Seifert, H., Wenzel, R. P. and Edmond, M. B. (2004). "Nosocomial bloodstream infections in US hospitals: analysis of 24,179 cases from a prospective nationwide surveillance study." Clinical Infectious Diseases **39**(3): 309-317.

Wolf, D. E. (1988). Probing The Lateral Organization And Dynamics of Membranes. Spectroscopic Membrane Probes. L. M. Loew. Boca Raton, CRC Press. **1:** 193-220.

Yeagle, P. L. (2016). Chapter 6 - Laboratory Membrane Systems. The Membranes of Cells. P. L. Yeagle. Boston, Academic Press**:** 95-114.

Yin, J., Howe, J. and Tan, K. S. W. (2010). "Staurosporine-induced programmed cell death in Blastocystis occurs independently of caspases and cathepsins and is augmented by calpain inhibition." Microbiology **156**(5): 1284-1293.

Young, M. E., Karpova, T. S., Brugger, B., Moschenross, D. M., Wang, G. K., Schneiter, R., Wieland, F. T. and Cooper, J. A. (2002). "The Sur7p family defines novel cortical domains in Saccharomyces cerevisiae, affects sphingolipid metabolism, and is involved in sporulation." Molecular and Cellular Biology **22**(3): 927-934.

Zahumensky, J. and Malinsky, J. (2019). "Role of MCC/Eisosome in Fungal Lipid Homeostasis." Biomolecules **9**(8): 305.

Zalokar, M. (1955). "Biosynthesis of carotenoids in Neurospora. Action spectrum of photoactivation." Archives of Biochemistry and Biophysics **56**(2): 318-325.

Zhang, L. and Takemoto, J. Y. (1989). "Syringomycin stimulation of potassium efflux by yeast cells." Biochimica et Biophysica Acta (BBA) - Biomembranes **987**(2): 171-175.

Zhang, Y. Q., Gamarra, S., Garcia-Effron, G., Park, S., Perlin, D. S. and Rao, R. (2010). "Requirement for ergosterol in V-ATPase function underlies antifungal activity of azole drugs." Plos Pathogens **6**(6): e1000939.

Zinser, E., Paltauf, F. and Daum, G. (1993). "Sterol composition of yeast organelle membranes and subcellular distribution of enzymes involved in sterol metabolism." Journal of Bacteriology **175**(10): 2853-2858.

CHAPTER X – ANNEXES

Table S 1 - Selected data from the transcriptional analysis of the 1h STS challenge of N. crassa conidial cells grown for 5 h, taken from Fernandes, A.S., Goncalves, A.P., Castro, A., Lopes, T.A., Gardner, R., Glass, N.L., and Videira, A. (2011) Fungal Genet Biol 48, 1130-1138.

gene	sample_1	sample_2	status	value_1	value_2	log2(fold_change)	test_stat	p_value	q_value	significant	BROAD_Annotation_March2011
NCU09975	wtDMSO	wtSTS	OK	6.78603	797.821	6.87735	-16.5023	0	0	yes	multidrug resistance protein 3
NCU09473	wtDMSO	wtSTS	OK	20.6851	290.81	3.81341	-8.97906	0	0	yes	3-ketoacyl-acyl carrier protein reductase
NCU03929	wtDMSO	wtSTS	OK	18.793000	170.309000	3.179890	-8.584620	0.000000	0.000000	yes	acyl-CoA synthetase
NCU08147	wtDMSO	wtSTS	OK	7.856650	108.687000	3.790120	-9.747290	0.000000	0.000000	yes	Na or K P-type ATPase
NCU03639	wtDMSO	wtSTS	OK	29.851900	266.787000	3.159790	-8.160950	0.000000	0.000000	yes	lipase
NCU05899	wtDMSO	wtSTS	OK	4.904470	60.893400	3.634120	-8.134920	0.000000	0.000000	yes	flotillin domain-containing protein
NCU09337	wtDMSO	wtSTS	OK	52.049000	4.835380	-3.428170	7.641030	0.000000	0.000000	yes	plasma membrane fusion protein prm-1
NCU06005	wtDMSO	wtSTS	OK	46.748800	4.212840	-3.472060	7.543640	0.000000	0.000000	yes	glycerol kinase
NCU02287	wtDMSO	wtSTS	OK	29.259000	176.423000	2.592080	-6.861070	0.000000	0.000000	yes	acyl-CoA dehydrogenase
NCU00130	wtDMSO	wtSTS	OK	2.403480	25.253500	3.393290	-6.615720	0.000000	0.000000	yes	beta-glucosidase
NCU01068	wtDMSO	wtSTS	OK	117.984000	21.670000	-2.444820	6.443370	0.000000	0.000000	yes	BAR domain-containing protein
NCU04479	wtDMSO	wtSTS	OK	42.493000	223.192000	2.392990	-6.189490	0.000000	0.000000	yes	LAP2
NCU08924	wtDMSO	wtSTS	OK	39.233900	184.905000	2.236620	-6.158780	0.000000	0.000000	yes	acyl-CoA dehydrogenase
NCU02544	wtDMSO	wtSTS	OK	8.622140	47.559900	2.463630	-5.951730	0.000000	0.000000	yes	ABC transporter
NCU07546	wtDMSO	wtSTS	OK	6.508890	33.511500	2.364170	-5.899320	0.000000	0.000000	yes	multidrug resistance protein MDR
NCU11109	wtDMSO	wtSTS	OK	71.734200	299.789000	2.063210	-5.818880	0.000000	0.000000	yes	ORM1
NCU04021	wtDMSO	wtSTS	OK	4.925710	25.286800	2.359980	-5.794680	0.000000	0.000000	yes	ABC transporter
NCU01107	wtDMSO	wtSTS	OK	5.716320	43.154000	2.916340	-5.626310	0.000000	0.000000	yes	short-chain dehydrogenase
NCU04736	wtDMSO	wtSTS	OK	30.484000	117.254000	1.943520	-5.535560	0.000000	0.000001	yes	plasma membrane calcium-transporting ATPase 3
NCU06694	wtDMSO	wtSTS	OK	138.923000	528.243000	1.926920	-5.488300	0.000000	0.000001	yes	fatty acid elongase
NCU03768	wtDMSO	wtSTS	OK	49.993500	9.591930	-2.381850	5.236550	0.000000	0.000002	yes	lysophospholipase, variant 2
NCU08372	wtDMSO	wtSTS	OK	0.519639	4.924010	3.244250	-5.162900	0.000000	0.000003	yes	triacylglycerol lipase
NCU06364	wtDMSO	wtSTS	OK	23.155600	3.728430	-2.634720	5.097590	0.000000	0.000005	yes	GDSL lipase/acylhydrolase
NCU08977	wtDMSO	wtSTS	OK	31.567300	117.428000	1.895280	-5.041450	0.000000	0.000006	yes	long chain fatty alcohol oxidase
NCU05207	wtDMSO	wtSTS	OK	2.058190	14.680200	2.834420	-5.039550	0.000000	0.000006	yes	MFS multidrug transporter
NCU12074	wtDMSO	wtSTS	OK	5.329910	28.140000	2.400440	-5.001480	0.000001	0.000007	yes	5-nitroimidazole antibiotic resistance protein
NCU06382	wtDMSO	wtSTS	OK	5.399280	0.894413	-2.593750	4.986180	0.000001	0.000008	yes	ABC transporter
NCU03497	wtDMSO	wtSTS	OK	22.075800	3.989470	-2.468190	4.916460	0.000001	0.000011	yes	plasma membrane iron permease
NCU05627	wtDMSO	wtSTS	OK	41.486200	142.091000	1.776110	-4.850080	0.000001	0.000015	yes	high affinity glucose transporter ght1
NCU02579	wtDMSO	wtSTS	OK	1.884410	12.033600	2.674890	-4.671830	0.000003	0.000033	yes	FAS1 domain-containing protein
NCU01378	wtDMSO	wtSTS	OK	7.163080	34.178300	2.254430	-4.597220	0.000004	0.000046	yes	acetoacetyl-CoA synthase
NCU09692	wtDMSO	wtSTS	OK	9.785690	1.477070	-2.727930	4.563700	0.000005	0.000053	yes	phosphatidic acid phosphatase beta
NCU02726	wtDMSO	wtSTS	OK	52.019100	152.866000	1.555160	-4.236950	0.000023	0.000200	yes	ethanolamine kinase
NCU01654	wtDMSO	wtSTS	OK	53.617000	133.763000	1.318910	-3.742520	0.000182	0.001255	yes	long-chain-fatty-acid-CoA ligase 1
NCU09497	wtDMSO	wtSTS	OK	544.225000	216.566000	-1.329400	3.740650	0.000184	0.001264	yes	bifunctional D12/D15 fatty acid desaturase
NCU08045	wtDMSO	wtSTS	OK	117.551000	312.121000	1.408820	-3.659310	0.000253	0.001672	yes	phosphatidylethanolamine N-methyltransferase
NCU01004	wtDMSO	wtSTS	OK	31.210300	75.905100	1.282180	-3.612380	0.000303	0.001957	yes	phosphatidylserine decarboxylase proenzyme
NCU03372	wtDMSO	wtSTS	OK	3.485350	11.710900	1.748470	-3.497490	0.000470	0.002856	yes	nonspecific lipid-transfer protein
NCU06874	wtDMSO	wtSTS	OK	4.772800	14.085100	1.561260	-3.423350	0.000619	0.003618	yes	HMG box-containing protein
NCU08976	wtDMSO	wtSTS	OK	344.536000	807.528000	1.228860	-3.419700	0.000627	0.003660	yes	fatty acid elongase
NCU01112	wtDMSO	wtSTS	OK	0.238675	3.270530	3.776400	-3.388280	0.000703	0.004039	yes	lipid binding protein
NCU04699	wtDMSO	wtSTS	OK	450.142000	1031.780000	1.196690	-3.373530	0.000742	0.004230	yes	methylene-fatty-acyl-phospholipid synthase
NCU04092	wtDMSO	wtSTS	OK	13.474900	33.867600	1.329630	-3.278820	0.001042	0.005642	yes	N-acylethanolamine amidohydrolase
NCU02175	wtDMSO	wtSTS	OK	5.431200	14.964700	1.462220	-2.977490	0.002906	0.013370	yes	phosphatidyl inositol-specific phospholipase C
NCU06761	wtDMSO	wtSTS	OK	41.666000	87.120900	1.064150	-2.948890	0.003189	0.014443	yes	sphingosine-1-phosphate lyase
NCU07307	wtDMSO	wtSTS	OK	176.841000	380.261000	1.104540	-2.942410	0.003257	0.014714	yes	fatty acid synthase beta subunit dehydratase
NCU07308	wtDMSO	wtSTS	OK	195.555000	407.017000	1.057520	-2.833550	0.004603	0.019585	yes	fatty acid synthase alpha subunit reductase
NCU01069	wtDMSO	wtSTS	OK	35.838900	73.054400	1.027440	-2.786030	0.005336	0.022090	yes	amphiphysin-like lipid raft protein
NCU05278	wtDMSO	wtSTS	OK	111.279000	217.775000	0.968661	-2.748650	0.005984	0.024305	yes	cytochrome P450 61
NCU05608	wtDMSO	wtSTS	OK	10.652800	21.556500	1.016890	-2.659850	0.007818	0.030214	yes	phosphatidylinositol 3-kinase tor2

3-oxo-acyl-[acyl-carrier-protein] reductase exhibits a marked preference for acyl-carrier protein derivatives over CoA derivatives as substrates. The enzyme shows activity towards both short and long chain saturated and unsaturated ß-ketoacyl-ACPs. The reductase functions in every cycle of the fatty acid elongation pathway. Other reductases of this type also exist in E. coli [Magnuson93, Heath96b]. The enzyme is also involved in the elongation of 3-ketoglutaryl-[acp]-methyl-ester to pimeloyl-[acp]-methyl-ester, part of the biotin biosynthesis pathway [Lin10].

Component of the SPOTS complex that acts as a negative regulator of sphingolipid synthesis. Acts by inhibiting serine palmitoyltransferases (LCB1 and LCB2) activity

(involved in C-22 desaturation of the ergosterol side-chain)

Table S 2 - Fluorescence Spectroscopy Parameters of t-PnA, DPH and di-4-ANEPPS in N. crassa at 30 ºC, 2 h growth.

Probes	Cells	Growth medium	α_1	τ_1 (ns)	α_2	τ_2 (ns)	α_3	τ_3 (ns)	τ_{av} (ns)	$\langle\tau\rangle$ (ns)
t-PnA	*WT*	MMV	0.68 ± 0.03	1.7 ± 0.1	0.26 ± 0.02	6.91 ± 0.26	0.07 ± 0.01	24.07 ± 0.20	4.54 ± 0.41	11.60 ± 0.76
	WT	SeM	0.719 ± 0.006	0.98 ± 0.08	0.25 ± 0.01	4.74 ± 0.35	0.028 ± 0.004	22.70 ± 2.00	2.55 ± 0.23	8.2 ± 1.3
	slime	SeM	0.66 ± 0.02	2.87 ± 0.63	0.19 ± 0.03	10.91 ± 2.59	0.154 ± 0.006	39.15 ± 1.21	9.94 ± 1.05	26.52 ± 0.60
DPH	*WT*	MMV	0.538 ± 0.007	1.17 ± 0.13	0.411 ± 0.008	4.0 ± 0.2	0.051 ± 0.009	10.09 ± 0.68	2.78 ± 0.12	4.46 ± 0.12
	WT	SeM	0.53 ± 0.02	1.13 ± 0.14	0.337 ± 0.009	3.86 ± 0.29	0.14 ± 0.02	8.58 ± 0.32	3.07 ± 0.07	5.14 ± 0.09
	slime	SeM	0.22 ± 0.11	1.05 ± 0.47	0.45 ± 0.19	4.35 ± 0.99	0.33 ± 0.09	8.14 ± 0.71	4.98 ± 0.81	6.35 ± 0.15
di-4-ANEPPS	*WT*	MMV	0.43 ± 0.07	0.53 ± 0.02	0.367 ± 0.001	1.74 ± 0.09	0.20 ± 0.07	3.22 ± 0.12	1.52 ± 0.14	2.17 ± 0.12
	WT	SeM	0.48 ± 0.02	0.483 ± 0.005	0.21 ± 0.03	1.314 ± 0.004	0.314 ± 0.009	2.682 ± 0.003	1.35 ± 0.01	2.03 ± 0.02
	slime	SeM	0.18 ± 0.01	0.35 ± 0.08	0.41 ± 0.05	1.73 ± 0.07	0.41 ± 0.05	3.07 ± 0.07	2.02 ± 0.02	2.51 ± 0.02

Table S 3 - Fluorescence Spectroscopy Parameters of t-PnA, DPH and di-4-ANEPPS in N. crassa at 30 ºC, 5 h growth.

Probes	Cells	Growth medium	α_1	τ_1 (ns)	α_2	τ_2 (ns)	α_3	τ_3 (ns)	τ_{av} (ns)	$\langle\tau\rangle$ (ns)
***t*-PnA**	*WT*	MMV	0.70 ± 0.01	1.62 ± 0.13	0.245 ± 0.009	5.92 ± 0.85	0.051 ± 0.006	24.00 ± 0.20	3.81 ± 0.46	10.41 ± 0.45
	WT	SeM	0.68 ± 0.02	1.42 ± 0.19	0.27 ± 0.02	5.11 ± 0.37	0.047 ± 0.001	25.51 ± 0.33	3.55 ± 0.16	11.04 ± 0.05
	slime	SeM	0.63 ± 0.03	2.41 ± 0.26	0.22 ± 0.01	9.43 ± 0.81	0.15 ± 0.02	38.03 ± 0.42	9.34 ± 1.05	25.75 ± 1.57
DPH	*WT*	MMV	0.54 ± 0.01	1.10 ± 0.17	0.404 ± 0.008	3.89 ± 0.20	0.06 ± 0.02	9.62 ± 0.77	2.74 ± 0.10	4.48 ± 0.16
	WT	SeM	0.41 ± 0.08	1.16 ± 0.02	0.36 ± 0.03	4.38 ± 0.33	0.23 ± 0.05	8.84 ± 0.19	4.05 ± 0.35	6.19 ± 0.18
	slime	SeM	0.08 ± 0.01	1.63 ± 0.87	0.59 ± 0.06	5.33 ± 0.16	0.32 ± 0.05	8.53 ± 0.32	6.04 ± 0.20	6.70 ± 0.05
di-4-ANEPPS	*WT*	MMV	0.45 ± 0.06	0.52 ± 0.08	0.36 ± 0.03	1.64 ± 0.21	0.19 ± 0.06	3.16 ± 0.16	1.42 ± 0.04	2.09 ± 0.06
	WT	SeM	0.21 ± 0.07	0.54 ± 0.02	0.46 ± 0.08	0.96 ± 0.02	0.34 ± 0.02	2.53 ± 0.02	1.40 ± 0.03	1.88 ± 0.02
	slime	SeM	0.17 ± 0.06	0.44 ± 0.19	0.42 ± 0.02	1.73 ± 0.09	0.42 ± 0.07	3.10 ± 0.05	2.08 ± 0.23	2.54 ± 0.09

Table S 4 - Maximal emission and excitation wavelengths for di-4-ANEPPS in N. crassa strains at 30 ºC, 2 h and 5 h growth.

Cells	Growth medium	2 h growth		5 h growth	
		$\lambda_{em,\,max}$ (nm)	$\lambda_{exc,\,max}$ (nm)	$\lambda_{em,\,max}$ (nm)	$\lambda_{exc,\,max}$ (nm)
WT	MMV	635 ± 3	487 ± 3	636 ± 3	489 ± 5
WT	SeM	629 ± 0	500 ± 0	636 ± 3	485 ± 1
slime	SeM	626 ± 3	482 ± 4	629 ± 5	480 ± 3

Table S 5 - Fluorescence Spectroscopy Parameters of t-PnA in N. crassa wt cells at 26 ºC, in MMV.

Growth time	α_1	τ_1 (ns)	α_2	τ_2 (ns)	α_3	τ_3 (ns)	τ_{av} (ns)	$\langle\tau\rangle$ (ns)
2 h	0.75 ± 0.03	1.84 ± 0.14	0.21 ± 0.03	7.25 ± 0.95	0.044 ± 0.005	33.32 ± 2.80	4.33 ± 0.19	14.19 ± 0.93
5 h	0.70 ± 0.01	1.95 ± 0.08	0.222 ± 0.004	7.78 ± 0.41	0.076 ± 0.004	37.14 ± 0.46	5.93 ± 0.27	20.47 ± 0.16

Table S 6 - Fluorescence spectroscopy parameters of t-PnA in N. crassa at 30 ºC, 2 h and 5 h growth, in the absence and presence of 1 h challenge with STS.

Time of growth (h)	Incubation time (min; h)	α_1	τ_1 (ns)	α_2	τ_2 (ns)	α_3	τ_3 (ns)	τ_{av} (ns)	$\langle\tau\rangle$ (ns)
2 h	1 h sts	0.64 ± 0.03	1.75 ± 0.09	0.30 ± 0.01	5.30 ± 0.19	0.06 ± 0.01	20.71 ± 1.11	3.88 ± 0.34	8.83 ± 1.15
	1 h ctrl	0.63 ± 0.01	1.52 ± 0.07	0.327 ± 0.008	4.91 ± 0.20	0.042 ± 0.003	20.44 ± 1.43	3.41 ± 0.03	7.81 ± 0.34
5 h	1 h sts	0.585 ± 0.004	2.03 ± 0.07	0.354 ± 0.005	5.90 ± 0.19	0.061 ± 0.008	24.51 ± 0.38	4.78 ± 0.27	10.78 ± 0.66
	1 h ctrl	0.64 ± 0.03	2.11 ± 0.09	0.31± 0.03	5.91 ± 0.28	0.047 ± 0.002	24.11 ± 0.59	4.31 ± 0.03	9.50 ± 0.10

Table S 7 - Fluorescence spectroscopy parameters of t-PnA in N. crassa at 30 ºC, 3 h and 6 h growth, in the absence and presence of 15 min challenge with STS.

Time of growth (h)	Incubation time (min; h)	α_1	τ_1 (ns)	α_2	τ_2 (ns)	α_3	τ_3 (ns)	τ_{av} (ns)	$\langle\tau\rangle$ (ns)
3 h	15 min sts	0.63 ± 0.04	1.73 ± 0.31	0.31 ± 0.04	6.13 ± 0.44	0.050 ± 0.005	26.27 ± 0.52	3.83 ± 0.49	11.98 ± 0.41
	15 min ctrl	0.581 ± 0.004	1.38 ± 0.07	0.356 ± 0.006	6.44 ± 0.25	0.058 ± 0.002	24.17 ± 0.36	4.71 ± 0.23	11.94 ± 1.18
6 h	15 min sts	0.474 ± 0.002	1.86 ± 0.06	0.44 ± 0.02	6.34 ± 0.40	0.08 ± 0.02	32.04 ± 0.99	5.99 ± 0.64	16.13 ± 1.65
	15 min ctrl	0.48 ± 0.06	1.59 ± 0.20	0.43 ± 0.04	5.71 ± 0.34	0.09 ± 0.02	31.77 ± 0.53	6.15 ± 0.49	17.64 ± 1.28

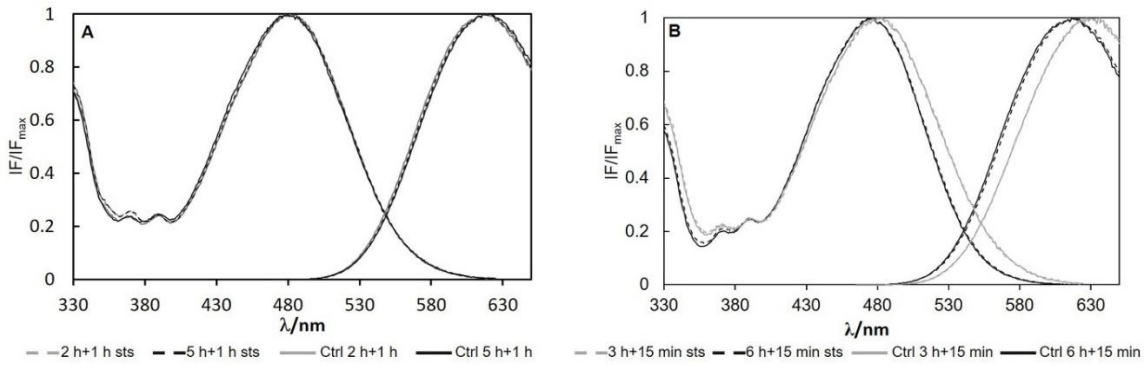

*Figure S 1 - Fluorescence excitation (λ_{em} = 635 nm) and emission spectra (λ_{exc} = 450 nm) of di-4-ANEPPS in N. crassa wt cells, at 30 ºC. **(A)** at 2 and 5 h growth plus 1 h incubation with STS, **(B)** at 3 and 6 h growth plus 15 min incubation with STS. The represented spectra are the mean of at least three independent experiments, n ≥ 3.*

Table S 8 - Maximal emission and excitation wavelengths for di-4-ANEPPS in N. crassa at 30 ºC, in the absence and presence of STS.

Time of growth (h)	2 h		5 h		3 h		6 h	
Incubation time (min;h)	1 h sts	1 h ctrl	1 h sts	1 h ctrl	15 min sts	15 min ctrl	15 min sts	15 min ctrl
$\lambda_{em\ max}$ (nm)	619 ± 1	619 ± 1	618 ± 1	617 ± 1	624 ± 3	627 ± 2	617 ± 3	617 ± 1
$\lambda_{exc\ max}$ (nm)	483 ± 1	484 ± 2	483 ± 2	480 ± 1	480 ± 3	483 ± 1	477 ± 2	476 ± 1

Table S 9 - Fluorescence spectroscopy parameters of di-4-ANEPPS in N. crassa at 30 ºC, 2 h and 5 h growth, in the absence and presence of 1 h challenge with STS.

Time of growth (h)	Incubation time (min; h)	α_1	τ_1 (ns)	α_2	τ_2 (ns)	α_3	τ_3 (ns)	τ_{av} (ns)	$\langle\tau\rangle$ (ns)
2 h	1 h sts	0.44 ± 0.05	0.25 ± 0.02	0.35 ± 0.02	1.49 ± 0.01	0.21 ± 0.03	3.46 ± 0.01	1.36 ± 0.12	2.44 ± 0.07
	1 h ctrl	0.48 ± 0.02	0.210 ± 0.009	0.32 ± 0.01	1.48 ± 0.07	0.21 ± 0.01	3.48 ± 0.06	1.28 ± 0.06	2.49 ± 0.08
5 h	1 h sts	0.51 ± 0.02	0.21 ± 0.02	0.31 ± 0.01	1.50 ± 0.08	0.18 ± 0.02	3.52 ± 0.06	1.20 ± 0.03	2.43 ± 0.03
	1 h ctrl	0.34 ± 0.04	0.50 ± 0.01	0.42 ± 0.03	1.736 ± 0.003	0.242 ± 0.005	3.63 ± 0.04	1.78 ± 0.06	2.56 ± 0.03

Table S 10 - Fluorescence spectroscopy parameters of di-4-ANEPPS in N. crassa at 30 ºC, 3 h and 6 h growth, in the absence and presence of 15 min challenge with STS.

Time of growth (h)	Incubation time (min; h)	α_1	τ_1 (ns)	α_2	τ_2 (ns)	α_3	τ_3 (ns)	τ_{av} (ns)	$\langle\tau\rangle$ (ns)
3 h	15 min sts	0.52 ± 0.02	0.37 ± 0.02	0.349 ± 0.008	1.63 ± 0.07	0.14 ± 0.02	3.38 ± 0.12	1.22 ± 0.04	2.08 ± 0.02
	15 min ctrl	0.49 ± 0.03	0.34 ± 0.08	0.348 ± 0.008	1.46 ± 0.12	0.17 ± 0.03	3.18 ± 0.09	1.20 ± 0.08	2.07 ± 0.04
6 h	15 min sts	0.18 ± 0.02	0.458 ± 0.006	0.46 ± 0.04	2.19 ± 0.01	0.36 ± 0.06	3.67 ± 0.05	2.40 ± 0.11	2.93 ± 0.08
	15 min ctrl	0.15 ± 0.08	0.94 ± 0.06	0.48 ± 0.06	2.51 ± 0.33	0.97 ± 0.10	3.64 ± 0.08	2.69 ± 0.05	3.01 ± 0.02

Table S 11 – Parameters describing the fluorescence intensity decay obtained from FLIM experiments of the transformed fluorescent proteins in S. cerevisiae wt and ipt1Δ plasma membrane. The values are the mean ± S.D. of at least four independent biological replicates with a total of at least 200 cells analyzed per replicate.

Strains	α_1	τ_1 (ns)	α_2	τ_2 (ns)	τ_{av} (ns)
wt Can1p-GFP	0.81 ± 0.08	1.82 ± 0.09	0.19 ± 0.08	3.59 ± 0.45	2.10 ± 0.04
*ipt1*Δ Can1p-GFP	0.83 ± 0.06	1.86 ± 0.04	0.17 ± 0.06	3.60 ± 0.15	2.14 ± 0.06
wt Pma1p-mRFP	0.90 ± 0.01	1.57 ± 0.01	0.10 ± 0.01	4.03 ± 0.16	1.80 ± 0.02
*ipt1*Δ Pma1p-mRFP	0.95 ± 0.02#	1.64 ± 0.02#	0.05 ±0.02#	4.45 ± 0.32	1.77 ± 0.03#

#p<0.001 vs. *wt* Pma1p-mRFP

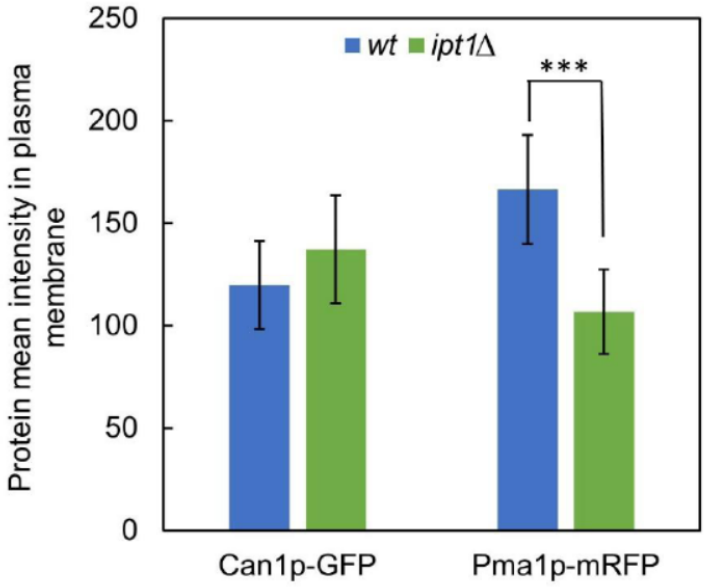

*Figure S 2 - Can1p-GFP and Pma1p-mRFP mean fluorescence intensity in the plasma membrane of wt (blue) and ipt1Δ (green) cells. The values are the mean ± S.D. of at least four independent biological replicates with a total of at least 200 cells analyzed per replicate. ***p ≤ 0.001.*